Charles University in Prague
Faculty of Mathematics and Physics

DOCTORAL THESIS

Dmytro Mulin

Laboratory studies of ion-molecule reactions with molecular and atomic hydrogen at temperatures relevant to astrochemistry

Department of Surface and Plasma Science

Supervisor: prof. RNDr. Juraj Glosík, DrSc.

Study programme: Physics

Specialisation: 4F2 - Physics of Plasmas and Ionised Media

Prague 2015

I hear and I forget.
I see and I remember.
I do and I understand.

– Confucius

Acknowledgements

I would like to express my gratitude to everyone who taught, helped, and supported me during this beautiful time of the PhD study. I had the good fortune to work in a team with excellent scientists and amazing people. Above all, I would like to thank my supervisor prof. Juraj Glosík, who believed in me and gave opportunity to study in Charles University in Prague. His lectures, sudden questions, homilies, combined with great sense of humour, were real engines for my personal and scientific promotion.

Special thanks go to Radek Plašil, whose experience, professionalism, and advice were priceless for conducting successful experiments. I am particularly indebted to Illia Zymak, who acquainted me with the technique and never refused to consult or help me, however busy he was. It was real pleasure to work on experiments together with Štěpán Roučka, Pavol Jusko, and Michal Hejduk, from whom I derived a lot of useful knowledge as well. I thank Petr Dohnal, Peter Rubovič, Tomáš Kotrík, Sergii Opanasiuk, Serhiy Rednyk, and Artem Kovalenko for a pleasant and friendly atmosphere of the team.

In sum, I wish to thank Czech Republic for making this thesis possible and for the financial support of our research.

Наостанок, я дякую всім рідним і друзям за взаємовиручку та підтримку протягом усієї доби навчання, але найбільше – моїй родині за те, що вони завжди поруч, навіть коли вони далеко.

I declare that I carried out this doctoral thesis independently, and only with the cited sources, literature, and other professional sources.

I understand that my work relates to the rights and obligations under the Act No. 121/2000 Coll., the Copyright Act, as amended, in particular the fact that the Charles University in Prague has the right to conclude a license agreement on the use of this work as a school work pursuant to Section 60 paragraph 1 of the Copyright Act.

Prague, March 2015

Dmytro Mulin

Název práce: Laboratorní výzkum reakcí iontů s molekuláním i atomárním vodíkem při teplotách relevantních pro astrochemii

Autor: Dmytro Mulin

Katedra / Ústav: Katedra fyziky povrchů a plazmatu

Vedoucí doktorské práce: prof. RNDr. Juraj Glosík, DrSc., Katedra fyziky povrchů a plazmatu

Abstrakt: V této práci jsou prezentovány výsledky laboratorního výzkumu ion-molekulových reakcí při nízkých teplotách, kde jedním z reaktantů byl atomární nebo molekulární vodík anebo molekulární deuterium. U reakcí atomárních iontů N^+ a H^+ s molekulárním vodíkem byl studován vliv konfigurace jaderných spinů a rotační excitace na rychlostní koeficienty těchto reakcí a jejich závislost na teplotě. Studium reakcí aniontů bylo spojeno s výzkumem reakcí izotopické výměny a izotopického efektu. Byla provedena měření rychlostních koeficientů tvorby molekul H_2O a D_2O v reakcích O^- s H_2 a D_2, reakcí izotopické výměny $OH^- + D_2$ a $OD^- + H_2$ a také byly studovány reakční kanály asociativního odtržení a přenosu náboje v reakci $D^- + H$. Experimenty byly prováděny na aparatuře AB-22PT s iontovou pastí. Tato aparatura zahrnuje systémy pro tvorbu, vedení, záchyt a detekci iontů a také samostatný zdroj atomárního H. Chladící systém umožnil měření teplotních závislostí rychlostních koeficientů při teplotách relevantních pro astrochemii (10 K – 300 K)

Klíčová slova: reakce iontů s atomárním a molekuláním vodíkem, izotopický efekt, jáderný spin, iontová past, asociativní odtržení

Title: Laboratory studies of ion-molecule reactions with molecular and atomic hydrogen at temperatures relevant to astrochemistry

Author: Dmytro Mulin

Department / Institute: Department of Surface and Plasma Science

Supervisor of the doctoral thesis: prof. RNDr. Juraj Glosík, DrSc., Department of Surface and Plasma Science

Abstract: The results of the laboratory study of reaction rate coefficients of several ion-molecule reactions with atomic and molecular hydrogen and molecular deuterium at low temperatures are presented in the thesis. The reaction rate coefficients of the N^+ and H^+ reaction with H_2 were measured with respect to the nuclear spin configuration and rotational excitation of H_2. The reactions of anions were a subject of the isotope exchange and isotope effect study. The measurements of the rate coefficients of H_2O and D_2O formation in the reaction of O^- with H_2 and D_2, isotope exchange reactions $OH^- + D_2$ and $OD^- + H_2$, and associative detachment and charge transfer channels of $D^- + H$ interaction were performed. Experiments were carried out using an AB-22PT instrument with an ion trap. It has producing, guiding, trapping, and detecting systems for ions and a separate source of atomic H. The cooling system allowed to measure the temperature dependencies of the reaction rate coefficients at temperatures relevant to astrochemistry (10 K – 300 K)

Keywords: ion-molecule reactions, isotope effect, nuclear spin state, ion trap, associative detachment

Contents

1 Introduction

This thesis focuses on the experimental study of the gas-phase ion-molecule reactions with atomic and molecular hydrogen, which are important for the astrochemistry. The information about the mentioned processes gives people not only some practical interest, but enriches the fundamental knowledge about the Universe and its formation after the Big Bang. Experiments as well as theoretical calculations are the main sources of information about physical and chemical processes. The most attention of this work is paid to the results of the laboratory studies of interaction of different ions, such as N^+, H^+, O^-, OH^-, OD^-, with molecular hydrogen or deuterium and the interaction of D^- ion with atomic H.

The paper consists of six sections, bibliography, two appendices, five attached publications, and lists of publications, studied reactions, figures, tables, and acronyms.

The importance of ion-molecule reactions for the formation of new species in space, the role of positive and negative ions in the production of the first molecules are explained in section 3 – *Theoretical background*. While studying hydrogen-containing reactions one should take into account the existence of para- and ortho-forms of H_2. So, the aspects of the nuclear spin state configuration of hydrogen and its influence on the reaction dynamics are also discussed there. As well as that, the isotope effect study is important for the understanding of the dynamics and specific features of ion-molecule reactions beyond the simple Langevin theory. Hence, it was also studied in some experiments.

To carry out the experiments relevant to astrochemistry, we had to operate a technique that created the experimental conditions, which allowed us to study the reactions important for the interstellar medium. The

laboratory measurements were conducted using a unique Atomic Beam with a 22-Pole Trap (AB-22PT) instrument firstly designed and operated by prof. Dieter Gerlich and co-workers in the Chemnitz University of Technology, and then transported to our laboratory in Prague in 2009. The cornerstone of the apparatus is a 22-pole ion trap (further 22PT, or just trap) that confines ions while they react with target gases. It can be cooled down to almost 10 K by a special cooling system. The background gas number density in the reaction volume can be reached as low as 10^8 cm^{-3} thanks to a powerful vacuum system. Production, guiding, and detection of ions as well as the formation of an effusive beam of atomic H are described in section 4 – *Experimental techniques* at length. Basic operation principles of a para-enriched hydrogen generator are also given there. Lastly, the section contains methodological aspects of the reaction rate coefficient calculation and evaluation of gas number densities in the ion trap.

Section 5 – *Experimental studies of ion-molecule reactions with atomic and molecular hydrogen* – provides us with the results of the measured rate coefficients of the mentioned reactions. The state-specific rate coefficients of the reactions of N^+ and H^+ with para- and ortho-hydrogen were determined. Moreover, the role of the fine structure of N^+ ions for collisional relaxation of internal states was studied in the reaction $N^+(^3P_{ja}) + H_2(J)$. In experiments with negative ions, such processes as isotope effect and isotope exchange are studied. The study of D^- + H reaction gives us further information about the H^- + H collision complex studied experimentally in our laboratory earlier in 2011 [*Gerlich et al., 2012*].

The studied reactions with the respective numeration in the text and denotation of the respective reaction rate coefficients can be found in a handy *List of studied reactions* at the end of the thesis.

During my study, I worked in a group, so I carried out the investigations of the ion-molecule reactions with co-workers. My work involved organising an experimental process as well as consequent experimental data analysis and preparation of the publications.

2 Goals of the thesis

The main goal of the work was to experimentally determine temperature-dependent rate coefficients of several ion-molecule reactions, which are essential for the understanding of astrochemical reaction processes.

Apart from the mentioned temperature dependencies, in reactions with positive ions

$$N^+(^3P_{ja}) + H_2(J) \rightarrow NH^+ + H,$$

$$H^+ + H_2(J) \rightarrow H_3^+$$

we studied state-specific rate coefficient dependencies on the H_2 rotational energy and on N^+ fine structure energy.

The experiments with negative ions were conducted using normal or atomic hydrogen and normal deuterium:

$$O^- + H_2(D_2) \rightarrow \text{products},$$

$$OH^- + D_2 \rightarrow OD^- + HD,$$

$$OD^- + H_2 \rightarrow OH^- + HD,$$

$$D^- + H \rightarrow \text{products}.$$

In these reactions we studied either isotope exchange or isotope effect under hydrogen-deuterium substitution. The ion kinetic temperature was evaluated with standard $He^+ + 2\,He$ ternary association reaction.

It is important to mention that the experiments presented had to be carried out at interstellar-relevant temperatures (down to 10 K). Accordingly, the goal of the work guided the calibration of the AB-22PT instrument in the whole as well as the design and construction of its separate units in particular.

3 Theoretical background

The necessity of the study of hydrogen-relevant chemistry is specified by the abundance of hydrogen in the Universe. It has been detected in all stars, atmospheres of giant planets, interstellar medium and comprises three quarters of the mass of the known matter [*Field et al., 1966*].

Hydrogen is mostly present in atomic, molecular, and proton forms. Furthermore, the H_2 molecular clouds played a basic role in the process of star formation and the cooling of primordial gas in the first protogalaxies [*Glover et al., 2006*]. The importance of the study of hydrogen isotopes, especially deuterium, is also discussed in the section.

The molecular hydrogen may occur in *ortho*- and *para*-forms that sign two different nuclear spin configurations. The influence of the nuclear spin configuration and rotational excitation on the reactivity of H_2 is discussed in chapter 3.4.

3.1 Positive and negative ions in the interstellar medium and their reactions with hydrogen

Ion-molecule reactions play an essential role in the astrochemistry. The study of these reactions at low temperatures can help to succeed in the understanding of the processes in the interstellar medium. Moreover, ion-molecule reactions, as well as reactions on the surface of dust grains, are the main source of production of more complex ions in space [*McSween and Huss, 2010*] and dominate the synthesis of molecules in the interstellar clouds [*Luine and Dunn, 1985*].

3.1.1 Ion-molecule reactions and conditions in the interstellar medium

The reactions between neutral particles are strongly inhibited at low temperatures because of well-known activation energy barriers associated with such interactions, however, it has been established that in most cases no such barrier retards reactions if one of the reacting particles is an ion. Reaction may take place at essentially every collision, even at interstellar-relevant temperatures, if the process is exothermic. For instance, there was shown that ion-molecule reactions could form small molecules (e.g., H_2O, NH_3, CO, etc.) in the interstellar medium much faster than other processes [*Watson, 1974*]. Ion-molecule reactions with hydrogen are also of particular importance due to the fact that the majority of nearly 150 detected in space molecules contain H.

The most of the observed species in the interstellar medium are present in diffuse and dense molecular clouds, which possess the most typical particle concentrations ~10 cm^{-3} – 100 cm^{-3} and ~10^4 cm^{-3} – 10^8 cm^{-3}, and kinetic temperatures ~10 K – 30 K and ~50 K – 100 K, respectively [*Herbst, 2001*]. The level of ionisation in such environments is relatively high and varies from 10^{-8} to 10^{-6} that supports the statement of the importance of ion-molecule reactions. The rest of the interstellar matter, spread out between the clouds, exists in atomic and ionised forms, where the temperatures may reach ~10^6 K values [*Ferriere, 2001*].

The low-pressure (hundreds of pascals and lower) experiments with ions have been carried out since the early 1950s, when conventional mass spectrometers with modified ion sources were used to study ion-molecule reactions [*Stevenson and Schissler, 1958*], [*Ferguson, 1975*]. The detection of a huge number of interstellar ions, atoms, and molecules and the recent development of detailed ion-molecule reaction schemes for the production of interstellar molecules also provide new impulse to laboratory investigations in this field. Nowadays the techniques for studying ion-molecule reactions,

such as tandem mass spectrometers, stationary and flowing afterglow apparatuses, beam technologies, drift tubes, trapping technique, have developed a lot comparing to the previous times and allow now experiments at different pressures in the range of interaction energies from several kelvins to several electron-volts.

3.1.2 H^- anion and formation of the first molecules in the Universe

The central role in the primordial chemistry and particularly the formation of the first H_2 molecules plays H^- anion [*Glover et al., 2006*], [*Glover and Abel, 2008*]. It also provides most of the continuum opacity, emission, and thermalisation in the photosphere of stars [*Gerlich et al., 2012*], [*Kutner, 2003*].

Firstly, H atoms were ionised by radiative attachment

$$H + e^- \rightarrow H^- + h\nu \tag{3.1}$$

and then the associative detachment (AD) reaction took place

$$H^- + H \rightarrow H_2 + e^-. \tag{3.2}$$

Several negative ion species have been detected directly in the interstellar medium since the first observation in 2006 [*McCarthy et al., 2006*], [*Cernicharo et al., 2007*], [*Brünken et al., 2007*]. However, due to the specific transition in the ultraviolet region, H^- anion has not been observed spectroscopically yet [*Ross et al., 2008*]. Nevertheless, there are some indirect observations that prove the presence of H^- anion in space [*Heap and Stecher, 1974*]. Theoretical calculations of the rate coefficient of the reaction (3.2) were in a quite disagreement among each other as well as with different selected ion flow tube (SIFT) and merged beams (MB) experimental results [*Sakimoto, 1989*], [*Bruhns et al., 2010*], [*Čížek et al., 1998*], [*Schmeltekopf et al., 1967*],

[*Fehsenfeld et al., 1973*], [*Martinez et al., 2009*]. In 2012 the first ion trap study of the reaction (3.2) at low temperatures was carried out in our laboratory and showed good accordance with Čížek and Sakimoto theories [*Gerlich et al., 2012*]. The comparison of the existing theoretical and experimental data is shown in figure 3.1.

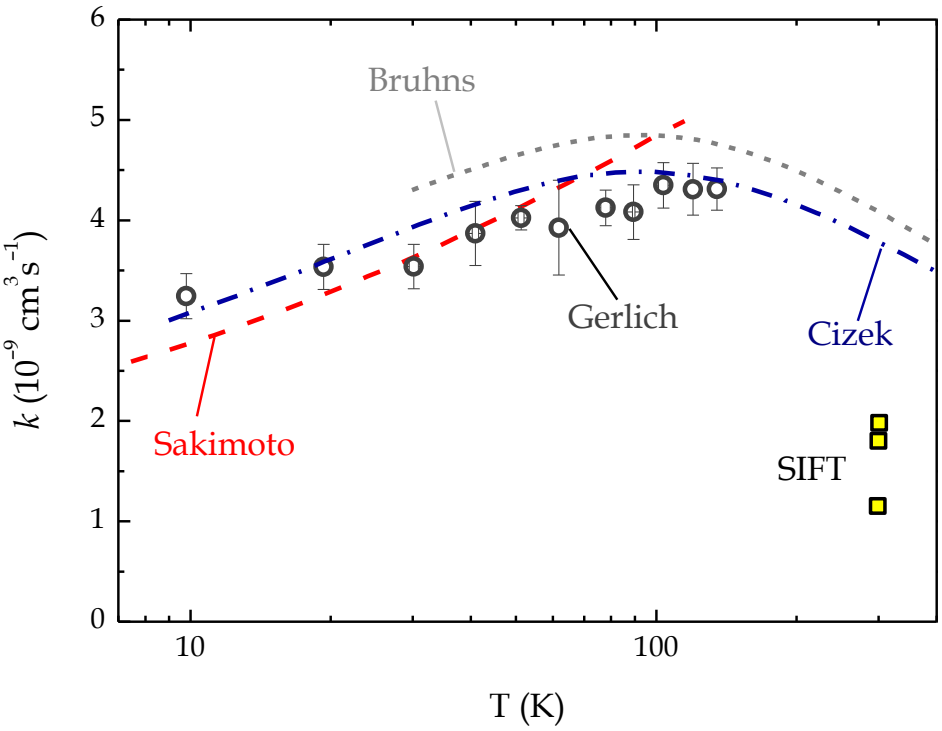

Figure 3.1. The $H^- + H$ reaction rate coefficients measured on ion trap (circles) [*Gerlich et al., 2012*], selected ion flow tube (squares) [*Schmeltekopf et al., 1967*], [*Fehsenfeld et al., 1973*], [*Martinez et al., 2009*], merged beams (short-dashed line) [*Bruhns et al., 2010*], and results from theoretical calculations [*Sakimoto, 1989*], [*Čížek et al., 1998*]. Figure adapted from [*Gerlich et al., 2012*].

As well as H atoms, deuterium particles also took an active part in the evolution of the primordial matter [*Hogan, 1996*]. As a sequel of that work the experimental study of deuterated variant of the reaction (3.2) $D^- + H$ was carried out. Despite the lower deuterium abundance in space comparing to hydrogen, the theoretical and experimental studies of isotope variances of hydrogen-containing reactions are also of a high importance (discussed in chapter 3.3).

The most of the interstellar deuterium is present in the form of HD [*Solomon and Woolf, 1973*]. In some regions a considerably higher HD/H_2 ratio was observed comparing to the D/H ratio obtained by other methods ($\sim 10^{-2}$ comparing to $\sim 10^{-4}$ [*Hoyle and Fowler, 1973*]) [*Watson, 1973[a]*], [*Watson, 1973[b]*], [*Spitzer et al., 1973*]. HD molecule and study of its formation is also important due to the fact that it has a dipole moment [*Glover et al., 2006*].

3.1.3 H_3^+ ion and $H^+ + H_2$ collision complex

It is a generally accepted fact that H_3^+ ions play an important role in the interstellar medium, hydrogen-containing plasmas, and discharges [*Oka, 2006*]. Since H_3^+ is the most produced polyatomic ion in the Universe, it must be involved in many reactions with other atoms, molecules, anions, or electrons. Therefore, it certainly is a powerful sensor for probing specific astrophysical environments [*Gerlich et al., 2013*]. It actually stands as a root of a huge tree of different ion-molecule reactions and serves as a cradle of more complex species [*Dalgarno, 1994*]. The combination of three protons (or deuterons) and two electrons represent a benchmark system for rigorous theoretical studies [*Morong et al., 2009*].

In hydrogen plasmas, containing molecular H_2^+ ion, the H_3^+ is predominantly produced via a fast proton transfer reaction [*Glosík, 1994*], [*Plašil et al., 2002*]:

$$H_2^+ + H_2 \rightarrow H_3^+ + H. \tag{3.3}$$

Another way of H_3^+ formation is association of H^+ ions with H_2, when an excited intermediate complex $(H_3^+)^*$ is formed and then relaxed by either binary radiative or ternary mechanisms. Radiative association plays an important role in the formation of interstellar molecules, whereas ternary process dominates in applications with higher hydrogen number densities [*Zymak et al., 2011*]:

$$H^+ + H_2 \rightarrow H_3^+ + h\nu, \tag{3.4}$$

$$H^+ + H_2 + H_2 \rightarrow H_3^+ + H_2. \tag{3.5}$$

Under our experimental conditions both association channels were significant. The methodology of evaluation of the respective rate coefficients is given in chapter 3.2.

For many decades, the determination of association rate coefficients has been the domain of swarm techniques operating at rather high pressures (with number densities above $10^{16}\,cm^{-3}$). The ternary rate coefficients were determined in a range of temperatures down to 135 K using a drift-tube mass spectrometer apparatus [*Graham et al., 1973*], [*Johnsen et al., 1976*]. Swarm techniques could not provide direct results for radiative association, the high densities led to the prevailing domination of the ternary process. This situation was changed after the development of ion-trapping techniques in the 1980s. First results for both channels (3.4) and (3.5) at 230 K were reported in [*Gerlich and Kaefer, 1989*]. The high sensitivity of ion traps allowed to carry out experiments at such low densities, where radiative association prevailed over the three-body process.

One should also take into account the role of internal energy of hydrogen in the reaction. It is particularly interesting in terms of evaluation the state-selective reactivity of both channels (3.4), (3.5). Temperature dependencies of the binary radiative and ternary rate coefficients may significantly help to understand the mechanisms of the stabilisation of $(H_3^+)^*$ collision complexes.

3.1.4 Water in the interstellar medium and its formation via $O^- + H_2$ reaction

Formation of H_2O molecules in space represents a fundamental problem for the astrochemistry due to its vital importance. The recent

observations of water in molecular clouds by NASA's[1] and ESA's[2] satellites have drawn a compelling connection between water in interstellar space and planetary water [*Bergin et al., 2008*]. These observations revealed a surprisingly low abundance of water particles in the dense cores of molecular clouds [*Snell et al., 2000*] and a relatively high abundance in diffuse clouds [*Neufeld et al., 2000*], [*Moneti et al., 2001*].

The reaction of O^- with H_2 is one of the simplest anion-neutral systems of H_2O formation in space. It has two exothermic channels corresponding to associative detachment and hydrogen atom transfer (channels (3.6) and (3.7), respectively) and an endothermic proton transfer (channel (3.8)) [*Li et al., 2009*]:

$$O^- + H_2 \rightarrow H_2O + e^-, \Delta H = -3.60 \text{ eV}, \quad (3.6)$$

$$O^- + H_2 \rightarrow OH^- + H, \Delta H = -0.30 \text{ eV}, \quad (3.7)$$

$$O^- + H_2 \rightarrow H^- + OH, \Delta H = 0.79 \text{ eV}. \quad (3.8)$$

Here ΔH is enthalpy change in the reaction. In low-energy collisions of reactants in ground electronic states, $O^-(^2P) + H_2(X^1\Sigma_g^+)$, the collision system has three accessible electronic states $1^2A'$, $1^2A''$, and $2^2A'$. Furthermore, the O^- ion is present in two fine structure states $O^-(^2P_{1/2})$ and $O^-(^2P_{3/2})$, which are separated by 22 meV [*Neumark et al., 1985*]. The AD reaction (3.6) is of particular interest because such reactions proceed through compound states, which then undergo autodetachment [*McFarland et al., 1973*].

Channels (3.6) and (3.7) received significant attention in previous experimental studies, but the endoergic proton transfer reaction was studied in less detail. The flow-drift tube study of $O^- + H_2$ interaction was carried out by McFarland, Fehsenfeld, Ferguson, and Schmeltekopf in Aeronomy Laboratory in Boulder at the beginning of the 1970s [*McFarland et al., 1973*].

[1] National Aeronautics and Space Administration. <http://www.nasa.gov/>. Retrieved 12 March 2015.
[2] European Space Agency. <http://www.esa.int/ESA>. Retrieved 12 March 2015.

In figure 3.2 one can see the collection of the respective reaction rate coefficients and the comparison with the values obtained in other experiments [*Martin and Bailey, 1968*], [*Parkes, 1972*], [*Mauer and Schulz, 1973*]. The total cross-sections for H^- production in the third endoergic channel (3.8) of the reaction at higher energies can be found in [*Li et al., 2009*].

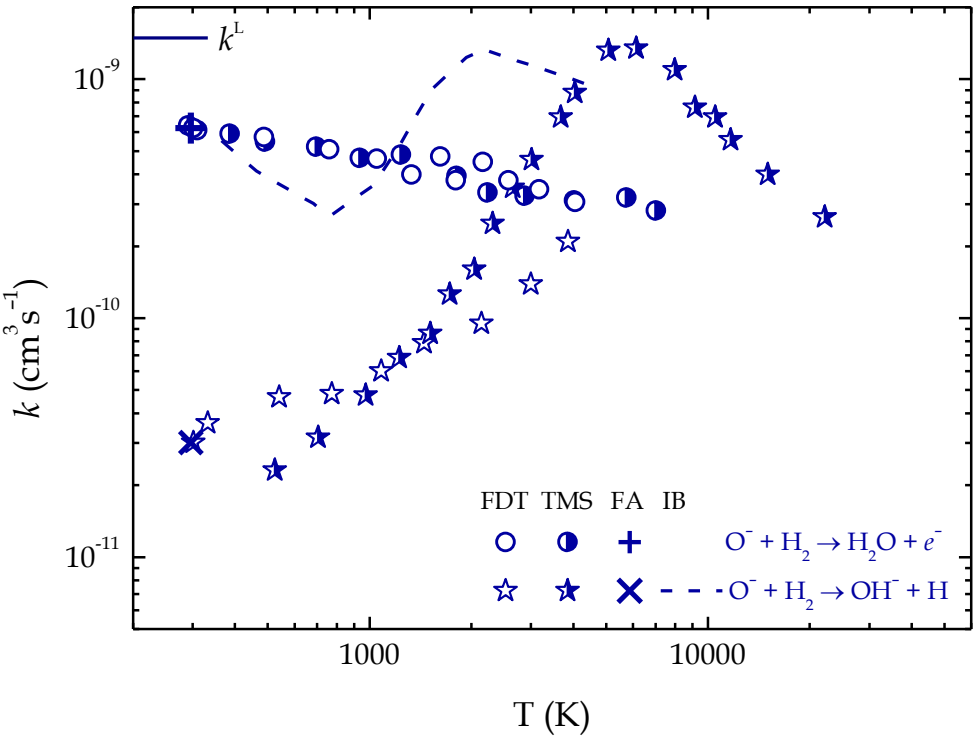

Figure 3.2. Rate coefficients of the $O^- + H_2$ reaction as function of collision temperature. Crosses are flowing afterglow (FA) data [*Parkes, 1972*], open symbols are flow-drift tube (FDT) [*McFarland et al., 1973*], half-closed symbols are tandem mass-spectrometer (TMS) [*Martin and Bailey, 1968*], dashed line is ion beam (IB) [*Mauer and Schulz, 1973*]. Circles refer to the reaction (3.6), stars refer to the reaction (3.7).

In the present work the results of the laboratory study of the rate coefficient of channels (3.6) and (3.7) and the respective reactions with deuterium at below-room temperatures down to 11 K are presented. Some notes on the theory of the $O^- + H_2$ interaction provided by theoreticians are given in subchapter 5.2.1.

3.2 Determination of the rate coefficient of an ion-molecule reaction

Ion-molecule collision takes place when the potential energy of the interaction between the particles exceeds the kinetic energy of their mutual motion. Ion induces a dipole moment in an atom or molecule so that at some distance the neutral particle «captures» the ion. Without a deep mathematical insight, the cross-section σ_0 of such collision can be expressed as [*Raizer, 1997*]

$$\sigma_0 = \pi\rho^2 = \frac{q}{2\varepsilon_0 v}\sqrt{\frac{\alpha}{\mu}}, \tag{3.9}$$

where ρ is capture radius, q is ion charge, v is relative velocity, α is neutral particle polarisability, μ is reduced mass, and ε_0 is vacuum permittivity. Collisional rate coefficient, or so-called Langevin rate coefficient, can be calculated from the collisional cross-section as

$$k^{\mathrm{L}} = \langle\sigma_0 v\rangle = \frac{q}{2\varepsilon_0}\sqrt{\frac{\alpha}{\mu}}. \tag{3.10}$$

Here the brackets signify velocity averaging. The coefficient is dependent only on the parameters of particles and is an essential unit in study and understanding of gas-phase ion-molecule reactions. Typical value of k^{L} is of 10^{-9} cm^3 s^{-1} in order.

Actually, not every single collision between ions and neutral particles leads to reaction due to the energy barriers, rotational excitation, state-selective reactivity, etc. Ion-molecule reactions by themselves have several particular parameters, but the reaction rate coefficient is mostly used to describe the rate of the reaction of the system in thermodynamic equilibrium

with temperature T. The usual formula describing a binary ion-molecule reaction is the following:

$$A^+ + B \rightarrow C^+ + D, \tag{3.11}$$

where A^+ and B are reactants, C^+ and D are products. Consequently, the time decay of the ion reactant number density is as follows:

$$\frac{d[A^+]}{dt} = -k[A^+][B], \tag{3.12}$$

where k is the reaction rate coefficient, $[A^+]$ and [B] are number densities of the reactants. If we put into the reaction zone far more reactant B than A^+, so that $[A^+] << [B]$, then we can count the density [B] as constant and the solution of the equation will be

$$[A^+] = [A_0^+]e^{-k[B]t}, \tag{3.13}$$

where $[A_0^+]$ is number density of reactant ions at time $t = 0$. As we can see, under equivalent conditions the reaction rate is faster with increasing [B] due to the increase of number of collisions.

Third body-assisted reactions are similar to binary except for the appearance of a particle M:

$$A^+ + B + M \rightarrow C^+ + D + M. \tag{3.14}$$

If $[A^+] << [B]$ and $[A^+] << [M]$, the change of the reactant ion number density in time is described with a ternary reaction rate coefficient k_3, and the respective solution is as follows:

$$\frac{d[A^+]}{dt} = -k_3[A^+][B][M], \tag{3.15}$$

$$[\mathrm{A}^+] = [\mathrm{A}_0^+]e^{-k_3[\mathrm{B}][\mathrm{M}]t}. \quad (3.16)$$

In case of associative ion-molecule reactions, the interaction between an ion and a neutral particle is usually followed by the creation of a highly excited complex that has to be then stabilised. The stabilisation can take place via emission of an electromagnetic quantum (binary radiative association) or by an interaction with a third particle (ternary association):

$$\mathrm{A}^+ + \mathrm{B} \rightarrow (\mathrm{AB}^+)^* \rightarrow \mathrm{AB}^+ + h\nu, \quad (3.17)$$

$$\mathrm{A}^+ + \mathrm{B} + \mathrm{M} \rightarrow (\mathrm{AB}^+)^* + \mathrm{M} \rightarrow \mathrm{AB}^+ + \mathrm{M}. \quad (3.18)$$

The binary radiative and ternary association processes are described by the respective binary and ternary reaction rate coefficients k_r and k_3. In case when association may proceed via both of the channels (3.17) and (3.18), an apparent binary reaction rate coefficient k^* is determined to evaluate the influence of both channels [*Gerlich and Horning, 1992*]:

$$\frac{\mathrm{d}[\mathrm{A}^+]}{\mathrm{d}t} = -k_r[\mathrm{A}^+][\mathrm{B}] - k_3[\mathrm{A}^+][\mathrm{B}][\mathrm{M}] = -(k_r + k_3[\mathrm{M}])[\mathrm{A}^+][\mathrm{B}], \quad (3.19)$$

$$k^* = k_r + k_3[\mathrm{M}]. \quad (3.20)$$

One can note that the apparent reaction rate coefficient k^* is linearly dependent on number density of the buffer gas.

In case of the presented in the thesis anion-molecule reactions, the stabilisation of the collision complex can also take place by the detachment of an electron that carries away the extra energy. Consequently, associative detachment reactions are binary and described by the binary reaction rate coefficient.

3.3 Isotope effect in hydrogen-containing ion-molecule reactions

The atomic mass of hydrogen was determined by Aston in 1927 [*Aston, 1927*] using a mass spectrometer. The result showed good agreement with the value obtained chemically. The later discovery that ordinary oxygen contained appreciable amounts of ^{17}O and ^{18}O isotopic variants [*Giauque and Johnston, 1929*] indicated that hydrogen might also have isotopes [*Birge and Menzel, 1931*].

The spectroscopic evidence for the existence of heavy hydrogen in a sample of ordinary hydrogen was firstly reported in 1932 by Urey, Brickwedde, and Murphy [*Urey et al., 1932*]. After the experimental confirmation of existence of deuterium both Cremer & Polanyi [*Cremer and Polanyi, 1932*], and Eyring & Sherman [*Eyring and Sherman, 1933*] predicted that hydrogen and deuterium should react at different rates due to the difference in zero-point energies. This feature was called deuterium isotope effect and it was found to be of great value in the study of the mechanisms and dynamics of ion-molecule reactions [*Wiberg, 1955*].

In the interactions between neutral species deuterium-containing molecules have lower vibrational states and thus higher dissociation energies than the respective ones with hydrogen. The typical energy difference associated with hydrogen isotope exchange in molecules is in the range of 0.03 eV – 0.07 eV that is appreciably lower than the thermal energy in both dense and diffuse interstellar clouds. Hence, the abundance of the deuterated molecular form can be considerably higher in thermodynamic equilibrium [*Watson, 1974*].

Concerning the interactions between ions and neutral particles, the respective Langevin collisional rate coefficient k^{L} is proportional to the value $\sqrt{\alpha/\mu}$, so, it is obvious that the ratio $k^{\mathrm{L}}_{\mathrm{H_2}}/k^{\mathrm{L}}_{\mathrm{D_2}}$ between its values for hydrogen-containing and deuterium-substituted reactions is $\sqrt{2}$.

In general, in many astrophysical environments and planetary atmospheres the abundance of ions and molecules containing isotopic constituents yields very useful information on the formation mechanisms of the different species [*McCaroll, 2010*].

A merged beam study of associative detachment reaction $H^- + H$ (3.2) and its deuterated analogue

$$D^- + D \rightarrow D_2 + e^- \tag{3.21}$$

conducted by the group of prof. D. W. Savin may serve as an example of the recent experimental and theoretical study of the isotope effect [*Miller et al., 2012*] (figure 3.3).

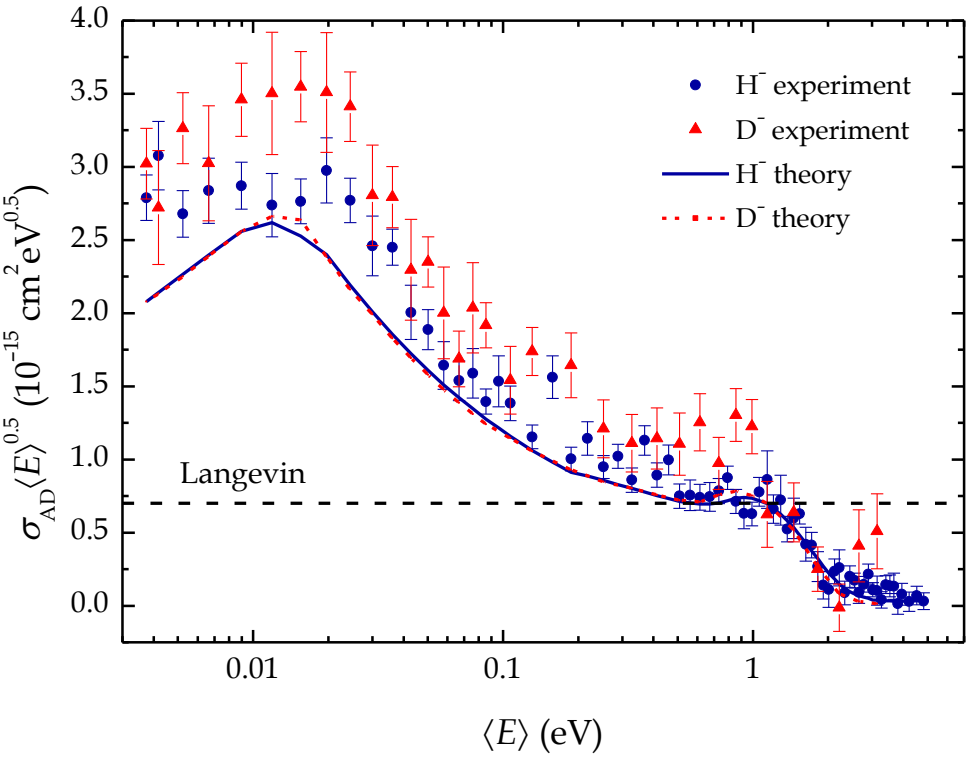

Figure 3.3. Scaled cross-section versus relative collision energy for $H^- + H$ (blue) and $D^- + D$ (red) AD reactions. Points and lines are the results of the experimental and theoretical studies of these reactions, respectively. Data adapted from [*Miller et al., 2012*].

The measurements were carried out in the range of collision energies from 3.74 meV to 4.83 eV and no isotope effect was reported. Predominantly they obtained slightly higher experimental cross-section values for deuterium, while theory gave almost identical results for both AD reactions. Nevertheless, the difference in their experimental values was not large to report a considerable isotope effect.

In the present work the results of the study of D^- with H reaction are reported. Unlike the reactions (3.2) and (3.21), associative detachment and charge transfer (CT) channels can be marked out in this interaction:

$$D^- + H \rightarrow HD + e-, \tag{3.22}$$

$$D^- + H \rightarrow H^- + D. \tag{3.23}$$

The data for both channels were obtained in the temperature range of 10 K – 160 K using an ion trapping technique to confine ions and an H-atom source to produce an effusive beam of thermalised H atoms. Lastly, the experimental results were compared with the recent theoretical calculations reported in [*Eliášek, 2014*] (subchapter 5.2.3).

Along with the above mentioned experimental and theoretical studies of the formation of interstellar H_2O and OH^- anion (reactions (3.6), (3.7)), a considerable insight was also given to their deuterated analogues [*McFarland et al., 1973*], [*Parkes, 1972*] in the same temperature ranges:

$$O^- + D_2 \rightarrow D_2O + e-, \tag{3.24}$$

$$O^- + D_2 \rightarrow OD^- + D. \tag{3.25}$$

The rate coefficients of the reactions (3.24), (3.25) reported in [*McFarland et al., 1973*] are shown in figure 3.4 as open orange triangles and diamonds. The values are given in comparison with the respective rate coefficients

obtained in the experiments with H_2, presented in figure 3.2. All measurements were conducted at energies higher than 300 K, so, low-temperature investigations are needed to fill in the gap in the knowledge about the water formation in the interstellar medium.

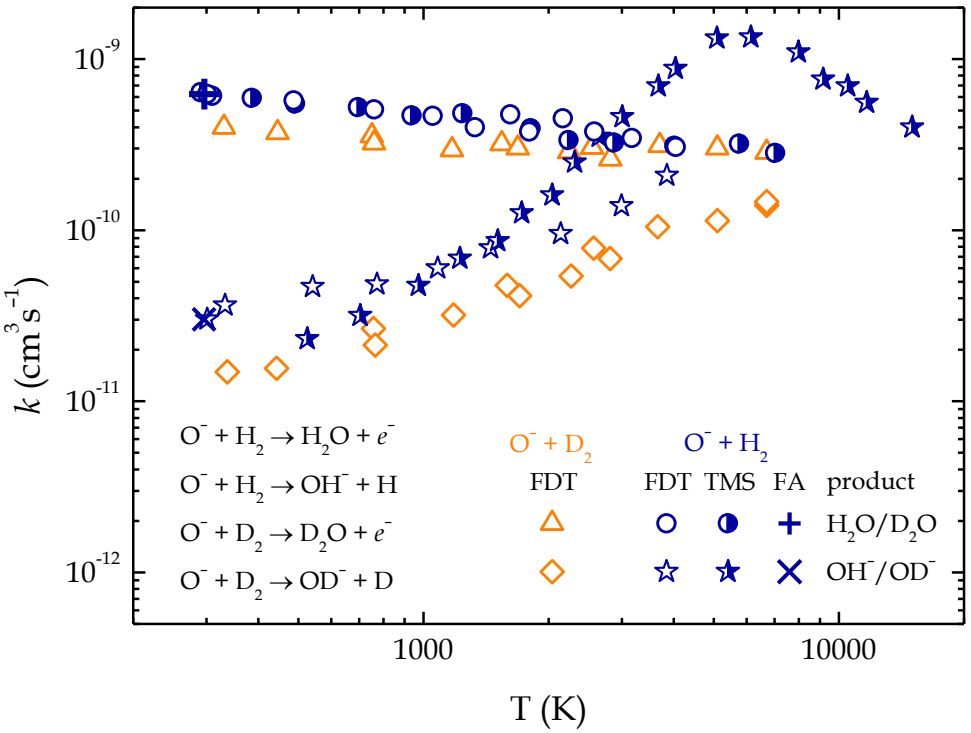

Figure 3.4. The dependence of $O^- + H_2/D_2$ reaction rate coefficients on temperature. Crosses are flowing afterglow (FA) data [*Parkes, 1972*], open symbols are flow-drift tube (FDT) [*McFarland et al., 1973*], half-closed symbols are tandem mass-spectrometer (TMS) (first reported in [*McFarland et al., 1973*]). Triangles refer to the reaction (3.24), diamonds to (3.25), circles to (3.6), stars to (3.7).

Reactions of anions with H, D, H_2, and D_2, leading to exchange of H atoms with D atoms, are also of particular importance for theoretical studies [*Martinez et al.*, 2009], [*Kreckel et al., 2010*], [*Yang et al., 2011*], [*Gerlich et al., 2012*], [*Miller et al., 2012*], [*Čížek et al., 1998*], [*Otto et al., 2008*]. Generally, the reactants in such isotope exchange reactions form an intermediate complex in which bond rearrangement takes place. The lifetime of the complex has to

be long enough to permit some degree of isotopic mixing [*Smith and Adams, 1984*].

The change of enthalpy of isotope exchange reactions are related to the recombination energies of reactants and products and the differences in the zero-point energies, which usually are near-thermoneutral (i. e., have reaction enthalpies up to tens of meV). Due to the considerable mass change in the molecule, these effects are most pronounced in hydrogen-deuterium exchange reactions, where significant differences in the bond vibrational energies take place [*Smith and Adams, 1984*]. The more particles a collisional system has, the harder is the interpretation of the experimental results and carrying out detailed quantum mechanical calculations. Such reactions served for determination of vibrational zero-point energies and relative bond strengths [*Smith and Adams, 1984*], assigning ion structures [*Stewart et al., 1977*], [*Hunt and Sethi, 1980*], etc. Isotope exchange reactions are also a useful instrument for the probation of chemical reaction mechanisms and examination of the nature of potential energy surfaces associated with these reactions [*Adams et al., 1982*], [*Lias, 1984*], [*Graul et al., 1990*], [*Lee and Farrar, 2000*].

In this work the H/D exchange process is investigated in one of the simplest proton transfer reaction complexes involving H_2O

$$OH^- + H_2 \rightarrow H_2O + H^-. \qquad (3.26)$$

This complex has been proven to be a stable species [*Kleingeld and Nibbering, 1983*] and serves as a model for negative ion-water complexes that governed high level of theoretical and experimental interest to its reaction dynamics. The reverse channel of the reaction (3.26) was also the first experimental report of a negative ion-molecule reaction [*Muschlitz, 1957*].

For better understanding of the H_3O^- collision complex, a sketch of the potential energies of different configurations of H_3O^- system is given in figure 3.5. The energies are corrected for the zero-point energies in order to

show the energy difference between the isotopic variants of the reactants. In case of the $OH^-\cdot(H_2)$ and $H^-\cdot(H_2O)$ clusters, the potential energies from [*Zhang et al., 2002*] and zero-point energies from [*Wang et al., 1997*] are used. The zero-point energies of the intermediate complexes have large uncertainties, but the energetics of the reactants is known with good precision.

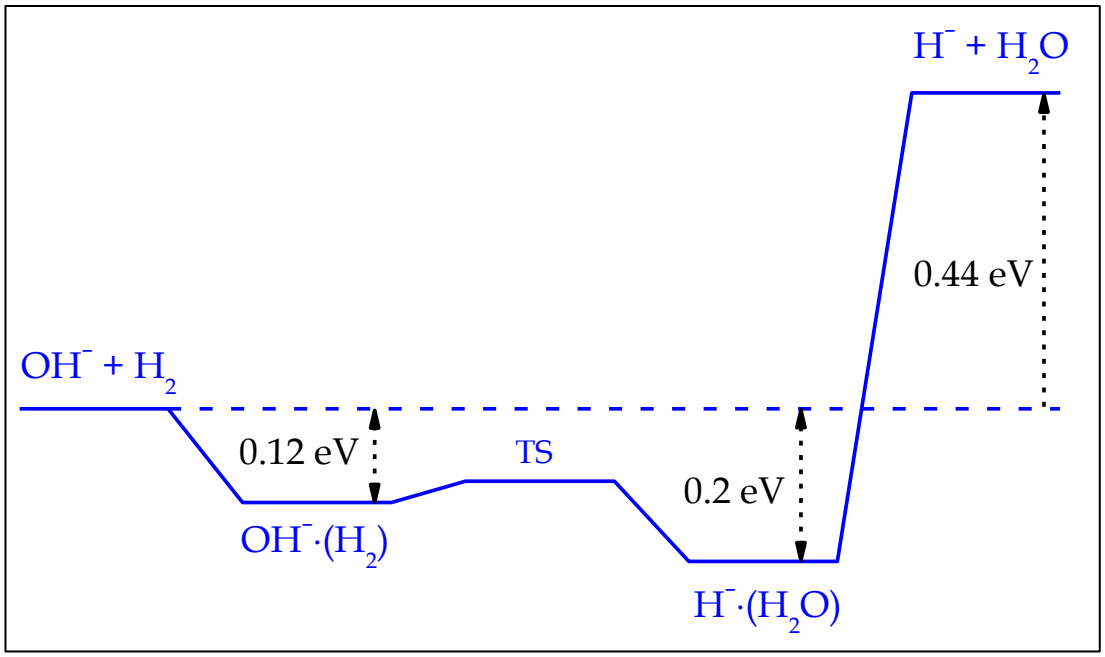

Figure 3.5. Sketch of the potential energy surface for the reaction of OH^- with H_2. The energies are theoretical values from [*Zhang et al., 2002*]. The dashed arrows indicate potential minimum corresponding to the intermediate complexes $OH^-\cdot(H_2)$ and $H^-\cdot(H_2O)$ and to the endothermicity of the reaction leading to $H^- + H_2O$.

The necessity of better understanding of the H_3O^- collision complex incited the low-temperature experimental study of deuterated variations of the reaction (3.26):

$$OH^- + D_2 \rightarrow OD^- + HD,\ \Delta H = -17.2\ \text{meV}, \qquad (3.27)$$

$$OD^- + H_2 \rightarrow OH^- + HD,\ \Delta H = 24.0\ \text{meV}. \qquad (3.28)$$

The changes of reaction enthalpies were calculated from electron affinities of OH and OD [*Smith et al., 1997*], [*Schulz et al., 1982*], zero-point energies of H_2, D_2, and HD [*Irikura, 2007*], and from zero-point energies of OH^- and OD^- [*Rosenbaum et al., 1986*], [*Rehfuss et al., 1986*] in the Born-Oppenheimer approximation. On the contrary, [*Lee and Farrar, 2000*] gives completely different values of changes of reactions enthalpies, but it might be due to a misprint.

The majority of previous experimental data were obtained for 300 K and above [*Grabowski et al., 1983*], [*Meot-Ner et al., 1980*], [*Henchman and Paulson, 1988*]. There is just one flow drift tube study conducted at 130 K and there are no data below this temperature [*Viggiano and Morris, 1994*]. Another endothermic channel $OH^- + D_2 \rightarrow D^- + HDO$ with change of enthalpy ΔH = 420 meV was also studied both theoretically and experimentally [*Li et al., 2005*].

Figure 3.6 provides a sketch of the potential energies of different isotopic and isomeric configurations of H_3O^- system involved in reaction (3.28). It is assumed [*Grabowski et al., 1983*], [*Viggiano and Morris, 1994*] that during the isotopic exchange reactions, the system passes through triple minima. In case of reaction (3.28) it is $OH^-\cdot(D_2)$ complex formation, followed by $D^-\cdot(DOH)$ complex, where the isotope positions can be exchanged to $D^-\cdot(HOD)$, and finally a breakup via $OD^-\cdot(HD)$ complex. The energies in the graph are corrected for the zero-point energies to show the energy difference between the isotopic variants of the reactants. The energies of the deuterated intermediate complexes are not known precisely, so the figure shows only schematically the H_3O^- energies from [*Zhang et al., 2002*] corrected by zero-point energies from [*Wang et al., 1997*]. It can be expected that complex formation, isotope exchange, and breakup of complex are reflected in the dependencies of the respective rate coefficients on rotational energy of reactants and on temperature.

To show the influence of internal excitation of reactants on endothermicity of the reaction (3.28), the energies of two lowest rotational

states of H_2 with para ($J_{H2} = 0$) and ortho ($J_{H2} = 1$) nuclear spin configuration (the details in chapter 3.4), as well as the lowest rotational states of OD^- with J_{OD^-} from 0 to 4 [*Rehfuss et al., 1986*], are included in the left panel of figure 3.6.

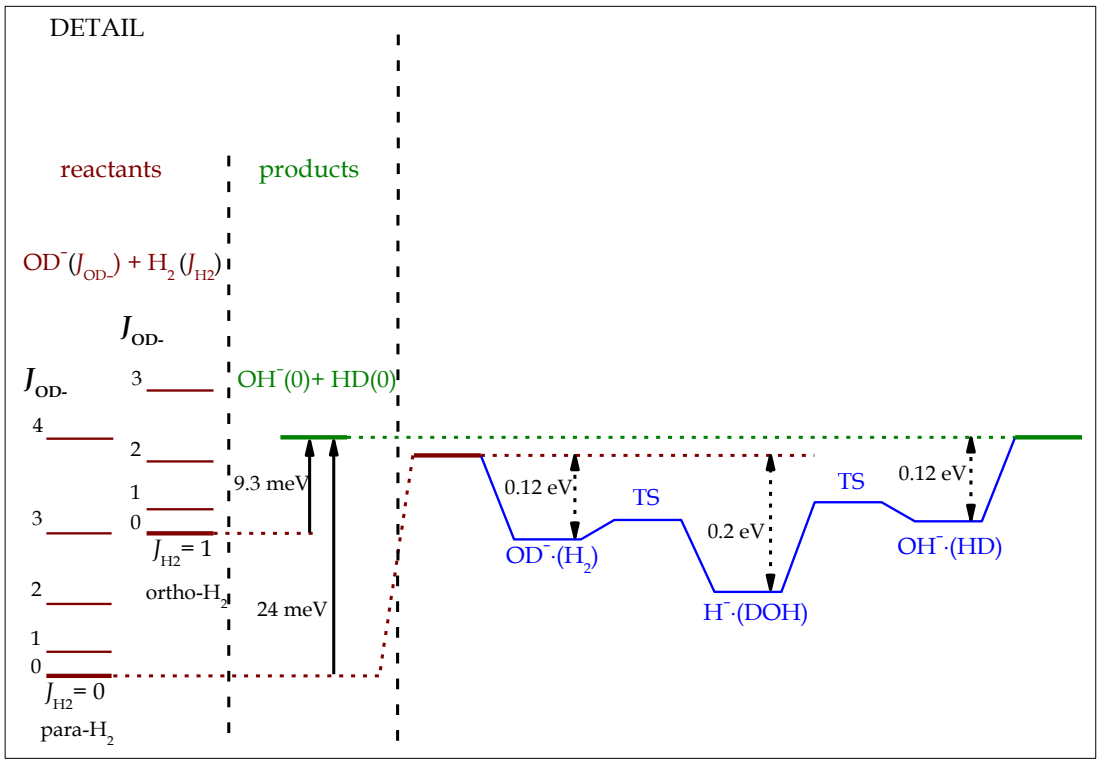

Figure 3.6. *Right panel*: Sketch of the potential energy surface for the reaction $OD^- + H_2 \rightarrow OH^- + HD$. The dashed arrows indicate potential minima corresponding to the intermediate complexes $OD^-\cdot(H_2)$, $OH^-\cdot(HD)$, and $H^-\cdot(DOH)$. *Left panel*: Detail of the rotational energy levels of the reactants OD^- and H_2. The energies of the rotational excitation of OD^- and H_2 are taken from [*Schulz et al., 1982*] and [*Monfils, 1965*]. The solid arrows indicate endothermicities of the reactions of $OD^-(J_{OD^-} = 0)$ with para-H_2 ($J_{H2} = 0$) and with ortho-H_2 ($J_{H2} = 1$).

3.4 Rotational excitation of H_2 and its influence on the reaction rate coefficient

H_2 molecule can exist in two different nuclear spin states known as para-hydrogen (antiparallel spin orientation) and ortho-hydrogen (parallel spin orientation). In this work we designate para-hydrogen as p-H_2 and ortho-hydrogen as o-H_2. More detailed view on the quantum-mechanical aspects of the hydrogen nuclear spin states can be found elsewhere [*Sugimoto and Fukutani, 2011*], [*Hejduk, 2013*], [*Zym*ak, *2013*], we will focus only on the basic features of para- and ortho-hydrogen.

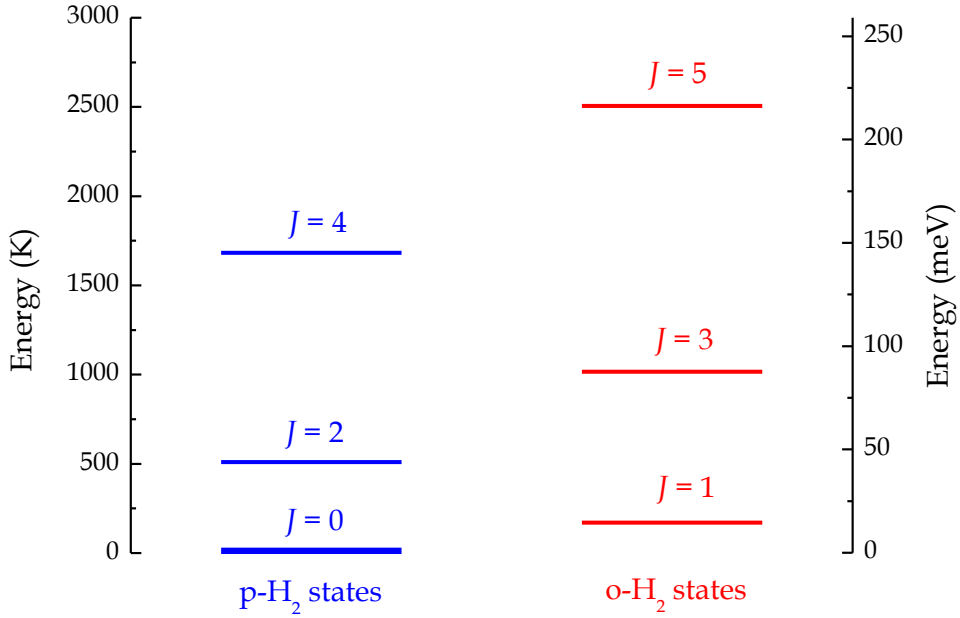

Figure 3.7. Rotational excitation levels of p/o-H_2(J) [*Monfils, 1965*].

Depending on the spin orientations, there may be several variations of the z-component S_z of the total nuclear spin. Para-hydrogen has one configuration with $S_z = 0$ (singlet) and its total spin number S equals 0. Ortho-hydrogen may be present in three configurations with $S_z = 0, \pm 1$ (triplet) and its total spin number S is 1. Nuclear spin state also affects the total angular momentum of a molecule. Due to the fact that protons are fermions, they are described by Fermi-Dirac statistics and are affected by Pauli Exclusion Principle. In the end, these restrictions lead to the coupling

between the nuclear spin states and rotational excitation levels J: the even states with J = 0, 2, 4 … correspond to para-hydrogen, while the odd states with J = 1, 3, 5 … correspond to ortho-hydrogen (figure 3.7).

The variations of the z-component of the total spin number S_z correspond to the ratio between the statistical weights of para- and ortho-states that equals 1:3 at room temperature. Consequently, in the thermodynamic equilibrium at 300 K the fractions of the molecules of H_2 present in para- and ortho-states are 0.25 and 0.75, respectively. We call such mixture normal hydrogen and designate as n-H_2. Spontaneous transitions between para- and ortho-states are very slow without catalysts, so a mixture of p/o-H_2 can be stored in a stainless steel container for a very long time without reaching equilibrium [*Buntkowsky et al., 2006*], [*Raich and Good, 1964*], [*Dislaire et al., 2012*]. However, at interstellar conditions the para/ortho conversion takes place in inelastic collisions of H^+ with H_2 in gas phase [*Gerlich, 1990*] and on the surface of dust grains [*Osterbrock, 1974*], [*Lique et al., 2014*]. The temperature dependence of relative populations of para- and ortho-states of H_2 in thermal equilibrium is presented in figure 3.8.

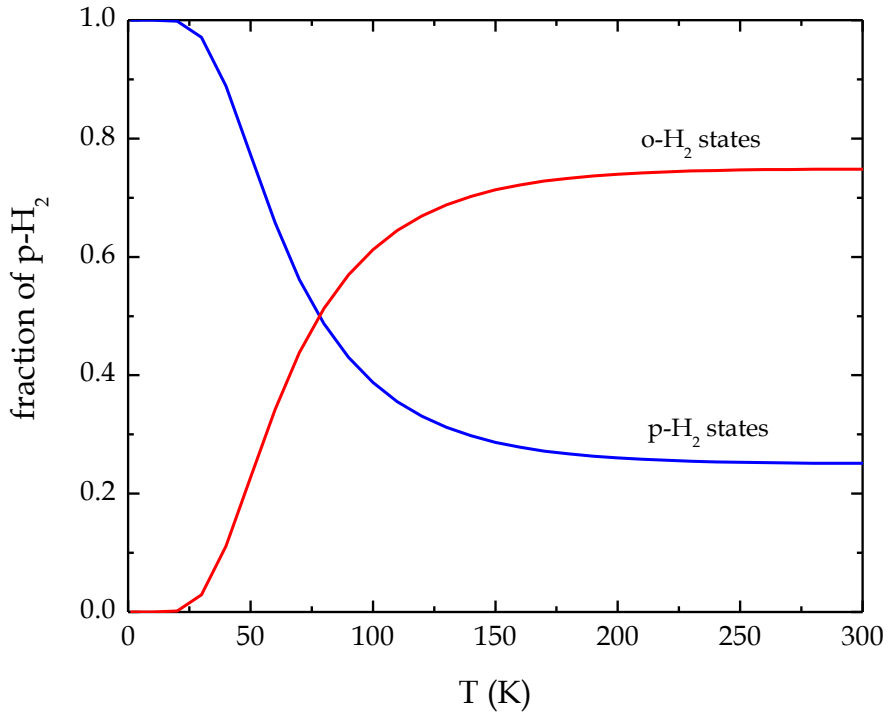

Figure 3.8. Thermal dependence of relative populations of para- and ortho-states of H_2 in thermal equilibrium.

Formation of H_3^+ in association reaction of H^+ with p/o-H_2 has already been previously studied using the 22-pole ion trap [*Gerlich and Horning, 1992*]. This work provides new experimental data on the mentioned reaction at interstellar-relevant temperatures (subchapter 5.1.2).

The difference of 170 K between the lowest $J = 0$ and $J = 1$ rotational levels of H_2 may have a considerable influence on the reaction rates of endothermic reactions at interstellar-relevant temperatures. A reaction of N^+ with H_2,

$$N^+ + H_2 \rightarrow NH^+ + H, \tag{3.29}$$

may serve as an example. Its typical endothermicity value varies from 11 meV [*Wilhelmsson and Nyman, 1992*] to 33 meV [*Gerlich, 2008*].

Atomic nitrogen and nitrogen-containing molecules are important tracers for understanding astrophysical objects [*Dislaire et al., 2012*]. The nitrogen hydrides NH, NH_2, NH_3, and their ions are of central importance in astrochemistry due to the high abundance of hydrogen and nitrogen (first and fifth abundant species in the range) [*Arnett, 1996*]. Furthermore, the reaction (3.29) stands in the beginning of the reaction chain leading to the formation of ammonia in dense interstellar clouds [*Herbst and Klemperer, 1973*].

Reaction (3.29) was previously studied experimentally using ion trap [*Gerlich et al., 1990*], CRESU[3] [*Marquette et al., 1988*], and selected ion flow drift tube (SIFDT) techniques [*Adams and Smith, 1985*], their results are presented in figure 3.9. The internal energy of o-H_2 decreases the endothermicity of the reaction (3.29), so the rate coefficients of the N^+ reaction with para- and ortho-H_2 differ extremely at low temperatures. Due to such difference, the reaction N^+ + p/o-H_2 is also a very useful instrument for the evaluation of the fraction of para-hydrogen in the p/o-H_2 mixture.

[3] Cinétique de Réaction en Ecoulement Supersonique Uniforme

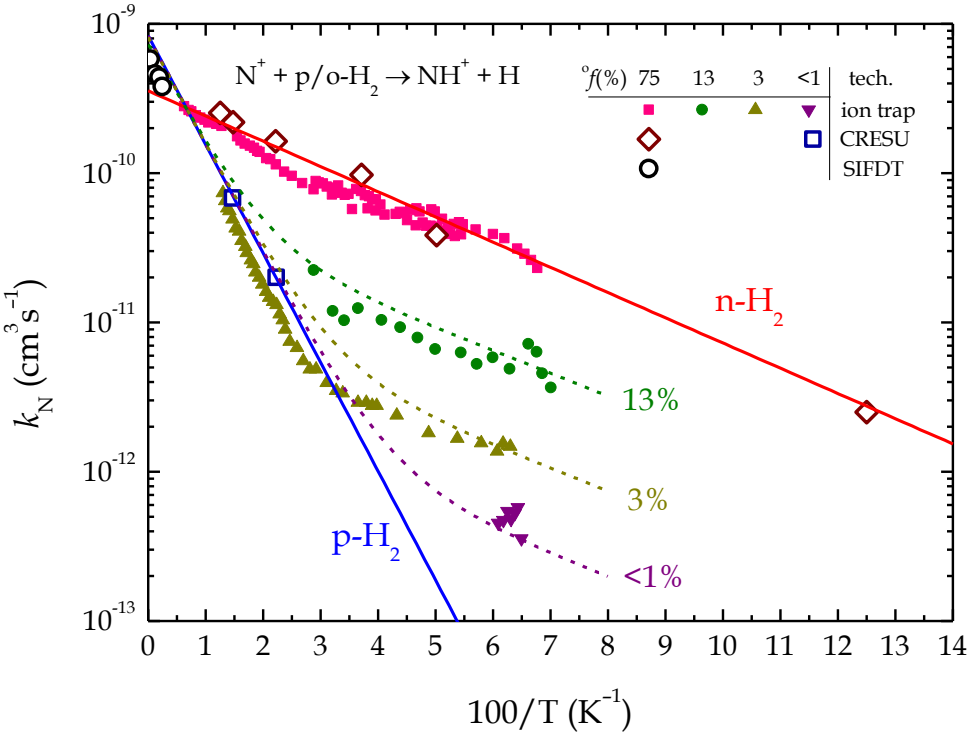

Figure 3.9. Temperature dependence of the reaction rate coefficient k_N of $N^+ + H_2$ reaction measured for different fractions of o-H_2 (given in percentage terms). Small closed symbols are trap experiment [*Gerlich et al., 1990*], open diamonds are CRESU [*Marquette et al., 1988*], and open circles are SIFDT data [*Adams and Smith, 1985*]. Some experimental data are fitted with biexponential functions (short-dashed lines) from [*Dislaire et al., 2012*].

Regarding N^+ ion, we can take into account $^3P_0$, $^3P_1$, $^3P_2$ states of fine structure energy that are dominantly populated in the studied temperature range of 10 K – 100 K. It is considered that the rotational energy can contribute to the reaction dynamics as efficiently as the kinetic energy and it was discussed whether the spin-orbit energy has a similar role for the reaction (3.29) (see discussion in [*Gerlich, 1989*]). In figure 3.10 the energy levels of reactants pair $N^+(^3P_{0,1,2}) + H_2(J)$ are shown. $X^2\Pi$ level of NH^+ (ground state) is drawn with the offset equal to the assumed endothermicity ~17 meV, the $^3P_2$ state of N^+ fine structure energy is reported to be non-reactive [*Russel and Manolopoulos, 1999*].

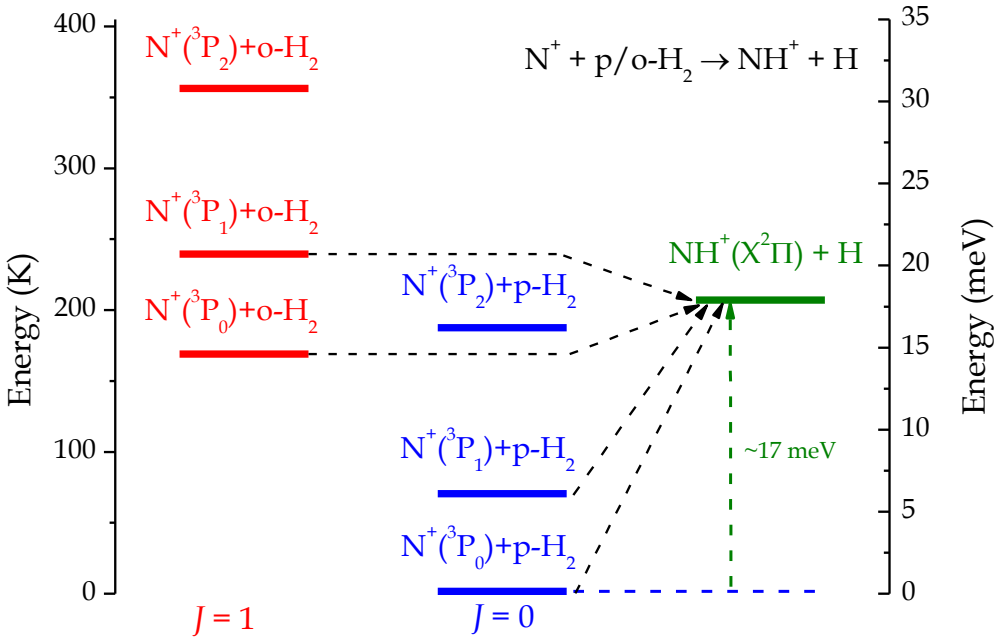

Figure 3.10. Schematic energy levels diagram of $N^+(^3P_{0,1,2})$ reaction with p/o-H_2. Only $^3P_0$, $^3P_1$ states of fine structure energy of N^+ are reported to be reactive, the respective transitions are marked as dashed arrows [*Russel and Manolopoulos, 1999*].

4 Experimental techniques

This section is focused on the description of the techniques used in the experiments. Apart from the description of an AB-22PT apparatus and a generator of para-enriched hydrogen, some methodological aspects of measurements – rate coefficient calculation procedure and the evaluation of number densities of gases in the trap volume – are presented here. The general theoretical principles of radiofrequency (RF) ion trapping are also briefly described in the section.

4.1 Trapping of ions in a radiofrequency trap

Trapping of ions is a fundamental element of the present work and its conception will be discussed in the text. Ion trapping technique is one of the basic instruments for investigation of gas-phase ion-molecule reactions. Such instrument allows to confine an ensemble of ions in all three dimensions using a combination of static, alternate electric, and sometimes magnetic fields.

There are several types of ion traps that have been developed up to the moment, but only multipole trap principles will be discussed further since this type of ion trap is a cornerstone of the instrument used in this work. For better understanding of the principles of ion trapping we have to investigate the motion of a charged particle in an inhomogeneous RF field. Here only the basics are discussed, the detailed description can be found in [*Gerlich, 1992*].

The classical equation of motion of a particle with mass m and charge q in an external electromagnetic field $\mathbf{E}(\mathbf{r},t)$, $\mathbf{B}(\mathbf{r},t)$ in nonrelativistic case is as follows:

$$m\ddot{\mathbf{r}} = q\mathbf{E}(\mathbf{r}, t) + q\dot{\mathbf{r}} \times \mathbf{B}(\mathbf{r}, t). \quad (4.1)$$

Here and further in the text bold font designates vector parameters. In our case magnetic component is not used in the instrument and we assume that quasistationary electric field $\mathbf{E}(\mathbf{r},t)$ is composed of static $\mathbf{E_s}(\mathbf{r})$ and time-variable $\mathbf{E_0}(\mathbf{r})\cos(\Omega t + \delta)$ components,

$$\mathbf{E}(\mathbf{r}, t) = \mathbf{E_s}(\mathbf{r}) + \mathbf{E_0}(\mathbf{r})\cos(\Omega t + \delta), \quad (4.2)$$

where $\mathbf{E_0}(\mathbf{r})$ is field amplitude, $\Omega = 2\pi f$ is angular frequency, and δ is phase shift. In this case the motion of a charged particle in the electric field is described by the differential equation

$$m\ddot{\mathbf{r}} = q\mathbf{E_s}(\mathbf{r}) + q\mathbf{E_0}(\mathbf{r})\cos(\Omega t + \delta). \quad (4.3)$$

We can eliminate the phase shift δ and set the static component to zero $\mathbf{E_s}(\mathbf{r}) = 0$ to make the survey easier. In case of homogeneous electric field $\mathbf{E_0}$ is independent on $\mathbf{r}$, the equation (4.3) is solved directly and in the end the trajectory amplitude $\mathbf{a}$ equals

$$\mathbf{a} = \frac{q\mathbf{E_0}}{m\Omega^2}. \quad (4.4)$$

In case of a weakly inhomogeneous field, the resulting trajectory deviates only slightly from the homogeneous one, so, we accept the expression (4.4) to remain the same. However, for stable motion of a particle the amplitude should not be very large and it has to satisfy some stability conditions. Hence, the angular frequency Ω of the field must be relatively high. This condition together with relations (4.2) and (4.3) will help to approximately describe the motion of a charged particle in the inhomogeneous field in the so-called *adiabatic approximation* [*Gerlich, 1992*].

The solution of the equation (4.3) in the inhomogeneous case is found with an assumption that RF field varies smoothly and slowly as a function of coordinate **r**. The motion vector **r** of a particle can be separated into smooth drift $\mathbf{R_0}(t)$ and rapidly oscillating $\mathbf{R_1}(t) = -\mathbf{a}(t)\cos\Omega t$ components. After expansion $\mathbf{E_0}(\mathbf{r}) = \mathbf{E_0}(\mathbf{R_0} - \mathbf{a}\cos\Omega t)$ into Taylor series and further mathematical operations, which we omit here, we get a differential equation for the drifting motion of a particle

$$m\ddot{\mathbf{R}}_\mathbf{0} = -\frac{q^2\,\nabla \mathrm{E}_0^2}{4m\Omega^2} \tag{4.5}$$

that shows the time-averaged effect of the oscillatory electric field. This effect is called *field gradient force* and is caused by the inhomogeneity of the field. Its direction and strength are determined by the gradient of squared E_0. Taking into account the electrostatic field $\mathbf{E_s}$ that can be described with its potential φ_s, as

$$\mathbf{E_s} = -\nabla\varphi_s\,. \tag{4.6}$$

The total average force acting on a particle can be expressed as gradient of

$$V^*(\mathbf{R_0}) = -\frac{q^2\mathrm{E}_0^2}{4m\Omega^2} + q\varphi_s\,, \tag{4.7}$$

where V^* is called *effective potential* [*Gerlich, 1992*]. With such parameter, the equation, describing the smooth trajectory of a particle, is simplified to the form

$$m\ddot{\mathbf{R}}_\mathbf{0} = -\nabla V^*(\mathbf{R_0}). \tag{4.8}$$

The range of validity of the adiabatic approximation is defined by the statement that the change of the field must be much smaller than the field

itself over the full distance of the oscillation 2**a**. Consequently, we can define a characteristic parameter η that establishes the relation between these two values:

$$\eta = \frac{|2\mathbf{a}\nabla\mathbf{E_0}|}{|\mathbf{E_0}|}. \tag{4.9}$$

This parameter is called *adiabadicity parameter* and it should be much smaller than 1. Inserting here parameter **a** from the equation (4.4), we obtain its final form:

$$\eta = \frac{2q|\nabla\mathbf{E_0}|}{m\Omega^2}. \tag{4.10}$$

According to empirical results and some numerical calculations, the maximum tolerable limit of the adiabadicity parameter was reported to be η_{max} = 0.3 [*Gerlich, 1992*]. This limit is also in agreement with the restriction η < 0.4 accepted for describing quadrupole fields using effective potential.

Concerning the construction, a linear multipole represents a set of 2n parallel rods mounted on a circle with radius r_0. Consequently, the effective potential of the trap is axially symmetric if no voltage difference is applied to the rods. Static potentials confine particles along the axis of the multipole. The potential inside the trap can be described by RF amplitude V_0, signal angular frequency Ω, and direct current (DC) voltage difference U_0 applied to the pairs of rods:

$$\varphi = U_0 - V_0 \cos \Omega t. \tag{4.11}$$

The approximation of the effective potential of a linear multipole with 2n rods at the radius r inside the trap is defined as follows [*Gerlich, 1992*]:

$$V^* = \frac{n^2 q^2 V_0^2}{4m\Omega^2 r_0^2}\left(\frac{r}{r_0}\right)^{2n-2} + qU_0\left(\frac{r}{r_0}\right)^n \cos n\theta, \tag{4.12}$$

where θ is cylindrical coordinate. This is valid for multipoles with the same shape of rods.

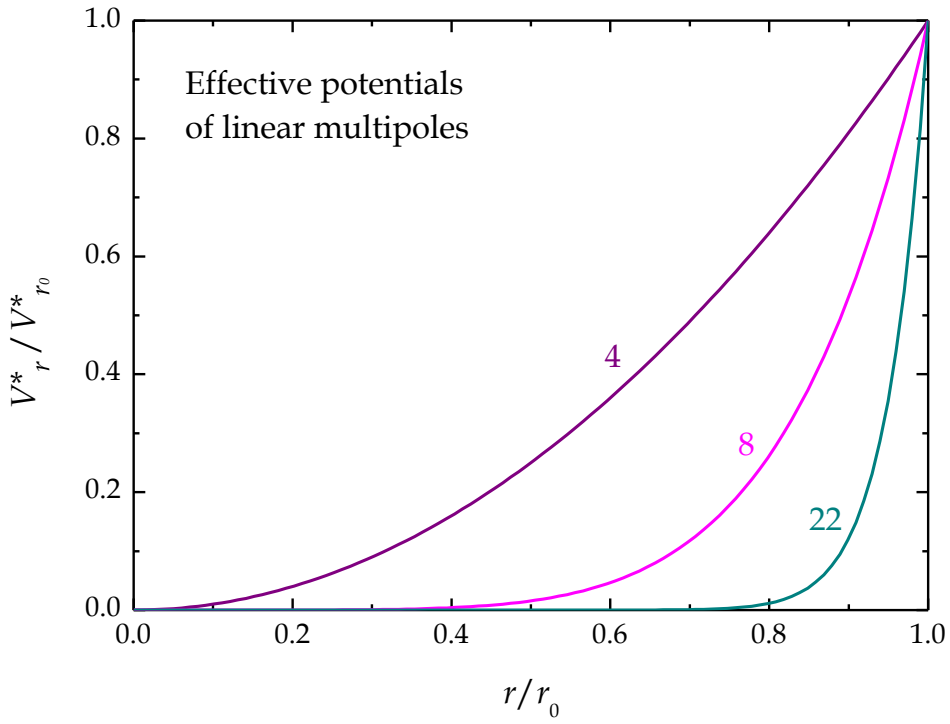

Figure 4.1. Diagram of effective potentials of different types of multipoles as function of distance from the centre of a trap when the DC difference U_0 equals 0. Numbers in graph designate numbers of rods in a multipole: quadrupole, octopole, and 22-pole, respectively.

In figure 4.1 we can see a comparison of effective potentials inside the most used types of multipoles as function of distance from the centre of a trap with DC difference $U_0 = 0$. Lines for quadrupole, octopole, and 22-pole are calculated there. One can note that the penetration of the effective potential inside the same-type multipole depends only on the number of rods. That is why these types of multipoles are used for different purposes: quadrupoles are usually used for mass-filtering of ions, octopoles – for their guiding. In this work a 22-pole ion trap was used for confining ions, the details of its construction and operation are given in the next chapter 4.2.

4.2 The AB-22PT instrument

The AB-22PT instrument is a very versatile and sensitive tool to study ion-molecule reactions experimentally. It was designed and constructed by prof. Dieter Gerlich and co-workers [*Gerlich and Horning, 1992*], [*Gerlich, 1995*], [*Asvany, 2003*], [*Borodi, 2008*] and it was operated by his group in Chemnitz University of Technology until the transfer to Prague in 2009. Each consisting part of the apparatus is described here as well as the principles of ion production, guiding, and detection. Constructive features of a unique source of atomic H and determination of the basic parameters of the H beam are also presented in the chapter. Lastly, a brief overview of principles of ortho-para conversion in a separate generator of para-enriched hydrogen is given as well.

4.2.1 Construction of the apparatus

The AB-22PT apparatus represents a set of separate components for producing, filtering, guiding, trapping, and counting of ions that are mounted in series in the vacuum chambers. An H-atom source (HAS) is used to produce and align an effusive beam of H atoms, which then interact with ions in the trap. The apparatus has also a cryogenic system that allows to carry out experiments at interstellar-relevant temperatures, down to 10 K. The instrument can be operated in two modifications. Experiments with an H-atom beam require operation of all the parts of the apparatus, while reactions with molecular gases may be studied with its simplified variant.

A complete scheme of the AB-22PT instrument is shown in figure 4.2. Ions are produced in a separate storage ion source (SIS) either by an electron impact ionisation of a target gas or by electron attachment. The source serves also as an ion trap where ions are stored by RF field and cooled in collisions until they are extracted by an opening pulse. Then desired ions are selected by a quadrupole mass filter, guided, and injected via the electrostatic

quadrupole bender into the 22-pole trap, which is the central part of the apparatus. Neutral particles can be transported into the trap either directly from the bottles with gases or in an effusive beam in case of experiment with hydrogen atoms. After defined time of the reaction, the trap opens and ions are extracted, mass-analysed by a quadrupole mass-spectrometer, and detected by a microchannel plate (MCP) detector.

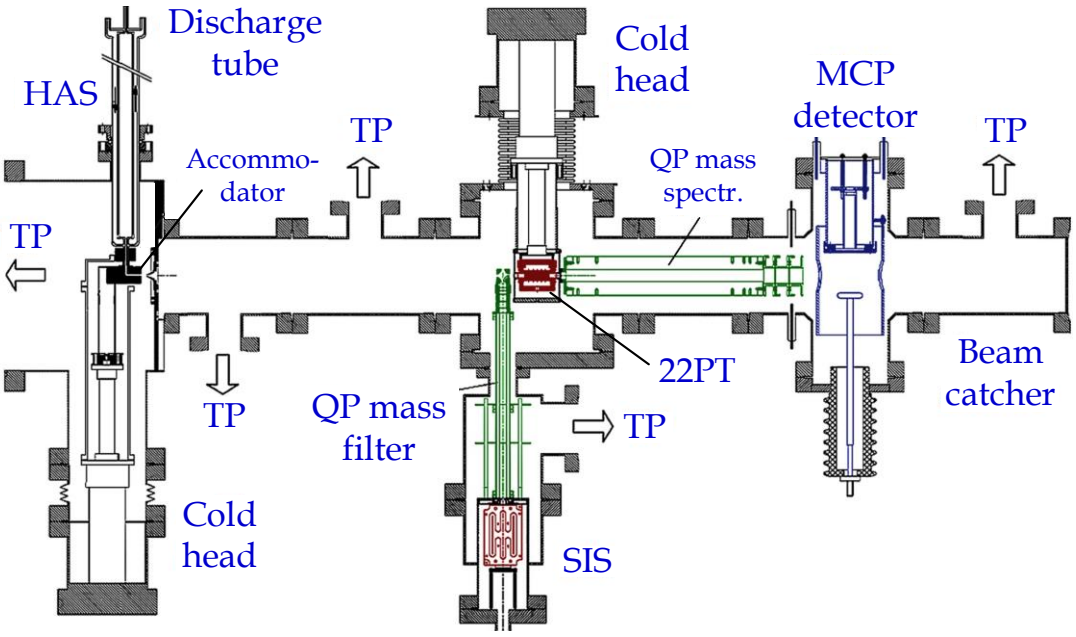

Figure 4.2. Complete scheme of the AB-22PT experimental setup. Ions are produced by an electron impact in a storage ion source (SIS), selected by a quadrupole (QP) mass filter, and injected to the 22-pole trap (22PT) via an electrostatic quadrupole deflector. The 22-pole trap is located in the central chamber and is mounted to a cold head. Extracted ions are mass-analysed by a quadrupole mass spectrometer and detected using an MCP detector. H-atom beam is produced in the separate H-atom source (HAS) where it is also cooled down by a cold head. Vacuum is formed by turbomolecular pumps (TP).

H atoms are produced by RF discharge in a glass tube. Cooling of atoms takes place in a special metal tube connected to the cold head that we call accommodator. Lastly, a nozzle forms a beam that is coaxial with the ion trap. Two differential pumping chambers are mounted between the H-atom

source and the trap chamber to minimise the penetration of the background molecular hydrogen from the HAS into the reaction volume.

The beam catcher chamber serves to prevent the reflection of the beam from the wall back to the trap. As well as that, it is used as an indicator of the proper direction of the beam. Cutting the beam off by a shutter causes a visible change of pressure in the beam catcher chamber, usually up to $4 \cdot 10^{-8}$ Pa.

Keeping the ultra-high vacuum (UHV) inside the instrument is essential for conducting precise experiments, so it is formed by a three-stage pumping system with 14 pumps of different types. The details of the vacuum system are given in subchapter 4.2.6.

H-atom source, differential pumping, and beam catcher chambers serve only for formation and detection of the beam, hence, the complete installation of the AB-22PT apparatus is used only while studying reactions with atomic hydrogen. The simplified configuration presented in figure 4.3 was used for experiments with noble or molecular gases.

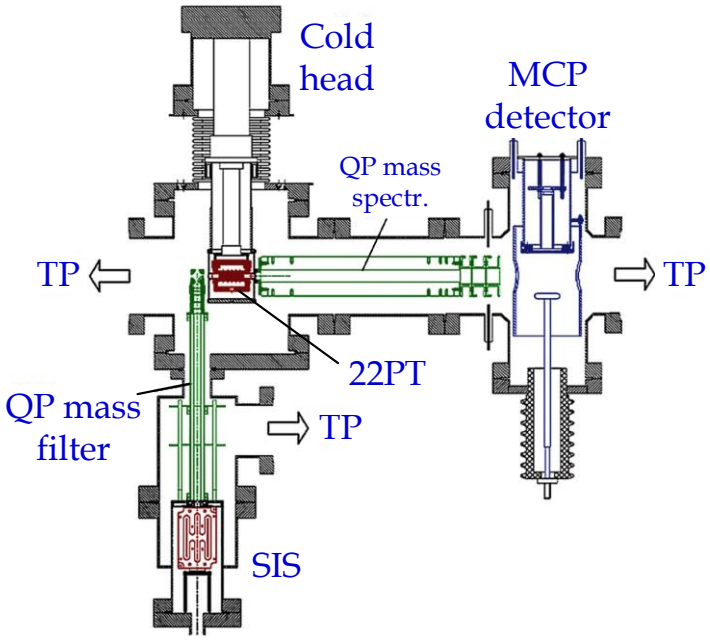

Figure 4.3. Scheme of the experimental setup used in experiments with molecular hydrogen. For simpler operation conditions and more effective pumping, the H-atom source, differential pumping, and beam catcher chambers were disengaged [*Zymak et al., 2011*].

Guiding, trapping, and detection of ions are synchronised by a delay pulse generator, which sends opening pulses to the necessary electrodes one after another from the ion source to the trap. Tuning and operation of the instrument is realised either from the control panel or from a computer with a set of special LabVIEW® programmes. For this purpose a Novation® Nocturn plug-in controller and a Meilhaus Electronic® RedLab 3105 USB-based digital-analogue converter (DAC) were used. Potentiometers of the plug-in controller set the necessary voltage values for the electrodes and send the proper signal to computer via USB interface, while DAC converts the USB signal from the computer into analogue voltage on the electrodes. Writing such programmes for operating and communication between the computer, plug-in controller, and analogue output was also a significant part of the experimental work during my PhD study. The details of the operating and remote control system are shown in appendix A.

4.2.2 Radiofrequency 22-pole ion trap

The central part of the AB-22PT instrument is a 22-pole RF ion trap firstly constructed in 1992 [*Gerlich and Horning, 1992*], its schematic diagram is shown in figure 4.4. The 22-pole is made from 22 stainless steel rods equally distributed on an inscribed radius $r_0 = 5$ mm. They create a 22-pole-shape effective potential that confines the ions in radial direction (figure 4.1). The diameter of each rod is $r_1 = 1$ mm. Axially the trap is closed by electrostatic fields of cylindrical entrance and exit electrodes. A set of five ring correction electrodes can be used to create a potential gradient in the axial direction for better extraction and to ensure that the ions are located in the centre of the trap.

The device is thermally connected to the cold head of a closed cycle helium refrigeration system, the nominal temperature of which can be varied between 10 K and 300 K. The temperature of the trap walls is measured by two silicon diodes. The pipes for the transportation of the neutral gas, one of

which is shown in figure 4.4, are in thermal contact with the cold head. The actual temperature of the ions was determined by a calibration reaction of He_2^+ formation [*Plašil et al., 2012*]. More information on the cooling system is given in subchapter 4.2.5.

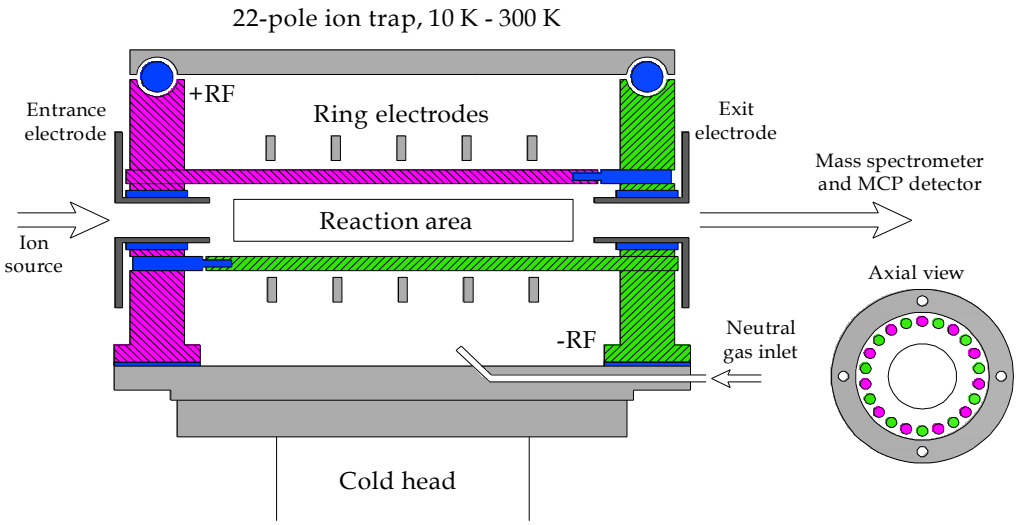

Figure 4.4. 22-pole ion trap, the central element of the instrument. Mass-selected ions are injected via the electrostatic entrance electrode. The confining RF voltage is applied to the two sets of rods in the opposite phases. After various storage times the exit electrode is opened by a suitable voltage pulse and ions escape towards the analysing system. The axial trapping potential created by the RF field can be corrected locally with five ring electrodes.

Extracted from the ion source and mass-selected, the beam of required ions is injected into the trap through an entrance electrode. The opening pulse is synchronised with the respective pulses in the ion source and guiding system. Reactant and buffer gases can be transported to the trap either continuously or injected through a pulsed valve. Such injection is used for better capture and cooling of ions and is synchronised with trap filling pulses. The length of the ion bunch can be adjusted in the ion source, it should be comparable with the axial length of the trap for more efficient

capture in order to prevent the escape of ions from the trap after reflecting from the closed exit electrode.

After the capture, ions are confined in the trap by its effective potential and form an ion cloud. The RF signal is applied to the two sets of 11 rods in the opposite phases. It allows to keep ions without any loss for a long time (up to tens of seconds). The confining static potentials at entrance and exit electrodes usually differ by ~0.5 V from the potential of the trap (the sign is different for positive and negative ions).

Various trapping time is set to check the change of ion composition in the trap, the exit electrode is opened by a suitable voltage pulse (usually several volts), and the ions travel to the analysing system. The taken data allow then to evaluate the reaction rate coefficients (chapter 4.4). Experimental study of ion-molecule reactions generally involves the repeating of this procedure under various conditions and further evaluation of the reaction rate coefficients and their dependencies on different parameters.

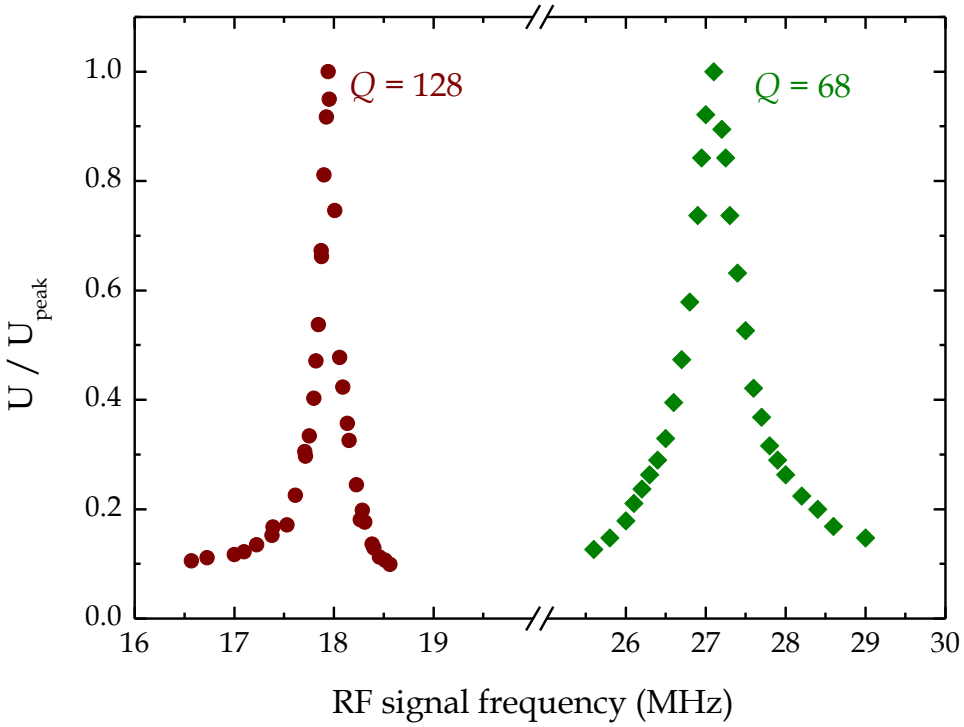

Figure 4.5. Resonator quality Q measurement of the trap-generator system.

The generator of RF voltage transmits the signal through a galvanically disconnected LC circuit. The RF frequency in this case should be set to a resonant value in order to decrease the energy dissipation. At first a circuit with $f = 17.9$ MHz resonant frequency was used, then a new circuit with frequency $f = 27.1$ MHz was mounted for better capture and confining of the lighter ions. The measurements of the resonator qualities in both cases are shown in figure 4.5.

An RM Italy® KL35 linear amplifier was used to amplify twice the RF signal amplitude from the generator for more effective capture of heavy ions and in order to control the influence of parasitic RF heating of ions on the evaluation of the reaction rate coefficients.

4.2.3 Producing, guiding, and detection of ions

Ions are prepared in a separate RF storage ion source that is designed using the principle of combination of ion production and RF ion trapping. The advantages of such sources are accumulation of ions with high collection efficiency without the use of energy-perturbing extraction fields, thermalisation by inelastic collisions, and possibility of additional chemical ionisation by secondary reactions.

A schematic view of the storage ion source from two sides is presented in figure 4.6. One or more neutral gases are added into the ion source chamber from the inlet system. Positive and negative ions are produced by an electron impact ionisation or electron attachment, respectively, and then stored in a cavity inside the RF plates (lower part of figure 4.6). Electrons are emitted from a cathode (filament), accelerated by a negative repeller potential, and accommodated by a focus electrode potential. The cathode is incandesced by an applied direct current of 3.5 A – 4.7 A. Electron emission current is measured by a picoammeter Keithley® 6485 and usually is in order of 0.1 mA. Produced ions usually have high internal excitation, but they are thermalised by inelastic collisions with the neutral gas before the extraction.

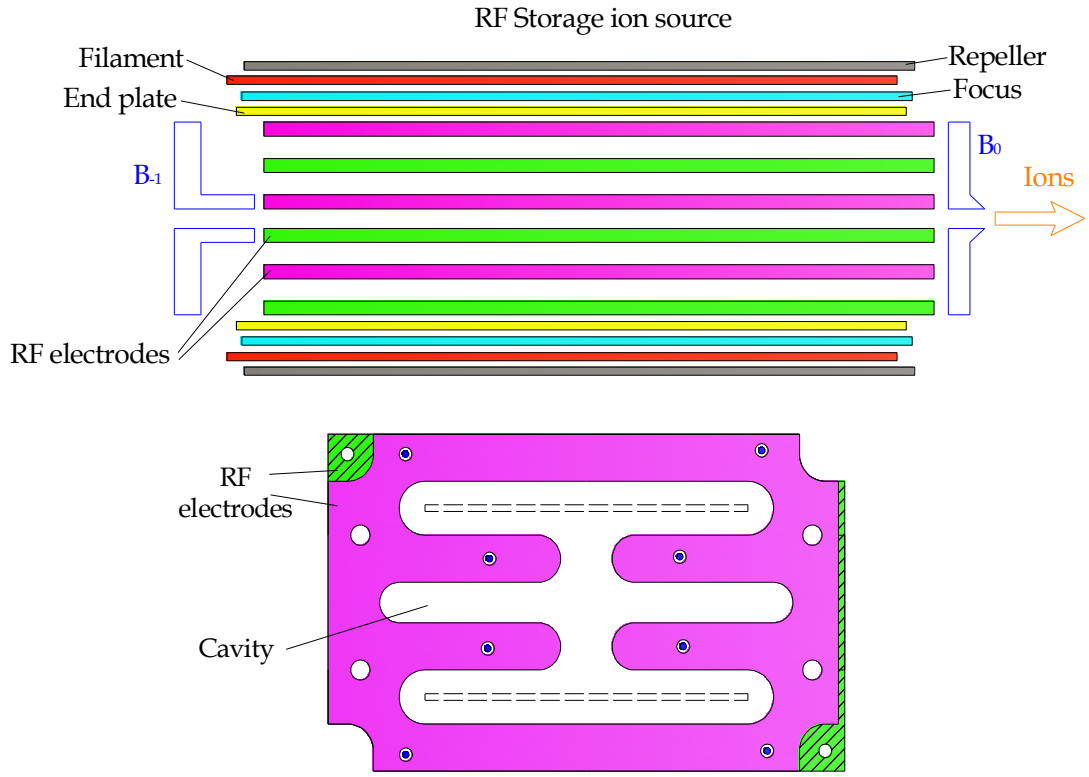

Figure 4.6. Schematic view of the radiofrequency storage ion source. Emitted, accelerated, and focused electrons penetrate into the RF trap and ionise the gas. Ions are confined inside a special cavity in planar electrodes by RF field. RF electrodes with the opposite signal phases are marked by green and pink colours. *Upper panel*: Arrangement of the electrodes of the storage ion source. The DC potentials of the B_0 and B_{-1} electrodes serve to confine the ions along the horizontal axis of the SIS. End plate electrodes confine ions in vertical direction. *Lower panel*: View from the top on the cavity in RF electrodes. Dashed rectangles show the locations of the apertures for the electrons in focus and end plate electrodes. Sapphire balls serve for electrical isolation of the plane electrodes.

There is a possibility to use RF signals with different resonant frequencies for confining different ions, so 19 MHz field was used to confine lighter ions (up to ion mass of 4 a. m. u.), whereas heavier ions were kept by the field with 3.3 MHz frequency.

The extraction takes place when an opening pulse of several volts comes to the B_0 electrode (upper part of figure 4.6). The length of the pulse is adjusted in the way to obtain a beam of ions dimensionally comparable to the length of the 22-pole ion trap (see subchapter 4.2.2) and usually lasts for ~10 μs. B_{-1} electrode serves as a potential barrier for confining of ions along the axis of the SIS and end plate electrodes are used for confining of ions in the direction perpendicular to the planar electrodes. All the electrodes are electrically separated by sapphire balls.

The ion source is equipped with two identical sets of ion production system (cathodes and focusing electrodes). The location of the apertures for the electrons is denoted as dashed rectangles in the lower part of figure 4.6. The specific ways of obtaining of ions in each experiment are described in the respective experimental chapters 5.1 and 5.2.

After the extraction, ions are selected in a quadrupole mass-filter that follows the ion source. The necessity of this is conditioned by the fact that several types of ions can be produced from a molecular gas via impact ionisation or electron attachment. Moreover, fast ion-molecule reactions in the SIS may serve as an additional source of other ions. The detailed information on the quadrupole mass-filters can be found elsewhere [*Gerlich, 1992*], here we stop on the basic priciples of its operation.

As it has already been mentioned, the motion of a charged particle in the field of a multipole is decribed by the formula (4.3). The electric fields are created by DC potential U_0 and AC voltage $V_0 \cos\Omega t$ applied to the rods of the quadrupole. The region of stable trajectories in the quadrupole field is completely characterised by the well-known Mathieu stability diagram (figure 4.7) with parameters a_2, q_2 defined as:

$$q_2 = \frac{4qV_0}{m\Omega^2 r_4^2}, \tag{4.13}$$

$$a_2 = \frac{8qU_0}{m\Omega^2 r_4^2}, \tag{4.14}$$

where m is ion mass, r_4 is inscribed radius of a quadrupole.

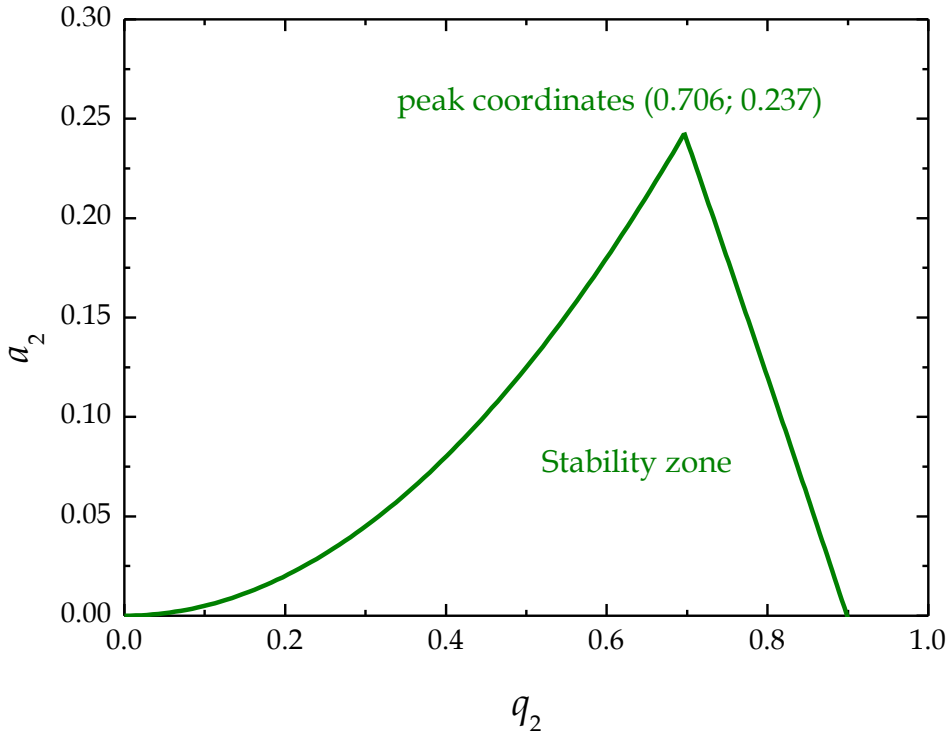

Figure 4.7. Lowest stability zone of the Mathieu (a_2, q_2) diagram. The region near the peak is used for high-resolution mass-filter operation [*Gerlich, 1992*].

A generator with $f = 6.7$ MHz frequency was used as a source of RF signal. In some cases the mass filtration is needed to cut off not only other types of ions, but also the neighbour isotopes of the required ion, as in case with N^+, O^-.

From the equations (4.13), (4.14) the values U_0, V_0 are calculated to obtain the stable trajectory for a particular ion. An example of U_0-V_0 diargam for several masses used in the experiments is presented in figure 4.8.

After the quadrupole mass filter, the ion beam is guided into the trap through an ion optic system shown in figure 4.9. B_1 is a pair of pulsed electrodes that serves as an additional potential barrier on the way of ions and prevents continuous filling of the 22PT. An opening pulse on B_1 electrodes is synchronised with the respective extraction pulse on B_0 electrode. B_2/B_3 is a pair of electrodes with a static voltage used for better focusing of the ion beam.

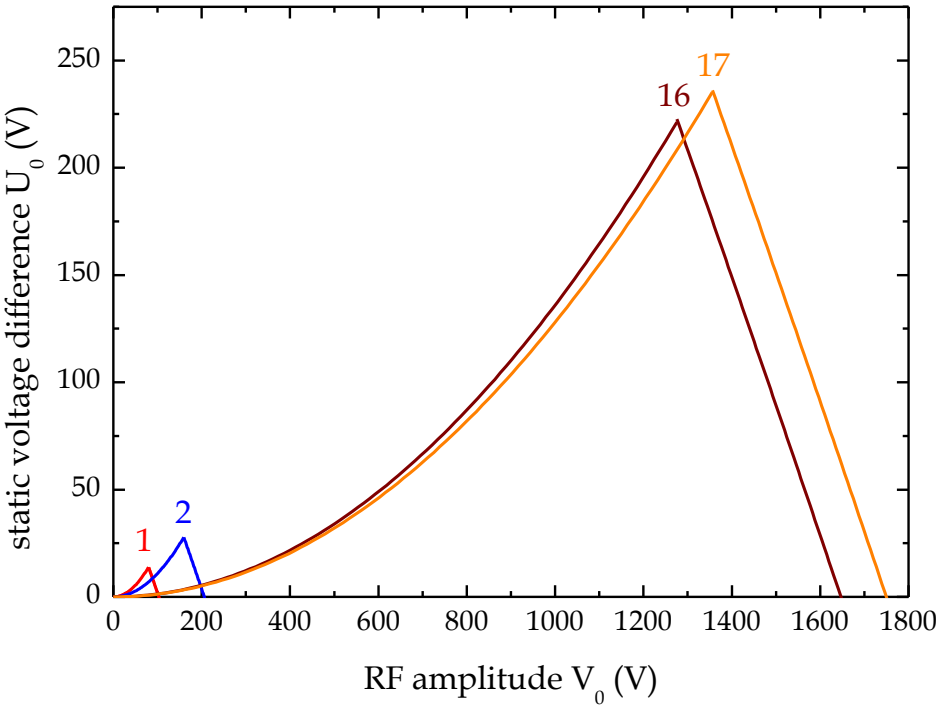

Figure 4.8. Stability regions for several ion trajectories in the quadrupole. Masses are marked in atomic mass units and refer to H^+, H^- (1 a. m. u.); H_2^+ and D^- (2 a. m. u.); O^- (16 a. m. u); OH^- (17 a. m. u.). The RF signal frequency f = 6.67 MHz and the inscribed radius of the quadrupole r_4 = 5 mm were used for the calculations.

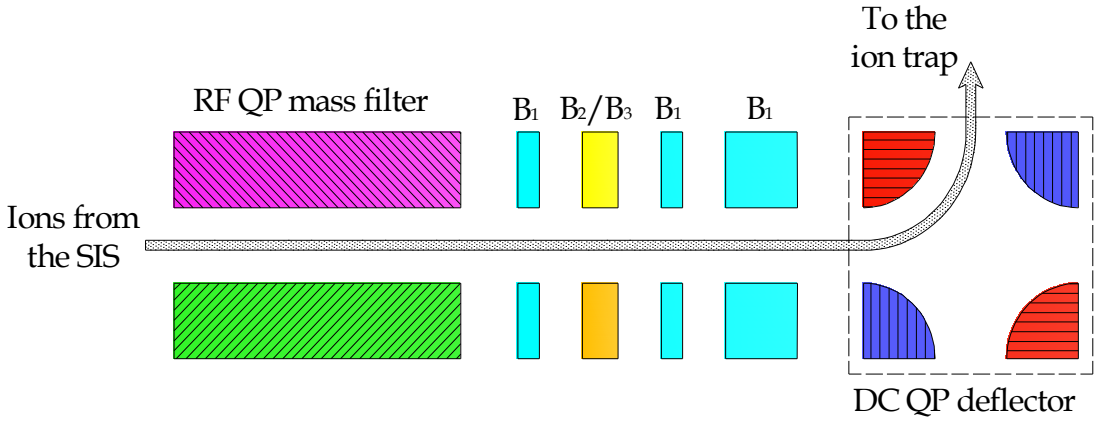

Figure 4.9. Schematic top view of the ion guiding system of the AB-22PT apparatus. A pair of pulsed electrodes B_1 prevents the continuous filling of the ion trap, a pair of electrodes B_2/B_3 serves for better focusing of the ion beam. A quadrupole DC deflector aligns the beam with the axis of the 22PT. Dashed square denotes two horizontal mutually parallel plates that focus the ion beam in the vertical direction.

The initial direction of the ion beam is perpendicular to the axis of the ion trap, so a quadrupole DC deflector is used to make a 90° bend of the beam trajectory. Two horizontal parallel rectangle plates focus the ion beam in the vertical direction (dashed square in figure 4.9).

Concerning the detecting system of the AB-22PT apparatus, it is used to analyse the composition of the ion ensemble after the reaction. Numbers of reactant and product ions represent essential information for further evaluation of the reaction rate coefficients. The analysing system consists of a quadrupole mass-spectrometer, a detector, and a counter of ions.

The quadrupole mass-spectrometer is used in combination with two electrodes that focus the ions flying from the trap. Balzers® QMH 400-5 RF generator is used to induce the signal on the quadrupole rods.

After the quadrupole, the ions are focused by three electrodes to the Hamamatsu® F-4655-12 microchannel plate detector. The detector detects only charged particles, when every single event is converted into a digital pulse that then comes to a 100 MHz ion counter. The ions are attracted to the detector by an applied high-voltage potential. A discriminator is used to distinguish the digital peaks caused by ions from minor oscillations. In order to achieve higher signal-to-noise ratio the counter is gated by a pulse synchronised with the extraction of ions from the trap. A slow-ramp filter is used for obtaining a smooth extracting pulse on the exit electrode of the 22PT. It allows elongating the ion cloud and prevents the counter from the saturation.

During the experiments one may face the problem of lower sensitivity (approximately by 30%) of the analysing system to H^+ ion comparing to ions with higher masses, or so-called discrimination of ions. This fact should be taken into account while working with H^+. The discrimination factor was calculated from the observation of the overall sum of ions. It was always controlled and the respective reaction rate coefficient was corrected during its evaluation.

4.2.4 Production of H atoms and formation of an effusive H-beam

H atoms are produced, cooled, and formed into an effusive beam in the separate H-atom source. The principle and schematic construction of the H-atom source are presented in figure 4.10. Molecular hydrogen flows from the bottle through a leak valve into a glass discharge tube. H_2 dissociates in a discharge, which is switched on by an RF field with 27.1 MHz frequency and 20 W power. Then the mixture of dissociated H and H_2 flows through an accommodator and is cooled by a cold head. The pipe in the accommodator is covered with a polytetrafluoroethylene (Teflon®) film to minimise the association of H back to H_2 on its surface. Then a cold effusive beam is formed by a skimmer. The axiality of the beam is set by moving the accommodator and adjusting the beam direction.

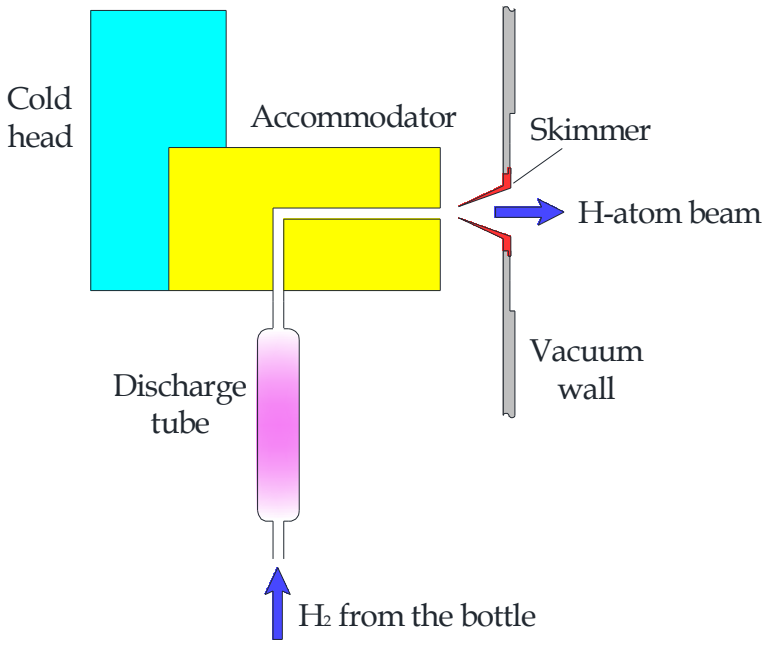

Figure 4.10. Schematic drawing of the H-atom source. Molecular hydrogen flows from the bottle through a leak valve into a glass discharge tube where H_2 partially dissociates into H. Then the mixture of H and H_2 flows through a cold accommodator. The pipe in the accommodator is covered with a polytetrafluoroethylene film to minimise the association of H back into H_2. A cold effusive beam is then formed by a skimmer.

For the calibration of the number density of the H-atom beam, a reaction of CO_2^+ ion with the beam was used. An advantage of CO_2^+ is that it gives different products in reactions with H and H_2:

$$CO_2^+ + H \rightarrow HCO^+ + O, \tag{4.15}$$

$$CO_2^+ + H_2 \rightarrow HCO_2^+ + H. \tag{4.16}$$

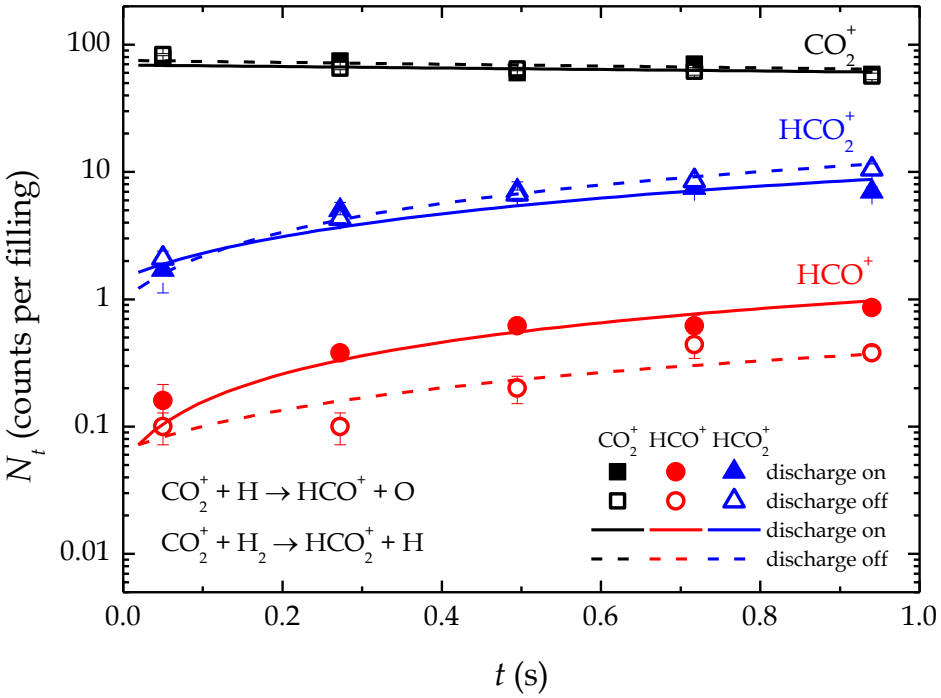

Figure 4.11. Time evolution of detected numbers of CO_2^+ (squares), HCO^+ (circles), and HCO_2^+ (triangles) ions in the trap in reaction of CO_2^+ with H and H_2. Solid and dashed lines represent fits of numbers of ions with the discharge switched on and off, respectively. The temperatures of the trap and accommodator were 40 K and 50 K, respectively.

Figure 4.11 shows the evolution of numbers of CO_2^+, HCO^+, and HCO_2^+ ions in time in the trap. After injecting into the trap, CO_2^+ ions begin to react with H atoms and H_2 molecules in the beam as well as with H_2, penetrating into the trap from the H-atom source. In these reactions HCO^+ and HCO_2^+ ions are produced, consequently, from the ratio between the product ions it

is possible to calculate the ratio between the number densities [H]/[H_2] in the trap.

The effective number density of the H-atom beam was derived from the fitting of the difference between the numbers of HCO^+ ions counted with the discharge switched on and off. Thus, the calibration showed the H-atom number density in the beam [H] = $1.5 \cdot 10^7$ cm^{-3}. Comparing to the experiment with H^- [*Gerlich et al., 2012*] it was lower due to the installed additional differential pumping chamber.

The cold head can cool the H atoms from 300 K down to 7 K. We observed a considerable decrease of the H-atom number density while operating the H-atom source in the range of temperatures 8 K – 50 K with a minimum at 20 K. Due to this fact in experiment with D^- ions, the mentioned range was not used. The H-atom source was operated at the lowest temperature of 7 K and at temperatures above 50 K. The possible reason is that cold H atoms have higher probability of the association to H_2. At the same time, at the lowest operating temperature of nearly 7 K, H_2 creates a frozen film on the accommodator surface that prevents H from association back to H_2 quite well [*Gerlich et al., 2012*].

4.2.5 Cooling of ions, molecules, and H atoms

Cooling system of the AB-22PT instrument serves for obtaining the interstellar-relevant temperatures for the studied ion-molecule reactions. There are two separate systems for cooling of ions in the trap and H atoms in the accommodator. As it was metioned before the accelerating potentials in the guiding system are in the range of volts, consequently, ions have to be cooled in the trap to the values of several meV. This cooling takes place in elastic collisions of kinetically hot ions with cold buffer gas (usually helium), which is specially added into the trap. The approximate frequency of the collisions is proportinal to the buffer gas number density, average ion velocity, and collisional cross-section:

$$f_c = n\langle v_i \sigma_0 \rangle = nk^{\mathrm{L}}, \tag{4.17}$$

where k^{L} is Langevin rate coefficient given by formula (3.10). The brackets designate here velocity averaging. According to the previously evaluated k^{L} and typical values of buffer gas number densities used in the experiments f_c were ~10^5 s^{-1} in order of magnitude. Ions are typically thermalised in at least 100 collisions, so cooling usually took several milliseconds. The process of cooling of ions can be seen when trapping times are comparable to the time of cooling (example in figure 5.1).

Nevertheless, due to the parasitic RF heating the temperature of the ions near the rods may differ from the buffer gas temperature. Ions are accelerated and deccelerated during each period of the RF oscillation and because of the collisions with the gas the average acceleration may be different from zero. Due to this reason the measurements are repeated with different RF signal amplitudes in order to exclude the factor of parasitic effects. A geometric distortion of the trap may also cause more intensive RF heating [*Asvany and Schlemmer, 2009*].

The cooling of the trap is realised by a two-stage closed-cycle helium refrigerator system, consisting of a Leybold® RGD 210 cold head and a compressor RW 2/3. The first stage of the cold head is cooled down to 50 K and serves as a shield from the RF heating and infrared radiation. The trap is mounted on the second stage of the cold head, its lowest achievable temperature is 10 K. Pipes for the neutral gases contact the second stage of the cold head to precool the gases and get rid of impurities.

The temperature of the trap (T_{22PT}) is set by heating up a resistive wire mounted on the cold head. The wire is heated by applying a DC voltage from a TTi® PL303 power supply. The system is secured to prevent the overheating of the trap when the cold head is switched off, that is why an automatic remote operation is realised using LabVIEW® programming environment.

In figure 4.12 one can see the dependence of the temperature of the trap on the applied heating power. The maximum power that can be applied is 15 W.

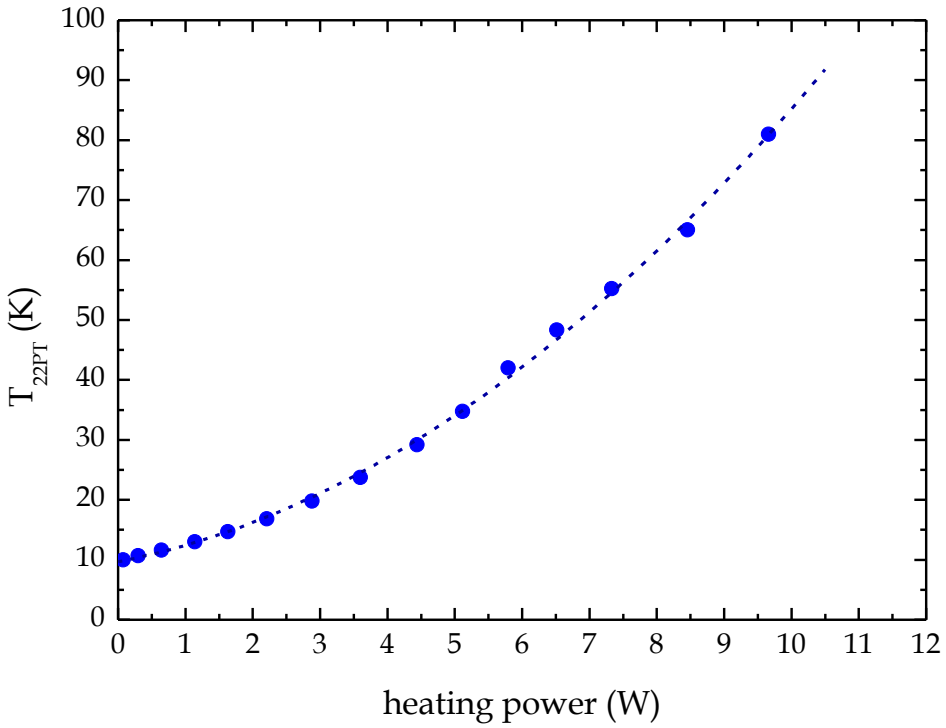

Figure 4.12. Dependence of the trap temperature on the applied heating power. The heating power is limited by 15 W. Dashed line is a polynomial fit for the measured points.

The temperature of the walls of the ion trap is measured by two silicon diodes Lakeshore® DT-471-C4 mounted directly on the copper wall of the trap. The data from the diodes are read and visualised by the Lakeshore® temperature monitor (model 218), the difference between the shown temperatures is within 0.3 K.

In order to test the actual temperature of ions in the trap, the ternary association reaction

$$He^+ + 2\,He \rightarrow He_2^+ + He \qquad (4.18)$$

was used. Although the obtained data shown in figure 4.13 are somehow larger than the previous ion-trapping results [*Gerlich and Horning, 1992*], within an error bar there is a good overall agreement with them and with the analytical function extrapolating the selected ion drift tube data reported in [*Böhringer et al., 1983*]. Hence, we can conclude that the temperature of the trap walls reflects actual temperature of the trapped ions.

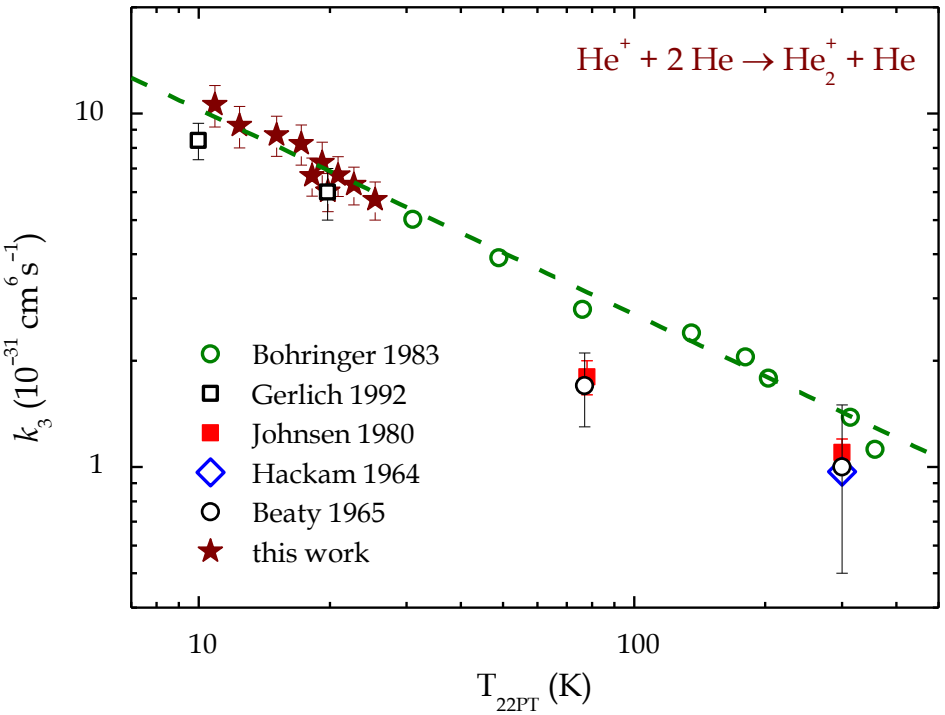

Figure 4.13. Dependence of the rate coefficient of He_2^+ formation on trap temperature. Stars show the measured k_3(T) used as a trap thermometer [*Plašil et al., 2012*], as proposed in [*Gerlich, 2008*]. The circles indicate previous results obtained using a selected ion drift tube [*Böhringer et al., 1983*] and open squares show a ring-electrode trap experiment [*Gerlich and Horning, 1992*]. Older data measured at higher temperatures are also shown in the graph [*Hackam and Lennon, 1964*], [*Beaty and Patterson, 1965*], [*Johnsen et al., 1980*]. The dashed line is an extrapolation of Böhringer's fit.

4.2.6 Vacuum and gas inlet systems of the instrument

Maintaining the ultra-high vacuum is essential requirement for conducting astrophysically-relevant experiments. The range of number densities of neutral gases used in experiments is of 10^{11} cm^{-3} – 10^{14} cm^{-3} that approximately corresponds to the pressures in a range of 10^{-6} Pa – 10^{-3} Pa at 11 K. The achievable background pressure in the chambers is ~10^{-8} Pa. Consequently, the fraction of probable impurities in the gas in the trap is less than 1%.

Measurement of the pressures of gases in the apparatus is essential due to two main reasons: we need to know the number densities of gases in the trap volume to calculate the reaction rate coefficients and we have to secure the turbopumps from the overpressure and control the technical parameters of the instrument.

For this purpose, almost every vacuum chamber of the instrument has at least one pressure gauge. Ionisation gauges (IG) AML® AIG NGS2 are mounted on the trap, beam catcher, differential pumping, and H-atom source chambers. They measure pressures below 10^{-2} Pa and provide the security for turbopumps. The IG are connected to the AML® NGC 2 electronic system. Forevacuum pressure is measured by Pfeiffer Vacuum® TPR 280 Pirani gauges. Another differential pumping chamber is equipped with Pfeiffer Vacuum® PKR 251 full range pirani gauge. For better visual control of the trap chamber a wide range Vacom® ATMS 0443-40 manometer is used. It contains both ionisation and pirani gauges and makes it possible to control the pressure when another IG are switched off.

There is a three-level pumping system, constantly maintaining ultra-high vacuum inside the apparatus. The system consists of a set of pumps and valves of different types. The H-atom source has its own pumping subsystem. The scheme of the vacuum system of the AB-22PT instrument is presented in figure 4.14, which refers to the complete installation shown in figure 4.2.

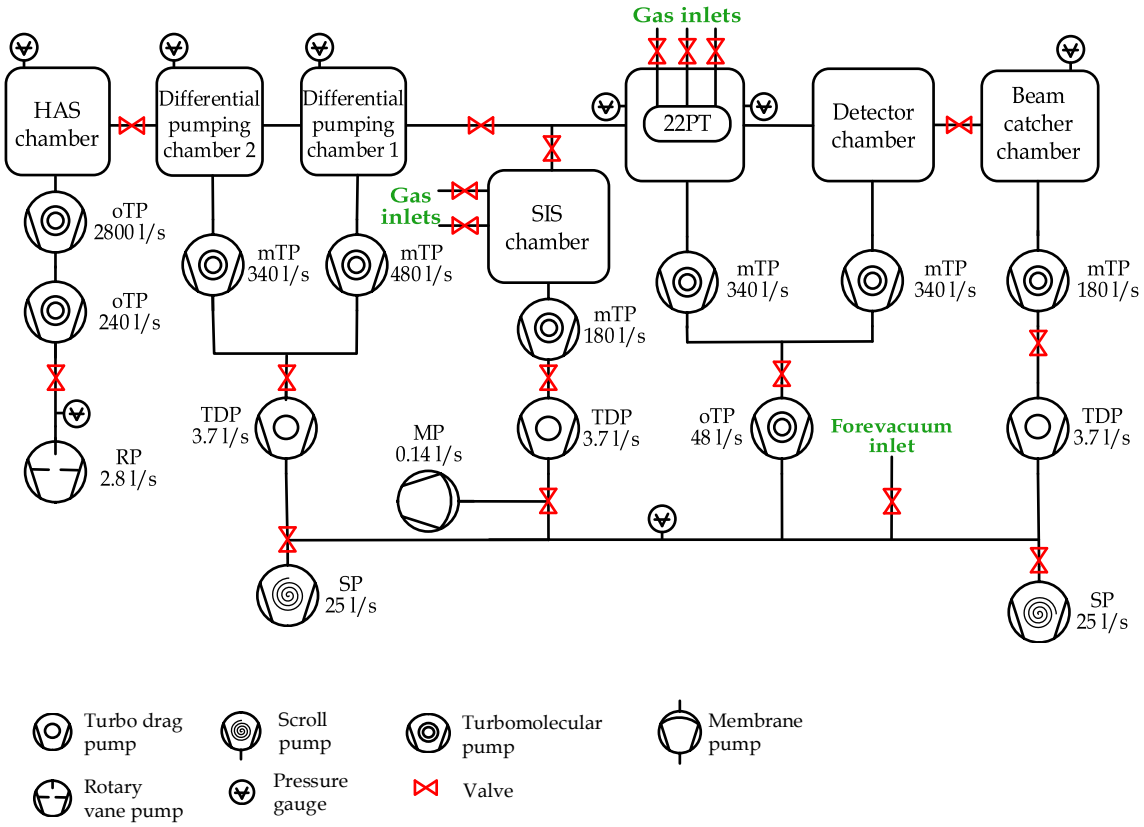

Figure 4.14. Scheme of the three-level pumping system of the AB-22PT apparatus. The chambers are pumped by turbomolecular pumps (mTP and oTP for magnetic-levitation and oil turbomolecular pumps, respectively). Forevacuum is made by scroll pumps (SP) and a rotary pump (RP). A separate forevacuum for ion source chamber can be also formed by a membrane pump (MP). The second-level turbomolecular and turbo drag pumps (TDP) serve to increase the pumping efficiency. The pumping efficiencies of each pump are shown for hydrogen in litres per second.

The apparatus is pumped by Pfeiffer Vacuum® magnetic-levitation turbomolecular pumps Turbovac 340M (22PT, detector, and differential pumping chambers), TMU 200M (beam catcher and ion source chambers), and TM 700 (another differential pumping chamber). Turbo drag pumps Pfeiffer Vacuum® HiPace 10 are used to increase the efficiency of turbomolecular pumps and are mounted in series with the last ones, except from the 22PT and detector chambers, where more efficient HiPace 80 is used. The forevacuum is formed separately for differential pumping

chambers and the other parts of the instrument by two scroll pumps Varian® SH 110. It is also possible to form a separate forevacuum for ion source by switching it to Pfeiffer Vacuum® MVP 015-4 membrane pump.

The H-atom source is pumped by two turbomolecular pumps Pfeiffer Vacuum® TPU 2200 and TPU 240, forevacuum for which is made by a Pfeiffer Balzers® Duo 008B rotary vane pump. The pumping speed values for hydrogen for each pump are written in figure 4.14 in litres per second. Such system allows to minimise the penetration of the unwanted gases into the reaction volume that, at the same time, guarantees higher precision and reliability of experiments.

Inlet system represents a set of reservoirs from which gases are transported to the trap or the ion source (figure 4.15). The bottles are filled up to the pressures of $1 \cdot 10^5$ Pa – $3 \cdot 10^5$ Pa from high-pressure bottles with gases of the required purity. The system is pumped by a Pfeiffer Vacuum® MVP 015-4 membrane pump. The gases from the high-pressure bottles come through a cryogenic filter with liquid nitrogen that freezes water and other unwanted impurities.

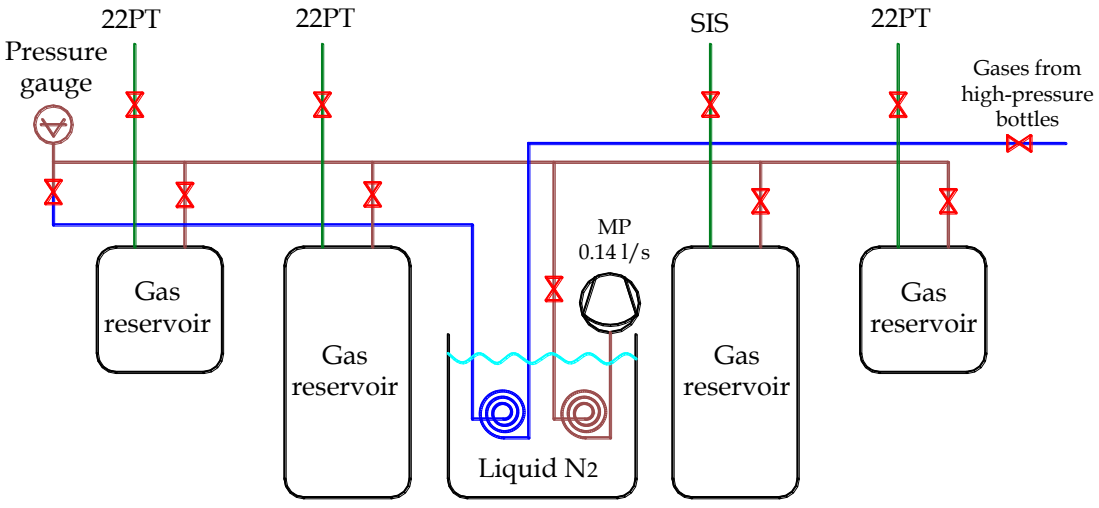

Figure 4.15. Schematic drawing of the inlet system of the AB-22PT apparatus. Gas reservoirs are filled with gases from high-pressure bottles up to the pressures of $1 \cdot 10^5$ Pa – $3 \cdot 10^5$ Pa. A cryogenic filter with liquid nitrogen is used to get rid of impurities (mainly water). The system is pumped by a membrane pump with 0.14 litres per second efficiency for hydrogen.

Flow of the gases from the containers is realised through UHV variable leak valves Balzers® UVD – 040, Varian® 91515106, and Leybold® 87395. They allow to set the required pressures in the trap and in the ion source with high sensitivity. The pressure in the system is controlled by a Swagelok® PTU series pressure transducer.

4.3 Measurement and calculation of number densities of gases in the trap volume

In case of ideal gas the number density n_{22} of a gas in the trap is calculated as follows:

$$n_{22} = \frac{p_{22}}{\mathrm{k_B} \cdot \mathrm{T_{22PT}}}, \tag{4.19}$$

where p_{22} is gas pressure inside the trap, k_B is Boltzman constant. Temperature of the gas is taken equal to the temperature of the walls of the trap, which is measured directly (discussed in subchapter 4.2.5). The pressure inside the trap can be measured with the calibrated spinning rotor gauge SRG-BF-CAL and VISCOVAC system MKS SRG 2 with 1% accuracy. It is not very practical to use in online mode, but it can be used for the calibration of the ionisation gauge.

Taking into account an assumption that in dynamic equilibrium the flow from the trap to the vacuum chamber is equal to the flow from the vacuum chamber to the turbopumps, after some mathematical transformations (you can find them in [*Zymak, 2013*]) we obtain the expression

$$n_{22} = \frac{C \cdot p_{\mathrm{IG}}}{\mathrm{k_B}\sqrt{\mathrm{T_{22PT}} \cdot \mathrm{T_{SRG}}}}, \tag{4.20}$$

where p_{IG} is pressure measured in the vacuum chamber by the IG, T_{SRG} is temperature of the head of the SRG (is taken equal to the temperature of environment, ~300 K), C is calibration factor between the pressures in the trap volume and the chamber.

This factor can be calculated from the measured dependence of the pressure in the trap measured directly by VISCOVAC on the pressure measured by the ionisation gauge in the 22PT vacuum chamber. In figure

4.16 we can see such dependence for helium that was introduced directly into the trap. SRG measures the pressure with an offset, so after its elimination we obtain a direct ratio between the respective pressures.

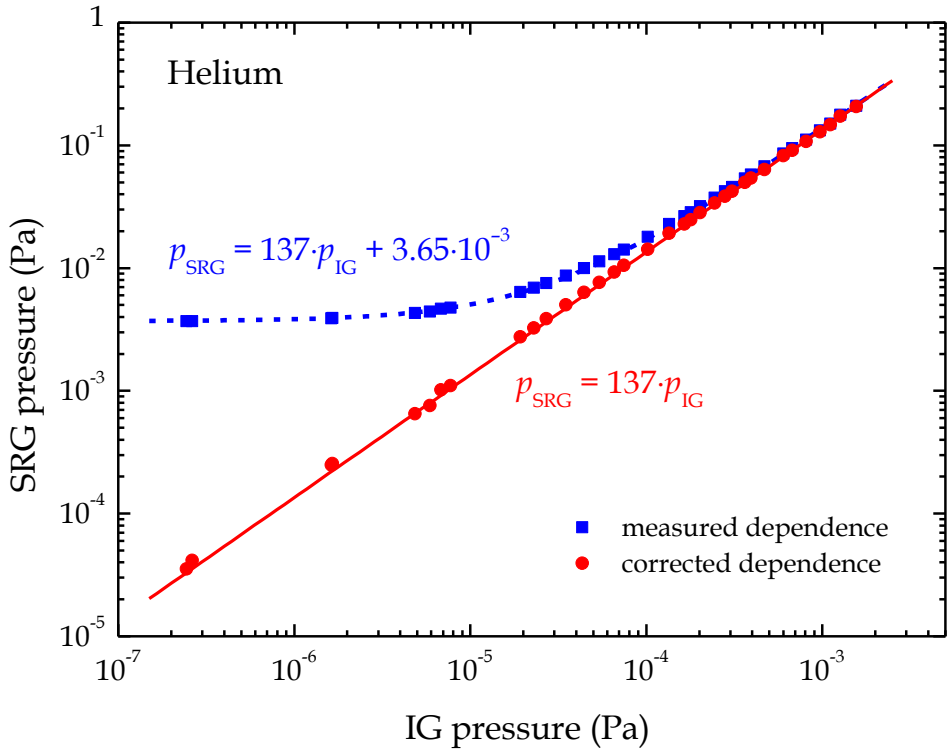

Figure 4.16. Measured dependence of the spinning rotor gauge pressure on ionisation gauge pressure for helium at 11 K. The gas was added directly into the trap. After the subtraction of the SRG offset pressure, the dependence actually reflects the ratio between pressures in the trap volume and 22PT vacuum chamber.

In cases of experiments with $H^+ + H_2(J)$, $OH^- + D_2 \rightarrow OD^- + HD$, and $OD^- + H_2 \rightarrow OH^- + HD$ reactions, it was important to know exactly how much H_2 or D_2 penetrated into the trap volume from the storage ion source, so the similar dependence could be measured also by changing the pressure in the SIS chamber. The measured calibration factors C for the gases used in this work are given in appendix B.

4.4 The rate coefficient measurement routine and methodology of its evaluation

Operation of ion trapping technique involves a standard procedure for the rate coefficient evaluation. It is based on iterative filling of the trap with a certain number of primary ions and analysis of the content after certain storage periods using the quadrupole mass spectrometer and MCP detector [*Gerlich and Horning, 1992*]. In the experiments the trapping time could reach 40 s.

From the chapter 3.2 and formulas (3.12), (3.15) we know that the reaction rate constant is a proportionality coefficient between the time decay of the reactant and the number densities of reactants. The solution of the respective balance equation gives

$$\frac{[\mathrm{A}^+]}{[\mathrm{A}_0^+]} = e^{-k[\mathrm{B}]t}. \tag{4.21}$$

In our case instead of number densities of A^+ ions in the trap $[A^+]$, we will use relative number of ions $N(A^+)$ detected by analysing system. During the experiment, the numbers of ions are counted and hence after taking the logarithm of the both parts of equation (4.21) the rate coefficient k is calculated.

The reaction rate coefficient can be calculated either from the decay of number of detected reactant ions or from the growth of number of product ions in a certain time using the expressions:

$$k = \frac{1}{[\mathrm{B}] \cdot t} \cdot ln \frac{N(\mathrm{A}^+)_0}{N(\mathrm{A}^+)_t} \tag{4.22}$$

for the calculation from the decay of relative number of reactant ions, and

$$k = \frac{1}{[\mathrm{B}] \cdot t} \cdot ln \frac{(N(\mathrm{A}^+) + N(\mathrm{C}^+))_t}{N(\mathrm{A}^+)_t} \tag{4.23}$$

for the calculation from the growth of relative number of product ions. Here [B] is number density of the reactant gas in the trap, t is trapping time, $N(\mathrm{A}^+)_0$ is number of detected primary ions at the beginning of the measurement, $N(\mathrm{A}^+)_t$ is number of detected primary ions after time t, $(N(\mathrm{A}^+) + N(\mathrm{C}^+))_t$ is the sum of numbers of detected primary and product ions after time t (that corresponds to the number $N(\mathrm{A}^+)_0$ at $t = 0$).

Calculation from the growth of the relative number of product ions is used to increase the precision of the measurement when $N(\mathrm{A}^+)_t >> N(\mathrm{C}^+)_t$. While measuring, some additional correcting parameters – such as mass discrimination or total loss of ions from the trap – can be also calculated.

The logics and procedure of the evaluation of the rate coefficient of third body-assisted reactions is the same as for binary reactions. Finally, we get the expressions

$$k_3 = \frac{1}{[\mathrm{B}][\mathrm{M}]t} \cdot ln \frac{N(\mathrm{A}^+)_0}{N(\mathrm{A}^+)_t} \tag{4.24}$$

for its calculation from the decay of the number of reactant ions, and

$$k_3 = \frac{1}{[\mathrm{B}][\mathrm{M}]t} \cdot ln \frac{(N(\mathrm{A}^+) + N(\mathrm{C}^+))_t}{N(\mathrm{A}^+)_t} \tag{4.25}$$

for its calculation from the growth of the number of product ions, where [M] is number density of the buffer gas in the trap.

The error in the reaction rate coefficient evaluation comprises statistical error and uncertainties of the reactant gas temperature and number density evaluation.

4.5 Generator of para-enriched hydrogen

In the study of $N^+(^3P_{ja}) + H_2(J)$ and $H^+ + H_2(J)$ reaction complexes a separate instrument was used to produce para-enriched hydrogen. It was designed by a colleague Michal Hejduk and all the details of its construction can be found in [*Hejduk, 2013*]. I will mention only the basic overview of the operation of the generator of para-enriched hydrogen.

o-H_2 is converted into p-H_2 at low temperature and in the thermodynamic equilibrium, so, in the generator H_2 is mostly relaxed to the lowest $J = 0$ para-state (figure 3.8). The efficiency of the conversion can be greatly increased by the presence of inhomogeneous magnetic field, so, a catalyst $HFeO_2$ (CAS number 20344-49-4) was used in the conversion volume.

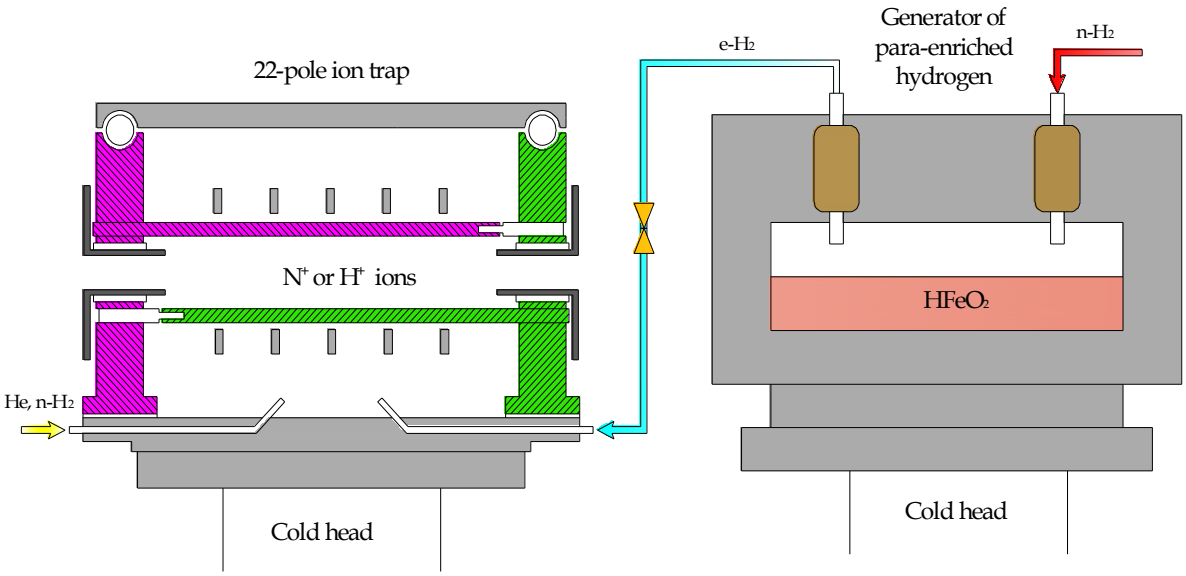

Figure 4.17. Schematic cross-section of the trap and the generator of para-enriched hydrogen. Normal hydrogen is introduced from a high-pressure reservoir into the volume with catalyst and cooled down to 10 K. Then para-enriched hydrogen (e-H_2) penetrates from the generator into the trap through a leak valve and reacts with trapped ions.

In figure 4.17 we can see a scheme of the experiments carried out with p/o-H_2. Normal hydrogen was introduced from a high-pressure reservoir

into the generator chamber with catalyst and cooled down to 10 K by a cooling system. When the temperature was increased to 14 K the converted hydrogen evaporated from the catalyst and was released into the 22PT through a leak valve.

The outer vacuum chamber of the generator was pumped by a turbomolecular pump to minimise the heat transfer from the walls to the catalyst container and the cold head. The pressure inside the chamber was always kept below 10^{-3} Pa. The forevacuum was pumped by a rotary pump. The cooling system consisted of a cold head Leybold RGD 210 and a helium compressor with water cooling [*Hejduk, 2013*].

The control measurements of the fraction ${}^{p}f$ of p-H_2 in the hydrogen from the generator yielded ${}^{p}f = 0.995$, the details are described in the next section. Due to a minor ortho-fraction we cannot strictly consider the after-conversion hydrogen to be pure p-H_2. So, in our work we designate such para-enriched hydrogen with ${}^{p}f = 0.995$ as e-H_2.

5 Experimental studies of ion-molecule reactions with atomic and molecular hydrogen

Experimental studies of the rate coefficients of ion-molecule reactions are of a certain importance due to the fact that there are few experimental and theoretical data for these reactions at interstellar-relevant temperatures. Moreover, sometimes experiment can show the reaction features that were not considered in the existing theoretical studies. The accordance between experimental and theoretical outcomes may serve as an indicator of high level of knowledge on the process, whereas the discrepancy between the results inspires both theoreticians and experimentalists for further research.

In this section the experimental data on the ion-molecule reactions with atomic and molecular hydrogen and molecular deuterium are presented. The studies touched such important issues as isotope effect and isotope exchange, state-selective reactivity of species, formation of HD and H_2O in the interstellar medium, as discussed in section 3.

Some of the experimental results, such as data on $O^- + H_2$, $D^- + H$ reactions, are compared with the recent quantum-mechanical calculations of the respective reaction rate coefficients. The theoretical studies were provided by the Martin Čížek group from the Institute of Theoretical Physics of the Faculty of Mathematics and Physics of Charles University in Prague. One can note very good overall agreement between the measured and calculated data that serves as an additional proof of reliability of our experiments.

5.1 Laboratory studies of the interaction of positive ions with para-/ortho-hydrogen

As it was mentioned in theoretical section, the change of the rotational energy of hydrogen may have a significant impact on the reaction dynamics. Rotation of a molecule as well as change of the energy barrier may lead to completely different behaviour in reactions with para- and ortho-hydrogen. From this point of view, the information about the state-selective rate coefficients is essential for filling in the gaps in the understanding of hydrogen reactivity.

Such experimental study of the interaction of N^+ and H^+ ions with p/o-H_2 was conducted using the combination of the AB-22PT instrument with the generator of para-enriched hydrogen. Such reactions are of great importance for the astrochemistry because they are a source of such species as interstellar ammonia and provide information on H_3^+ ion formation via binary radiative and ternary association of H^+ with H_2. Here the results for the state-specific rate coefficients are reported at temperatures down to 11 K.

5.1.1 Temperature dependence of the rate coefficient and state-selective reactivity of $N^+(^3P_{ja}) + H_2(J)$ reaction

The primary N^+ ions were produced via dissociative ionisation of N_2 in the SIS using energetic electrons (~60 eV). Helium was also added into the SIS to increase the efficiency of ion production via fast reaction

$$He^+ + N_2 \rightarrow N^+ + N + He \qquad (5.1)$$

with the near-Langevin reaction rate coefficient ~$1 \cdot 10^{-9}$ $cm^3\ s^{-1}$ [*Anicich, 2003*].

A typical set of raw data recorded at the trap temperature 52 K and with buffer and reactant gases in the trap ([He] = $5.2 \cdot 10^{11}$ cm^{-3}, [n-H_2] = $1.6 \cdot 10^{11}$ cm^{-3}) is shown in figure 5.1. The injected N^+ ions react with

hydrogen and form NH^+, which reacts to NH_2^+ and then to NH_3^+ in subsequent collisions with H_2. As discussed in [*Herbst and Klemperer, 1973*] and [*Gerlich, 1993*], NH_4^+ may also be formed, however, very slowly, most probably via tunnelling. In the first 10 ms one can note the increase of the sum of all detected ions (Σ). It takes place due to the phase-space compression of the injected ion cloud via collisions with the cold buffer gas leading to an increase of the detection efficiency mainly due to the better acceptance and transmission of the quadrupole mass-filter [*Zymak et al., 2013*].

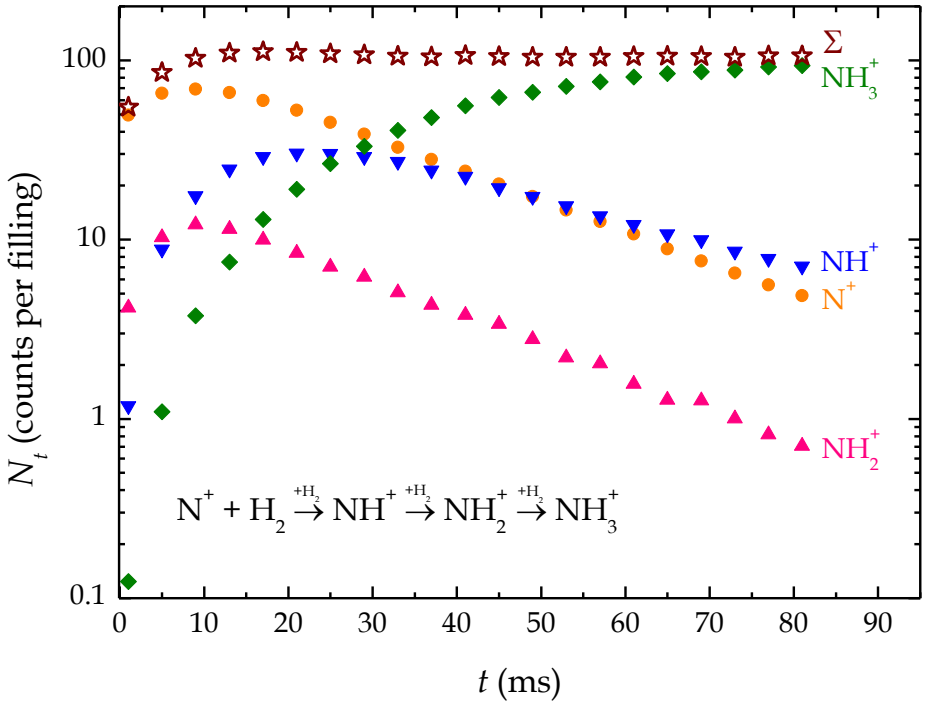

Figure 5.1. Sequential hydrogenation of trapped N^+ ions to NH_i^+ ions (i = 1, 2, 3) as function of storage time t [*Zymak et al., 2013*]. The measurement was carried out at T_{22PT} = 52 K at hydrogen number density [n-H_2] = $1.6 \cdot 10^{11}$ cm^{-3} and helium buffer gas number density [He] = $5.2 \cdot 10^{11}$ cm^{-3}. The increase of the sum of all detected ions (Σ) at the beginning is commented in the text.

In the present study, the information about the $N^+ + H_2$ reaction rate coefficient k_N was derived simply from the decay of the primary ions. Figure 5.2 shows measured dependencies of the rate coefficients on

temperature between 11 K and 100 K for different fractions ${}^{o}f$ of o-H_2, which were ranged from 0.75 to 0.005.

The data were analysed with respect to the fine structure of N^+ ion and rotational excitation of H_2 molecule. Arrhenius type dependencies were used to describe the reaction of N^+ ion at different fine structure levels with p/o-H_2. The respective reaction rate coefficients are

$$ {}^{p/o}k_{Nja}(T) = {}^{p/o}k^{A}_{Nja} \cdot e^{-\frac{{}^{p/o}E^{A}_{Nja}}{T}}, \tag{5.2} $$

where ja marks a N^+ fine structure level (ja = 0, 1, 2, corresponding to $^3P_0$, $^3P_1$, $^3P_2$, respectively), ${}^{p/o}k^{A}_{Nja}$ and ${}^{p/o}E^{A}_{Nja}$ are Arrhenius parameters [*Menzinger and Wolfgang, 1969*].

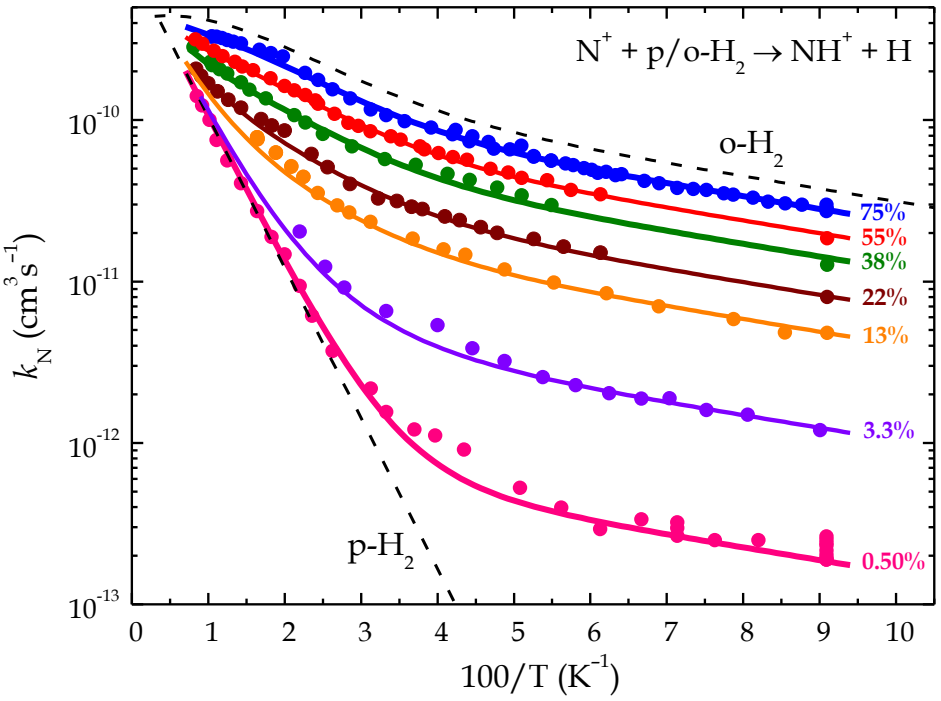

Figure 5.2. Arrhenius plot of experimental rate coefficients k_N for the reaction of N^+ with p/o-H_2 (3.29), measured with different fractions of o-H_2 (given in percentage terms). The solid lines are fits (5.3) for thermally weighted superpositions of state-specific rate coefficients. The fit parameters are listed in table 5.1. The dashed lines are the analytical fits for ${}^{o}f$ = 0 (pure p-H_2) and ${}^{o}f$ = 1 (pure o-H_2).

As it was mentioned before, according to the assumption in [*Russel and Manolopoulos, 1999*], the $^3P_2$ FS level of N^+ is non-reactive due to the fact that only three lowest adiabatical states of the nine $N^+(^3P)$ states are reactive (i. e., the $^3P_0$ level and two of three $^3P_1$ states). Moreover, the recognition of the reaction of N^+ ion in different FS levels with e-H_2 was hard due to the higher endothermicity of the respective reaction and lower sensitivity, comparing to the measurements with hydrogen with considerable ${}^o f$ (13% and higher). Hence, the reaction of N^+ with p-H_2 is described by overall ${}^p k_N$ rate coefficient only. Lastly, the model of evaluation of the $N^+ + H_2$ reaction rate coefficient is represented by the following expression:

$$k_N = {}^o f \cdot ({}^o k_{N0} \cdot \xi_0 + {}^o k_{N1} \cdot \xi_1) + (1 - {}^o f) \cdot {}^p k_N. \qquad (5.3)$$

Here the coefficients ξ_0, ξ_1 account for the thermal population of the two lowest FS states $^3P_0$, $^3P_1$, shown in figure 5.3.

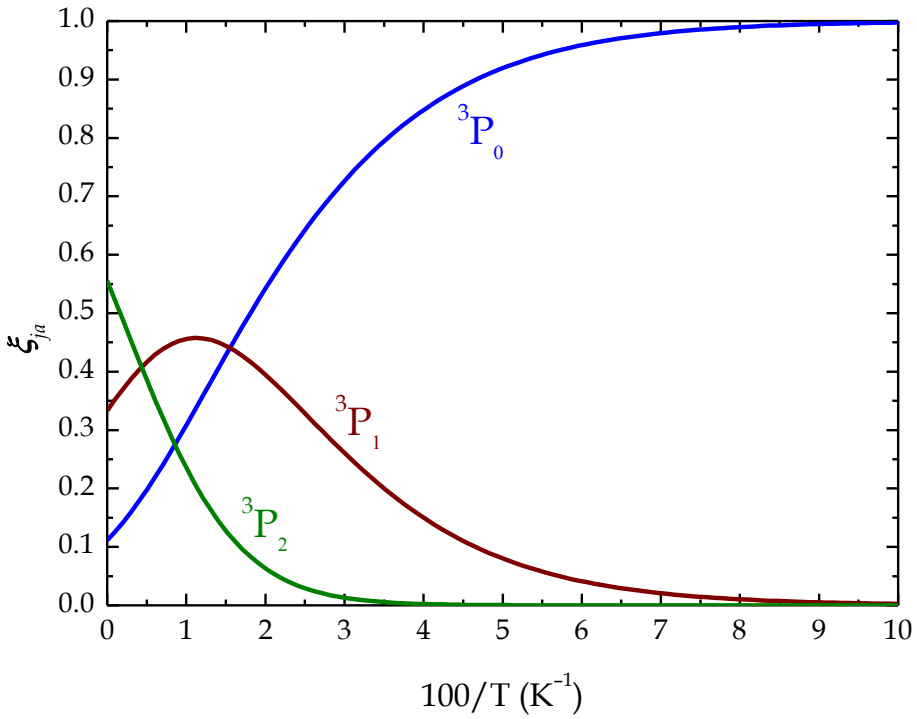

Figure 5.3. Thermal distribution of the population of the three FS levels ξ_{ja} of $N^+(^3P_{ja})$ ion evaluated from the Maxwell-Boltzmann distribution function [*Tosi et al., 1994*].

Obviously, the expression in the first brackets in equation (5.3) represents the overall rate coefficient of the $N^+(^3P_{ja})$ reaction with o-H_2:

$$ {}^{o}k_{\mathrm{N}} = {}^{o}k_{\mathrm{N0}} \cdot \xi_0 + {}^{o}k_{\mathrm{N1}} \cdot \xi_1. \tag{5.4} $$

The thermal populations of the FS levels were calculated from the Maxwell-Boltzmann distribution and according to the numerical values the dependencies for $^3P_0$ and $^3P_1$ levels equalled [*Tosi et al., 1994*]:

$$ \xi_0 = \frac{1}{1 + 3 \cdot e^{-\frac{70.76\ \mathrm{K}}{\mathrm{T}}} + 5 \cdot e^{-\frac{187.9\ \mathrm{K}}{\mathrm{T}}}}, \tag{5.5} $$

$$ \xi_1 = \frac{3 \cdot e^{-\frac{70.76\ \mathrm{K}}{T}}}{1 + 3 \cdot e^{-\frac{70.76\ \mathrm{K}}{\mathrm{T}}} + 5 \cdot e^{-\frac{187.9\ \mathrm{K}}{\mathrm{T}}}}. \tag{5.6} $$

Nevertheless, we also had to take into account the population of the «non-reactive» $^3P_2$ level as it was quite significant at temperatures above 50 K (figure 5.3).

For the state-specific rate coefficients, individual Arrhenius functions were chosen according to the equation (5.2). Contribution of $H_2(J = 2)$ (3% in pure p-H_2 at 100 K) was neglected.

The rate coefficient ${}^{p}k_{\mathrm{N}}$ was extracted directly from the least-squares fitting of the points of the measurement with ${}^{o}f = 0.005$ in the para-dominant region (~40 K – 100 K temperature range). Then the overall rate coefficient ${}^{o}k_{\mathrm{N}}$ of the reaction with o-H_2 can be extracted from the expressions (5.3) and (5.4):

$$ {}^{o}k_{\mathrm{N}} = \frac{k_{\mathrm{N}} - {}^{p}f \cdot {}^{p}k_{\mathrm{N}}}{{}^{o}f}. \tag{5.7} $$

The result is plotted in figure 5.4 as a black solid line. The points in the graph are measured data divided by the respective ortho-fractions; hence, we

extracted the ortho-component from each data set. One can note the excellent agreement for the values measured in reaction with hydrogen with a considerable fraction of o-H_2 (^{o}f in range from 13% to 75%) that proves that the restricted model fits all experimental data quite well.

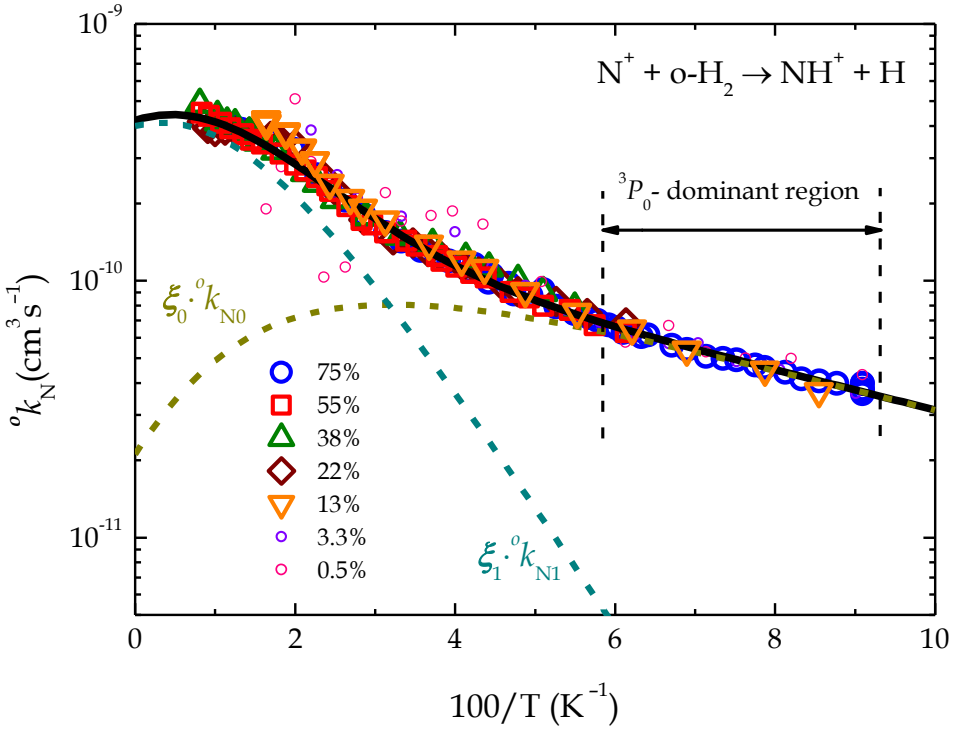

Figure 5.4. Dependence of $^{o}k_{\mathrm{N}}$ on temperature. The resulting calculated rate coefficient of the reaction of N^+ with o-H_2 is shown as a solid line. Dashed lines are contributions $^{o}k_{\mathrm{N}ja}$ weighted by the populations of N^+ FS states. Points are experimental data divided by the respective ortho-fractions.

Figure 5.3 provides us with the information that below ~16 K more than 95% of N^+ ions are thermalised in the lowest FS state $^3P_0$, consequently, the coefficient $^{o}k_{\mathrm{N0}}$ was extracted directly by fitting the measured points in the $^3P_0$-dominating region in figure 5.4. Hence, the rate coefficient $^{o}k_{\mathrm{N1}}$ was calculated from the equation (5.4) using already known $^{o}k_{\mathrm{N}}$ and $^{o}k_{\mathrm{N0}}$:

$$ {}^{o}k_{\mathrm{N1}} = \frac{{}^{o}k_{\mathrm{N}} - \xi_0 \cdot {}^{o}k_{\mathrm{N0}}}{\xi_1}. \qquad (5.8) $$

The rate coefficients ${}^{o}k_{\mathrm{N0}}$ and ${}^{o}k_{\mathrm{N1}}$, weighted by the FS states population, are shown in figure 5.5 as dashed lines. The sum of the separate coefficients ${}^{o}k_{\mathrm{N}}$, ${}^{p}k_{\mathrm{N}}$ weighted by the respective ${}^{o}f_{\mathrm{n}} = 0.75$, ${}^{p}f_{\mathrm{n}} = 0.25$, and FS level populations gives the overall fit for n-H_2 (solid line in figure 5.5). The same fits for all measured sets of data are drawn in figure 5.2 as solid lines. The Arrhenius temperatures ${}^{p/o}\mathrm{T}^{\mathrm{A}}_{\mathrm{N}ja} = {}^{p/o}E^{\mathrm{A}}_{\mathrm{N}ja}/\mathrm{k_B}$, where $\mathrm{k_B}$ is Boltzmann constant, are given in kelvins. The obtained parameters of fits are presented in table 5.1.

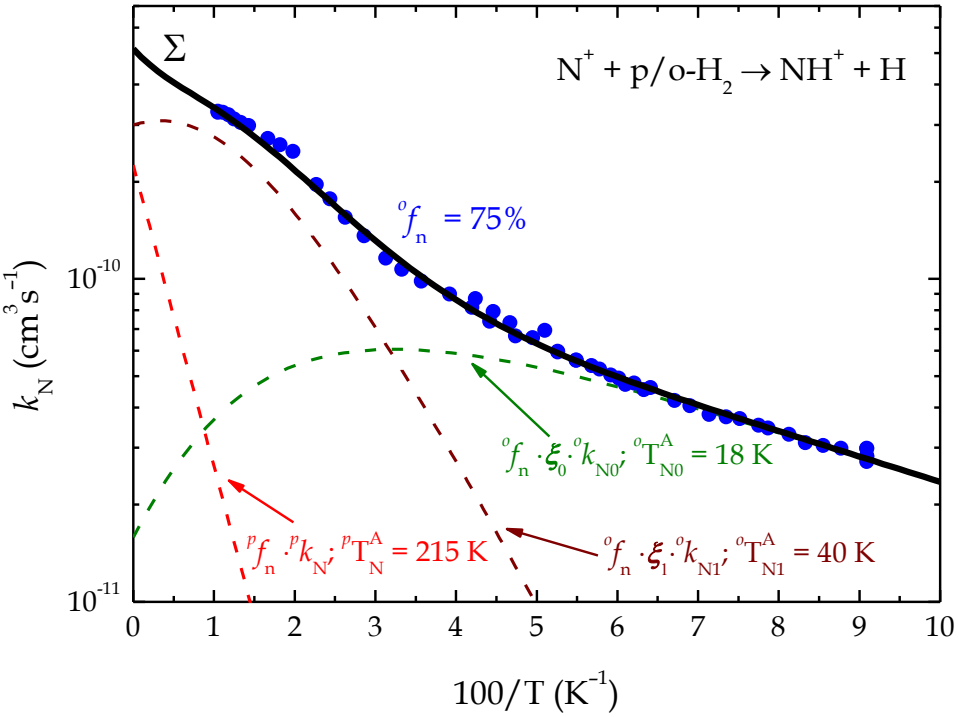

Figure 5.5. Influence of each partial rate coefficient ${}^{o}k_{\mathrm{N}ja}$ (dashed lines) on the summing $\mathrm{N^+}(^3\mathrm{P}_{ja})$ + n-H_2 reaction rate coefficient k_{N} (solid line). The respective Arrhenius temperatures ${}^{p/o}\mathrm{T}^{\mathrm{A}}_{\mathrm{N}ja}$ are given in kelvins (see text). Points represent data measured with normal hydrogen.

Due to the ionisation process, the initially injected primary $\mathrm{N^+}$ ions are in the $^3\mathrm{P}_2$ state with a probability of 5/9. Thermalisation of the trapped ions and hydrogen abstraction reactions occur in competition with each other, so the probable FS relaxation should be also taken into account.

A kinetic model, including the collisional transitions $^3P_2 \rightarrow {}^3P_1$ and $^3P_1 \rightarrow {}^3P_0$, was developed and its notable result was that the model was in good agreement with the exponential shape of the decay curve of number of N^+ ions in figure 5.1. The study also yielded that that the excitation of N^+ to the $^3P_2$ state reduces its reactivity, but not completely to zero as predicted from strict adiabatic assumptions in [*Wilhelmsson and Nyman, 1992*] and [*Russel and Manolopoulos, 1999*].

The details about the kinetic model, adaptation of fit functions for astrochemical purposes, and also discussions about the quantum mechanical problems of availability of FS energy accumulated in $N^+(^3P_{ja})$ ions in the reactions with hydrogen can be found in [*Zymak et al., 2013*], [*Hejduk, 2013*].

	k^{A}_{Nja} (10^{-10} cm^3 s^{-1})	T^{A}_{Nja} (K)
$^{p}k_{N}$	9.0	215
$^{o}k_{N0}$	1.9	18
$^{o}k_{N1}$	12	40

Table 5.1. Parameters of the model (5.3) evaluated by the method of gradual fitting. Arrhenius temperature T^{A}_{Nja} is used instead of the respective energy for clarity.

5.1.2 Binary and ternary association of H^+ and $H_2(J)$

In the experimental study of radiative binary and ternary association $H^+ + H_2$ (+ H_2) to H_3^+ (+ H_2) ion (3.4), (3.5) H^+ ions were produced from H_2 in the SIS, the ion beam was filtered from H_2^+ and H_3^+, and guided to the trap.

A typical set of measured data, showing the reaction of H^+ ions with para-enriched and normal hydrogen, recorded at the 22-pole trap temperature of 11 K, is presented in figure 5.6. About 100 – 200 H^+ ions were injected each time. For better comparison of the results, the numbers of the remaining primary ions are normalised to the number of initially injected ones.

Without target gas, the number of stored ions was independent on the trapping time. The ions were cooled in collisions either with helium buffer gas or with background gas in the trap. Adding normal or para-enriched hydrogen led to a decrease of number of H^+ in time. In both measurements the same reactant gas number density was used, so, it is obvious that e-H_2 is more reactive than n-H_2. The apparent binary rate coefficient k_H^* (see equation (3.20)) of the H^+ association with H_2 was determined from the exponential decrease of number of H^+ ions in time with the rate $r_H = k_H^* \cdot [H_2]$.

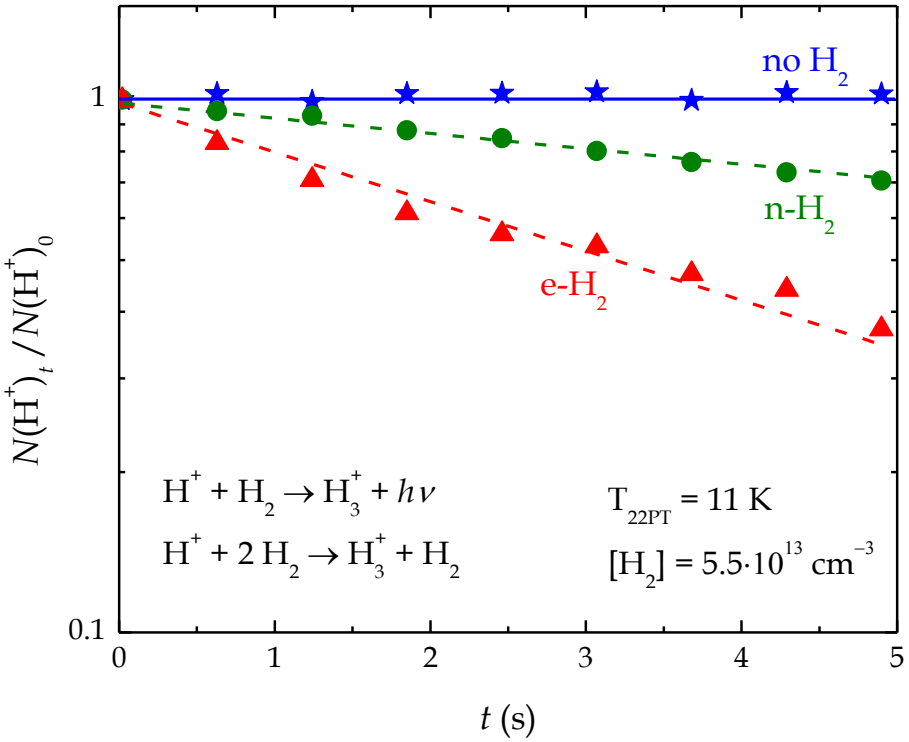

Figure 5.6. Normalised numbers of trapped H^+ as function of storage time t. Addition of hydrogen ($[H_2] = 5.5 \cdot 10^{13}$ cm^{-3} in both cases) leads to a decay of number of H^+ due to formation of H_3^+ in collisions with H_2.

Here we mark ternary and binary radiative rate coefficients of $H^+ + H_2$ association as k_{H3} and k_{Hr}, respectively. Figure 5.7 shows the apparent binary rate coefficients k_H^* measured in the range of temperatures from 11 K to 33 K in experiment with e-H_2 and 11 K – 22 K in experiment with n-H_2. The experiments also covered more than two orders of magnitude of hydrogen

number densities, $[H_2] = 4{\cdot}10^{11}$ cm^{-3} – $2{\cdot}10^{14}$ cm^{-3}. At lower number densities the measurements were limited by statistical errors. The dash-dotted and dash-dot-dotted lines in figure 5.7 are the contributions from the binary radiative and ternary association to $k_H^*(T_{22PT} = 22\ K)$, respectively. The data analysis reveals that at number densities below 10^{11} cm^{-3} – 10^{12} cm^{-3} most products are $H_3^+ + h\nu$, while above ~10^{13} cm^{-3}, the ternary stabilisation of the $H^+ + H_2$ collision complex prevails and k_H^* rises proportionally to the hydrogen number density.

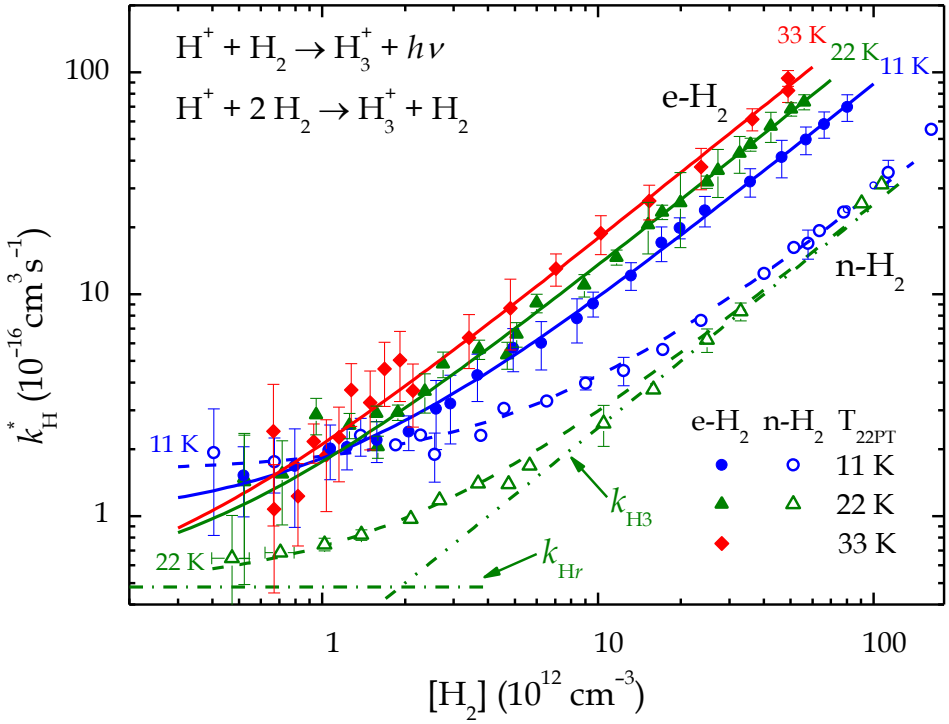

Figure 5.7. Dependence of the apparent binary association rate coefficients k_H^* on hydrogen number density at different temperatures. The measured points were fitted with equation (3.20) (dashed lines for n-H_2 and solid lines for e-H_2). Dash-dotted and dash-dot-dotted lines are radiative and ternary components of the apparent rate coefficient k_H^* for n-H_2 at T_{22PT} = 22 K.

The ternary and binary radiative rate coefficients, obtained from the fits, are shown as function of nominal temperature in the upper and lower panels of figure 5.8 (open circles with crosses). The values for k_{H3} were determined at the highest measured hydrogen number densities by

correcting k_H^* for the small contributions from the radiative association. Correspondingly, the values for k_{Hr} were obtained from k_H^* at $[H_2] = 7.0 \cdot 10^{11}$ cm^{-3} by subtracting the mean value of $k_{H3} \cdot [H_2]$ (stars, lower panel).

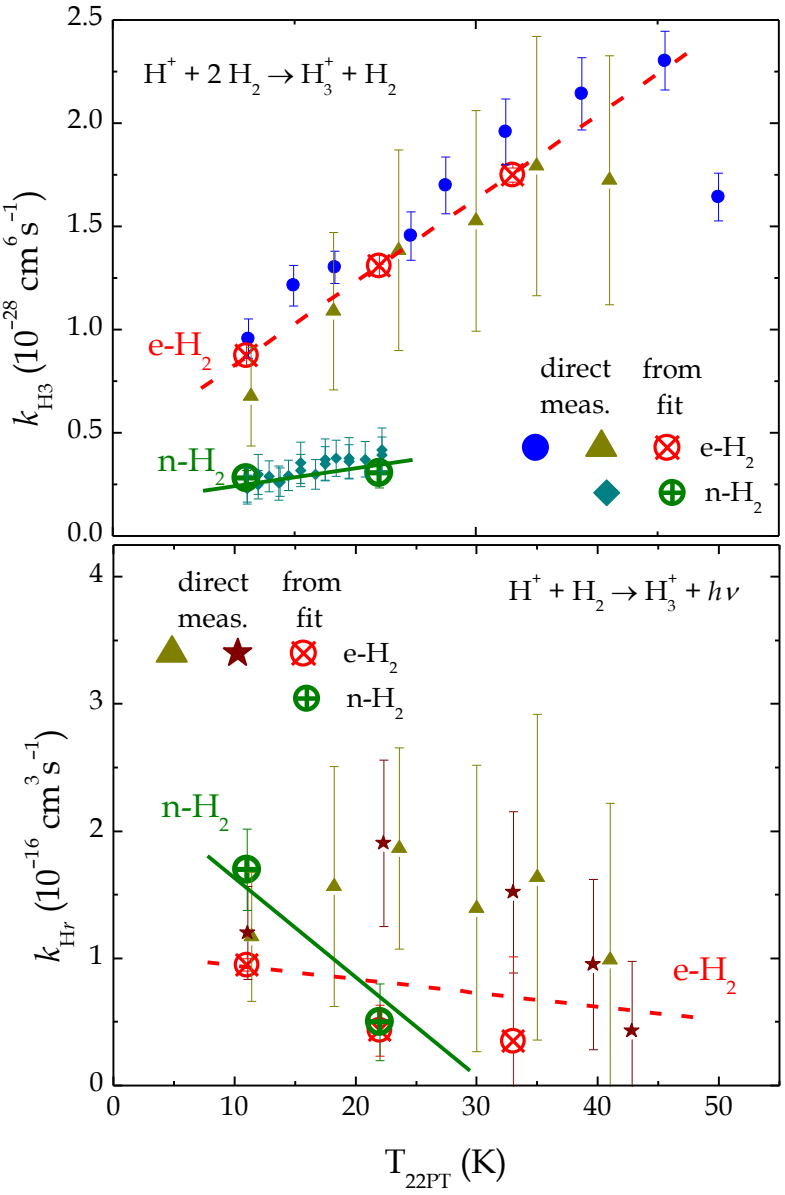

Figure 5.8. Temperature dependencies of k_{H3} (*upper panel*) and k_{Hr} (*lower panel*). The large circles with crosses inside are fits of the density dependencies of k_H^* (from figure 5.7), dashed lines correspond to the temperature trends for e-H_2 and solid for n-H_2. Small symbols (circles, triangles, diamonds, and stars) are k_{H3} and k_{Hr} determined at different fixed H_2 number densities by correcting the measured k_H^* values individually (see text).

The filled triangles in the upper and lower panels of figure 5.8 indicate that correction of k_H^* with nominal values of k_{H3} and k_{Hr} was also reasonable at a density $[H_2] = 1.9 \cdot 10^{12}$ cm^{-3}, where the two contributions $k_{H3} \cdot [H_2]$ and k_{Hr} are nearly equal. The solid and dashed lines in figure 5.8 indicate the trends of the corresponding temperature dependencies of the k_{H3} and k_{Hr} rate coefficients for n-H_2 and e-H_2, respectively.

The ternary rate coefficient for H^+ association with e-H_2 has visible positive temperature dependence that follows the linear function

$$k_{H3}(T; \text{e-}H_2) = (4.4 + 0.4 \cdot T) \cdot 10^{-29} \text{ cm}^6 \text{ s}^{-1} \quad (5.9)$$

in a range of T from 11 K to 50 K. For n-H_2 (data from [*Plašil et al., 2012*]), the trend is not so evident, partly due to the smaller temperature interval. The only definite conclusion, which we can make, is that at low temperatures the ternary rate coefficient $k_{H3}(T; \text{o-}H_2)$ is far lower than the respective coefficient for p-H_2 (see figure 5.9). The minor increase indicated by the solid line in the upper panel of figure 5.8 can be fully explained with the 25% contribution of p-H_2 in n-H_2. This may probably lead to the conclusion that $k_{H3}(J = 1)$ is several times lower than $k_{H3}(J = 0)$.

The stabilisation of the intermediate complex by a collision with a third particle takes place on the rather well characterised potential energy surface of H_5^+ [*Aguado et al., 2010*]. Hence, one of the possible explanations of the increasing temperature dependence for e-H_2 is that a proton can easily be exchanged between the two hydrogen molecules [*de Tudela et al., 2011*] and that the H_2 approaching the $(H_3^+)^*$ complex pulls out the proton in many cases instead of stabilising the collision complex. Such specific processes certainly may have quite different temperature dependencies [*Gerlich et al., 2013*].

The results for n-H_2 showed k_{Hr} (11 K) > k_{Hr} (22 K) that is in accordance with the expectations, while it is hard to make some definite conclusion

about the thermal dependence of the radiative rate coefficient for e-H_2 due to the low sensitivity and, hence, large error bars. Therefore, the two functions

$$k_{Hr}(T; \text{e-}H_2) = (1 - 0.01 \cdot T)\ 10^{-16}\ \text{cm}^3\,\text{s}^{-1}, \tag{5.10}$$

$$k_{Hr}(T; \text{n-}H_2) = (2.3 - 0.07 \cdot T)\ 10^{-16}\ \text{cm}^3\,\text{s}^{-1} \tag{5.11}$$

were evaluated from the measured data sets (T in kelvins). However, it is rather obvious that radiative association decreases with temperature and does not follow the temperature trend of ternary association.

From the difference between the reactivity of e-H_2 and n-H_2 we can derive the state-specific rate coefficient for o-H_2. In figure 5.9 the mean ternary rate coefficient is plotted as function of ortho-fraction ${}^{o}f$ at the trap temperature 11 K. The two large symbols (open squares with crosses inside) represent the results determined from the density dependencies of k_H^* (from figure 5.7), while the other points were measured directly at the indicated ${}^{o}f$ values. As discussed above, the contributions from k_{Hr}, which were subtracted from k_H^*, were negligible at the indicated hydrogen densities.

A systematic increase of the deviations toward pure p-H_2 may be caused due to additional loss of H_3^+ in conversion into H_5^+ ions. It is known from ion trap experiments that in pure p-H_2 H_5^+ clusters grow 4 times as fast as those in n-H_2 [*Paul et al., 1995*]. The overall dependence on ${}^{o}f$ can be reasonably well described with a linear function

$$k_{H3}({}^{o}f) = (1 - {}^{o}f) \cdot k_{H3}(J = 0) + {}^{o}f \cdot k_{H3}(J = 1), \tag{5.12}$$

however, deviations from linearity could also be expected [*Gerlich et al., 2013*]. The fit of equation (5.12) results in two state-specific rate coefficients

$$k_{H3}(11\ \text{K}; \text{p-}H_2) = 8.8 \cdot 10^{-29}\ \text{cm}^6\,\text{s}^{-1}, \tag{5.13}$$

$$k_{H3}(11\ \mathrm{K};\ o\text{-}H_2) = 0.6{\cdot}10^{-29}\ \mathrm{cm^6\ s^{-1}}. \qquad (5.14)$$

It is an open question whether this large difference is caused by complex formation, complex stabilisation, or due to both these processes. H^+ ions may also have higher kinetic energy thanks to ortho-para transitions (when more hydrogen molecules are rotationally excited).

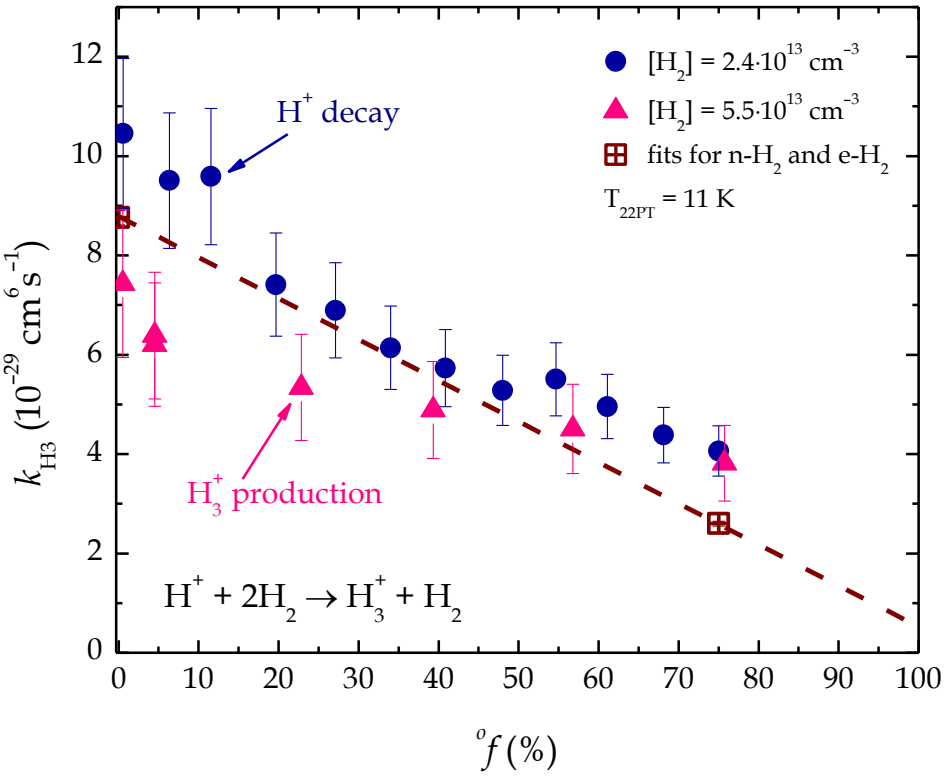

Figure 5.9. Ternary rate coefficients k_{H3} measured at T_{22PT} = 11 K as function of ortho-fraction $^o\!f$. The open squares with crosses inside were determined from fits of the density dependencies of k_H^* at 11 K (figure 5.7), while the other points were measured directly at fixed hydrogen number densities. The filled circles were derived from the decay of primary H^+ ions, the triangles show rate coefficients determined from the production of H_3^+. The dashed line indicates that $^o\!f$ dependence can be approximated with a linear function resulting in state-specific rate coefficients for pure p-H_2 and o-H_2.

The result from the present work – that ternary association is significantly more efficient with $H_2(J = 0)$ – is in accordance with previous

ion trap studies performed with C^+, CH_3^+, and $C_2H_2^+$ ions [*Gerlich, 1994*]. The similar situation when a reaction with a non-rotating particle is faster is also discussed for the reaction of OH^- with H_2 in subchapter 5.2.2.

5.2 Experimental investigations of the reactions of anions with atomic and molecular (normal) hydrogen and normal deuterium

The importance of negative ions in the interstellar medium has been discussed before in section 3.1. Here we just note that for a long time anions were species that did not deserve much attention due to their difficulty in surviving in an environment rich of ionising radiation [*Carelli, 2011*]. Only in the last decade a new theoretical and experimental interest to negative ions has been arisen after their detection in space.

In the present chapter the data on the experimental studies of interaction of some anions with atomic and normal hydrogen and deuterium are summarised. Such important issues as H_2O and HD formation in the anion-molecule reactions were investigated at temperatures, ranging from 260 K down to 10 K. Moreover, isotope exchange and isotope effect were studied in experiments with negative ions.

5.2.1 Isotope effect study in the reaction of O^- with H_2 and D_2

Studying the temperature dependencies of the reaction rate coefficients provides a probe for investigating the structure of the fundamental H_2O^- system. The measurement of the rate coefficients of associative detachment and H atom transfer channels (3.6), (3.7) of O^- reaction with H_2 at temperatures below 300 K is described in the present work. The isotopic effect of replacing the reactant H_2 with D_2 was also investigated.

O^- ions were produced by dissociative attachment to N_2O in the SIS, the usual routine was implemented for study of the reactions (3.6), (3.7), (3.24), (3.25). The measurements were repeated at various trap temperatures and the examples of data are shown in figure 5.10.

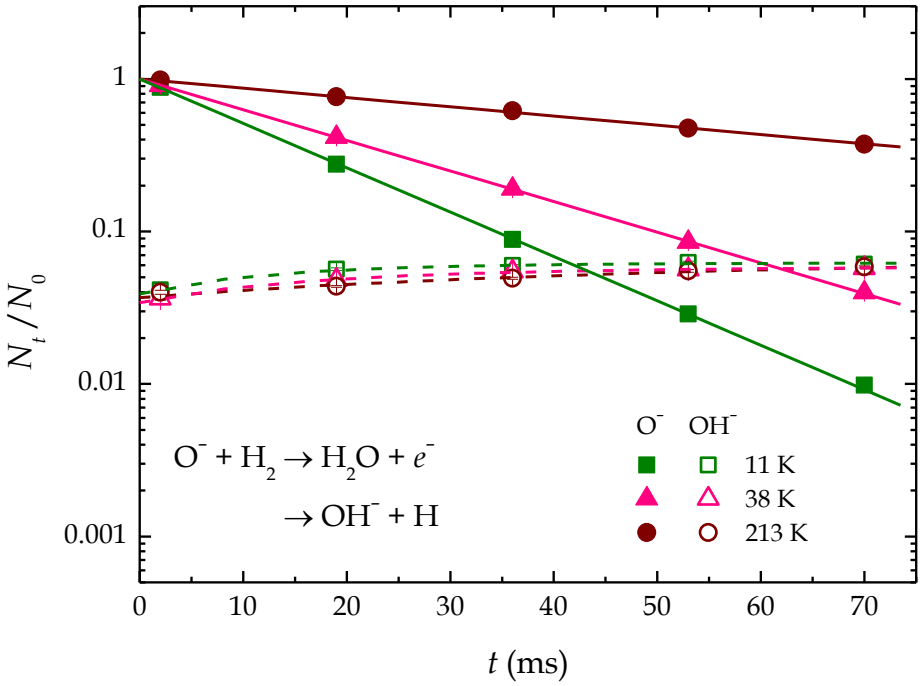

Figure 5.10. The destruction of O^- by interaction with H_2 in time and formation of OH^- at various trap temperatures (indicated in the graph). The number of ions relative to the fitted initial number of O^- at $t = 0$ as function of trapping time is plotted. The relative numbers of ions are indicated by closed and open symbols and the fitted curves are indicated by solid and dashed lines for O^- and OH^-, respectively.

The measurements were analysed by least-squares fitting of the measured numbers of ions with the following formulas:

$$N(O^-)_t = N(O^-)_0 \cdot e^{-(k_{O1}+k_{O2})[H_2]t}, \tag{5.15}$$

$$N(OH^-)_t = N(OH^-)_0 + N(O^-)_0\left(1 - e^{-k_{O2}[H_2]t}\right) \cdot \frac{k_{O2}}{k_{O1}+k_{O2}}. \tag{5.16}$$

Here k_{O1} and k_{O2} are the respective rate coefficients of the reactions (3.6) and (3.7), $N(O^-)_t$ and $N(OH^-)_t$ are numbers of the respective O^- and OH^- ions after storage time t, and $[H_2]$ is used hydrogen number density. $N(O^-)_0$, $N(OH^-)_0$, k_{O1}, and k_{O2} are free parameters of the fit. One can see a good agreement of

the fit with the measured data in figure 5.10. The evaluation routine of the k_{O3} and k_{O4} rate coefficients of the O^- reaction channels with deuterium, (3.24) and (3.25), respectively, was identical.

Varying the trap temperature, we were able to measure the rate coefficients in the temperature range of 11 K – 300 K. For reaction channels with OH^- and OD^- formation (3.7) and (3.25), the temperature range was limited by 200 K due to reaction with evaporating impurities. At temperatures above 200 K, a certain loss of O^- ions was observed even without added H_2. In such cases, the loss rate was measured separately and the obtained results were corrected in the analysis.

The binary character of the studied reactions can be seen from the dependence of the reaction rate on the reactant gas number density. Such dependence for the reaction with deuterium is shown in figure 5.11. The linearity confirms that the loss of O^- ions is caused by binary ion-molecule reaction with D_2.

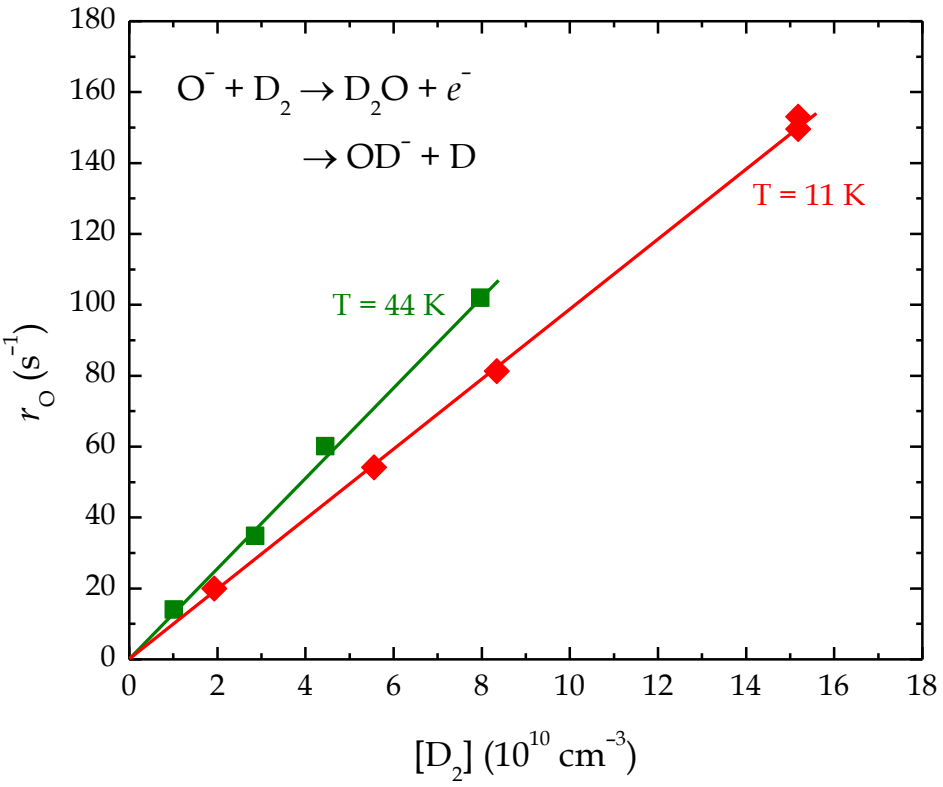

Figure 5.11. The observed O^- decay rate $r_O = (k_{O3} + k_{O4})\cdot[D_2]$ as function of D_2 number density at 11 K and 44 K.

The measured reaction rate coefficients as well as the previous results can be seen in figure 5.12. Our data for both isotopic variants (closed symbols) appear as an extension of the values from [*McFarland et al., 1973*] (open symbols). However, the rate coefficients of H_2O/D_2O formation (3.6) and (3.24) obtained in this work at near-room temperature are nearly one and a half times as high as those measured by flowing afterglow technique, while the values for the OH^-/OD^- formation are in excellent agreement with the old ones.

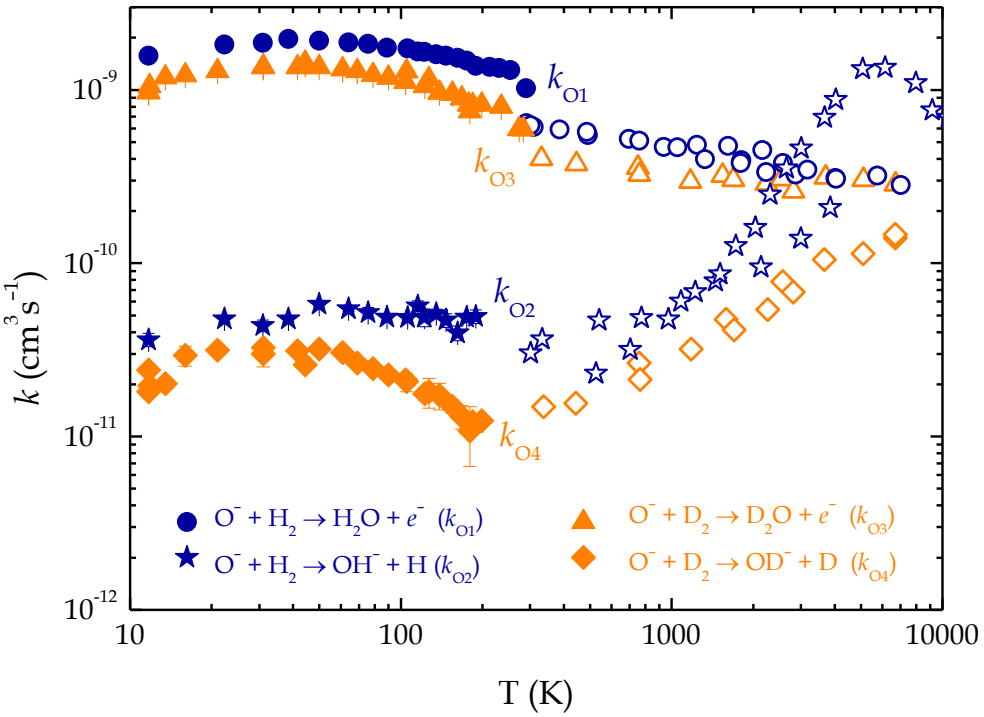

Figure 5.12. The measured rate coefficients of $O^- + H_2/D_2$ reactions in comparison with the previous values. The data obtained in this work are indicated by the filled symbols. Circles and stars denote H_2O and OH^- production, respectively; triangles and diamonds denote D_2O and OD^- production, respectively. The rate coefficients of these reactions reported in [*McFarland et al., 1973*] are indicated by the respective open symbols.

To emphasise the isotopic effects beyond the simple Langevin theory, the measured reaction rate coefficients were normalised by the corresponding Langevin collisional rate coefficients (figure 5.13). The

polarisabilities of n-H_2 and n-D_2 at 77 K were used to calculate these Langevin rate coefficients [*Milenko et al., 1972*] neglecting the slight temperature dependence. Concerning the associative detachment H_2O/D_2O production channels (3.6) and (3.24), the isotope effect is negligible near the prominent maximum at 40 K, but away from the maximum at higher temperatures the reaction with D_2 proceeds slower by 10% – 25%. However, a very significant isotope effect can be seen for the OH^-/OD^- production channels at 200 K, where the formation of OD^- proceeds approximately three times slower than the formation of OH^-.

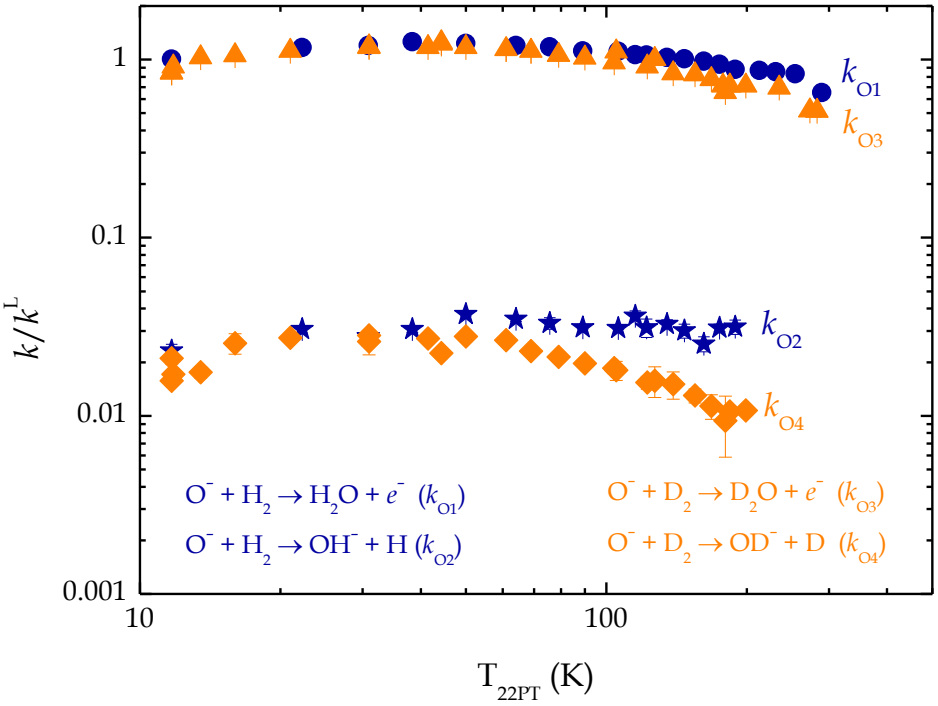

Figure 5.13. The measured $O^- + H_2/D_2$ reaction rate coefficients normalised by the respective Langevin rate coefficients. Circles and stars denote H_2O and OH^- production, respectively; triangles and diamonds denote D_2O and OD^- production, respectively.

The $O^- + H_2$ reaction rate coefficients measured previously at collision energies higher than 300 K were at nearly 1/3 fraction level of the Langevin rate. It was generally accepted due to the fact that one of the three potential

energy surfaces (PES) was reactive, whereas the other two were not [*McFarland et al., 1973*].

After we had obtained the experimental rate coefficients, which even exceeded the Langevin rate, we initiated cooperation with a group of theoreticians who helped us to interpret the outcomes. They calculated the PES for the lowest three ($1^2A'$, $1^2A''$, and $2^2A'$) electronic states connected to the $O^-(^2P) + H_2(X^1\Sigma_g^+)$ asymptote to understand the dynamics of the $O^- + H_2$ collisions (figure 5.14). There one can see that the autodetachment (responsible for H_2O channel) may occur in the region where the anionic potential is higher than neutral (dashed lines in figure 5.14).

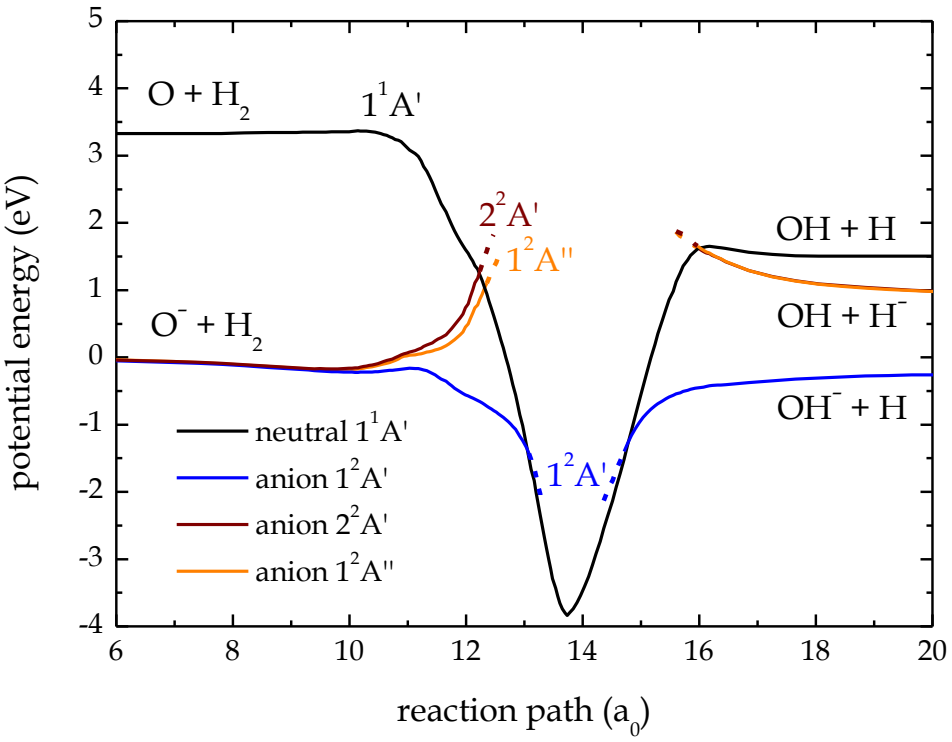

Figure 5.14. Potential energy surfaces of H_2O^- and H_2O along the minimum energy path going from $O^- + H_2$ to $OH^- + H$ on the $1^2A'$ potential energy surface. The anionic curves in the autodetachment region, where they are above the neutral OH + H PES, are indicated by dashed lines [*Jusko et al., 2015*].

According to the simulations, at low collision energies a long-lived complex is formed on the non-reactive PES ($1^2A''$ and $2^2A'$) and there is high

probability of its transition to the reactive PES ($1^2A'$) due to the conical intersection. This effect increases the reaction rate coefficient to near-Langevin values. With increasing temperature, the lifetime of the collision complex decreases and the rate coefficient approaches the 1/3 fraction of the Langevin rate.

The resulting theoretical capture rates for $O^- + H_2$ reaction (3.6) are shown in figure 5.15 together with experimental data for the respective reaction ($k_{O1} + k_{O2}$), however, variations of the arbitrary strength and the position of the absorbing function cause the uncertainty of the capture model. As well as in figure 5.13, the rate coefficient of reaction (3.6) normalised by the corresponding Langevin collisional rate coefficient is shown in figure 5.15.

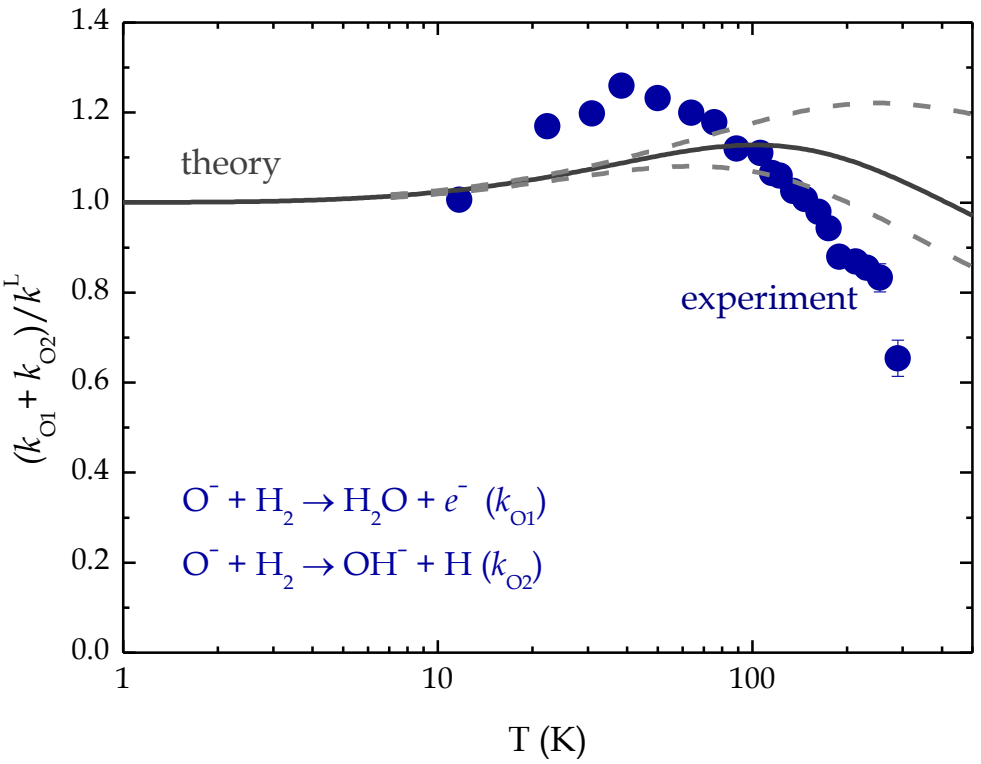

Figure 5.15. The measured $O^- + H_2$ rate coefficient normalised by the Langevin rate coefficient (circles) in comparison with the capture rates calculated with 1D capture model [*Jusko et al., 2015*]. Dashed lines indicate limits of the uncertainty of the model.

The ~5% contribution of the H atom transfer channel is explained by the fact that its reaction path passes through autodetachment region and the reaction paths, which avoid the autodetachment, have the respective low probabilities. The further details of the calculation can be found in [*Jusko et al., 2015*].

The uncertainty of the theoretical model increases at higher temperatures because the terms, which account for the specific features of high-temperature interaction, were not considered in the model. Nevertheless, there is an overall agreement between the experimental data and theoretical capture rate coefficient despite some shift of the respective peaks.

5.2.2 The OH^- + D_2 and OD^- + H_2 isotope exchange reactions

OH^- and OD^- ions for the experiment were produced in the storage ion source in a chain of two reactions. Firstly, O^- ions were produced from N_2O in the SIS in the same way as in the previous experiment, and then O^- reacted in the ion source with added H_2 or D_2.

The reaction rate coefficients were determined by fitting the measured time evolutions of numbers of OH^- and OD^- ions in the trap with the following expressions:

$$\frac{dN(\mathrm{OH^-})}{\mathrm{d}t} = -k_{\mathrm{OH}} \cdot N(\mathrm{OH^-}) \cdot [\mathrm{D_2}] + k_{\mathrm{OD}} \cdot N(\mathrm{OD^-}) \cdot [\mathrm{H_2}] \qquad (5.17)$$

for the decay of number of OH^- and

$$\frac{\mathrm{d}N(\mathrm{OD^-})}{\mathrm{d}t} = -k_{\mathrm{OD}} \cdot N(\mathrm{OD^-}) \cdot [\mathrm{H_2}] + k_{\mathrm{OH}} \cdot N(\mathrm{OH^-}) \cdot [\mathrm{D_2}] \qquad (5.18)$$

for the decay of number of OD^-, where k_{OH} is the rate coefficient of the reaction (3.27), k_{OD} is the rate coefficient of the reaction (3.28), t is trapping

time, [H_2] and [D_2] are hydrogen and deuterium number densities in the trap, $N(OH^-)$ is number of detected OH^- ions, $N(OD^-)$ is number of detected OD^- ions.

In figure 5.16 we can see the change of the normalised numbers of trapped primary and product ions in reaction of OH^- with D_2. The normalisation was made to the sum $N(OH^-) + N(OD^-)$ of numbers of detected OH^- and OD^- ions, the sum was checked to remain constant during each measurement.

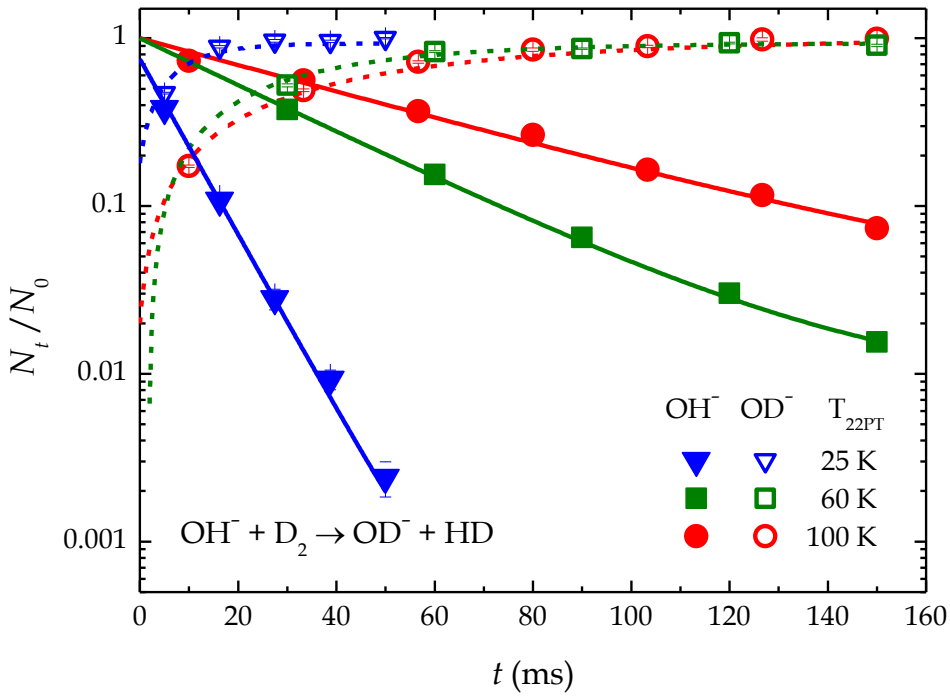

Figure 5.16. Measured time evolutions of normalised numbers of primary and product ions for the reaction (3.27) at different trap temperatures. Solid and dashed lines are fits for the decay of number of OH^- and production of OD^-, respectively. The used number densities of D_2, He, and background H_2 in the trap in these measurements can be found in table 5.2.

The binary character of the reaction (3.27) was observed by measuring the dependencies of the rate r_{OH} of the reaction on the deuterium number density. The measurements were carried out in a wide range of number

densities of D_2 and at various temperatures of the trap (figure 5.17). The plotted data confirm the expected linear relationship $r_{OH} = k_{OH} \cdot [D_2]$.

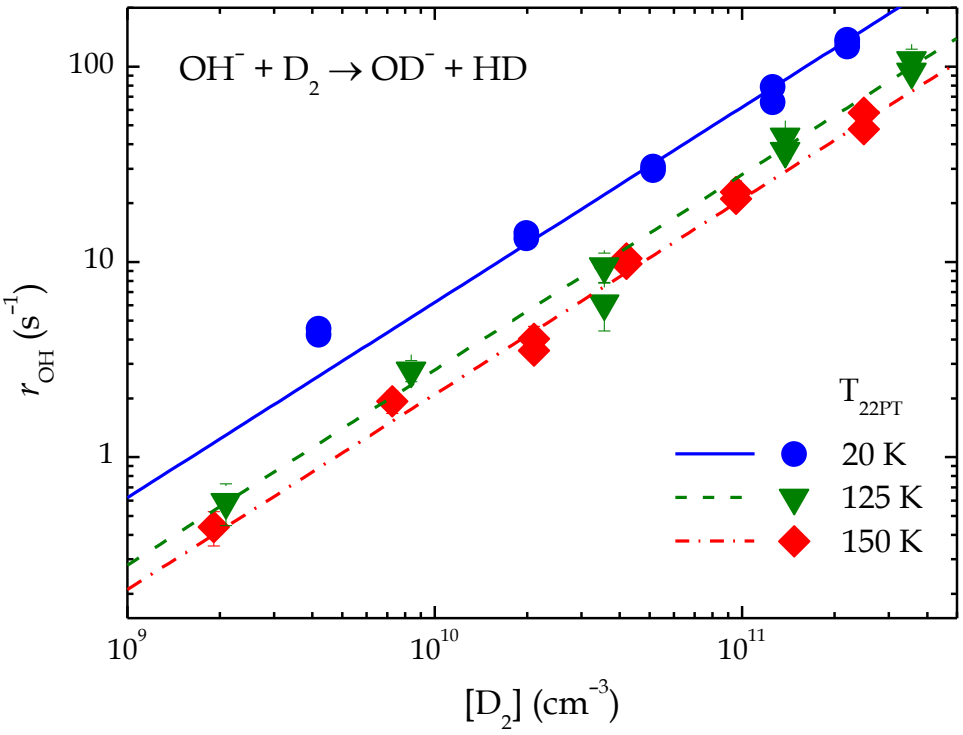

Figure 5.17. Dependencies of the rate r_{OH} of the reaction (3.27) on number density of D_2.

In the experiments small amounts of H_2 and D_2 always penetrated into the trap from the ion source. These gases reacted with the product OD^- and OH^- ions and converted them back to the reactant ions via reactions (3.28) and (3.27). Note that these processes are not the reverse reactions of the studied reactions (3.27) and (3.28). Actually, in our case, the reactions (3.27) and (3.28) are backward processes for each other. Furthermore, the presence of HD in the trap volume was negligible.

Although the number densities of those gases from the SIS were approximately 100 times lower compared to the reactant number densities, the correction for the slow endothermic reaction $OD^- + H_2$ due to fast exothermic backward converting process $OH^- + D_2$ at 11 K can be substantial. These backward processes were always considered in the data analysis (see expressions (5.17) and (5.18)).

The used density of He buffer gas was high enough, so that reactant ion would have at least 10 collisions with He prior to the interaction with a molecule of the target gas to ensure the thermalisation of trapped OH^- or OD^- (see data in table 5.2). According to the recent low-temperature studies of rotational relaxation of OH^- in collisions with He [*Otto et al., 2013*], ions were expected to be vibrationally and rotationally relaxed close to the temperature of the He buffer gas.

T_{22PT}	$[D_2]$ (cm^{-3})	[He] (cm^{-3})	$[H_2]_{SIS}$ (cm^{-3})
25 K	$2.1 \cdot 10^{11}$	$6.0 \cdot 10^{12}$	$\sim 6 \cdot 10^{9}$
60 K	$6.0 \cdot 10^{10}$	$2.4 \cdot 10^{12}$	$\sim 3 \cdot 10^{9}$
100 K	$4.7 \cdot 10^{10}$	$4.1 \cdot 10^{12}$	$\sim 1 \cdot 10^{9}$

Table 5.2. The number densities of the gases in the trap during the measurements plotted in figure 5.16. Lower index SIS indicates the background number density of hydrogen, penetrating into the trap from the ion source.

The measured rate coefficients for the reaction (3.27) are presented in figure 5.18. It includes data reported in both [*Mulin et al., 2013*] and [*Mulin et al., 2015*] publications. The experiment was conducted in the range of trap temperatures T_{22PT} = 11 K – 200 K. The present data show almost constant value of the rate coefficient at the lowest temperatures and negative temperature dependence above 60 K. The previous data from the selected ion flow tube (SIFT) [*Grabowski et al., 1983*], flow drift tube (FDT) [*Viggiano and Morris, 1994*], and high pressure mass spectrometer (HPMS) [*Meot-Ner et al., 1980*] experiments are included in the graph and are in quite good overall agreement with the present values.

In the FDT study k_{OH} was measured as function of temperature of D_2 and as function of elevated collisional energy KE_{CM}. They observed negative temperature dependence with only slight dependence on KE_{CM} that gave

them a conclusion that the reactivity of OH^- with deuterium depends on the rotational excitation of D_2 (for details see [*Viggiano and Morris, 1994*]).

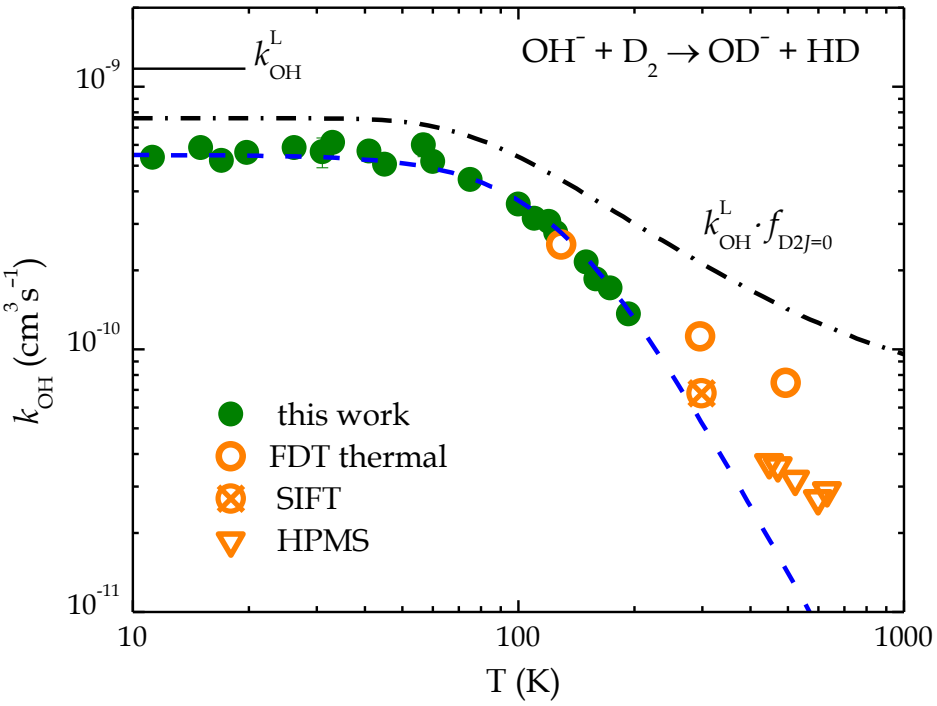

Figure 5.18. The measured temperature dependence of the reaction rate coefficient k_{OH} for H/D exchange reaction $OH^- + D_2 \rightarrow OD^- + HD$. The calculated value of Langevin collisional rate coefficient is indicated as k_{OH}^{L}. Dash-dotted line shows the calculated temperature dependence of a fictive rate coefficient k_{OH}^{F} (5.19). Here are also included thermal flow drift tube (FDT) [*Viggiano and Morris, 1994*], selected ion flow tube (SIFT) [*Grabowski et al., 1983*], and high pressure mass spectrometer (HPMS) [*Meot-Ner et al., 1980*] data. The dashed line is the fit expressed by formula (5.20).

To support this statement a fictive rate coefficient

$$k_{OH}^{F} = k_{OH}^{L} \cdot f_{D2J=0} \tag{5.19}$$

of the reaction of OH^- with nonrotating D_2 (in $J = 0$ state) was calculated. For simplicity we assume that k_{OH}^{F} is given by the product of the Langevin rate coefficient k_{OH}^{L} and of the relative population $f_{D2J=0}$ of normal D_2 in the ground rotational state (ortho nuclear spin state). The obtained temperature

dependence of the rate coefficient k_{OH}^{F} is plotted in figure 5.18 as dash-dotted line. The correlation between the measured k_{OH} and the calculated k_{OH}^{F} is clear at low temperatures, but the decrease of the measured data at higher temperatures is faster than the decrease of population of ortho-D_2 in $J = 0$.

The measured negative temperature dependence of the reaction rate coefficient k_{OH} for exothermic H/D exchange reaction (3.27) above 50 K may be also described and discussed by assuming that the reaction proceeds via the formation of the long-lived intermediate complex. This complex is subsequently either decomposed back to reactants or forward to products. Such negative temperature dependence was observed for many ion-molecule reactions, proceeding via formation of intermediate complex. For this type of reactions it was deduced that the temperature dependence of the overall rate coefficient can be approximated by power law dependence in the form:

$$\left(\frac{k_{OH}^{0}}{k_{OH}} - 1\right) = \left(\frac{T}{T_{OH}}\right)^{m} \tag{5.20}$$

with parameters k_{OH}^{0}, T_{OH}, and m (see [*Glosík et al., 1993*], [*Glosík et al., 1995[a]*], [*Glosík et al., 1995[b]*], [*Glosík et al., 1995[c]*], [*Glosík et al., 2003*]). From the least squares fit plotted in figure 5.18, the parameter values $k_{OH}^{0} = 5.5 \cdot 10^{-10}$ cm^3 s^{-1}, $T_{OH} = 130$ K, and $m = 2.7$ were obtained.

The validity of equation (5.20) for describing the measured data can also be appreciated from the plot of $log(\frac{k_{OH}^{0}}{k_{OH}} - 1)$ versus $log(T)$ (figure 5.19), where the dependence is linear with slope m. The plot also includes data from the earlier FDT [*Viggiano and Morris, 1994*], HPMS [*Meot-Ner et al., 1980*], and SIFT [*Grabowski et al., 1983*] experiments.

The procedure used here is considered as semiempirical based on statistical arguments. It is useful for extrapolation and characterisation of experimental data and similar to the procedure used for description of ternary association reactions [*Gerlich and Horning, 1992*]. In any case, the fit through data plotted in figure 5.18 and the linearity of the plot in figure 5.19

are excellent. Moreover, the extrapolation of the fit to higher temperatures (energies) gives a good overlap with the previous data. The discrepancy between the line and the data of [*Meot-Ner et al., 1980*] at higher temperatures may be caused by the presence of another mechanism, which is not described by formula (5.20). The significant contribution of the present study is the coverage of a large range of reaction temperatures and thermal character of the data (having in mind rotational excitation of normal D_2).

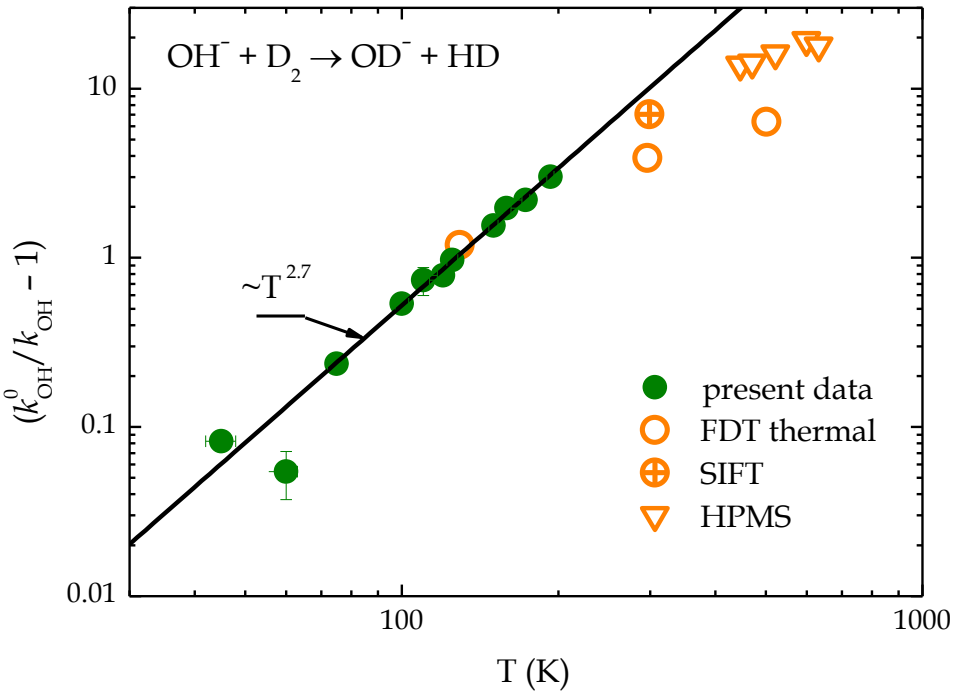

Figure 5.19. Plot of $(\frac{k^0_{OH}}{k_{OH}} - 1)$ value versus T for the reaction of OH^- with normal D_2. Present data (closed circles) are fitted by power function (5.20) (solid line). Plotted are also previous FDT [*Viggiano and Morris, 1994*], SIFT [*Grabowski et al., 1983*], and HPMS data [*Meot-Ner et al., 1980*]. Data with statistical error larger than 100% are not shown here.

In the similar way the temperature dependence of the rate coefficient of the OD^- reaction with H_2 (3.28) was measured in the range of trap temperatures from 11 K to 260 K. High number densities of H_2 were used to obtain a clear decay of number of primary OD^- anions because at low temperatures the endothermic reaction (3.28) is slow. The examples of the

measured time evolutions of numbers of reactant and product ions at different temperatures are shown in figure 5.20.

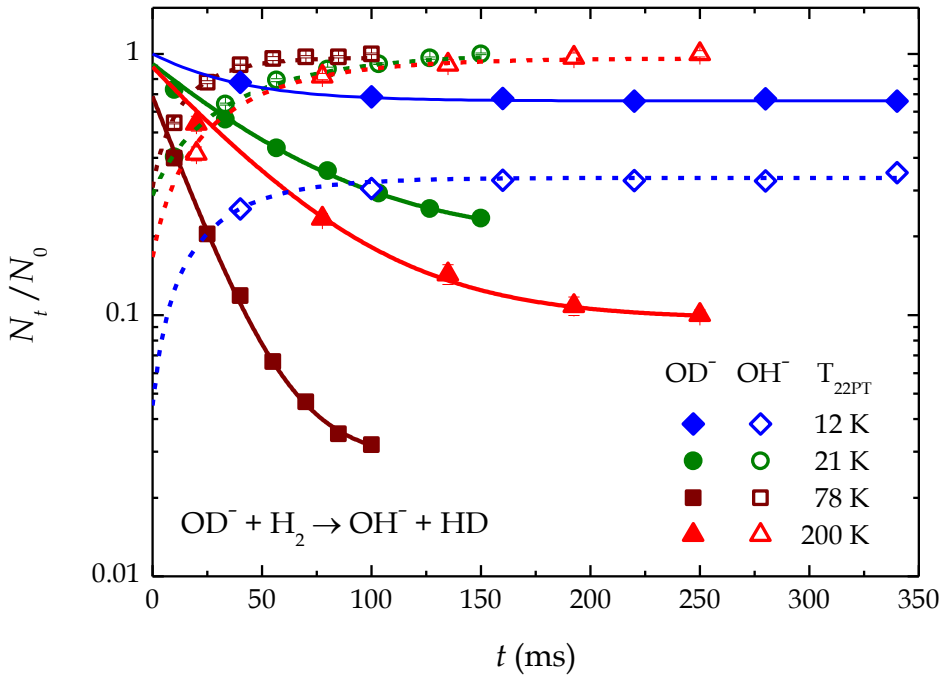

Figure 5.20. Measured time evolutions of normalised numbers of primary OD^- (closed symbols) and product OH^- (open symbols) ions for the reaction (3.28) at different trap temperatures. The normalisation was made to the sum of the detected ions. Solid and dashed lines are fits for the decay of OD^- and production of OH^-, respectively. The used densities of H_2, He, and background D_2 in the trap in these measurements can be found in table 5.3.

T_{22PT}	$[H_2]$ (cm^{-3})	$[He]$ (cm^{-3})	$[D_2]_{SIS}$ (cm^{-3})
12 K	$1.2 \cdot 10^{13}$	$3.4 \cdot 10^{13}$	$\sim 1 \cdot 10^{10}$
21 K	$6.7 \cdot 10^{12}$	$4.5 \cdot 10^{13}$	$\sim 1 \cdot 10^{10}$
78 K	$2.0 \cdot 10^{12}$	$2.3 \cdot 10^{13}$	$\sim 5 \cdot 10^{9}$
200 K	$3.4 \cdot 10^{11}$	$2.5 \cdot 10^{12}$	$\sim 3 \cdot 10^{9}$

Table 5.3. The number densities of the gases in the trap during the measurements plotted in figure 5.20. Lower index SIS indicates the background number density of deuterium, penetrating into the trap from the ion source.

The obtained temperature dependence of the rate coefficient of the reaction (3.28) (plotted in figure 5.21) was fitted by Arrhenius function

$$k_{OD} = k_{OD}^{A} \cdot e^{-\frac{E_{OD}^{A}}{k_B \cdot T}}, \tag{5.21}$$

where k_{0D}^{A} is a pre-exponential factor and E_{0D}^{A} is Arrhenius activation energy [*Menzinger and Wolfgang, 1969*]. The values of the parameters k_{0D}^{A} = 7.5·10^{-11} cm^3 s^{-1} and E_{0D}^{A} = 7.9 meV (or 92 K in Kelvins) were obtained from the data analysis.

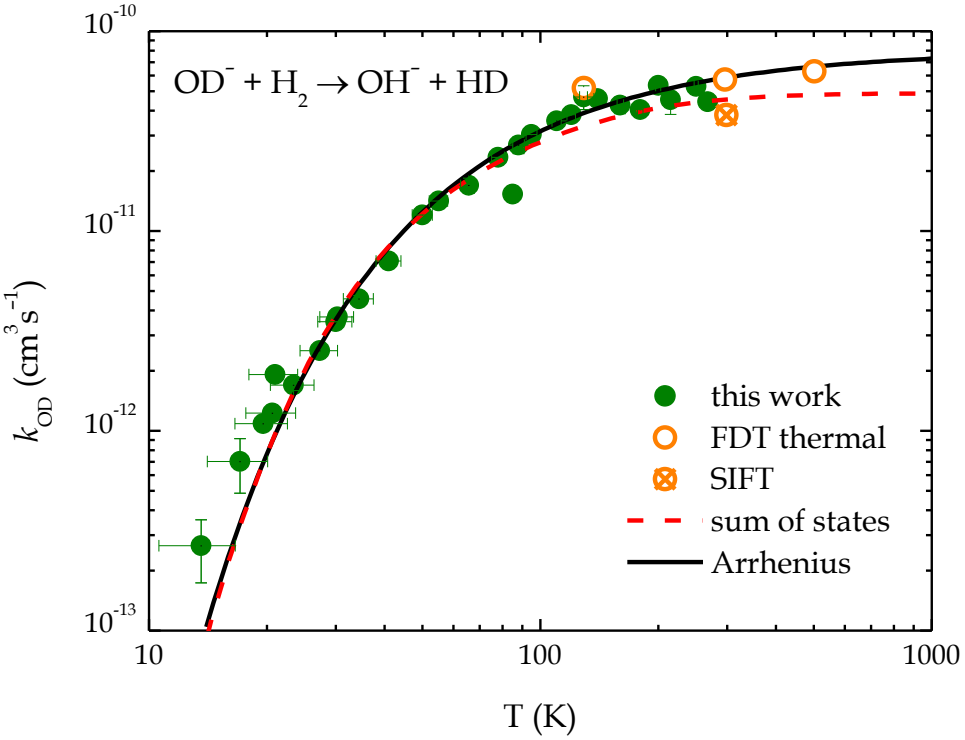

Figure 5.21. The measured temperature dependence of the reaction rate coefficient k_{OD} of the endothermic reaction $OD^- + H_2 \rightarrow OH^- + HD$. The present data (closed circles) are fitted by Arrhenius temperature dependence (5.21) (indicated by solid line). Plotted are also previous FDT [*Viggiano and Morris, 1994*] and SIFT data [*Grabowski et al., 1983*]. Dashed curve indicates the fit with function (5.23). The vertical error bars of the two points at the lowest temperatures include the estimated error due to the oscillations of temperature and pressure. At temperatures above 20 K these effects are negligible and only statistical errors are shown (mostly within data points).

As well as in case of the reaction (3.27), the dependence of the rate $r_{OD} = k_{OD} \cdot [H_2]$ on H_2 number density also shows that the reaction (3.28) is binary.

At low temperatures the backward exothermic reaction of product ion OH^- with D_2, penetrating from the SIS, is very fast in comparison with the reaction (3.28), that is why the influence of the backward process cannot be neglected despite the very large ratio $[H_2]/[D_2]$ (see table 5.3). Non-monoexponential decay of N_{OD^-} is a clear indication of that fact. From the data measured at $T_{22PT} = 12$ K we can observe an approach to equilibrium between forward and backward processes already after 50 ms. At such low temperatures this is a limiting factor for the accuracy of k_{OD} determination.

Due to its endothermicity, the reaction (3.28) may serve as a thermometer of the collision temperature by comparing the measured data with Arrhenius dependence. The accordance of the fit with both our and FDT data [*Viggiano and Morris, 1994*] is exceptionally good and it covers the variation of k_{OD} within almost three orders of magnitude. The corresponding Arrhenius plot is shown further in figure 5.22. The discrepancy between the fit and data is only at temperatures below 25 K that can be caused by many more or less substantiated reasons. The most obvious may be either a higher energy group in energy distribution of the stored OD^- ions or presence of rotationally excited OD^-. We cannot also exclude technical reasons, like small gradients of temperature on the metal envelope of the trap and on the rods of the trap when T_{22PT} approaches to its lowest limit of ~11 K. Due to a very large ratio k_{OH}/k_{OD} at low temperatures, the backward process plays an essential role in the accuracy of determination of k_{OD} from the measured data as well. The temperature variation from up to +3 K can explain the deviation of the fit from the measured coefficients. Here +5 K is used as a more conservative error estimate.

For the endothermic reaction (3.28) with $\Delta H = 24.0$ meV we have to take into account the fact that in normal hydrogen 75% of H_2 molecules are in ortho nuclear spin state configuration (figure 3.8). The corresponding lowest

rotational energy is 14.7 meV, thus, the endothermicity is lowered to approximately 9.3 meV, (figure 3.6). Although this is in rather good agreement with obtained activation energy E_{OD}^{A} = 7.9 meV, the difference is larger than our estimated error of 0.3 meV that may refer to unknown isotopic electronic shifts. However, the small difference may be also explained by thermal population of rotational states of OD^-, so our model was improved beyond the simple Arrhenius dependence [*Mulin et al., 2015*].

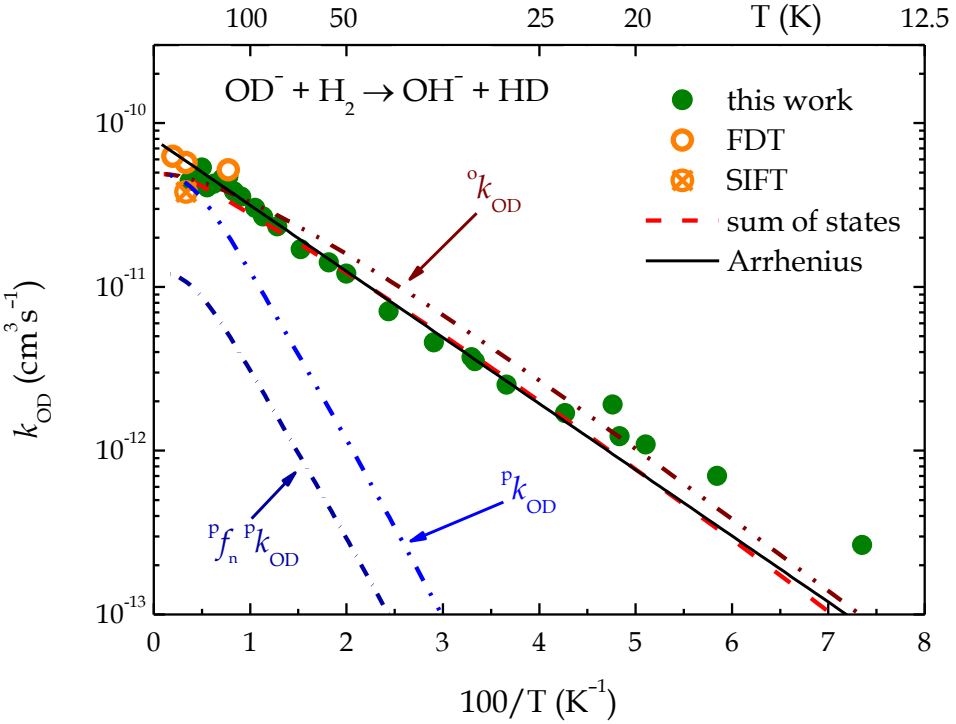

Figure 5.22. Arrhenius plot of the measured reaction rate coefficients k_{OD} for the reaction (3.28). The data were measured in experiments with n-H_2. The present data were fitted by Arrhenius function (5.21), indicated by a solid black line. Dashed line denotes the fit with function (5.22). The dash-dot-dotted lines indicate temperature dependencies of the state-specific rate coefficients ${}^{o}k_{OD}$ and ${}^{p}k_{OD}$. The estimated contribution from p-H_2 to the k_{OD} is also plotted as dash-dotted line. Previous thermal FDT [*Viggiano and Morris, 1994*] and SIFT [*Grabowski et al., 1983*] data are also shown in the plot.

Despite the fact that the $J = 1$ state of H_2 plays a central role in promoting the endothermic reaction in covered temperature range, for a

more precise quantitative evaluation we have to account for all initial states of reactants with their temperature dependent populations. We introduce a state-specific rate coefficient $k_{J_{H_2}J_{OD-}}$ of each combination of rotational states of both reactants and temperature-dependent populations of rotational states of reactants $P_{J_{H_2}}$ and $P_{J_{OD-}}$. Hence, the overall reaction rate coefficient k_{OD} can be calculated by the formula:

$$k_{OD} = \sum_{J_{H_2}} \sum_{J_{OD-}} \left(P_{J_{H_2}} \cdot P_{J_{OD-}} \cdot k_{J_{H_2}J_{OD-}} \right) \tag{5.22}$$

Actually, the model applies Arrhenius fitting for every single rotational level J_{H2}, J_{OD-}, so the result is in agreement with the theoretical value ΔH = 24.0 meV. For simplicity we assume that all states contribute with the same pre-exponential factor k_{OD}^{0} and all energies are equivalent in reducing the endothermicity of the reaction,

$$k_{J_{H_2}J_{OD-}} = k_{OD}^{0} \cdot e^{\frac{-\max\left\{\left(\Delta H - E_{J_{H_2}} - E_{J_{OD-}}\right);0\right\}}{k_B T}}, \tag{5.23}$$

where $E_{J_{H_2}}$ and $E_{J_{OD-}}$ are the energies of rotational states of reactants J_{H2}, J_{OD-}. The data for energies of rotational states are taken from [*Rehfuss et al., 1986*], [*Huber and Herzberg, 1979*], the fit of the measured data according to formula (5.23) gives k_{OD}^{0} = 4.9·10^{-11} cm^3 s^{-1}. The examples of the contributions of rotational levels J_{H2}, J_{OD-} to the overall reaction rate coefficient k_{OD} at temperatures 30 K and 200 K are shown in figure 5.23.

The obtained fit is shown as dashed line in figure 5.21 and figure 5.22. The state-specific rate coefficients of the OD$^-$ reaction with pure p-H_2 and o-H_2 indicated as ${}^{p}k_{OD}$ and ${}^{o}k_{OD}$, are shown in figure 5.22 as dash-dot-dotted lines. According to the expectations, the contribution of para-hydrogen ${}^{p}f_n \cdot {}^{p}k_{OD}$ to the overall rate coefficient k_{OD} is very small almost in the whole

range of the studied temperatures, here ${}^{p}f_{n}$ is the fraction of p-H_2 and equals 0.25.

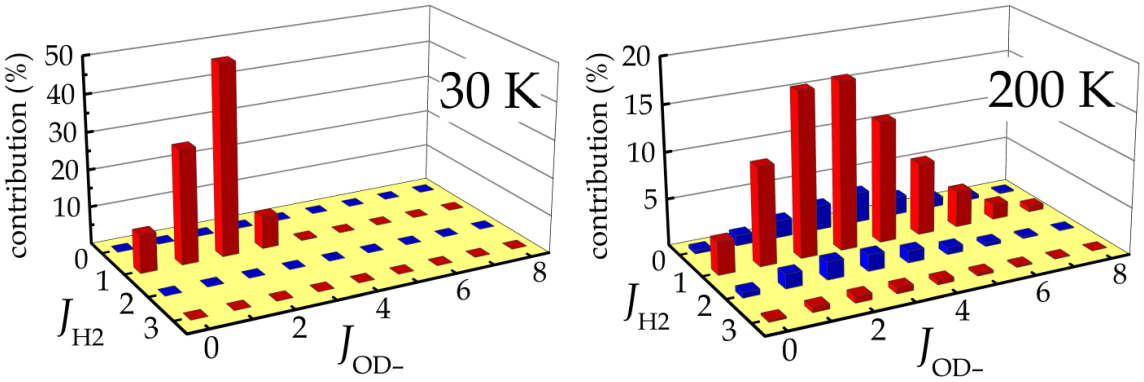

Figure 5.23. Contributions of the rotational levels of reactants J_{H2}, J_{OD^-} to the overall rate coefficient k_{OD} at reaction temperatures 30 K (*left panel*) and 200 K (*right panel*).

Comparing this model to the pure Arrhenius fit, one can note that the agreement between two models is excellent. At the same time, the advantage of this approach is that it fully agrees with theory because the theoretical endothermicity value ΔH = 24.0 meV was used here as a fixed parameter.

5.2.3 Associative detachment and charge transfer channels of D^- + H reaction

After the first report of the experimental H^- + H associative detachment reaction rate coefficients at interstellar-relevant temperatures [*Gerlich et al., 2012*], an analogue ion trap study of D^- + H reaction was carried out. D^- ions for the experiment were produced in the ion source via dissociative attachment reaction

$$D_2 + e^- \rightarrow D^- + D \qquad (5.24)$$

and were confined there by 3.2 MHz RF field.

After the mass-selection and injection of D^- ions into the trap they reacted with H in the beam and produced either HD in associative detachment reaction (3.22) or H^- in the charge transfer reaction (3.23) (figure 5.24). At the same time, produced H^- ions also reacted with H atoms, producing H_2.

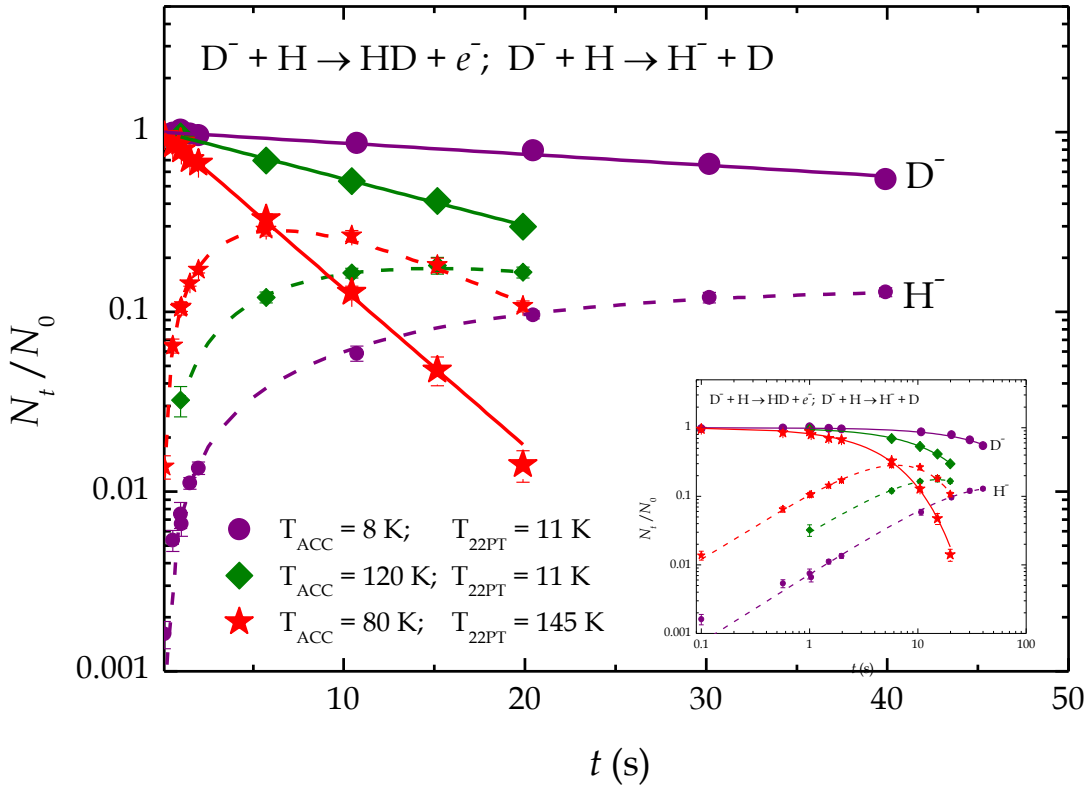

Figure 5.24. The time evolution of normalised numbers of trapped D^- and H^- ions. The same data in log-log scale is in the insert. The measurements were conducted with different combinations of the trap (T_{22PT}) and accommodator (T_{ACC}) temperatures. The larger symbols denote D^- number and the smaller symbols denote H^- number. The respective fits with the theoretical curves (5.25) and (5.26) are indicated by the solid and dashed lines.

If we mark the rate coefficient of the associative detachment reaction (3.22) as k_{AD}, charge transfer reaction (3.23) as k_{CT}, and associative detachment reaction of H^- with H (3.2) as k_{HH}, the chemical kinetics of all the processes in the trap can be written with the following balance equations:

$$\frac{dN(\mathrm{D}^-)}{\mathrm{d}t} = -k_{\mathrm{AD}} \cdot N(\mathrm{D}^-) \cdot [\mathrm{H}] - k_{\mathrm{CT}} \cdot N(\mathrm{D}^-) \cdot [\mathrm{H}], \tag{5.25}$$

$$\frac{dN(\mathrm{H}^-)}{\mathrm{d}t} = -k_{\mathrm{HH}} \cdot N(\mathrm{H}^-) \cdot [\mathrm{H}] + k_{\mathrm{CT}} \cdot N(\mathrm{D}^-) \cdot [\mathrm{H}], \tag{5.26}$$

where [H] is effective number density of the H-atom beam (see subchapter 4.2.4), $N(\mathrm{H}^-)$ is number of detected H^- ions, $N(\mathrm{D}^-)$ is number of detected D^- ions. Fitting equations (5.25) and (5.26) with already known value k_{HH} can provide us with unknown coefficients k_{AD} and k_{CT}.

The ion distribution in the trap usually changes with trap temperature $T_{22\mathrm{PT}}$. The behaviour of the ion cloud was checked using the photodetachment reactions of D^- and H^- ions with an expanded laser beam:

$$\mathrm{D}^-(\mathrm{H}^-) + h\nu \rightarrow \mathrm{D}(\mathrm{H}) + e^-. \tag{5.27}$$

The expanded laser beam (655 nm, 200 mW) was comparable to the H-atom beam in diameter, approximately 1 cm. The scheme of the experiment with the laser beam is shown in figure 5.25.

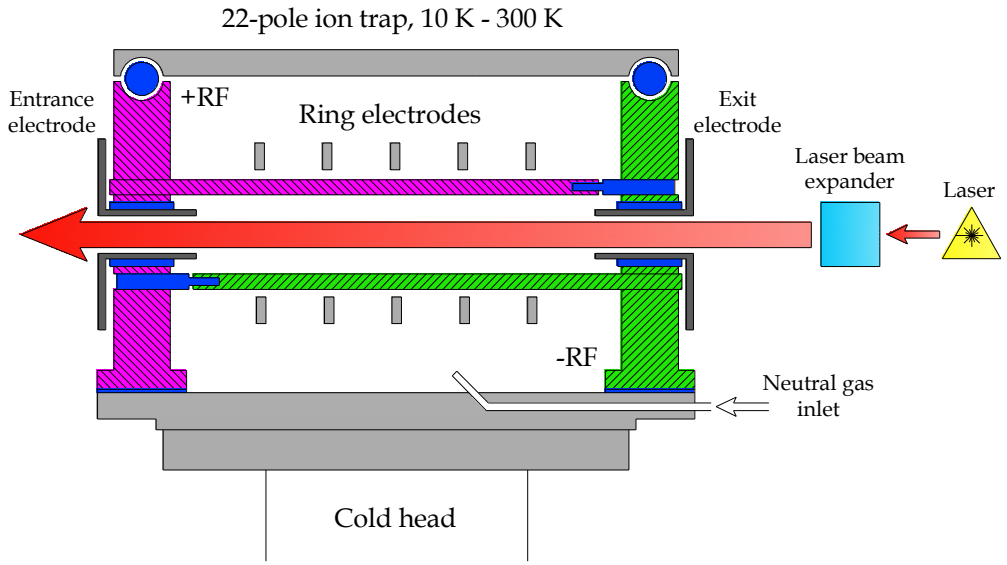

Figure 5.25. Scheme of the photodetachment $\mathrm{D}^-(\mathrm{H}^-) + h\nu$ experiment. The laser beam after expansion remained almost homogeneous. It scanned the trap volume and photodetached D^- and H^- ions.

The results of the experiment can be seen in figure 5.26. At higher temperatures of the trap an ion cloud seemed to be located in the volume that completely crosses the laser beam and, consequently, the H-atom beam. At the same time, the study showed that below 60 K the cross-section of the ion cloud with the beam lowered and the ions began to move into a «blind» zone. The discrepancy between the photodetachment rates of D^- and H^- at these temperatures may be due to the sensitivity of the ion distribution to very small variations of the effective potential in the order of meV.

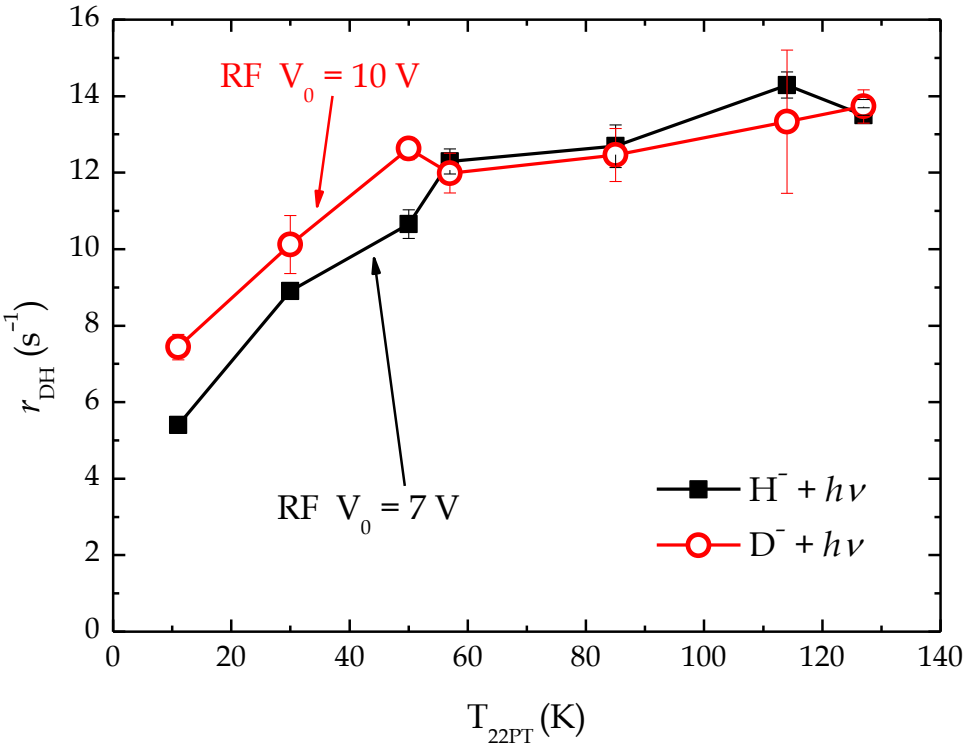

Figure 5.26. The dependence of the photodetachment rate of D^- and H^- on temperature of the trap. The measured data indicate that at temperatures of the trap lower than 60 K we can observe a shift of the ion cloud into the «blind» zone of the trap. 10 V and 7 V peak-to-peak signal amplitudes on the RF generator were used in the measurements of D^- and H^- photodetachment rates, respectively.

As well as that, comparing of the loss ratios of D^- and H^- reaction with H, measured at the same reaction temperatures with T_{22PT} = 11 K and with T_{22PT} > 60 K, yielded that the discrepancy between the loss rates was also

~1.63. Hence, the intermediate trap temperatures 11 K < T_{22PT} < 60 K were not used in the present experiment, the measurements with T_{22PT} = 11 K were corrected by the respective coefficient.

The efficiency of the confining of ions in the trap is different for ions with different masses, so, the shapes of ion clouds of D^- and H^- are also different. This is obvious from the concept of effective potential, which affects the trapped ions, described in chapter 4.1. For precise calculation we needed to have the similar conditions of the reactions of both D^- and H^- with H that could be reached by applying the same effective potential V^* to both ions. Hence, if we assume $V^*_{D^-} = V^*_{H^-}$, the following relations are valid for a certain point in the trap:

$$\frac{(V_0^2)_{D^-}}{m_{D^-}} = \frac{(V_0^2)_{H^-}}{m_{H^-}}, \tag{5.28}$$

$$(V_0)_{D^-} = (V_0)_{H^-}\sqrt{\frac{m_{D^-}}{m_{H^-}}}, \tag{5.29}$$

where V_0 is RF amplitude, m_{D^-} and m_{H^-} are atomic masses of D^- and H^-.

As D^- mass is twice higher than that of H^-, we repeated each measurement twice with 10 V peak-to-peak RF signal amplitude and 7 V RF signal amplitude on the generator ($10 \approx 7 \cdot \sqrt{2}$, see equation (5.29)). In figure 5.26 one can also note that the photodetachment rates of D^- and H^- ions are almost equal, except from some discrepancy below 60 K.

In the experiment the temperatures of the D^- and H reactants were defined by the temperatures of the trap and H-atom source accommodator, respectively (see subchapters 4.2.4, 4.2.5). Hence, the reaction temperature T was set by changing the respective temperatures and it was calculated according to the following expression:

$$T = \frac{T_{D^-} m_H + m_{D^-} T_H}{m_H + m_{D^-}}, \tag{5.30}$$

where m_H and m_{D^-} were masses of H and D^-, T_H and T_{D^-} were temperatures of H and D^-. Further in the chapter we will use the denotation T or T(K) for this reaction temperature. The used temperatures of the 22PT was 11 K and in the range from 60 K to 190 K. The temperatures of the H-atom source accommodator were 7 K and 50 K – 150 K due to technical reasons mentioned in subchapter 4.2.4.

The ratio between the overall rate coefficient ($k_{AD} + k_{CT}$) of the reaction $D^- + H$ and the rate coefficient k_{HH} of the AD reaction of H^- with H (3.2) was calculated from the decays in figure 5.24 using the expressions (5.25) and (5.26). The results after averaging and correction are presented in figure 5.27. Error bars are caused by low H-atom beam number density and hence, low measurement statistics.

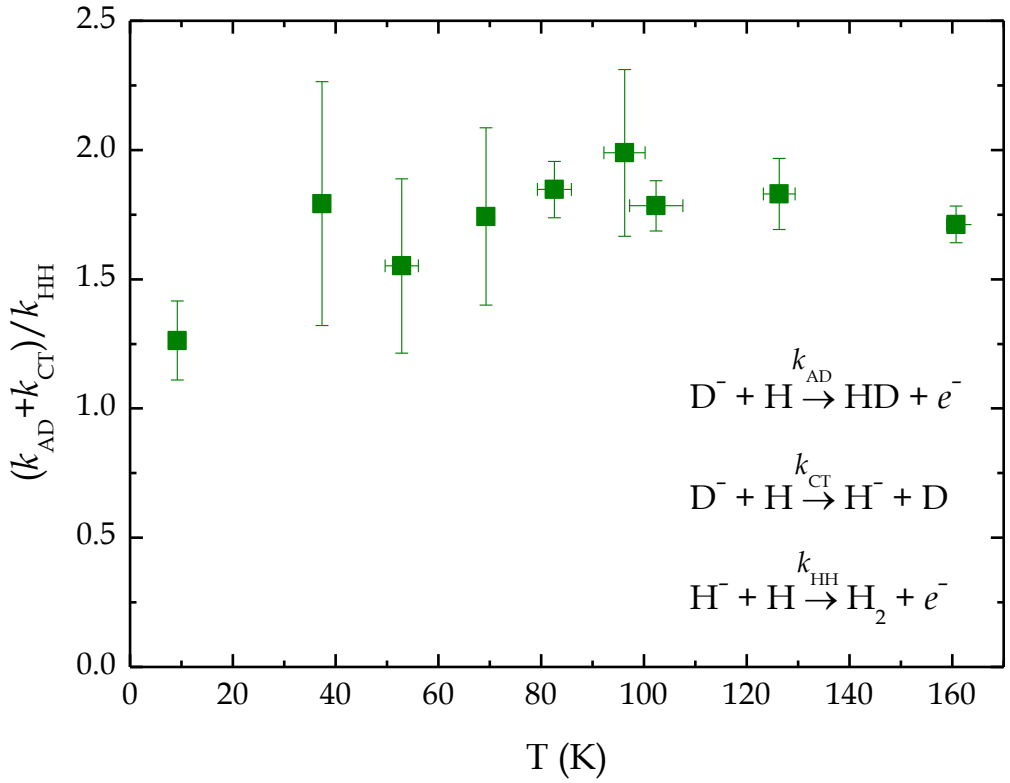

Figure 5.27. The dependence of the ratio between the rate coefficient ($k_{AD} + k_{CT}$) of the reaction $D^- + H$ and the rate coefficient k_{HH} of the AD reaction $H^- + H$ (3.2) on reaction temperature. Data are averaged and corrected according to the results of the study of photodetachment of D^- and H^- ions in the trap.

As well as total rate coefficient, the branching ratio between charge transfer (3.23) and associative detachment (3.22) rate coefficients was also calculated from the measured data. The charge transfer channel had dominating tendency with increasing temperature and reached 90% at 160 K (figure 5.28).

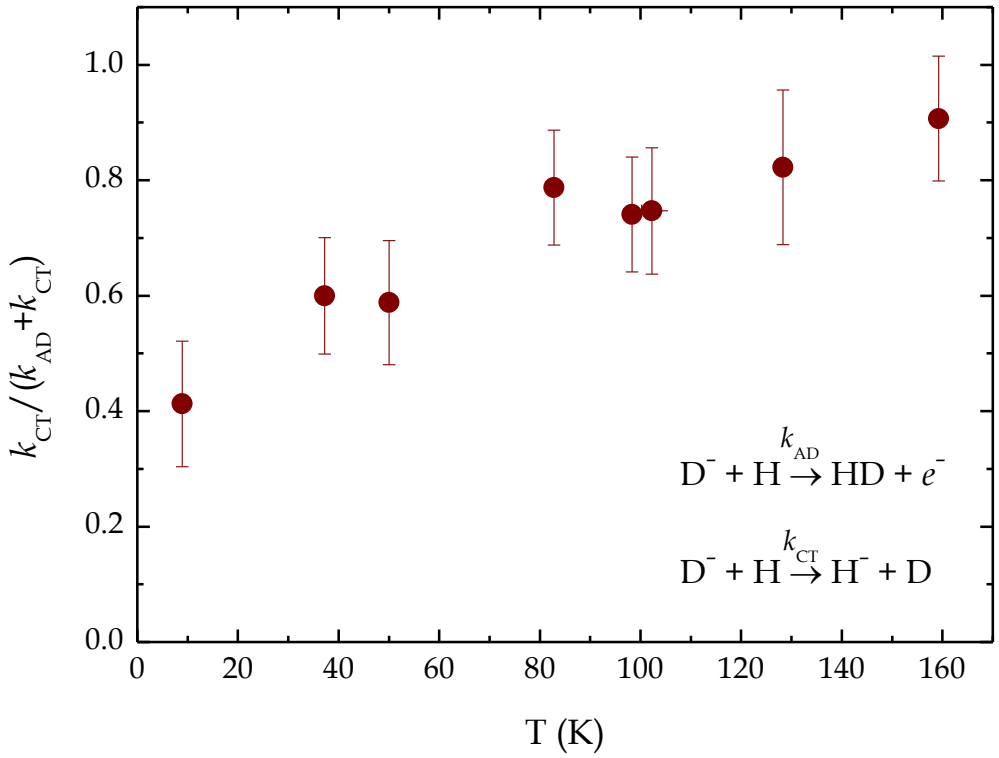

Figure 5.28. The dependence of the branching ratio between the charge transfer (3.23) rate coefficient k_{CT} and the overall rate coefficient ($k_{AD} + k_{CT}$) of the D^- + H reaction on reaction temperature.

According to the data shown in figures 5.27 and 5.28 and known values of the rate coefficient of the reaction (3.2), the rate coefficients of both AD and CT channels (3.22), (3.23) of D^- + H interaction were calculated. In figure 5.29 the dependencies of k_{AD} and k_{CT} on reaction temperature in the range of 10 K – 160 K are shown in comparison with the data on the previously studied reaction (3.2). H^- data are consistently increasing in the whole studied temperature range, while the rate coefficient for D^- association with H decreases above 60 K. At the relevant temperatures, the theoretical cross-

sections for AD of H^- + H and D^- + H are nearly identical [*Eliášek, 2014*] and the differences in rate coefficients are simply due to the different thermal velocities of D^- and H^-. The difference in the behaviour of AD reactions (3.22) and (3.2) still remains an open question.

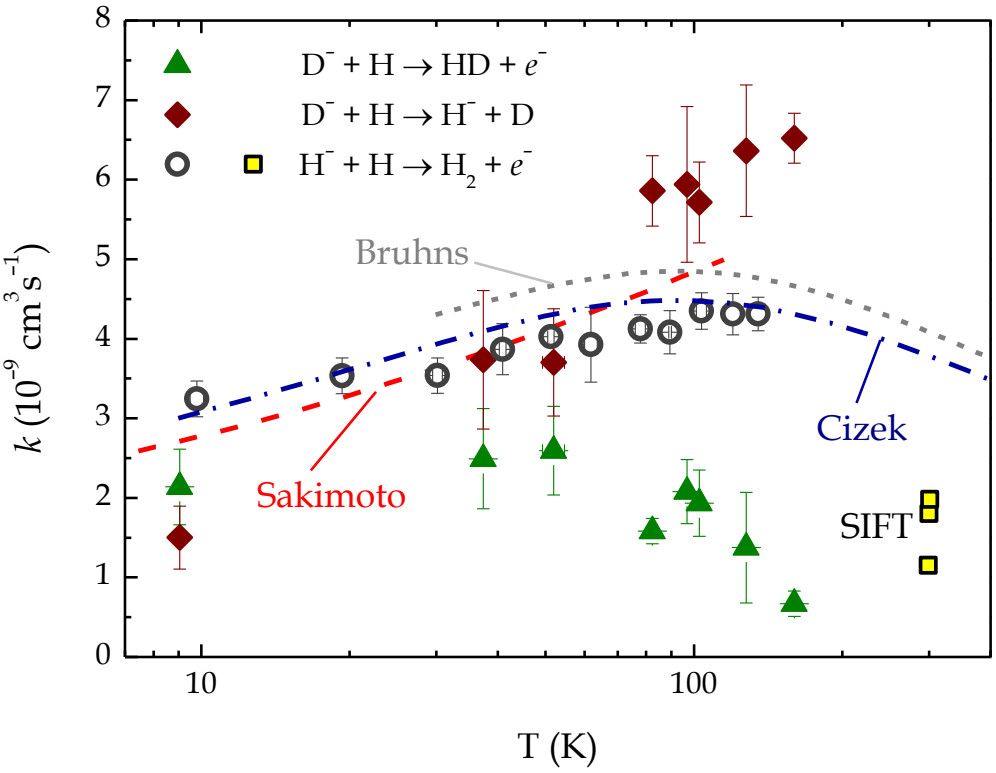

Figure 5.29. Comparison of the measured rate coefficients of D^- + H (closed diamonds and triangles) with previously measured AD H^- + H reaction rate coefficient (open circles – trap experiment, closed squares – SIFT experiment, short dashed line – merged beams experiment) and theoretically calculated rate coefficients (dashed and dash-dotted lines) for the H^- + H reaction (the respective references are given in the description of figure 3.1).

As well as in O^- + H_2/D_2 experiments, theoreticians provided us with quantum-mechanical study of the dynamics of H^- + H collision complex together with all its isotopic variants (D^- + H, H^- + D, D^- + D).

In figure 5.30 we can see the calculated rate coefficients for both charge transfer and associative detachment channels (dashed and dash-dot-dotted lines, respectively). The result for CT is in very good agreement with the

measured data. However, in case of AD channel theoretical values and experimental data have similar behaviour, but the discrepancy between them begins to increase with increasing temperature. This discrepancy still remains an open question, but it may be partly due to uncertainty of the discrimination of ions.

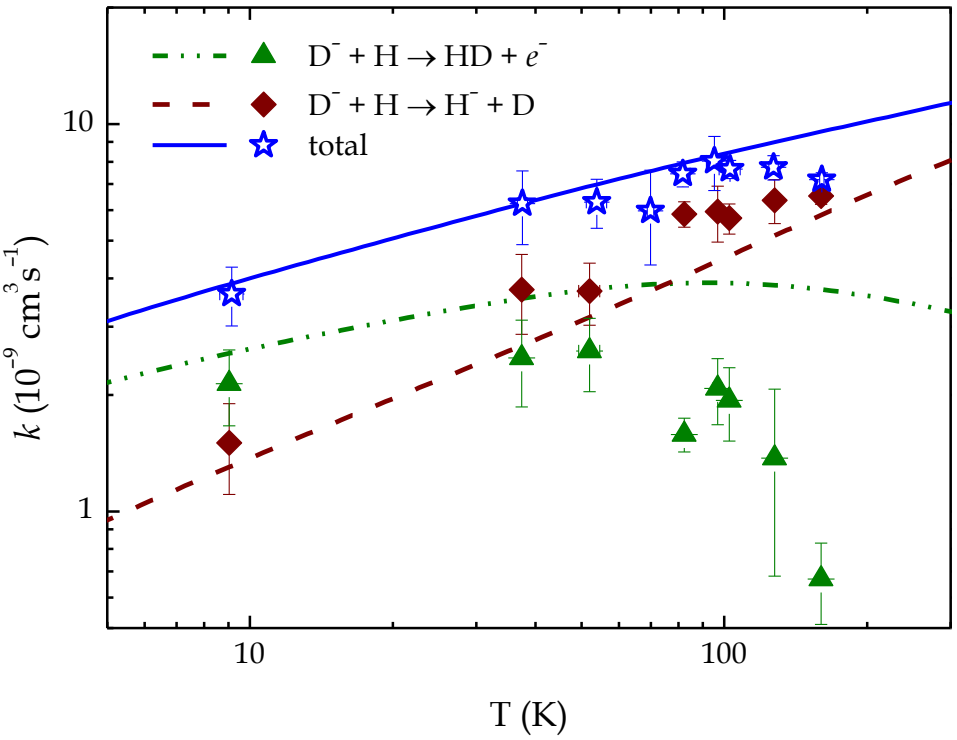

Figure 5.30. Comparison of the measured (closed diamonds and triangles and open stars) and calculated (dashed, dash-dot-dotted, and solid lines) rate coefficients for the reaction of D^- with H [*Eliášek, 2014*].

Deep theoretical insight in the study of H^- + H collision complexes and its isotope variations, including D^- + H, can be found in [*Eliášek, 2014*].

6 Summary

This section summarises all the materials presented in the thesis and gives some outlines for the future projects. This work is focused on the experimental study of the gas-phase ion-molecule reactions with atomic and molecular hydrogen and molecular deuterium at interstellar-relevant temperatures.

Studying hydrogen-containing ion-molecule reactions is essential for the astrochemistry. Their importance is specified not only by the high abundance of hydrogen in the Universe, but also by the fact that these reactions are an effective source of more complex ions and molecules in space (such as H_3^+, H_2, HD, H_2O, NH_3, etc.) due to the absence of energy barriers at typical astrochemical temperatures (10 K – 100 K).

All the results presented in the thesis were obtained in a research team. In the experiments studying the reactions of N^+, H^+, and O^- ions with hydrogen, I was involved in the experimental routine and data analysis. Afterwards I was in charge of conducting the majority of experiments with $OH^- + D_2$, $OD^- + H_2$, and $D^- + H$ reactions and I participated in the data analysis and preparation of the publications. The rate coefficients for the majority of the studied reactions (except for $N^+ + H_2$) reported by our group are the first experimental data on these reactions at temperatures below 77 K (the temperature of the liquid nitrogen).

The sections *Theoretical background* and *Experimental techniques* give some theoretical, methodological, technological, and constructional aspects of the experimental work. Such issues as importance of ion-molecule reactions for astrochemistry, isotope effect, nuclear spin state configuration of hydrogen and its influence on the reaction dynamics are discussed.

Constructional features of the AB-22PT apparatus and of the generator of para-enriched hydrogen are also presented there.

The $N^+(^3P_{ja}) + H_2(J)$ reaction for $J = 0$ and $J = 1$ was studied in range of temperatures 11 K – 100 K (subchapter 5.1.1). This reaction is endothermic, so it is quite sensitive to the nuclear spin state configuration of H_2. The reaction was also used as a probe of ortho-fraction in the used p/o-H_2 mixture. The obtained results are in some disagreement with the previous data, it could be explained by different reactivity of N^+ ion in different fine structure states. A kinetic model that includes the reactivity of the separate fine structure levels and collisional relaxation of the $N^+(^3P_{ja})$ levels was used to describe the studied reaction. The deep insight can be found in [*Zymak et al., 2013*]. The measurements of the rate coefficient of the inverse reaction $NH^+ + H$ are in progress now.

Another study that included measurements of the state-specific rate coefficients was the study of binary radiative and ternary association of H^+ and H_2 at temperatures 11 K – 44 K (subchapter 5.1.2). The experiments with a wide range of H_2 number densities (~10^{11} cm^{-3} – 10^{14} cm^{-3}) allowed us to obtain reaction rate coefficients for both channels. The positive temperature dependence of the ternary rate coefficient for para-enriched hydrogen was observed. The probable explanation may be that the approaching H_2 pulls out the proton from the excited $(H_3^+)^*$ complex in many cases instead of stabilising the collision complex. The ternary rate coefficient for pure ortho-hydrogen is considerably lower than that for para that is obvious from figure 5.8 and figure 5.9.

The interpretation of the results for binary radiative association is far harder due to the larger errors, but in both cases with n-H_2 and e-H_2 it has negative temperature dependence that is in accordance with theoretical predictions. The details of the experiments, studying association of H^+ ion with n-H_2 and e-H_2, were published in [*Plašil et al., 2012*] and [*Gerlich et al., 2013*].

Studies of the reactions of negative ions in this work touched the studies of H_2O formation, isotope effects, and isotope exchange reactions. The results of the study of AD reaction of O^- with H_2 in the range of temperatures from 11 K to 300 K are presented in subchapter 5.2.1. The measured reaction rate coefficient at 300 K is in general accordance with the previously measured values. Furthermore, the experimental data are in good agreement with the calculated capture rates for the reaction (3.6). Apart from H_2O formation, $O^- + H_2$ reaction has another H atom transfer channel with ~5% contribution. Such low value is caused by passing of its reaction path through autodetachment region, hence, the reaction paths, which avoid the autodetachment, have the respective low probabilities. The study of $O^- + H_2$ reaction was conducted in collaboration with theoreticians from the Institute of Theoretical Physics and the results are published in [*Jusko et al., 2015*].

Beyond the simple Langevin theory, experiments with deuterium shows no isotope effect for AD channel, whereas the formation of $OD^- + D$ proceeds approximately three times slower than the formation of $OH^- + H$ at 200 K. The experiments with p/o-H_2 are going to be carried out for further progress in the understanding of H_2O formation.

The isotope-exchange exothermic reaction $OH^- + D_2$ and endothermic reaction $OD^- + H_2$ were studied at temperatures, ranging from 11 K to 275 K (subchapter 5.2.2). Consequently, we obtained different temperature dependencies of the respective reaction rate coefficients. The measured reaction rate coefficient k_{OH} of the exothermic reaction of OH^- with D_2 (reaction (3.27)) has negative temperature dependence, which can be expressed by a power law function $k_{OH} \sim T^{-m}$, where $m = 2.7$ (see figure 3.6). That may confirm that the studied H/D exchange reaction proceeds via formation of a long-lived complex and the lifetime of this complex determines the kinetics of this reaction.

The negative temperature dependence of the reaction rate coefficient can be also discussed in terms of the state selectivity of the reaction, i.e., the reactivity is dependent on rotational excitation of D_2, as proposed in

[*Viggiano and Morris, 1994*]. This would be in agreement with the conclusion of [*Lee and Farrar, 2000*] that the reaction takes place only with preferable alignment of OH^- and D_2, when D_2 in $J = 0$ state adjusts its orientation into reactive position. The rotational excitation of D_2 disrupts such alignment. In our experiment it is valid below 60 K only, the decrease of the measured data at higher temperatures is faster than the decrease of population of $D_2(J = 0)$.

The endothermicity of the $OD^- + H_2$ reaction causes its positive temperature dependence. The fit by the Arrhenius function gives pre-exponential factor $k_{OD}^{A} = 7.5 \cdot 10^{-11}$ cm^3 s^{-1} and Arrhenius activation energy $E_{OD}^{A} = 7.9$ meV. The obtained value is quite close to the enthalpy change of the reaction of OD^- with $H_2(J = 1)$, whose population is 75% in the experiment with normal hydrogen. The respective state-specific rate coefficient for the reaction (3.28) with ortho-hydrogen at low temperatures results in a dependence ${}^{o}k_{OD} = 1 \cdot 10^{-10} e^{-\frac{92\,K}{T}}$ cm^3 s^{-1}.

The measured data were also fitted with function (5.23), which included contributions from all populated states of reactants at given temperature under assumption that all states contributed with the same pre-exponential factor k_{OD}^{0} and all energies were equivalent in reducing the endothermicity of the reaction. This fit has an excellent accordance with the Arrhenius-type fit (figures 5.21, 5.22) and theoretical predictions. The results of the research of H/D exchange in H_3O^- isotope reaction complex are published in [*Mulin et al., 2015*].

Finally, the interaction between D^- and H was studied using the source of an effusive H-atom beam (subchapter 5.2.3). This work is a logical sequel of the H^- + H experiment carried out in our laboratory in 2011 [*Gerlich et al., 2012*]. D^- + H has associative detachment and charge transfer channels and the rate coefficients for both of them are reported at reaction temperatures from 10 K to 160 K. The charge transfer channel has dominating tendency throughout the whole temperature range and reaches 90% at 160 K. The discrepancy between the rate coefficients of the associative detachment reactions of H^- and D^- with H also increases with temperature. Theoretical

study of the dynamics of $D^- + H$ collision complexes has recently been performed by J. Eliášek [*Eliášek, 2014*]. In the studied temperature range, the theoretical cross-sections for associative detachment $H^- + H$ and $D^- + H$ reactions are nearly equal, hence, the differences in the respective theoretical rate coefficients are caused just by the different thermal velocities of D^- and H^-.

One can note good overall agreement of theoretical rate coefficients with the measured values for both channels that also proves the reliability of the experiment. The difference between the calculated and measured rate coefficients for $D^- + H$ associative detachment reaction (3.22) may be partly due to uncertainty of the discrimination of ions (see subchapter 4.2.2). The publication, summarising experimental and theoretical insight into the interaction of D^- with H, is in preparation at the current moment [*Roučka et al., 2015*].

Bibliography

Adams N. G., Smith D., and Henchman M. J. (1982), Isotope Exchange in the Reactions $H_3O^+ + D_2O$, $NH_4^+ + ND_3$, $CH_5^+ + CD_4$ and Their Mirror Reactions at Thermal Energies, *International Journal of Mass Spectrometry and Ion Physics*, **42**, 11.

Adams N. G. and Smith D. (1985), A Study of the Nearly Thermoneutral Reactions of N^+ with H_2, HD and D_2, *Chemical Physics Letters*, **117**, 67.

Aguado A., Barragán P., Prosmiti R., Delgado-Barrio G., Villarreal P., and Roncero O. (2010), A New Accurate and Full Dimensional Potential Energy Surface of H_5^+ Based on a Triatomic-in-Molecules Analytic Functional Form, *The Journal of Chemical Physics*, **133**, 024306.

Anicich V. G. (2003), *An Index of the Literature for Bimolecular Gas Phase Cation-Molecule Reaction Kinetics*, NASA JPL – Pasadena.

Arnett D. (1996), *Supernovae and Nucleosynthesis: An Investigation of the History of Matter, from the Big Bang to the Present*, Princeton University Press – New Jersey. ISBN 0-691-01148-6.

Aston F. W. (1927), Bakerian Lecture. A New Mass-Spectrograph and the Whole Number Rule, *Proceedings of the Royal Society of London A*, **115**, 487.

Asvany O. (2003), Experiments with Ions and Clusters in a Variable Temperature 22-pole Ion Trap, PhD thesis, Technische Universität Chemnitz.

Asvany O., Schlemmer S. (2009), Numerical Simulations of Kinetic Ion Temperature in a Cryogenic Linear Multipole Trap, *International Journal of Mass Spectrometry*, **279**, 147.

Beaty E. C. and Patterson P. L. (1965), Mobilities and Reaction Rates of Ions in Helium, *Physical Review*, **137**(**2A**), A346.

Bergin E., Blake G., Goldsmith P., Harris A., Melnick G., Zmuidzinas J. (2008), *Water in Space: Comets and the Interstellar Medium*, SOFIA Science Steering Committee Design Reference Mission Study.

Birge R. T. and Menzel D. H. (1931), The Relative Abundance of the Oxygen Isotopes and the Basis of the Atomic Weight System, *Physical Review*, **37**, 1670.

Borodi G. (2008), On the Combination of a Low Energy Hydrogen Atom Beam with a Cold Multipole Ion Trap, PhD thesis, Technische Universität Chemnitz.

Böhringer H., Glebe W., Arnold F. (1983), Temperature Dependence of the Mobility and Association Rate Coefficient of He^+ Ions in He from 30 – 350 K, *Journal of Physics B: Atomic and Molecular Physics*, **16**, 2619.

Bruhns H., Kreckel H., Miller K. A., Urbain X., and Savin D. W. (2010), Absolute Energy-Resolved Measurements of the $H^- + H \rightarrow H_2 + e^-$ Associative Detachment Reaction Using a Merged-Beam Apparatus, *Physical Review A*, **82**, 042708-1.

Brünken S., Gupta H., Gottlieb C. A., McCarthy M. C., and Thaddeus P. (2007), Detection of the Carbon Chain Negative Ion C_8H^- in TMC-1, *The Astrophysical Journal Letters*, **664.1**, L43.

Buntkowsky G., Walaszek B., Adamczyk A., Xu Y., Limbach H.-H., and Chaudret B. (2006), Mechanism of Nuclear Spin Initiated para-H_2 to ortho-H_2 Conversion, *Physical Chemistry Chemical Physics*, **8**, 1929.

Carelli F. (2011), Molecular Anions in Circumstellar Envelopes, Interstellar Clouds and Planetary Atmospheres: Quantum Dynamics of

Formation and Evolution, PhD thesis, University of Rome «Sapienza».

Cernicharo J., Guélin M., Agündez M., Kawaguchi K., McCarthy M., and Thaddeus P. (2007), Astronomical Detection of C_4H^-, the Second Interstellar Anion, *Astronomy and Astrophysics*, **467**, L37.

Čížek M., Horáček J., and Domcke W. (1998), Nuclear Dynamics of the H_2^- Collision Complex Beyond the Local Approximation: Associative Detachment and Dissociative Attachment to Rotationally and Vibrationally Excited Molecules, *Journal of Physics B: Atomic, Molecular and Optical Physics*, **31**, 2571.

Cremer E. and Polanyi M. (1932), Eine Prüfung der «Tunneltheorie» der Heterogenen Katalyse am Beispiel der Hydrierung von Styrol, *Zeitschrift für Physikalische Chemie*, **B19**, 443.

Dalgarno A. (1994), Terrestrial and Extraterrestrial H_3^+, *Advances in Atomic, Molecular, and Optical Physics*, **32**, 57.

Dislaire V., Hily-Blant P., Faure A., Maret S., Bacmann A., and Pineau des Forêts G. (2012), Nitrogen Hydrides and the H_2 ortho-to-para Ratio in Dark Clouds, *Astronomy and Astrophysics*, **537**, A20.

Eliášek J. (2014), Collisions of Negative Particles with Atoms and Molecules, PhD thesis, Charles University in Prague.

Eyring H. and Sherman A. (1933), Theoretical Considerations Concerning the Separation of Isotopes, *The Journal of Chemical Physics*, **1**, 345.

Fehsenfeld F. C., Howard C. J., and Ferguson E. E. (1973), Thermal Energy Reactions of Negative Ions with H Atoms in the Gas Phase, *The Journal of Chemical Physics*, **58**, 5841.

Ferguson E. E. (1975), Ion-Molecule Reactions, *Annual Review of Physical Chemistry*, **26**, 17.

Ferriere K. M. (2001), The Interstellar Environment of Our Galaxy, *Reviews of Modern Physics*, **73**, 1031.

Field G. B., Somerville W. B., Dressler K. (1966), Hydrogen Molecules in Astronomy, *Annual Review of Astronomy and Astrophysics*, **4**, 207.

Gerlich D. (1989), Reactive Scattering of $N^+ + H_2$ and Deuterated Analogs: Statistical Calculation of Cross Sections and Rate Coefficients, *The Journal of Chemical Physics*, **90**, 3574.

Gerlich D. and Kaefer G. (1989), Ion Trap Studies of Association Processes in Collisions of CH_3^+ and CD_3^+ with n-H_2, p-H_2, D_2, and He at 80 K, *The Astrophysical Journal*, **347**, 849.

Gerlich D. (1990), Ortho-para Transitions in Slow $H^+ + H_2$ Collisions, *The Journal of Chemical Physics*, **92**, 2377.

Gerlich D., Kaefer G., Paul W. (1990), Ion Trap Studies of Ternary and Radiative Association Processes, *Symposium on Atomic and Surface Physics*, edited by T. D. Märk and F. Howorka, Obertraun, 332.

Gerlich D. (1992), Inhomogeneous Electrical Radio Frequency Fields: A Versatile Tool for the Study of Processes with Slow Ions, in: *State-Selected and State-to-State Ion-Molecule Reaction Dynamics*, *Advances in Chemical Physics Series LXXXII*, edited by C. Y. Ng and M. Baer, Wiley & Sons. ISBN 0-471-53258-4.

Gerlich D. and Horning S. (1992), Experimental Investigation of Radiative Association Processes as Related to Interstellar Chemistry, *Chemical Reviews*, **92**(**7**), 1509.

Gerlich D. (1993), General Discussion, *Journal of the Chemical Society, Faraday Transactions*, **89**, 2199.

Gerlich D. (1994), Recent Progress in Experimental Studies of Ion−Molecule Reactions Relevant to Interstellar Chemistry, in *Molecules and Grains in Space*, edited by I. Nenner, AIP Press – New York. ISBN 1-56396-355-8.

Gerlich D. (1995), Ion-Neutral Collisions in a 22-Pole Trap at Very Low Energies, *Physica Scripta*, **T59**, 256.

Gerlich D. (2008), The Study of Cold Collisions Using Ion Guides and Traps, in *Low Temperatures and Cold Molecules*, edited by I. W. M. Smith, Imperial College Press – Singapore. ISBN-13 978-1-84816-209-9.

Gerlich D., Jusko P., Roučka Š., Zymak I., Plašil R., and Glosík J. (2012), Ion Trap Studies of $H^- + H \rightarrow H_2 + e^-$ Between 10 and 135 K, *The Astrophysical Journal*, **749**, 22.

Gerlich D., Plašil R., Zymak I., Hejduk M., Jusko P., Mulin D., Glosík J. (2013), State Specific Stabilization of $H^+ + H_2(J)$ Collision Complexes, *The Journal of Physical Chemistry A*, **117**(**39**), 10068.

Giauque W. F. and Johnston H. W. (1929), An Isotope of Oxygen of Mass 18, *Nature*, **123**, 318.

Glosík J., Freysinger W., Hansel A., Španěl P., and Lindinger W. (1993), Energy Dependencies of Fast Reactions of Positive Ions X^+ with HCl from Near Thermal to ≈2 eV Center-of-Mass Collision Energy ($X^+ = H^+, H_2^+, H_3^+, N^+, N_2^+, AR^+, C^+, CH^+, CH_2^+, CH_3^+, CH_4^+, CH_5^+$), *The Journal of Chemical Physics*, **98**, 6995.

Glosík J. (1994), Measurement of the Reaction Rate Coefficients of Reactions of H_2^+ with Ne, Ar, Kr, Xe, H_2, D_2, N_2, and CH_4 at Thermal Energy, *International Journal of Mass Spectrometry*, **139**, 15.

Glosík J., Zakouřil P., and Lindinger W. (1995[a]), Selected Ion Flow Drift Tube Studies of the Reaction of $Si^+(^2P)$ with C_2H_4. Observation of the Ternary Reaction with Two Channels: Collisional Stabilization and Collisional Dissociation, *International Journal of Mass Spectrometry*, **145**, 155.

Glosík J., Zakouřil P., V. Skalský, and Lindinger W. (1995[b]), Selected Ion Flow Drift Tube Studies of the Kinetics of the Reactions of $Si^+(^2P)$ with C_2H_2 and C_6H_6, *International Journal of Mass Spectrometry*, **149**, 499.

Glosík J., Zakouřil P., and Lindinger W. (1995[c]), Selected Ion Flow Drift Tube Studies of the Reactions of $Si^+(^2P)$ with HCl, H_2O, H_2S, and NH_3: Reactions Which Produce Atomic Hydrogen, *The Journal of Chemical Physics*, **103**, 6490.

Glosík J., Zakouřil P., and Luca A. (2003), The Reaction of SiH^+ and SH^+ with Small Molecules, *International Journal of Mass Spectrometry*, **223**, 539.

Glover S. C., Savin D. W., and Jappsen A. (2006), Cosmological Implications of the Uncertainty in H^- Destruction Rate Coefficients, *The Astrophysical Journal,* **640**, 553.

Glover S. and Abel T. (2008), Uncertainties in H_2 and HD Chemistry and Cooling and Their Role in Early Structure Formation, *Monthly Notices of the Royal Astronomical Society*, **388**, 1627.

Grabowski J. J., DePuy C. H., and Bierbaum V. M. (1983), Gas-Phase Hydrogen-Deuterium Exchange Reactions of HO^- and DO^- Ions with Weakly Acidic Neutrals, *Journal of the American Chemical Society*, **105**, 2565.

Graham E., James D. R., Keever W. C., Gatland I. R., Albritton D. L., McDaniel E. W. (1973), Measurement of the Rate Coefficient of the Reactions $H^+ + 2\ H_2 \rightarrow H_3^+ + H_2$ and $D^+ + 2\ D_2 \rightarrow D_3^+ + D_2$ in a Drift Tube Mass Spectrometer, *The Journal of Chemical Physics*, **59**, 4648.

Graul S. T., Brickhouse M. D., and Squires R. R. (1990), Deuterium Isotope Fractionation Within Protonated Water Clusters in the Gas Phase, *Journal of the American Chemical Society*, **112**, 631.

Hackam R. and Lennon J. J. (1964), Positive Ion Mobilities and Conversion Rates in a Helium Afterglow, *Proceedings of the Physical Society*, **84**(**1**), 133.

Heap S. and Stecher T. (1974), Two New Physical Processes in the Far-Ultraviolet Spectrum of Zeta Tauri, *The Astrophysical Journal Letters*, **187**, L27.

Hejduk M. (2013), Reactions of Hydrogen Molecules with Ions and Recombination of H_3^+ Ions with Electrons at Cryogenic Temperatures, PhD thesis, Charles University in Prague.

Henchman M. and Paulson J. F. (1988), The Gas-Phase and Solution Mechanism of the Isotope Exchange Reaction $OH^- + D_2 \rightarrow OD^- + HD$: Beam Study of the Solvated-Ion Reaction OH^-

·$H_2O + D_2$ in the Collision Energy Range 0 – 2 eV, *Radiation Physics and Chemistry*, **32**, 417.

Herbst E. (2001), The Chemistry of Interstellar Space, *Chemical Society Review,* **30**, 168.

Herbst E. and Klemperer W. (1973), The Formation and Depletion of Molecules in Dense Interstellar Clouds, *The Astrophysical Journal,* **185**, 505.

Hogan J. C. (1996), Primordial Deuterium and the Big Bang, *Scientific American*, **Dec96**, 68.

Hoyle F. and Fowler W.A. (1973), On the Origin of Deuterium, *Nature*, **241**, 384.

Huber K. and Herzberg G. (1979), *Molecular Spectra and Molecular Structure: Constants of Diatomic Molecules, vol. IV*, Van Nostrand Reinhold – New York. ISBN 0-442-23394-9.

Hunt D. F. and Sethi S. K. (1980), Gas-Phase Ion/Molecule Isotope-Exchange Reactions: Methodology for Counting Hydrogen Atoms in Specific Organic Structural Environments by Chemical Ionization Mass Spectrometry, *Journal of the American Chemical Society*, **102**, 6953.

Irikura K. K. (2007), Experimental Vibrational Zero-Point Energies: Diatomic Molecules, *The Journal of Physical Chemistry Reference Data*, **36**, 389.

Johnsen R., Huang C.-M., and Biondi M. A. (1976), Three-Body Association Reactions of H^+ and H_3^+ Ions in Hydrogen from 135 to 300 K, *The Journal of Chemical Physics*, **65**(**4**), 1539.

Johnsen R., Chen A., and Biondi M. A. (1980), Three-Body Association Reactions of He^+, Ne^+, and Ar^+ Ions in Their Parent Gases From 78 to 300 K, *The Journal of Chemical Physics*, **73**, 1717.

Jusko P., Roučka Š., Mulin D., Zymak I., Plašil R., Gerlich D., Čížek M., Houfek K., Glosík J. (2015), Interaction of O^- and H_2 at Low Temperatures, *The Journal of Chemical Physics*, **142**(**1**), 014304.

Kleingeld J. C., Nibbering N. M. M. (1983), The Long-Lived H_3O^- Ion in the Gas Phase: Its Formation, Structure and Reactions, *International Journal of Mass Spectrometry and Ion Physics*, **49**, 311.

Kreckel H., Bruhns H., Čížek M., Glover S. C. O., Miller K. A., Urbain X., and Savin D. W. (2010), Experimental Results for H_2 Formation from H^- and H and Implications for First Star Formation, *Science*, **329**, 69.

Kutner M. L. (2003), *Astronomy: A Physical Perspective, Second Edition*, Cambridge University Press – Cambridge. ISBN 0-521-82196-7.

Lee S. T. and Farrar J. (2000), Dynamics of the $OH^- + D_2$ Isotope Exchange Reaction: Reactive and Nonreactive Decay of the Collision Complex, *The Journal of Chemical Physics*, **113**, 581.

Li Y., Liu L., and Farrar J. (2005), Quantum State-Resolved Study of the Four-Atom Reaction $OH^-(X^1\Sigma_g^+) + D_2\ (X^1\Sigma_g^+, \upsilon = 0) \rightarrow HOD(X^1A', \upsilon') + D^-(^1S)$, *The Journal of Physical Chemistry A Letters*, **109**(**29**), 6392.

Li Y., Liu L., and Farrar J. (2009), Vibrational-Rotational Energy Distributions in the Reaction $O^- + D_2 \rightarrow OD + D^-$, *The Journal of Physical Chemistry A*, **113**, 15233.

Lias S. G. (1984), Thermoneutral Isotope Exchange Reactions in Proton-Bound Complexes of Water with Organic Molecules: Correlations with Energetics of Formation of the Corresponding Association Ions, *The Journal of Physical Chemistry*, **88**, 4401.

Lique F., Honvault P., and Faure A. (2014), Ortho–Para-H_2 Conversion Processes in Astrophysical Media, *International Reviews in Physical Chemistry*, **33**(**1**), 125.

Luine J. A. and Dunn G. H. (1985), Ion-Molecule Reaction Probabilities Near 10 K, *The Astrophysical Journal Letters*, **299**, L67.

Marquette J. B., Rebrion C., and Rowe B. R. (1988), Reactions of $N^+(^3P)$ Ions with Normal, Para, and Deuterated Hydrogens at Low Temperatures, *The Journal of Chemical Physics*, **89**, 2041.

Martin J. D. and Bailey T. L. (1968), Reactions of Low-Energy O^- Ions with D_2 and H_2, *The Journal of Chemical Physics*, **49**, 1977.

Martinez O., Yang Z., Betts N. B., Snow T. P., and Bierbaum V. M. (2009), Experimental Determination of the Rate Constant for the Associative Detachment Reaction $H^- + H \rightarrow H_2 + e^-$ at 300 K, *The Astrophysical Journal Letters*, **705**, L172.

Mauer J. L. and Schulz G. J. (1973), Associative Detachment of O^- with CO, H_2, and O_2, *Physical Review A*, **7**, 593.

McCaroll R. (2010), Isotopic Effects in Ion-Molecule Reactions, *Journal of Physics: Conference Series*, **257**, 012003.

McCarthy M. C., Gottlieb C. A., Gupta H., and Thaddeus P. (2006), Laboratory and Astronomical Identification of the Negative Molecular Ion C_6H^-, *The Astrophysical Journal Letters*, **652**.**2**, L141.

McFarland M., Albritton D. L., Fehsenfeld F. C., Ferguson E. E., and Schmeltekopf A. L. (1973), Flow-Drift Technique for Ion Mobility and Ion-Molecule Reaction Rate Constant Measurements. III. Negative Ion Reactions of O^- with CO, NO, H_2, and D_2, *The Journal of Chemical Physics*, **59**, 12.

McSween H. Y. and Huss G. R. (2010), *Cosmochemistry*, Cambridge University Press – Cambridge. ISBN 9780521878623.

Menzinger M. and Wolfgang R. (1969), The Meaning and Use of the Arrhenius Activation Energy, *Angewandte Chemie International Edition*, **8**, 438.

Meot-Ner M., Lloyd J. R., Hunter E. P., Agosta W. A., and Field F. H. (1980), Isotope Exchange Reactions of OH^- or OD^- Ions with Hydrogen and Water, *Journal of the American Chemical Society*, **102**, 4672.

Milenko Y., Karnatsevich L., Kogan V. (1972), On temperature dependence of the polarizability of H_2 and D_2 molecules, *Physica*, **60**, 90.

Miller K. A., Bruhns H., Čížek M., Eliášek J., Cabrera-Trujillo R., Kreckel H., O'Connor A. P., Urbain X., and Savin D. W. (2012), Isotope Effect

for Associative Detachment: $H(D)^- + H(D) \rightarrow H_2$ (D_2) + e^-, *Physical Review A*, **86**, 032714.

Moneti A., Cernicharo J., and Pardo J. R. (2001), Cold H_2O and CO Ice and Gas Toward the Galactic Center, *The Astrophysical Journal Letters*, **549**, L203.

Monfils A. (1965), The Absorption Spectra of the Molecules H_2, HD, and D_2: Part VI. Rotational Analysis of the B′, B″, D, D′, and D″ States, *Journal of Molecular Spectroscopy*, **15**, 265.

Morong C. P., Gottfried J. L., Oka T. (2009), H_3^+ as the Benchmark for Rigorous *ab initio* Theory, *Journal of Molecular Spectroscopy*, **255**, 13.

Mulin D., Jusko P., Roučka Š., Zymak I., Plašil R., Glosík J. (2013), Experimental Study of $OH^- + D_2 \rightarrow OD^- + HD$ Reaction at Low Temperatures, in *WDS'13 Proceedings of contributed papers: Part II – Physics of Plasmas and Ionised Media*, edited by J. Šafránkova, J. Pavlů, Matfyzpress – Prague. ISBN 978-80-7378-251-1.

Mulin D., Roučka Š., Jusko P., Zymak I., Plašil R., Gerlich D., Wester R., and Glosík J. (2015), H/D Exchange in Reactions of OH^- with D_2 and of OD^- with H_2 at Low Temperatures, *Physical Chemistry Chemical Physics*, accepted 23 February 2015.

Muschlitz E. E. (1957), Formation of Negative Ions in Gases by Secondary Collision Processes, *Journal of Applied Physics*, **28**, 1414.

Neufeld D. A., Snell R. L., Ashby M. L. N., Bergin E. A. Chin G., Erikson N., Goldsmith P. F., Harwit M., Howe J. E., Kleiner S. C., Koch D. G., Patten B. M., Plume R., Schieder R., Stauffer J. R., Tolls V., Wang Z., Winnewisser G., Zhang Y. F., and Melnick G. J. (2000), Observations of Interstellar Water Vapor in Outflow Regions, *The Astrophysical Journal Letters*, **539**, L107.

Neumark D. M., Lykke K. R., Andersen T., Lineberger W. C. (1985), Laser Photodetachment Measurement of the Electron Affinity of Atomic Hydrogen, *Physical Review A*, **32**(**3**), 1890.

Oka T. (2006), Interstellar H_3^+, *Proceedings of the National Academy of Sciences of the United States of America*, **103**(**33**), 122335.

Osterbrock D. E. (1974), *Astrophysics of Gaseous Nebulae*, W. H. Freeman and Co. – San Francisco. ISBN 0-935702-22-9.

Otto R., Mikosch J., Trippel S., Weidemuller M., and Wester R. (2008), Nonstandard Behavior of a Negative Ion Reaction at Very Low Temperatures, *Physical Review Letters*, **101**, 063201.

Otto R., Zastrow A. v., Best T., and Wester R. (2013), Internal State Thermometry of Cold Trapped Molecular Anions, *Physical Chemistry Chemical Physics*, **15**, 612.

Parkes D. A. (1972), Reactions of the O^- Negative Ion with Hydrogen and the Lower Hydrocarbons, *Journal of Chemical Society, Faraday Transactions 1*, **68**, 613.

Paul W., Lu̇cke B., Schlemmer S., Gerlich D. (1995), On the Dynamics of the Reaction of Positive Hydrogen Cluster Ions (H_5^+ to H_{23}^+) with Para and Normal Hydrogen at 10 K, *International Journal of Mass Spectrometry and Ion Physics*, **150**, 373.

Plašil R., Glosík J., Poterya V., Kudrna P., Rusz J., Tichý M., Pysanenko A. (2002), Advanced Integrated Stationary Afterglow Method for Experimental Study of Recombination of Processes of H_3^+ and D_3^+ Ions with Electrons, *International Journal of Mass Spectrometry*, **218**, 105.

Plašil R., Zymak I., Jusko P., Mulin D., Gerlich D., Glosík J. (2012), Stabilization of $H^+ – H_2$ Collision Complexes Between 11 and 28 K, *Philosophical Transactions of the Royal Society A*, **370**, 5066.

Raich J. C., Good R. H. (1964), Ortho-Para Transition in Molecular Hydrogen, *The Astrophysical Journal*, **139**, 1004.

Raizer Y. P. (1997), *Gas Discharge Physics, Corrected 2nd Printing*, edited by J. E. Allen, Springer – New York. ISBN 3-540-19462-2.

Rehfuss B. D., Crofton M. W., and Oka T. (1986), Infrared Spectrum of the Fundamental Vibration-Rotation Band of OD^-, *The Journal of Chemical Physics*, **85**, 1785.

Rosenbaum N. H., Owrutsky J. C., Tack L. M., and Saykally R. J. (1986), Velocity Modulation Laser Spectroscopy of Negative Ions: The Infrared Spectrum of Hydroxide (OH^-), *The Journal of Chemical Physics*, **84**, 5308.

Ross T., Baker E., Snow T., Destree J., Rachford B., Drosback M., and Jensen A. G. (2008), The Search for H^- in Astrophysical Environments, *The Astrophysical Journal*, **684**, 358.

Roučka Š., Mulin D., Jusko P., Plašil R., Gerlich D., Glosík J. (2015), Experimental Study of D^- + H Reaction at Low Temperatures Using 22-Pole Ion Trap with H-Atom Beam, *The Journal of Physical Chemistry Letters*, in preparation.

Russel C. L. and Manolopoulos D. E. (1999), Time-Dependent Wave Packet Study of the $N^+ + H_2$ Reaction, *The Journal of Chemical Physics*, **110**, 177.

Sakimoto K. (1989), Ion-Molecule Reactions at Extremely Low Energies: $H^- + H \rightarrow H_2 + e^-$, *Chemical Physics Letters*, **164**, 294.

Schmeltekopf A. L., Fehsenfeld F. C., and Ferguson E. E. (1967), Laboratory Measurement of the Rate Constant for $H^- + H \rightarrow H_2 + e^-$, *The Astrophysical Journal Letters*, **118**, L155.

Schulz P. A., Mead R. D., Jones P. L., and Lineberger W. C. (1982), OH^- and OD^- Threshold Photodetachment, *The Journal of Chemical Physics*, **77**, 1153.

Smith D. and Adams N. G. (1984), Isotope Exchange in Ion-Molecule Reactions, in *Ionic Processes in the Gas Phase*, NATO ASI Series C, Volume **118**, edited by M. A. A. Ferreira, Reidel – Dordrecht. ISBN 978-94-009-7248-3.

Smith J. R., Kim J. B., and Lineberger W. C. (1997), High-Resolution Threshold Photodetachment Spectroscopy of OH^-, *Physical Review A*, **55**, 2036.

Snell R. L., Howe J. E., Ashby M. L. N., Bergin E. A. Chin G., Erikson N.R., Goldsmith P. F., Harwit M., Kleiner S. C., Koch D. G., Neufeld D., Patten B. M., Plume R., Schieder R. G., Stauffer J. R., Tolls V., Wang Z., Winnewisser G., Zhang Y. F., and Melnick G. J. (2000), Water Abundance in Molecular Cloud Cores, *The Astrophysical Journal Letters*, **539**, L101.

Solomon P. M. and Woolf N. J. (1973), Interstellar Deuterium: Chemical Fractionation, *The Astrophysical Journal Letters*, **180**, L89.

Stevenson D. P. and Schissler D. O. (1958), Reactions of Gaseous Molecule Ions with Gaseous Molecules. IV. Experimental Method and Results, *The Journal of Chemical Physics*, **29**, 282.

Spitzer L., Drake J. F., Jenkins E. B., Morton D. C., Rogerson J. B., York D. G. (1973), Spectrophotometric Results from the Copernicus Satellite. IV. Molecular Hydrogen in Interstellar Space, *The Astrophysical Journal Letters*, **181**, L116.

Stewart J. H., Shapiro R. H., DePuy C. H., and Bierbaum V. (1977), Hydrogen-Deuterium Exchange Reactions of Carbanions with D_2O in the Gas Phase, *Journal of the American Chemical Society*, **99**(**23**), 7650.

Sugimoto T., Fukutani K. (2011), Electric-Field-Induced Nuclear-Spin Flips Mediated by Enhanced Spin-Orbit Coupling, *Nature Physics*, **7**, 307.

Tosi P., Dmitrijev O., Bassi D., Wick O., Gerlich D. (1994), Experimental Observation of the Energy Threshold in the Ion-Molecule Reaction $N^+ + D_2 \rightarrow ND^+ + D$, *The Journal of Chemical Physics*, **100**, 4300.

de Tudela R. P., Barragán P., Prosmiti R., Villarreal P., Delgado-Barrio G. (2011), Internal Proton Transfer and H_2 Rotations in the H_5^+

Cluster: A Marked Influence on Its Thermal Equilibrium State, *The Journal of Physical Chemistry A*, **115**, 2483.

Urey H. C., Brickwedde F. G., and Murphy G. M. (1932), A Hydrogen Isotope of Mass 2, *Physical Review*, **39**, 164.

Viggiano A. A. and Morris R. A. (1994), Effects of Rotational, Vibrational, and Translational Energy on the Rate Constants for the Isotope Exchange Reactions $OH^- + D_2$ and $OD^- + H_2$, *The Journal of Chemical Physics*, **100**, 2748.

Wang D., Zhang J. Z. H., and Yu C.-H. (1997), Quantum Calculation of Photodetachment Spectrum of $OH^-\cdot(H_2)$, *Chemical Physics Letters*, **273**, 171.

Watson W. D. (1973[a]), Formation of the HD Molecule in the Interstellar Medium, *The Astrophysical Journal Letters*, **182**, L73.

Watson W. D. (1973[b]), The Rate of Formation of Interstellar Molecules by Ion-Molecule Reactions, *The Astrophysical Journal Letters*, **183**, L17.

Watson W. D. (1974), Ion-Molecule Reactions, Molecule Formation, And Hydrogen-Isotope Exchange in Dense Interstellar Clouds, *The Astrophysical Journal Letters*, **188**, 35.

Wiberg K. B. (1955), The Deuterium Isotope Effect, *Chemical Reviews*, **55**(**4**), 713.

Wilhelmsson U. and Nyman G. (1992), A Low Energy Quasiclassical Trajectory Study of $N^+ + H_2$. Potential Energy Surface Effects, *The Journal of Chemical Physics*, **96**, 1886.

Yang Z., Cole C.A., Martinez O., Carpenter M.Y., Snow T. P., and Bierbaum V. M. (2011), Experimental and Theoretical Studies of Reactions Between H Atoms and Nitrogen-Containing Carbanions, *The Astrophysical Journal*, **739**, 19.

Zhang D. H., Yang M., Collins M. A., and Lee S.-Y. (2002), Probing the Transition State via Photoelectron and Photodetachment Spectroscopy of H_3O^-, *Proceedings of the National Academy of Sciences of the United States of America*, **99**, 11579.

Zymak I., Jusko P., Roučka Š., Plašil R., Rubovič P., Gerlich D., and Glosík J. (2011), Ternary Association of H^+ Ion with H_2 at 11 K, Experimental Study, *The European Physical Journal – Applied Physics*, **56**, 24010.

Zymak I. (2013), Study of State Selected Interactions of Ions with Molecular Hydrogen at Temperatures Relevant to Astrochemistry, PhD thesis, Charles University in Prague.

Zymak I., Hejduk M., Mulin D., Plašil R., Glosík J., and Gerlich D. (2013), Low-Temperature Ion Trap Studies of $N^+(^3P_{ja}) + H_2(J) \rightarrow NH^+ + H$, *The Astrophysical Journal*, **768**, 86.

List of publications

Publications in impacted journals

Mulin D., Roučka Š., Jusko P., Zymak I., Plašil R., Gerlich D., Wester R., and Glosík J. (2015), H/D Exchange in Reactions of OH^- with D_2 and of OD^- with H_2 at Low Temperatures, *Physical Chemistry Chemical Physics*, accepted 23 February 2015.

Plašil R., Zymak I., Jusko P., **Mulin D.**, Gerlich D., Glosík J. (2012), Stabilization of H^+-H_2 Collision Complexes Between 11 and 28 K, *Philosophical Transactions of the Royal Society A*, **370**, 5066.

Gerlich D., Plašil R., Zymak I., Hejduk M., Jusko P., **Mulin D.**, Glosík J. (2013), State Specific Stabilization of $H^+ + H_2(J)$ Collision Complexes, *The Journal of Physical Chemistry A*, **117**(**39**), 10068.

Zymak I., Hejduk M., **Mulin D.**, Plašil R., Glosík J., and Gerlich D. (2013), Low-Temperature Ion Trap Studies of $N^+(^3P_{ja}) + H_2(J) \rightarrow NH^+ + H$, *The Astrophysical Journal*, **768**(**1**), 86.

Jusko P., Roučka Š., **Mulin D.**, Zymak I., Plašil R., Gerlich D., Čížek M., Houfek K., Glosík J. (2015), Interaction of O^- and H_2 at Low Temperatures, *The Journal of Chemical Physics*, **142**(**1**), 014304.

Publications in *Web of Science* registered proceedings

Plašil R., Zymak I., Jusko P., **Mulin D.**, Gerlich D., and Glosík J. (2012), Radiative Association of H^+ and H_2 – Experimental Study, *Journal of Physics: Conference Series*, **388**(**8**), 012041.

Roučka Š., Jusko P., Zymak I., **Mulin D.**, Plašil R., Gerlich D., Glosík J. (2012), Interactions of H^- Anions with Atomic Hydrogen – Ion Trap study at 10 – 100 K, *Journal of Physics: Conference Series*, **388**(**8**), 082057.

Plašil R. , Zymak I., Hejduk M., **Mulin D.**, Glosík J., Gerlich D. (2014), Formation of NH^+ in Collisions of N^+ with para- or ortho-H_2 at Low Temperatures – an Experimental Study, *Journal of Physics: Conference Series*, **488**(**12**), 122003.

Publications in conference proceedings

Mulin D., Jusko P., Roučka Š., Zymak I., Plašil R. and Glosík J. (2011), Review of Ion-Molecule Reactions with Atomic and Molecular Hydrogen Suitable for Future Studying Using 22-Pole Ion Trap, in *WDS'11 Proceedings of contributed papers: Part II – Physics of Plasmas and Ionised Media*, edited by J. Šafránkova, J. Pavlů, Matfyzpress – Prague. ISBN 978-80-7378-185-9.

Mulin D., Zymak I., Hejduk M., Dohnal P., Plašil R., Gerlich D., and Glosík J. (2012), Limits for the $N^+ + p/o\text{-}H_2$ Reaction Study Using 22-Pole Ion Trap Apparatus, in *WDS'12 Proceedings of Contributed Papers: Part II - Physics of Plasmas and Ionized Media*, edited by J. Šafránkova, J. Pavlů, Matfyzpress – Prague. ISBN 978-80-7378-225-2.

Mulin D., Jusko P., Roučka Š., Zymak I., Plašil R., Glosík J. (2013[a]), Experimental Study of $OH^- + D_2 \rightarrow OD^- + HD$ Reaction at Low Temperatures, in *WDS'13 Proceedings of contributed papers: Part II – Physics of Plasmas and Ionised Media*, edited by J. Šafránkova, J. Pavlů, Matfyzpress – Prague. ISBN 978-80-7378-251-1.

Mulin D., Plašil R., Zymak I., Gerlich D., Glosík J. (2013[b]), Experimental Study of the D^+ and $H^+ + D_2$ Reaction Using a 22-Pole Ion Trap, in *19th Symposium on Applications of Plasma Processes (SAPP XIX), Book of Contributed Papers*, edited by J. Országh, P. Papp, Š. Matejčík, Society for Plasma Research and Applications in cooperation with Library and Publishing Centre CU – Bratislava. ISBN 978-80-89186-77-8.

Hejduk M., Zymak I., **Mulin D.**, Plašil R., Gerlich D., Glosík J., Gaertner S. (2012), In-situ Determination of Population of Nuclear Spin States of H_2 Injected to the 22-Pole Trap, in *WDS'12 Proceedings of Contributed Papers: Part II - Physics of Plasmas and Ionized Media*, edited by J. Šafránkova, J. Pavlů, Matfyzpress – Prague. ISBN 978-80-7378-225-2.

Jusko P., Roučka Š., **Mulin D.**, Plašil R., Glosík J. (2011), Atomic Beam Calibration for the $H^- + H$ Experiment, in *WDS'11 Proceedings of contributed papers: Part II – Physics of Plasmas and Ionised Media*, edited by J. Šafránkova, J. Pavlů, Matfyzpress – Prague. ISBN 978-80-7378-185-9.

Jusko P., Zymak I., **Mulin D.**, Roučka Š., Plašil R., Gerlich D., Glosík J. (2012), Experimental Determination of Conditions in the Trap: Reaction Temperature and Reactant Density, in *SASP 2012, Book of Contributed Papers*, edited by M. Lewerenz, O. Dutuit, R. Marquardt, Innsbruck University Press – Innsbruck. ISBN 978-3-902719-52-2.

Roučka Š., Jusko P., Zymak I., **Mulin D.**, Plašil R., Glosík J. (2011), Influence of the 22-pole Trap Imperfections on the Interaction of Ions with a Neutral Beam, in *WDS'11 Proceedings of contributed papers: Part II – Physics of Plasmas and Ionised Media*, edited by J. Šafránkova, J. Pavlů, Matfyzpress – Prague. ISBN 978-80-7378-185-9.

Zymak I., Jusko P., Roučka Š., **Mulin D.**, Plašil R., and Glosík J. (2011), Association of H^+ with H_2 at low temperatures, in *WDS'11 Proceedings of contributed papers: Part II – Physics of Plasmas and Ionised Media*, edited by J. Šafránkova, J. Pavlů, Matfyzpress – Prague. ISBN 978-80-7378-185-9.

List of studied reactions

The studied reactions with the respective numbers in the text and designations of the rate coefficients are listed here.

$H^- + H \rightarrow H_2 + e^-$	k_{HH}	(3.2)
$H^+ + H_2 \rightarrow H_3^+ + h\nu$	k_{Hr}	(3.4)
$H^+ + H_2 + H_2 \rightarrow H_3^+ + H_2$	k_{H3}	(3.5)
$O^- + H_2 \rightarrow H_2O + e^-$	k_{O1}	(3.6)
$O^- + H_2 \rightarrow OH^- + H$	k_{O2}	(3.7)
$D^- + H \rightarrow HD + e-$	k_{AD}	(3.22)
$D^- + H \rightarrow H^- + D$	k_{CT}	(3.23)
$O^- + D_2 \rightarrow D_2O + e-$	k_{O3}	(3.24)
$O^- + D_2 \rightarrow OD^- + D$	k_{O4}	(3.25)
$OH^- + D_2 \rightarrow OD^- + HD$	k_{OH}	(3.27)
$OD^- + H_2 \rightarrow OH^- + HD$	k_{OD}	(3.28)
$N^+ + H_2 \rightarrow NH^+ + H$	k_N	(3.29)

List of figures

List of tables

List of used acronyms

22PT	22-Pole ion Trap
AB-22PT	Atomic Beam with a 22-Pole ion Trap
AC	Alternate Current
AD	Associative Detachment
AML®	Arun Microelectronics®
CRESU	Cinétique de Réaction en Ecoulement Supersonique Uniforme apparatus
CT	Charge Transfer
DAC	Digital-to-Analogue Converter
DC	Direct Current
FA	Flowing Afterglow apparatus
FDT	Flowing Drift Tube apparatus
FS	Fine Structure
HAS	H-Atom Source
IB	Ion Beam experiment
IG	Ionisation Gauge
MP	Membrane Pump
mTP	Magnetic-levitation Turbomolecular Pump
oTP	Oil Turbomolecular Pump
QP	Quadrupole
RF	Radio Frequency
RP	Rotary Pump
SIFDT	Selected Ion Flow Drift Tube apparatus
SIFT	Selected Ion Flow Tube apparatus
SIS	Storage Ion Source
SP	Scroll Pump

SRG	Spinning Rotor Gauge
TDP	Turbo Drag Pump
TMS	Tandem Mass Spectrometer apparatus
TP	Turbomolecular Pump
UHV	Ultra-High Vacuum

Appendix A

AB-22PT remote control and operation system

AB-22PT remote control and operation block diagram is shown in figure A.1.

The advantages of the digital remote operation and control of the instrument comparing to the analogue are as follows:

– fast response to the driving signals;

– stability and lower sensitivity to the noise and environment conditions (e. g., temperature);

– possibility to save and load the appropriate settings and electrode voltages for the particular ions;

– possibility to operate the instrument from different computers and places;

– possibility to use any device from the Novation® Nocturn series.

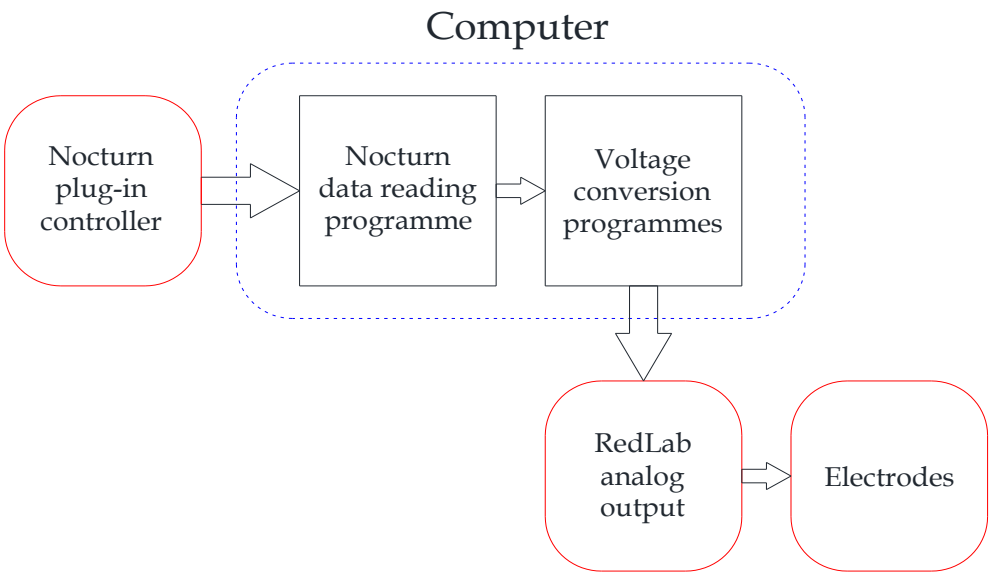

Figure A.1. AB-22PT remote control and operation block diagram.

Appendix B

Measured calibration coefficient *C* between the pressures in the trap volume and vacuum chamber

The pressures in the trap volume and outer vacuum chamber were measured by a spinning-rotor gauge SRG-BF-CAL and an AML® AIG ionisation gauge, respectively. The temperature of the trap was 11 K, the temperature of the environment was 300 K.

The serial number of the ball of the spinning-rotor gauge was G191941. Ball diameter was 4.5 mm, ball density was 7.70 g/cm^3.

AML® AIG17G nude ionisation gauge is a high-sensitivity UHV Bayard-Alpert gauge with two Tungsteen filaments, covering the pressure range of $3 \cdot 10^{-9}$ to $1 \cdot 10^{-1}$ Pa, and is intended for electron-bombardment degas.

Gas inlet	Gas	*C*
SIS	H_2	1.81
22PT	H_2	42.2
	D_2	56.7
	He	137

Table B.1. Measured pressure calibration coefficients *C* for different gases, which penetrated into the trap directly (22PT rows) or through the storage ion source (SIS row).

Attached publications

I. H/D Exchange in Reactions of OH^- with D_2 and of OD^- with H_2 at Low Temperatures

II. Low-Temperature Ion Trap Studies of $N^+(^3P_{ja}) + H_2(J) \rightarrow NH^+ + H$

III. State Specific Stabilization of $H^+ + H_2(J)$ Collision Complexes

IV. Stabilization of $H^+–H_2$ Collision Complexes between 11 and 28 K

V. Interaction of O^- and H_2 at Low Temperatures

I. H/D Exchange in Reactions of OH^- with D_2 and of OD^- with H_2 at Low Temperatures

Mulin D., Roučka Š., Jusko P., Zymak I., Plašil R., Gerlich D.,
Wester R., and Glosík J. (2015)

Physical Chemistry Chemical Physics, accepted 23 February 2015.

PCCP

PAPER

View Article Online
View Journal

Cite this: DOI: 10.1039/c5cp00516g

H/D exchange in reactions of OH^- with D_2 and of OD^- with H_2 at low temperatures

Dmytro Mulin,[a] Štěpán Roučka,*[a] Pavol Jusko,[a] Illia Zymak,[a] Radek Plašil,[a] Dieter Gerlich,[b] Roland Wester[c] and Juraj Glosík[a]

Received 27th January 2015,
Accepted 23rd February 2015

DOI: 10.1039/c5cp00516g

www.rsc.org/pccp

Using a cryogenic linear 22-pole rf ion trap, rate coefficients for H/D exchange reactions of OH^- with D_2 (1) and OD^- with H_2 (2) have been measured at temperatures between 11 K and 300 K with normal hydrogen. Below 60 K, we obtained $k_1 = 5.5 \times 10^{-10}$ cm^3 s^{-1} for the exoergic reaction (1). Upon increasing the temperature above 60 K, the data decrease with a power law, $k_1(T) \sim T^{-2.7}$, reaching $\approx 1 \times 10^{-10}$ cm^3 s^{-1} at 200 K. This observation is tentatively explained with a decrease of the lifetime of the intermediate complex as well as with the assumption that scrambling of the three hydrogen atoms is restricted by the topology of the potential energy surface. The rate coefficient for the endoergic reaction (2) increases with temperature from 12 K up to 300 K, following the Arrhenius equation, $k_2 = 7.5 \times 10^{-11} \exp(-92\ \mathrm{K}/T)$ cm^3 s^{-1} over two orders of magnitude. The fitted activation energy, $E_{A\text{-}Exp} = 7.9$ meV, is in perfect accordance with the endothermicity of 24.0 meV, if one accounts for the thermal population of the rotational states of both reactants. The low mean activation energy in comparison with the enthalpy change in the reaction is mainly due to the rotational energy of 14.7 meV contributed by *ortho*-H_2 ($J = 1$). Nonetheless, one should not ignore the reactivity of pure *para*-H_2 because, according to our model, it already reaches 43% of that of *ortho*-H_2 at 100 K.

1 Introduction

Interactions of ions with neutral particles and the formation of new molecules play an important role in natural and technical plasmas. The various ways to form interstellar molecules, including gas phase processes involving cations, radicals and gas-grain interactions, have attracted a lot of attention in the last four decades. The role of anions in the interstellar medium has been discussed for the first time by Dalgarno and McCray already in 1973.[1] However, the interest in anions diminished because, due to a lack of spectroscopic data, they could not be detected. This has changed recently when the first anions were observed in the interstellar medium,[2–4] reactivating the interest in theory[5,6] and experiments[7–13] with anion-molecule reactions, including associative detachment reactions. Also photodetachment of electrons from anions including interstellar anions has been reported.[14–17] The anions are interesting not only due to their role in astrochemistry, but they also play an important role in plasma physics, in technical discharges, in radiation chemistry *etc.*[18–20]

Experimental and theoretical studies of gas phase reactions provide a good basis for understanding the detailed dynamics of fundamental chemical reactions. Here, reactions of hydrogen atoms or molecules are of particular importance, because at low temperature, the influence of specific molecular quantum states can be probed.[9–11,21–23] Furthermore, theoretical treatments of the reactive scattering process, while still challenging, become feasible for few-atom systems.[24,25] A particular class of reactions is the hydrogen/deuterium isotopic exchange,[26] which forms products that are chemically equivalent to the reactants and whose energies vary only by their change in vibrational zero-point energy.

We recently studied H/D isotope effects in the reactions $H^-(D^-)$ + H and O^- + $H_2(D_2)$ using the AB-22-pole ion trap apparatus[10,27,28] and we measured the temperature dependencies of their reaction rate coefficients for temperatures from 11 K up to 300 K. In the present study we investigate the H/D exchange process at a low temperature in a more complex collision system, OH^- + H_2 and its isotopic variants, where isotopic exchange occurs *via* the H_3O^- complex and requires several chemical rearrangement steps. As such, this system is different from H/D exchange in many cation–molecule reactions.[26]

The first experimental observation of the long-lived H_3O^- anion has been reported in 1983 by Kleingeld and Nibbering.[29] One of the formation mechanisms is ternary association of OH^- + H_2, with He or H_2 as a third body. A ternary rate coefficient of 10^{-30} cm^6 s^{-1} was measured at 88 K,[30] which increases for OD^- + D_2 to 3×10^{-29} cm^6 s^{-1} at 15 K.[31] The stability of this anion made it possible to probe the transition state of OH + H_2 → H_2O + H by starting the neutral reaction *via* photodetachment from the anion.[32–34] These very interesting experiments stimulated

[a] Department of Surface and Plasma Science, Faculty of Mathematics and Physics, Charles University in Prague, Czech Republic. E-mail: Stepan.Roucka@mff.cuni.cz; Tel: +420 22191 2344
[b] Department of Physics, Technische Universität Chemnitz, Germany
[c] Institute for Ion Physics and Applied Physics, University of Innsbruck, Austria

state of the art calculations including accurate potential energy surfaces of H_3O^- and the neutral H_3O complex.[32,33]

The endothermic proton transfer reaction $OH^- + H_2 \rightarrow H^- + H_2O$ proceeds *via* the H_3O^- collision complex. The enthalpy change in this reaction is in the range ΔH = 0.37–0.46 eV, the uncertainty of ΔH reflects values given in previous publications.[30,32,33,35,36] Collisions of H^- with H_2O were studied in the first anion-molecule experiment.[37] Crossed molecular beam experiments indicated that the reaction proceeds *via* a direct mechanism at collision energies above 0.7 eV.[38] In a 4 K 22-pole ion trap, this reaction could be promoted by exciting the first vibrational state of the anion with 2.85 μm IR radiation.[36]

A common way to probe reaction dynamics and to learn more about the H_3O^- collision complex is to use isotope labelling and to look for scrambling of the chemically equivalent atoms. In the following, we will discuss the two isotope exchange reactions, which have been studied experimentally before,[38–42]

$$OH^- + D_2 \rightarrow OD^- + HD, \quad \Delta H = -17.2 \text{ meV}, \qquad (1)$$

$$OD^- + H_2 \rightarrow OH^- + HD, \quad \Delta H = 24.0 \text{ meV}. \qquad (2)$$

The majority of previous studies of these reactions were carried out at 300 K and above.[39,41,43] There is just one flow drift tube study at 130 K and there are no data available for lower temperatures.[40]

The reaction enthalpies at 0 K given in eqn (1) and (2) were calculated from electron affinities of OH and OD,[44,45] zero point energies of H_2, D_2, and HD,[46] and from zero point energies of OH and OD[47,48] in the Born–Oppenheimer approximation. However, at sub-meV accuracy, the isotopic electronic shifts of the energy eigenvalues need to be accounted for. It has been shown for several isotope exchange reactions with H_2 and D_2 that the change of enthalpy due to adiabatic correction of the Born–Oppenheimer approximation is on the order of 1 meV.[49–51] In particular, spectroscopic studies of OH and OD suggest that the isotopic shift of the electronic ground state potential energy surface in this system can be up to 2.5 meV (see note 78 in Ruscic *et al.*[52]). To our knowledge, there are no published results concerning the OH/OD isotopic shift, so in the worst case, the error of the above determined endothermicities can be up to 2.5 meV.

For a better understanding of the collision complex, Fig. 1 provides a sketch of the stationary points of different isotopic and isomeric configurations of the H_2DO^- system involved in reaction (2). It has already been discussed[39,40] that, for H/D exchange, the system has to pass through three minima, separated by submerged transition states (TSs). The energies shown in Fig. 1 are corrected for zero point energies. As already mentioned above, the endothermicity of 24.0 meV is known with good precision. The values for the deuterated intermediates are estimated from H_3O^- energies calculated by Zhang *et al.*[33] corrected for the rather uncertain zero point energies reported by Wang *et al.*[35] Inspection reveals that, during the approach of the reactants, first an $OH^-\cdot(H_2)$ complex is formed, which can undergo rearrangement to the most stable form of H_3O^-, a H^- ion bound to a perturbed H_2O molecule. With exception of the zero point energies, the exit channel is symmetric. It is not so easy to predict, where scrambling of H and D atoms actually occurs, most probably in the transition states where both the H_2 bond and one of the HO bonds are weakened. Extending this picture to all dimensions one may expect that the outcome of complex formation in the first minimum, isotope exchange around the minimum, and breakup either back to reactants or to products may be predictable with a statistical model. However, the submerged barriers, centrifugal barriers, and the rather rigid structures in the potential minima may hinder full scrambling. In total the probability for H/D exchange may depend on the relative orientation of the reactants during the approach, on the initial rotational states of both reactants, on the relative velocity, and certainly also on the total orbital angular momentum of the collision complex.

To compare quantitatively rotational excitation of both reactants with the endothermicity of reaction (2), we included in the left panel of Fig. 1 the energies of two lowest rotational states of H_2 with *para* (J_{H_2} = 0) and *ortho* (J_{H_2} = 1) nuclear spin configuration as well as the four lowest rotational states of the OD^- ion.[53]

2 Experimental

The experiments have been carried out using the AB-22PT instrument.[54,55] The principle of operating a 22-pole ion trap

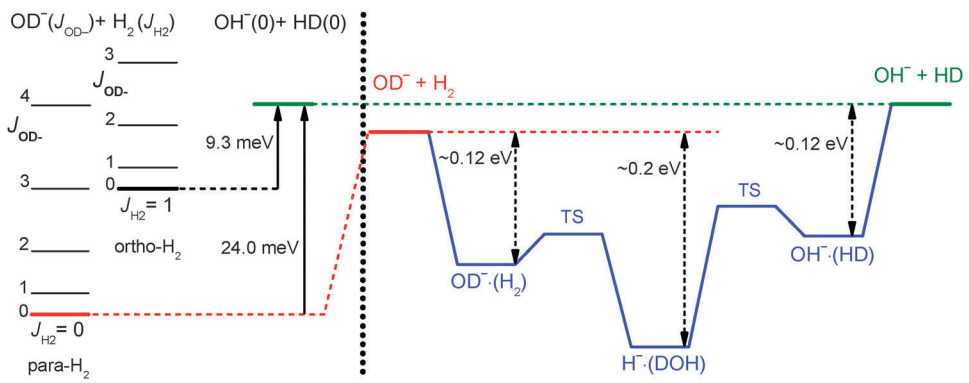

Fig. 1 Right panel: stationary points of the potential energy surface for the reaction $OD^- + H_2 \rightarrow OH^- + HD$. The energies are corrected for zero point energies, for details, see the text. The arrows (with dashed lines) indicate the binding energies of the intermediate complexes $OD^-\cdot(H_2)$, $OH^-\cdot(HD)$ and $H^-\cdot(DOH)$. Left panel: rotational energy levels[47,53] of OD^- and H_2. The two arrows indicate the energies required for forming ground state products.

has been described many times so only a few essential details will be given here. For detailed descriptions, discussions of specific features, and comparisons between 22-pole trap experiments see ref. 10, 54, 56–61.

The 22-pole trap was operated at an RF frequency of 27 MHz, the amplitude has been set to values up to 40 V (peak to peak). The temperature has been varied from 11 K to 300 K. The instrument uses ultra-high vacuum technology, the background number density of residual gas in the trap volume was at most 10^8 cm^{-3} at 11 K. High purity H_2 or D_2 gases were used in the experiments as reactants and He as buffer gas. Hydrogen or deuterium was used in its "normal" composition, *i.e.*, with an *ortho* : *para* ratio of 3 : 1 or 2 : 1, respectively. Tests have indicated that this population does not change while passing the gas into the cooled trap *via* the inlet system.[62,63]

OH^- or OD^- ions are produced in the electron impact storage ion source using a mixture of N_2O and H_2 or D_2.[27,28] The desired ions are then selected by a quadrupole mass filter and guided into the trap, where they are stored. A He–D_2 or a He–H_2 gas mixture is introduced directly into the trap volume. After various well-defined trapping times the trap is opened, the ions are mass selected using a second quadrupole mass spectrometer, and finally counted using an MCP detector. The actual reactant density is adjusted so that the decay of the number of trapped reactant ions due to the reaction is statistically significant. For the fast exothermic reaction (1), the D_2 number density was varied between 10^{10} cm^{-3} and 10^{12} cm^{-3} while for the slow endoergic reaction (2) the H_2 number density has been increased up to 10^{13} cm^{-3}.

Helium buffer gas was added to the trap volume to cool the reactant ions. The actual density of He was such that reactant ions would have at least 10 collisions with He prior to collision with a molecule of reactant gas. This ensures that the kinetic and internal temperatures of OH^- or OD^- ions are thermalized at temperature of the He buffer gas prior to the reaction.

The temperature of trapped ions thermalized by the buffer gas was studied and discussed in many experimental studies. It was found that trap imperfections or patch potentials may lead to acceleration of the ions (*i.e.*, higher kinetic energies). It was concluded several times for the present trap that the interaction temperature is close to the trap temperature (see *e.g.* ref. 57 and 63). In some previous studies the ion temperature was obtained by measuring the temperature dependence of reaction rate coefficients where this dependence could be extrapolated, *e.g.* the rate of the ternary association reaction of $He^+ + He + He$.[57] In the present experiments, the reaction of OD^- with H_2 is endothermic and has an Arrhenius-type temperature dependence of the reaction rate coefficient. Relying on the endothermicity allows us to estimate that the collision temperature deviates from the trap temperature T_{22PT} by less than 5 K.

In the experimental studies of reactions (1) or (2), a small amount of H_2 or D_2, respectively, always leaks into the trap from the ion source, and the product ions react with these gases *via* reactions (2) or (1), respectively. In this way products are reconverted back to reactant ions. Note that these reactions are not the reverse reactions of (1) or (2), the presence of HD is negligible. Although the number density of gas from the ion source is very small compared to the reactant number density (see Table 1), it is necessary to include its influence in the data analysis, especially for the endothermic reaction (2). Consequently, the reaction rate coefficients for reactions (1) and (2) are determined by fitting the time dependence of the measured number of ions with the solution of the balance equations

Table 1 Experimental conditions used for the results shown in Fig. 2. Lower index SIS indicates the density of hydrogen penetrating into the trap from the storage ion source (SIS)

T_{22PT} (K)	$[D_2]$ (cm^{-3})	[He] (cm^{-3})	$[H_2]_{SIS}$ (cm^{-3})
25	2.1×10^{11}	6.0×10^{12}	$\approx 6 \times 10^9$
60	6.0×10^{10}	2.4×10^{12}	$\approx 3 \times 10^9$
100	4.7×10^{10}	4.1×10^{12}	$\approx 1 \times 10^9$

$$\frac{d}{dt}N_{OH^-} = -k_1 N_{OH^-}[D_2] + k_2 N_{OD^-}[H_2] \quad (3)$$

$$\frac{d}{dt}N_{OD^-} = k_1 N_{OH^-}[D_2] - k_2 N_{OD^-}[H_2] \quad (4)$$

where k_1 and k_2 are the binary reaction rate coefficients of the reactions (1) and (2), respectively. $[H_2]$ and $[D_2]$ are hydrogen and deuterium number densities in the trap, respectively. N_{OH^-} and N_{OD^-} are numbers of detected OH^- and OD^- ions, respectively. The free parameters of the fit were the reaction rates $r_1 = k_1[D_2]$ and $r_2 = k_2[H_2]$ as well as the initial numbers of trapped ions.

3 Results and discussion

3.1 Reaction $OH^- + D_2$

As a typical result, Fig. 2 shows the decline of primary ions, N_{OH^-}, and the increase of products, N_{OD^-}, at three temperatures. For normalizing, the numbers of ions are divided by the sum $N_{OH^-} + N_{OD^-}$. This sum did not change with time indicating that there is no loss of ions or that there are no other products. The experimental conditions for these results are summarized in Table 1. Note that the number density of He

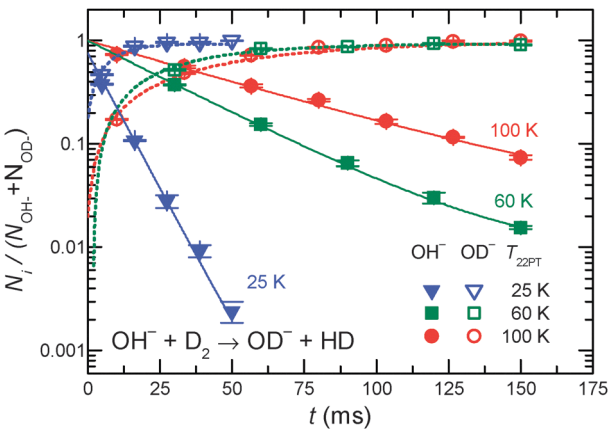

Fig. 2 Normalized number of primary ions (OH^-, closed symbols) and product ions (OD^-, open symbols) as a function of storage time. Operating conditions were T_{22PT} = 25, 60, 100 K, the densities of D_2, He, and H_2 are listed in Table 1.

buffer gas is at least 10 times higher than that of the reactant gas D_2. The density of the perturbing H_2 gas, originating from the ion source, is more than 10 times lower. The monoexponential decay of the primary ions in Fig. 2 indicates that reconversion of products can be neglected in the case of the exothermic reaction (1). The binary character of reaction (1) was checked by varying the number density $[D_2]$ from 2×10^9 cm^{-3} up to 4×10^{11} cm^{-3}. The data plotted in Fig. 3 for 3 temperatures confirm the linear relationship $r_1 = k_1[D_2]$.

The measured temperature dependence of the rate coefficient k_1 for reaction (1) is shown in Fig. 4. As already mentioned, normal D_2 is used as the reactant. For comparison, the Langevin collisional rate coefficient k_{1L} for $OH^- + D_2$ capture is indicated. The measurements were conducted in the range of trap temperatures T_{22PT} from 11 K up to 200 K. The data show that above 60 K the reaction is getting slower with increasing temperature. The previous thermal data from the selected ion flow tube (SIFT) of Grabowski *et al.*[39] and the flow drift tube (FDT) obtained by Viggiano and Morris[40] are included in the graph. High temperature data obtained in high pressure mass spectrometer experiment (HPMS) are also plotted.[41] We did not include FDT data at elevated collisional energy (KE_{CM}) because of unclear internal excitation of the ions.[40] In their FDT study, Viggiano and Morris[40] measured k_1 both as a function of the D_2 temperature and of KE_{CM} (kinetic energy in the center of mass for collision between D_2 and OH^- ions). They observed a significant negative dependence on the temperature but only a slight dependence on the kinetic energy. Therefore they concluded that the negative temperature dependence must be due to the increasing rotational temperature of D_2. To illustrate the influence of the rotational population of deuterium in our temperature range, Fig. 4 shows a simple model rate coefficient (dash-dotted line), calculated with the assumptions that only the rotational ground state can react and this with the Langevin rate coefficient k_{1L}. At first sight there seems to be a similarity in the temperature dependence of this function to the measured data; however, the decline of our experimental data is much steeper. In our temperature range, it must be due to the increase of the energy contributed from all degrees of freedom. This leads to a decrease of the life time of the collision complex in the first minimum (see Fig. 1). In this context we note that the comparison of k_{1L} with the data measured below 60 K also leads to the supposition that, even at these low energies, many collision complexes decay back to reactants rather quickly. To gain more insight into the detailed dynamics of this reaction, more detailed experiments as well as theoretical studies are needed.

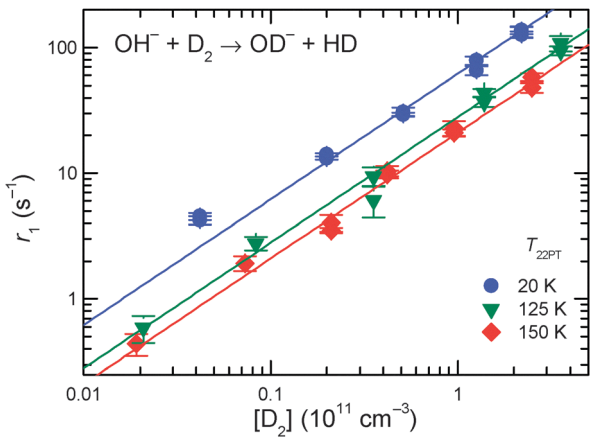

Fig. 3 Rate r_1 of the reaction (1) as a function of deuterium number density $[D_2]$ at trap temperatures T_{22PT} = 20, 125, 150 K.

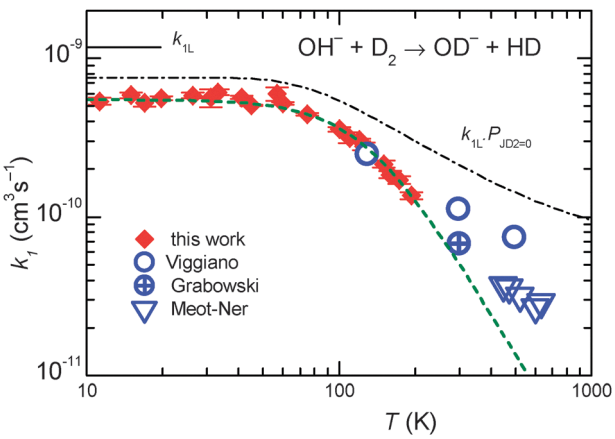

Fig. 4 Measured temperature dependence of the rate coefficient k_1 for H/D exchange reaction (1). The calculated Langevin collisional rate coefficient is indicated as k_{1L}. The assumption that exclusively the rotational ground state of D_2 can react leads to the dash-dotted line (see text). Thermal FDT data of Viggiano and Morris,[40] SIFT data of Grabowski *et al.*,[39] and HPMS data of Mautner *et al.*[41] are also included. The dashed line shows $k_1(T)$ calculated from eqn (5) with the parameters given there.

Negative temperature dependencies have been observed for many binary reactions proceeding *via* formation of the intermediate complex. For such reactions it was deduced that the temperature dependence of the rate coefficient can be approximated by a power law dependence[64–70] in analogy with the mechanism of ternary reactions described by Bates[71] and Herbst.[72]

To describe the studied reaction (1), we are going to use a semi-empirical method given *e.g.* by Glosik *et al.*[70] The general conclusion of this semi-empirical description is that the reaction rate coefficient k_1 can be described by the dependence:

$$\frac{k_{10}}{k_1} - 1 = \left(\frac{T}{T_0}\right)^m \qquad (5)$$

with parameters k_{10}, T_0 and m. From the fit plotted in Fig. 4 we obtained the parameters $k_{10} = 5.5 \times 10^{-10}$ cm^3 s^{-1}, $T_0 = 130$ K, and $m = 2.7 \pm 0.5$. The error estimate of m includes the statistical error as well as the error due to possible deviations from the power law, which was estimated by fitting subsets of data in different temperature ranges. The validity of eqn (5) for describing the measured data can be more easily seen from the plot of $\log(k_{10}/k_1 - 1)$ *versus* $\log(T)$, shown in Fig. 5. This plot includes also data from FDT,[40] HPMS[41] and SIFT.[39]

The empirical model leading to eqn (5) can also be derived from RRKM theory and the exponent m can be explained with the number of "active" degrees of freedom of both the reactants and of the intermediate complex. However, looking at Fig. 1, it is not obvious, where the rate limiting bottlenecks

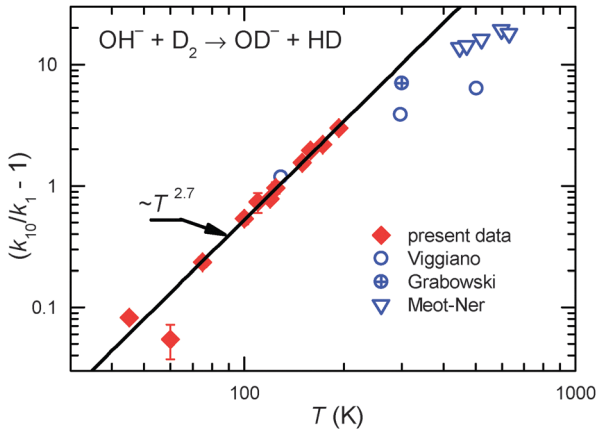

Fig. 5 Plot of $(k_{10}/k_1 - 1)$ *versus* T for the data shown in Fig. 4 emphasizing on the power law T^m. Data with a statistical error above 100% in this representation are not shown.

really are. In any case, the fit through the data plotted in Fig. 4 and the linearity of the plot in Fig. 5 may be significant. The extrapolation of our fit towards higher temperatures gives a reasonable prediction for previous data, see Fig. 4 and 5. The discrepancy between the empirical curve and the data of Mautner *et al.*[41] at higher temperatures must be due to direct mechanisms, which is not accounted for in eqn (5). Similar behavior has been observed before for several ion molecule reactions.[65] The significant contribution of the present study is the coverage of a large interval at low temperatures.

3.2 Reaction $OD^- + H_2$

Examples of the measured time evolutions of normalized numbers of primary OD^- and product OH^- ions at four different temperatures are plotted in Fig. 6. The actual densities of H_2, He and D_2 in the trap are listed in Table 2. High number densities of H_2 are necessary to obtain a significant decay of the number of primary OD^- anions because at low temperatures the endothermic reaction (2) is slow. Note that, in comparison

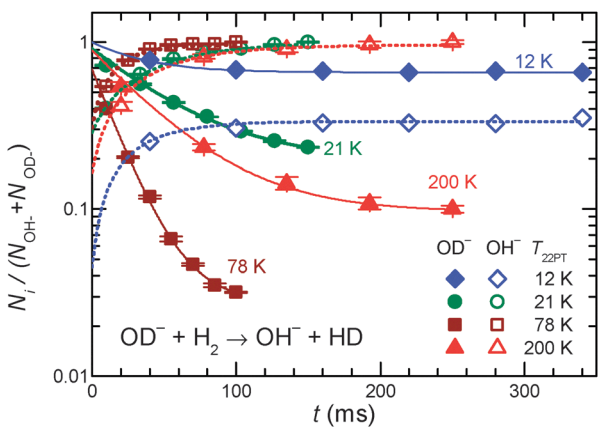

Fig. 6 Normalized number of primary ions (OD^-, closed symbols) and product ions (OH^-, open symbols) as a function of storage time. The trap was at T_{22PT} = 12, 21, 78, 200 K, the densities of D_2, He and H_2 in the trap are listed in Table 2.

Table 2 Experimental conditions used for the results shown in Fig. 6. $[D_2]_{SIS}$ is the density of deuterium penetrating from the storage ion source into the trap

T_{22PT} (K)	$[H_2]$ (cm^{-3})	[He] (cm^{-3})	$[D_2]_{SIS}$ (cm^{-3})
12	1.2×10^{13}	3.4×10^{13}	$\approx 1 \times 10^{10}$
21	6.7×10^{12}	4.5×10^{13}	$\approx 1 \times 10^{10}$
78	2.0×10^{12}	2.3×10^{13}	$\approx 5 \times 10^{9}$
200	3.4×10^{11}	2.5×10^{12}	$\approx 3 \times 10^{9}$

with the density of reactant H_2, the density of D_2 from the SIS is at least 100 times lower. In spite of this, back conversion of the OH^- products *via* exothermic H/D exchange with D_2 dominates at low temperatures. Therefore, the influence of reconversion cannot be neglected. Non-monoexponential decay is a clear indication of this fact. From this we can observe an approach towards equilibrium already at $t > 50$ ms at 12 K (see Fig. 6). The reconversion is the factor limiting the accuracy of k_2.

The temperature dependence of reaction (2) was studied in the range of trap temperatures T_{22PT} from 11 K to 300 K. Varying the target density, it was confirmed that the products are formed *via* a bimolecular reaction. Our data shown in Fig. 7 were fitted by the Arrhenius function $k_2 = k_{2A} \exp(-E_{A\text{-}Exp}/k_B T)$, where k_{2A} is pre-exponential factor and $E_{A\text{-}Exp}$ is the Arrhenius activation energy.[73] From the fit we obtained $k_{2A} = 7.5 \times 10^{-11}$ cm^3 s^{-1} and $E_{A\text{-}Exp} = (7.9 \pm 0.3)$ meV, corresponding to $T_{A\text{-}Exp} = E_{A\text{-}Exp}/k_B = (92 \pm 3)$ K. The obtained function agrees with the data obtained in previous FDT experiments of Viggiano and Morris[40] as well. To emphasize the low temperature region, Fig. 8 shows the data as the Arrhenius plot, revealing a linear decay over two orders of magnitude. Minor deviations are only at $T_{22PT} < 25$ K.

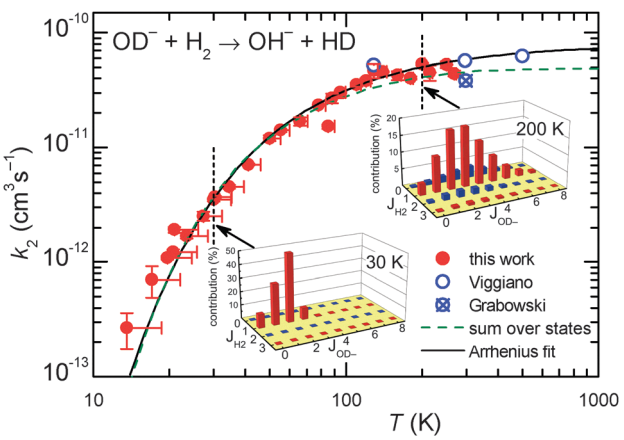

Fig. 7 Temperature dependence of the rate coefficient k_2 (filled circles) for the endothermic reaction (2). The vertical error bars of the two points at the lowest temperatures include the estimated error caused by the oscillations of temperature and pressure. At temperatures above 20 K, these effects are negligible and only statistical errors are shown. The results have been fitted using an Arrhenius temperature dependence (solid line). Previous FDT data of Viggiano and Morris[40] and SIFT data of Grabowski *et al.*[39] are also plotted. The dashed curve is a fit with function (7) (see the text for details). The insets indicate the $k_{J_{H_2}J_{OD^-}}/k_{2\Sigma}$ in percent (eqn (6) and (7)) at 30 K and 200 K.

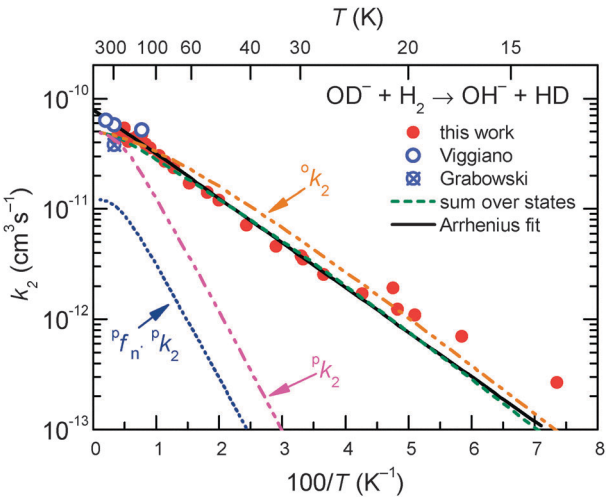

Fig. 8 Arrhenius plot of rate coefficient k_2 for reaction (2) measured with normal H_2. Shown are two almost identical fits, the two-parameter Arrhenius (solid line) and the sum over all relevant rotational states of the ion and of normal hydrogen (no *ortho–para* relaxation, dashed line). For details see the text. Previous FDT data of Viggiano and Morris[40] and SIFT data of Grabowski *et al.*[39] are also included in the plot. The plots marked with ${}^{o}k_2$ and ${}^{p}k_2$ are predictions for pure *ortho*- and *para*-hydrogen. In normal hydrogen, the contribution of *para*-hydrogen is only ${}^{p}f_n\,{}^{p}k_2 = \frac{1}{4}{}^{p}k_2$.

For explaining the difference between the endothermicity of reaction (2), ΔH = 24.0 meV, and the obtained activation energy $E_{\text{A-Exp}}$ = (7.9 ± 0.3) meV, one is tempted to account simply for the rotational energy contributed from the hydrogen target. We use normal hydrogen with 75% in the *ortho* nuclear spin state. This means that, even at very low temperatures, 3/4 of the H_2 molecules are rotationally excited with odd quantum numbers. If the rotational energy for J = 1, 14.7 meV, is available for promoting the reaction, the threshold onset is already lowered to 9.3 meV. For a more consistent comparison, one has to account for all rotational energies provided by both reactants (see Fig. 1). Introducing a state specific rate coefficient $k_{J_{H_2}J_{OD^-}}$ for each combination of rotational states, J_{H_2}, J_{OD^-} and accounting for their thermal populations $P_{J_{H_2}}$ and $P_{J_{OD^-}}$, the thermal rate coefficient can be calculated using the sum

$$k_{2\Sigma}(T) = \sum_{J_{OD^-},J_{H_2}} P_{J_{H_2}} P_{J_{OD^-}} k_{J_{H_2}J_{OD^-}} \qquad (6)$$

This general formula can account for all dependencies, *e.g.* rotational inhibition or special nuclear spin effects. In the following we use the crude assumptions that all energies are equivalent in driving the reaction and that we can use a global pre-exponential factor k_{20} in an Arrhenius representation for the state specific rate coefficients,

$$k_{J_{H_2}J_{OD^-}}(T) = k_{20}\exp\left(-\frac{\Delta E_{J_{H_2}J_{OD^-}}}{k_B T}\right). \qquad (7)$$

The activation energy is given by

$$\Delta E_{J_{H_2}J_{OD^-}} = \max\left\{0; \left(\Delta H - E_{J_{H_2}} - E_{J_{OD^-}}\right)\right\}. \qquad (8)$$

The energies of the rotational states, $E_{J_{H_2}}$ and $E_{J_{OD^-}}$, have been calculated using the rotational constants from Huber and Herzberg,[47] Rehfuss *et al.*[53] Using ΔH = 24.0 meV as fixed and putting eqn (7) into eqn (6), the averaged rate coefficient $k_{2\Sigma}(T)$ is completely determined with the exception of one free parameter, k_{20}. Accounting for the temperature dependence of the rotational population of OD^- and the constant 1 : 3 population of even and odd J of normal H_2, the experimental data could be fitted leading to $k_{20} = 4.9 \times 10^{-11}$ cm^3 s^{-1}. Comparison of this result (dashed line) with the data points in Fig. 7 and 8 reveals good agreement over a wide range of T. The small deviations at low temperatures are most probably due to experimental uncertainties in the translational and rotational temperatures (they may differ slightly). It cannot also be excluded that ΔH is slightly smaller. The problem of determining the endothermicity with sub-meV accuracy from the difference of zero point energies has been discussed above.

Based on our simple model, specific rate coefficients can be calculated for various conditions of the trapping experiment. The two insets in Fig. 7 show the relative contributions as a function of the two rotational states (J_{H_2}, J_{OD^-}). At 30 K, the largest rate coefficient is predicted for (1,2) while at 200 K, also contributions from J_{H_2} = 0 and 2 show up. Summing exclusively over even or odd rotational states of H_2 leads to rate coefficients for pure *ortho* or pure *para* hydrogen, respectively. The results are shown in Fig. 8 as ${}^{o}k_2$ and ${}^{p}k_2$. The lowest curve in this plot, ${}^{p}f_n{}^{p}k_2$, shows the contribution of *para*-H_2 in the present experiment, where normal-H_2 has been used (${}^{p}f_n$ = 0.25). Such predictions are important for preparing experiments with *para*-enriched H_2 or for estimating the product signal for a hydrogen beam, passing a trapped OD^- cloud.

4 Conclusion

We have studied the temperature dependence of proton–deuteron exchange for the two reactions (1) and (2). The experiments have been carried out using the AB-22PT instrument, the cold head of which can reach nominal temperatures as low as 10 K. Both the He buffer gas and the hydrogen reactant gas have been leaked into the trap directly resulting in a nearly thermalized system.

Isotope scrambling *via* the 0.2 eV bound intermediate H_3O^- is rather inefficient. This can be concluded from a comparison of the measured rate coefficients for the two isotopic combinations (1) and (2) with each other as well as with the corresponding capture values (Langevin: $k_{1L} = 1.16 \times 10^{-9}$ cm^3 s^{-1} and $k_{2L} = 1.55 \times 10^{-9}$ cm^3 s^{-1}). Only at low temperatures, reaction (1) reaches almost 70% of $\frac{2}{3}k_{1L}$ (the pre-factor accounts for the 1 : 2 ratio of H : D). Reaction (2) is always slower than (1) and increases only to 5% of $\frac{2}{3}k_{2L}$. All this may indicate steric hindrance during complex formation or weak coupling between the various H_3O^- intermediates.

More information has been gained from the change of reactivity with increasing temperature. The measured negative temperature dependence of the exoergic reaction (1) has been

approximated using the function $k_1 \approx k_{10}/(1 + (T/130\ \mathrm{K})^{2.7})$. This power law and its similarity to the T dependence of three body association reactions leads to the supposition that a decrease of the complex lifetime may be responsible for the fall-off of the experimental data. A different explanation, proposed by Viggiano and Morris,[40] postulates that rotation of D_2 hinders the reaction. This idea has been partly supported by Lee and Farrar[42] who concluded that the reaction needs favorable alignments of OH^- and D_2. This may be easier to reach with non-rotating deuterium. We have tested this idea by comparing our data with a simple simulation assuming that exclusively D_2 ($J = 0$) reacts. As can be seen from the dash-dotted line in Fig. 4, the resulting temperature dependence is not falling off steeply enough.

So far our results have not been detailed enough for extracting state specific rate coefficients $k_{J_{H_2} J_{OD^-}}$; however, the results for the endoergic reaction (2) give additional hints. For modeling the increase of $k_2(T)$ we have assumed that each combination of rotational states of the two reactants contributes with the same rate coefficient multiplied with a state specific Arrhenius factor (see eqn (7) and (8)). The dashed line in Fig. 7 shows that this leads to a very good fit of our data with only one free parameter, k_{20}. It is also in accord with previous data.[39,40]

In spite of our new results and their good agreement with the simple models, many questions remain open and ask for more experimental and theoretical activities. An obvious task is to use pure HD as target gas and to study reactions (1) and (2) in their reverse direction. The use of *para*-enriched hydrogen for separating $J = 0$ and $J = 1$ contributions already has been mentioned and work is in progress. For testing the dependence of k_1 on the rotation of the D_2 molecule, the AB-22PT instrument can be operated with a cold effusive D_2 beam instead of leaking the gas directly into the trap.[54] The combination neutral beam–trap allows one to control the rotational population of the ions separately from that of the neutrals.

For a deeper understanding of the reaction dynamics, theoretical investigations are required. Potential energy surfaces are available.[33,34,38] First hints to a possible orientation dependence during the approach of the reactants may be obtained from trajectory calculations. Trajectories, started somewhere in the three potential minima, may provide information on the efficiency of H/D scrambling. To look closer to the H_3O^- transitions state, the spectroscopic characterization of this stable molecular anion is of great interest. Moreover, photofragmentation of the 0.2 eV bound H_3O^- may start selected half-collisions, complementary to the neutral reactions initiated by photo detachment of the electron from H_3O^-.[34]

Acknowledgements

The 22-pole ion trap instrument has been developed in Chemnitz and since 2009 it has been operated in the Faculty of Mathematics and Physics of the Charles University in Prague. We thank Chemnitz University of Technology and the DFG for making this transfer possible. This work was partly supported by GACR Grant No. P209/12/0233, 14-14715P, UNCE Grant No. 204020/2012, SV Grant No. 260 090, GAUK Grant No. 572214, 692214, 659112, AKTION 7AMB14AT023.

References

1 A. Dalgarno and R. A. McCray, *Astrophys. J.*, 1973, **181**, 95–100.
2 M. C. McCarthy, C. A. Gottlieb, H. Gupta and P. Thaddeus, *Astrophys. J.*, 2006, **652**, L141.
3 J. Cernicharo, M. Guélin, M. Agundez, K. Kawaguchi, M. McCarthy and P. Thaddeus, *Astron. Astrophys.*, 2007, **467**, L37–L40.
4 S. Brunken, H. Gupta, C. A. Gottlieb, M. C. McCarthy and P. Thaddeus, *Astrophys. J.*, 2007, **664**, L43.
5 P. Botschwina and R. Oswald, *J. Phys. Chem. A*, 2010, **114**, 4875–4880.
6 Z. Yang, B. Eichelberger, O. Martinez, M. Stepanovic, T. P. Snow and V. M. Bierbaum, *J. Am. Chem. Soc.*, 2010, **132**, 5812–5819.
7 N. J. Demarais, Z. Yang, O. Martinez, N. Wehres, T. P. Snow and V. M. Bierbaum, *Astrophys. J.*, 2012, **746**, 32.
8 Z. Yang, B. Eichelberger, M. Y. Carpenter, O. Martinez, Jr., T. P. Snow and V. M. Bierbaum, *Astrophys. J.*, 2010, **723**, 1325–1330.
9 H. Kreckel, H. Bruhns, M. Čížek, S. C. O. Glover, K. A. Miller, X. Urbain and D. W. Savin, *Science*, 2010, **329**, 69–71.
10 D. Gerlich, P. Jusko, Š. Roučka, I. Zymak, R. Plašil and J. Glosík, *Astrophys. J.*, 2012, **749**, 22.
11 K. Miller, H. Bruhns, M. Čížek, J. Eliášek, R. Cabrera-Trujillo, H. Kreckel, A. OConnor, X. Urbain and D. Savin, *Phys. Rev. A: At., Mol., Opt. Phys.*, 2012, **86**, 032714.
12 C. A. Cole, N. J. Demarais, Z. Yang, T. P. Snow and V. M. Bierbaum, *Astrophys. J.*, 2013, **779**, 181.
13 E. S. Endres, O. Lakhmanskaya, D. Hauser, S. E. Huber, T. Best, S. S. Kumar, M. Probst and R. Wester, *J. Phys. Chem. A*, 2014, **118**, 6705–6710.
14 S. Trippel, J. Mikosch, R. Berhane, R. Otto, M. Weidemuller and R. Wester, *Phys. Rev. Lett.*, 2006, **97**, 193003.
15 P. Hlavenka, R. Otto, S. Trippel, J. Mikosch, M. Weidemuller and R. Wester, *J. Chem. Phys.*, 2009, **130**, 061105.
16 T. Best, R. Otto, S. Trippel, P. Hlavenka, A. v. Zastrow, S. Eisenbach, S. Jézouin, R. Wester, E. Vigren, M. Hamberg and W. D. Geppert, *Astrophys. J.*, 2011, **742**, 63.
17 S. S. Kumar, D. Hauser, R. Jindra, T. Best, Š. Roučka, W. D. Geppert, T. J. Millar and R. Wester, *Astrophys. J.*, 2013, **776**, 25.
18 J. E. Parr and J. L. Moruzzi, *J. Phys. D: Appl. Phys.*, 1972, **5**, 514.
19 Y. Okuyama, M. Sabo, H. Itoh and S. Matejcík, *Eur. Phys. J.: Appl. Phys.*, 2013, **61**, 7.
20 M. Kučera, M. Stano, J. Wnorowska, W. Barszczewska, D. Loffhagen and Š. Matejčík, *Eur. Phys. J. D*, 2013, **67**, 1–8.
21 O. Martinez, Z. Yang, N. B. Betts, T. P. Snow and V. M. Bierbaum, *Astrophys. J.*, 2009, **705**, L172.

22 Z. Yang, C. A. Cole, J. Oscar Martinez, M. Y. Carpenter, T. P. Snow and V. M. Bierbaum, *Astrophys. J.*, 2011, **739**, 19.
23 R. Otto, J. Mikosch, S. Trippel, M. Weidemuller and R. Wester, *Phys. Rev. Lett.*, 2008, **101**, 063201.
24 M. Cížek, J. Horáček and W. Domcke, *J. Phys. B: At., Mol. Opt. Phys.*, 1998, **31**, 2571–2583.
25 T. González-Lezana, P. Honvault, P. G. Jambrina, F. J. Aoiz and J.-M. Launay, *J. Chem. Phys.*, 2009, **131**, 044315.
26 D. Gerlich and S. Schlemmer, *Planet. Space Sci.*, 2002, **50**, 1287–1297.
27 P. Jusko, Š. Roučka, R. Plašil and J. Glosík, *Int. J. Mass Spectrom.*, 2013, **352**, 19–28.
28 P. Jusko, Š. Roučka, D. Mulin, I. Zymak, R. Plašil, D. Gerlich, M. Čížek, K. Houfek and J. Glosík, *J. Chem. Phys.*, 2015, **142**, 014304.
29 J. C. Kleingeld and N. M. M. Nibbering, *Int. J. Mass Spectrom.*, 1983, **49**, 311–318.
30 T. M. Miller, A. A. Viggiano, A. E. S. Miller, R. A. Morris, M. Henchman, J. F. Paulson and J. M. V. Doren, *J. Chem. Phys.*, 1994, **100**, 5706–5714.
31 D. Hauser, O. Lakhmanskaya, S. Lee, Š. Roučka and R. Wester, *New J. Phys.*, 2015, submitted.
32 E. de Beer, E. H. Kim, D. M. Neumark, R. F. Gunion and W. C. Lineberger, *J. Phys. Chem.*, 1995, **99**, 13627–13636.
33 D. H. Zhang, M. Yang, M. A. Collins and S.-Y. Lee, *PNAS*, 2002, **99**, 11579–11582.
34 D. M. Neumark, *Phys. Chem. Chem. Phys.*, 2005, **7**, 433–442.
35 D. Wang, J. Z. H. Zhang and C.-h. Yu, *Chem. Phys. Lett.*, 1997, **273**, 171–178.
36 P. Jusko, O. Asvany, A.-C. Wallerstein, S. Brunken and S. Schlemmer, *Phys. Rev. Lett.*, 2014, **112**, 253005.
37 E. E. J. Muschlitz, *J. Appl. Phys.*, 1957, **28**, 1414–1418.
38 Y. Li, L. Liu and J. M. Farrar, *J. Phys. Chem. A*, 2005, **109**, 6392–6396.
39 J. J. Grabowski, C. H. DePuy and V. M. Bierbaum, *J. Am. Chem. Soc.*, 1983, **105**, 2565–2571.
40 A. A. Viggiano and R. A. Morris, *J. Chem. Phys.*, 1994, **100**, 2748–2753.
41 M. M.-N. Mautner, J. R. Lloyd, E. P. Hunter, W. A. Agosta and F. H. Field, *J. Am. Chem. Soc.*, 1980, **102**, 4672–4676.
42 S. T. Lee and J. M. Farrar, *J. Chem. Phys.*, 2000, **113**, 581–595.
43 M. Henchman and J. F. Paulson, *Int. J. Radiat. Appl. Instrum., Part C*, 1988, **32**, 417–423.
44 J. R. Smith, J. B. Kim and W. C. Lineberger, *Phys. Rev. A: At., Mol., Opt. Phys.*, 1997, **55**, 2036–2043.
45 P. A. Schulz, R. D. Mead, P. L. Jones and W. C. Lineberger, *J. Chem. Phys.*, 1982, **77**, 1153–1165.
46 K. K. Irikura, *J. Phys. Chem. Ref. Data*, 2007, **36**, 389–397.
47 K. Huber and G. Herzberg, *Molecular Spectra and Molecular Structure: Constantso Diatomic Molecules*, Van Nostrand Reinhold, New York, 1979, vol. IV.
48 N. H. Rosenbaum, J. C. Owrutsky, L. M. Tack and R. J. Saykally, *J. Chem. Phys.*, 1986, **84**, 5308–5313.
49 L. I. Kleinman and M. Wolfsberg, *J. Chem. Phys.*, 1973, **59**, 2043–2053.
50 L. I. Kleinman and M. Wolfsberg, *J. Chem. Phys.*, 1974, **60**, 4740–4748.
51 A. Adohi-Krou, F. Martin, A. J. Ross, C. Linton and R. J. L. Roy, *J. Chem. Phys.*, 2004, **121**, 6309–6316.
52 B. Ruscic, A. F. Wagner, L. B. Harding, R. L. Asher, D. Feller, D. A. Dixon, K. A. Peterson, Y. Song, X. Qian, C.-Y. Ng, J. Liu, W. Chen and D. W. Schwenke, *J. Phys. Chem. A*, 2002, **106**, 2727–2747.
53 B. D. Rehfuss, M. W. Crofton and T. Oka, *J. Chem. Phys.*, 1986, **85**, 1785–1788.
54 D. Gerlich, G. Borodi, A. Luca, C. Mogo and M. A. Smith, *Z. Phys. Chem.*, 2011, **225**, 475–492.
55 G. Borodi, A. Luca and D. Gerlich, *Int. J. Mass Spectrom.*, 2009, **280**, 218–225.
56 I. Zymak, P. Jusko, Š. Roučka, R. Plašil, P. Rubovič, D. Gerlich and J. Glosík, *Eur. Phys. J.: Appl. Phys.*, 2011, **56**, 24010.
57 R. Plašil, I. Zymak, P. Jusko, D. Mulin, D. Gerlich and J. Glosík, *Philos. Trans. R. Soc., A*, 2012, **370**, 5066–5073.
58 D. Gerlich and S. Horning, *Chem. Rev.*, 1992, **92**, 1509–1539.
59 D. Gerlich, *Phys. Scr.*, 1995, **1995**, 256.
60 R. Wester, *J. Phys. B: At., Mol. Opt. Phys.*, 2009, **42**, 154001.
61 O. Asvany, S. Brunken, L. Kluge and S. Schlemmer, *Appl. Phys. B: Lasers Opt.*, 2014, **114**, 203–211.
62 M. Hejduk, P. Dohnal, J. Varju, P. Rubovič, R. Plašil and J. Glosík, *Plasma Sources Sci. Technol.*, 2012, **21**, 024002.
63 I. Zymak, M. Hejduk, D. Mulin, R. Plašil, J. Glosík and D. Gerlich, *Astrophys. J.*, 2013, **768**, 86.
64 J. Glosik, D. Smith, P. Španl, W. Freysinger and W. Lindinger, *Int. J. Mass Spectrom.*, 1993, **129**, 131–143.
65 J. Glosik, W. Freysinger, A. Hansel, P. Spanel and W. Lindinger, *J. Chem. Phys.*, 1993, **98**, 6995–7003.
66 J. Glosik, P. Zakouřil and W. Lindinger, *Int. J. Mass Spectrom.*, 1995, **145**, 155–163.
67 J. Glosik, P. Zakouřil, V. Skalský and W. Lindinger, *Int. J. Mass Spectrom.*, 1995, **149–150**, 499–512.
68 J. Glosík, P. Zakouřil and W. Lindinger, *J. Chem. Phys.*, 1995, **103**, 6490–6497.
69 P. Zakouřil, J. Glosik, V. Skalsky and W. Lindinger, *J. Phys. Chem.*, 1995, **99**, 15890–15898.
70 J. Glosik, P. Zakouřil and A. Luca, *Int. J. Mass Spectrom.*, 2003, **223–224**, 539–546.
71 D. R. Bates, *J. Phys. B: At. Mol. Phys.*, 1979, **12**, 4135.
72 E. Herbst, *J. Chem. Phys.*, 1979, **70**, 2201–2204.
73 M. Menzinger and R. Wolfgang, *Angew. Chem., Int. Ed. Engl.*, 1969, **8**, 438–444.

II. Low-Temperature Ion Trap Studies of $N^+(^3P_{ja}) + H_2(J) \rightarrow NH^+ + H$

Zymak I., Hejduk M., Mulin, D., Plašil R., Glosík J., and Gerlich D. (2013)

The Astrophysical Journal, **768**(**1**), 86.

The Astrophysical Journal, 768:86 (8pp), 2013 May 1 doi:10.1088/0004-637X/768/1/86

LOW-TEMPERATURE ION TRAP STUDIES OF $N^+(^3P_{ja}) + H_2(j) \rightarrow NH^+ + H$

I. Zymak[1], M. Hejduk[1], D. Mulin[1], R. Plašil[1], J. Glosík[1], and D. Gerlich[1,2,3]
[1] Faculty of Mathematics and Physics, Charles University, Prague, Czech Republic
[2] Department of Physics, Technische Universität Chemnitz, D-09107 Chemnitz, Germany
Received 2012 December 30; accepted 2013 February 22; published 2013 April 17

ABSTRACT

Using a low-temperature 22-pole ion trap apparatus, detailed measurements for the title reaction have been performed between 10 K and 100 K in order to get some state specific information about this fundamental hydrogen abstraction process. The relative population of the two lowest H_2 rotational states, $j = 0$ and 1, has been varied systematically. NH^+ formation is nearly thermo-neutral; however, to date, the energetics are not known with the accuracy required for low-temperature astrochemistry. Additional complications arise from the fact that, so far, there is no reliable theoretical or experimental information on how the reactivity of the N^+ ion depends on its fine-structure (FS) state $^3P_{ja}$. Since in the present trapping experiment, thermalization of the initially hot FS population competes with hydrogen abstraction, the evaluation of the decay of N^+ ions over long storage times and at various He and H_2 gas densities provides information on these processes. First assuming strict adiabatic behavior, a set of state specific rate coefficients is derived from the measured thermal rate coefficients. In addition, by recording the disappearance of the N^+ ions over several orders of magnitude, information on nonadiabatic transitions is extracted including FS-changing collisions.

Key words: astrochemistry – ISM: abundances – molecular processes

Online-only material: color figures

1. INTRODUCTION

As discussed recently by Dislaire et al. (2012) atomic nitrogen and nitrogen-containing molecules are important tracers for understanding astrophysical objects. Due to the abundance of hydrogen, the nitrogen hydrides, NH, NH_2, and NH_3, and their ions are of central importance in astrochemistry. For example, subsequent hydrogen abstraction reactions, starting with N^+, finally lead to the formation of interstellar ammonia (Le Bourlot 1991). In order to obtain quantitative abundances in various environments, e.g., in dark clouds, the reaction

$$N^+(^3P_{ja}) + H_2(j) \rightarrow NH^+ + H \quad (1)$$

and its dependence on the rotational ($j = 0, 1, \ldots$) and the FS ($j_a = 0$, 1, and 2) states plays a special role. In the 1980s and early 1990s, there were several experimental activities in which this reaction was studied at room temperature and below. Various techniques such as SIFDT (selected ion flow and drift tube; Adams & Smith 1985), CRESU (Cinétique de réactions en écoulement supersonique uniforme; Marquette et al. 1988), low-temperature penning ion trap (Barlow et al. 1986), and guided ion beams with scattering cells (Sunderlin & Armentrout 1994) provided detailed results. First applications of low-temperature radio frequency (RF) ion traps to the title reaction were mentioned in Gerlich (1989) and extended results have been given in Gerlich (1993). Probably the most sophisticated experiments have been based on crossing or merging a guided N^+ ion beam with a supersonic hydrogen beam (Tosi et al. 1994); however, the ambitious goal of determining state specific cross sections has not been reached so far. There have also been various theoretical studies (see Gerlich 1989; Nyman & Wilhelmsson 1992; Wilhelmsson & Nyman 1992; Russell & Manolopoulos 1999, and references therein), and interesting aspects have been discussed; however, concerning reactions at low temperature, they raise more questions than they answer.

A basic problem is that one does not yet know whether the formation of $NH^+ + H$ is really endothermic or whether somewhere a barrier hinders the reaction. As reviewed by Gerlich (2008a), the analysis of measured temperature dependencies of reaction (1) with a statistical theory leads to an endothermicity of 17 meV if one presupposes that FS and rotational states are in thermal equilibrium and that, in promoting the reaction, their energies are as equally efficient as translational energy. If FS energy is not available at all, the assumed endothermicity has to be lowered to 11 meV to match the experimental results. High-level ab initio computations are not yet sufficiently accurate to predict this value with the required accuracy, i.e., within a few meV. This is rather unexpected since one has to calculate only the binding energy of NH^+. Discussions of different high-level ab initio computations, calculated potentials, bond dissociation energies, and heat of formation for NH and NH^+ can be found in Tarroni et al. (1997), Jursic (1998), and Amero & Vazquez (2005). Also related to this subject are the quantum chemical calculations of the adiabatic ionization energy of the NH_2 radical (Willitsch et al. 2006), the accuracy of which has been estimated to be about 100 cm^{-1}.

In order to understand reaction dynamics, one needs more than just the asymptotic energies. In the present case, several potential energy surfaces are involved. The situation is illustrated in Figure 1 with a simplified electronic correlation diagram (Mahan & Ruska 1976; Russell & Manolopoulos 1999). Inspection reveals that, at kinetic energies below 1 eV, only the $NH^+(X^2\Pi)$ product can be formed, if the two reactants N^+ and H_2 are in their ground state. For C_s symmetry the reaction can proceed adiabatically via the more than 6 eV deep double-well structure, as indicated by the dashed lines avoiding the crossings. An analytical fit of this lowest adiabatic $^3A''$ potential energy surface has been published by Wilhelmsson et al. (1992). This surface has been used for low-energy quasi-classical trajectory

[3] Author to whom any correspondence should be addressed.

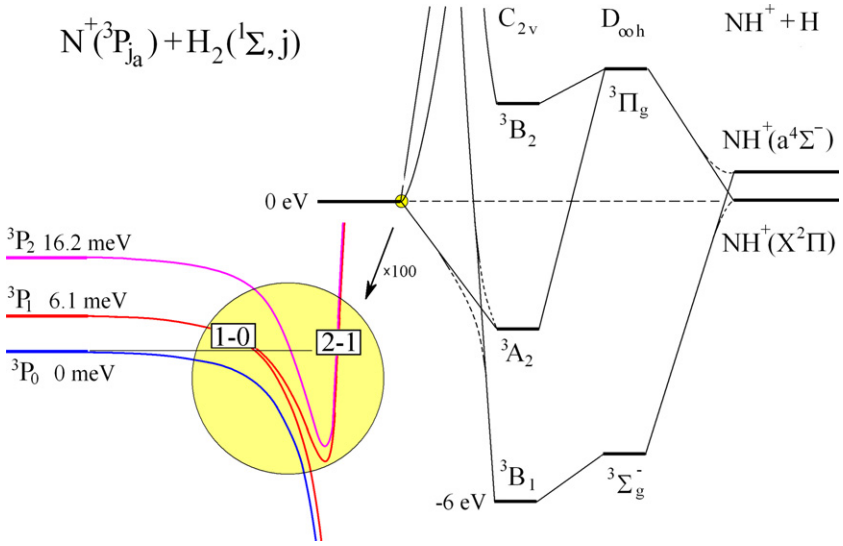

Figure 1. Schematic view of the electronic state correlation diagram for the NH_2^+ system (not to scale; for details see Mahan & Ruska 1976; González et al. 1986; Russell & Manolopoulos 1999). The horizontal dashed line indicates that reaction (1) is nearly thermoneutral. Typical experimental and theoretical values for the endothermicity (or barrier) range from 11 meV (Gerlich 2008a) to 33 meV (Wilhelmsson et al. 1992). The formation of a strongly bound NH_2^+ complex is possible via avoided intersections (C_s symmetry; dashed lines). Important for low-temperature collisions is the coupling between the nine near-degenerate spin–orbit potential-energy surfaces during the approach of the reactants. This can lead both to FS changes and reaction. The situation is illustrated in the lower left corner on a magnified scale in adiabatic approximation but also indicating schematically nonadiabatic transitions. The potential curves have been estimated in analogy to the N^+–He collision complex (Soldan & Hutson 2002).

(A color version of this figure is available in the online journal.)

calculations (Nyman & Wilhelmsson 1992; Wilhelmsson & Nyman 1992) as well as for time-dependent wave packet studies (Russell & Manolopoulos 1999). Problematic for the comparison of calculated reaction probabilities with low-temperature experimental data is that, on this surface, the reaction endothermicity is certainly too large with 33 meV.

Another shortcoming of the calculations mentioned above is that the role of FS splitting is included using only rather crude approximations. As can be seen from the electronic correlation diagram in Figure 1, only one of the three triplet surfaces that correlates with the entrance channel, allows direct access to the deep well, while the other two are repulsive. In statistical theories, this is accounted for by using suitable electronic degeneracy factors concerning the $N^+ + H_2$ system this is discussed in Gerlich (1989). A closer look at the initial splitting region (small circle in Figure 1) reveals that the open-shell structure of $N^+(^3P_{ja})$ results in at least nine spin–orbit coupled potential-energy surfaces. As plotted schematically in Figure 1 (large circle), they converge at large distances toward the three states $^3P_0$, $^3P_1$, and $^3P_2$. The question remains of how one can reach the product channel on these nine surfaces. Is there access to the deep well without any activation barrier? The assumption that only the three lowest spin–orbit surfaces lead to products, while reaction on the other six is not possible at low energies is very restrictive. This model, which is based on strict adiabatic behavior, was applied by Wilhelmsson & Nyman (1992) and Nyman & Wilhelmsson (1992). It has also been used by Russell & Manolopoulos (1999). Therefore, we also start the evaluation of our data on this basis. However, strict adiabatic behavior not only forbids reactions of ions in the $^3P_2$ state but also inhibits FS-changing collisions. As a consequence, N^+ ions in the highest fine structure would be completely insensitive to collisions with H_2. Since in our experiment, however, all N^+ ions are hydrogenated sooner or later, a more sophisticated kinetic model is required to account for the competition between reaction and thermalization of all three FS states.

Disregarding the details of any multi-surface model, a simpler question is how the different forms of energy, stored in the excited states of the reactants, can help to promote the reaction in the endothermic direction. Comparison of the thermal motion of the reactants (here up to 100 K, corresponding to $3/2\ k_B T = 12.9$ meV) with the electronic energy of N^+ ($^3P_1$ 6.1 meV, $^3P_2$ 16.2 meV) and rotational energy of H_2 (14.4 meV for $j = 1$) reveals that all these values are comparable to the endothermicity or barrier (11 or 17 meV, see above).

The equivalence of rotational and translational energy was first shown in the pioneering work from Marquette et al. (1988). In their low-temperature flow experiment, reaction (1) was studied using para hydrogen (p-H_2) as well as normal hydrogen (n-H_2). Note that p-H_2 has a total nuclear spin $I = 0$ and only even rotational states are allowed while ortho hydrogen has $I = 1$ and odd rotational states. Normal hydrogen is the 300 K statistical mixture consisting of 1/4 p-H_2 and 3/4 o-H_2. In what follows, other mixtures are characterized with the abbreviation f, indicating the fraction of o-H_2. The results from Marquette et al. (1988) were corroborated in a low-temperature trapping experiment (Gerlich 1993) and were extended using mixtures with $f = 0.13$, 0.03, and <0.01. More systematic studies of the f dependence are reported in this work.

In all experimental papers prior to 1994 it was postulated that the energy of the excited FS states is equivalent to translational and rotational energy. In addition it has been assumed that, in flow (Marquette et al. 1988) or trapping experiments (Gerlich 1993), thermal populations of the $^3P_{ja}$ states are reached rather quickly. There has never been any proof of this. In a guided ion beam experiment (Sunderlin & Armentrout 1994), FS energy was simply accounted for using the thermal mean value (9.5 meV at 300 K). As already mentioned, an analysis of all these experimental results, based on a detailed statistical model (Gerlich 1989), came to the conclusion that 17 meV is needed to promote the reaction. First doubts concerning the efficiency of the FS energy were formulated in

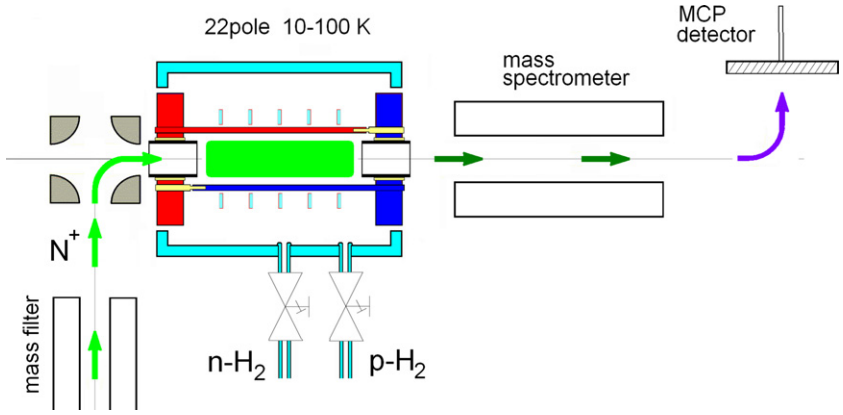

Figure 2. Schematic view of the 22 pole ion trap instrument used for studying reaction (1). The copper box surrounding the trap can be cooled down to 10 K. N^+ ions are produced from N_2 gas in a storage ion source (not shown), using electrons with a kinetic energy of 60 eV. After mass selection, they are transferred to the trap via an electrostatic quadrupole bender. In the radial direction the ions are confined by the RF field ($\Omega/2\pi = 19$ MHz, $V_0 = 20$ V). The potential inside the trap can be corrected locally with five ring electrodes. The entrance and exit electrode are used to open and close the trap with electrostatic barriers of some tens of meV. To the right, ions move through the quadrupole mass spectrometer toward the detector.

(A color version of this figure is available in the online journal.)

Tosi et al. (1994), especially in the context of Figure 4 of that publication.

This contribution reports new experimental results measured with a variable temperature RF ion trap. After a brief description of the instrument and typical measuring and calibration procedures, different sets of data are presented including the dependence of rate coefficients on the temperature and on the ortho fraction f and the time dependence of converting primary ions into products. The data are evaluated using first the adiabatic model resulting in state specific rate coefficients $k_{j,ja}(T)$ for $j = 0$, 1 and $j_a = 0$–2. In Section 4, additional information on the reactivity of $j_a = 2$ and the FS relaxation rate coefficient is presented. Some remarks concerning planned and possible extension of this work will conclude this paper.

2. EXPERIMENTAL

The instrument used in this study is the Chemnitz AB 22 pole trapping apparatus (Gerlich et al. 2011) which has been operated since 2009 at Charles University in Prague. It has been used recently in combination with an effusive beam of H atoms (Plasil et al. 2011; Gerlich et al. 2012). In the present study, the neutral target gas is leaked directly into the trap. The basics of storing ions in RF fields have been described thoroughly in Gerlich (1992, 1995). A summary of typical applications in low-temperature ion chemistry has been given in Gerlich (2008a, 2008b).

The central part of the instrument is shown schematically in Figure 2. The trap (22 rods with 1 mm diameter) is surrounded by a copper box which is mounted onto the cold head of a closed-cycle helium refrigerator. Stationary temperatures between 10 K and 100 K are set by simultaneously cooling and heating. Alternatively, temperature-dependent measurements are performed during the cooling down or warming up phases of the cold head. Hydrogen gas can be introduced into the trap via two leak valves, allowing us to produce any mixture from almost pure p-H_2 ($f < 0.01$) to n-H_2 ($f = 0.75$). A few collisions of the neutral gas with the walls are sufficient to get it into thermal equilibrium with the trap temperature, with the exception of the ortho/para ratio. The gas density inside the trap is determined using a spinning rotor gauge or a calibrated ionization gauge. The background pressure of the main chamber is lower than 10^{-7} Pa. With the exception of HD, most gas impurities are frozen out below 100 K; nonetheless, the small concentrations left can lead to errors as discussed below.

The primary N^+ ions are produced via dissociative ionization of N_2 in a storage ion source using energetic electrons (60 eV). Under such conditions it is safe to assume that the three fine-structure states $^3P_0$, $^3P_1$, and $^3P_2$ are populated according to their statistical weights, i.e., with 1, 3, and 5, respectively. Attempts to thermalize this population prior to reaction have been described in Gerlich (1993) and Tosi et al. (1994); however, no changes in the reactivity have been observed. After passing a mass filter and an electrostatic quadrupole bender, the primary ions are transferred into the trap. During the filling period, the electrostatic barrier at the entrance electrode is slightly negative relative to the potential of the trap. After various storage times, the trap exit is opened and the ions move through the quadrupole mass spectrometer and are converted into a fast negative pulse using an MCP detector followed by a discriminator. The standard measuring procedure is based on filling the trap at a fixed frequency with a well-defined number of primary ions (typically a few thousand) and analyzing the content after different storage times.

A typical set of raw data, recorded at a 22 pole temperature of 52 K and with buffer and reactant gas in the trap ([He] = 5.2×10^{11} cm^{-3}, [n-H_2] = 1.6×10^{11} cm^{-3}), is shown in Figure 3. The injected N^+ ions react with hydrogen and form NH^+. In subsequent collisions, these products react to form NH_2^+ and finally NH_3^+. As discussed by Gerlich (1993), NH_4^+ is also formed at length, however, very slowly, most probably via tunneling. In the first 10 ms, the sum of all detected ions (Σ) is increasing. This is due to phase-space compression of the injected ion cloud via collisions with the cold buffer gas leading to an increase of the detection efficiency (mainly acceptance and transmission of the quadrupole). Usually such time dependences are fitted with the solutions of a suitable rate equation system. In the present study, most information is derived simply from the decay of the primary ions. Quick information on the decay time constant is obtained by recording the number of N^+ ions at two or three suitable storage times. In order to get deeper insight into the kinetics, the disappearance of N^+ is followed in small time steps over several orders of magnitude (see below).

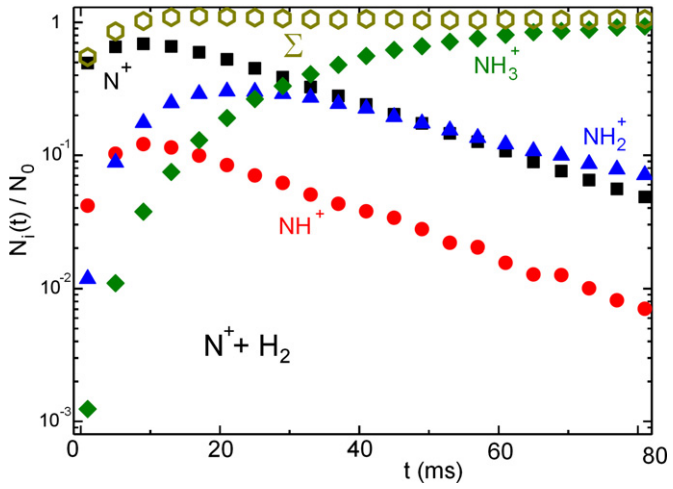

Figure 3. Sequential hydrogenation of trapped N^+ ions leading to NH_i^+ (i = 1–3) as a function of the storage time t. The measurements were performed at 52 K with helium buffer gas [He] = 5.2×10^{11} cm^{-3} and at a hydrogen number density of [n-H_2] = 1.6×10^{11} cm^{-3}. The sum of all ions (Σ) increases at the beginning (phase-space compression) and decays than very slowly. The 3.6% loss is most probably due to reactions with impurities. Evaluation of the decay of N^+ leads to a mean rate coefficient of 2.67×10^{10} cm^3 s^{-1}.

(A color version of this figure is available in the online journal.)

3. RESULTS AND FIRST EVALUATION

The upper part of Figure 4 shows a collection of rate coefficients, measured for the title reaction between 100 K and 10 K for different o-H_2 fractions f, ranging from 0.75 to 0.005. As explained in Section 2, most data have been taken during the cooling down phase of the cold head. In addition, some tests at selected temperatures have been made. Several sets of data, taken on different days, have confirmed the reproducibility.

One approach to evaluating such a manifold of experimental results is to use simple Arrhenius-type functions,

$$k = k_A \exp(-T_A/T), \quad (2)$$

where $T_A = E_A/k$ is the activation temperature, E_A is the activation energy, and k is the Boltzmann constant. In order to limit the number of free parameters, the restrictions imposed by the adiabatic model mentioned in Section 1 have been implemented. This means only the lowest three FS states can lead to products while the other six are so repulsive that there is no low-energy reaction path. In addition, it is postulated that the population of the FS states relaxes efficiently to the temperature of the trap. This assumption has also been made in the evaluation of all previous experimental data (Marquette et al. 1988; Gerlich 1993), although there has never been a direct proof. Under these boundary conditions, the measured rate coefficient k can be fitted using the ansatz

$$k = f(\xi_0 k_{1,0} + \xi_1 k_{1,1}) + (1 - f)(\xi_0 k_{0,0} + \xi_1 k_{0,1}). \quad (3)$$

In this equation, f is the selected ortho fraction, and the coefficients ξ_{ja} account for the thermal population of the two lowest FS states j_a. For the state specific rate coefficients, $k_{j,ja}(T)$ (with $j = 0$, 1 and $j_a = 0$ and 1), individual Arrhenius functions have been chosen. Contributions from $j = 2$ (3% in pure p-H_2 at 100 K) have been neglected. Inspection of the upper part of Figure 4 reveals that the lines follow the data points rather precisely, i.e., the restricted model fits all experimental data

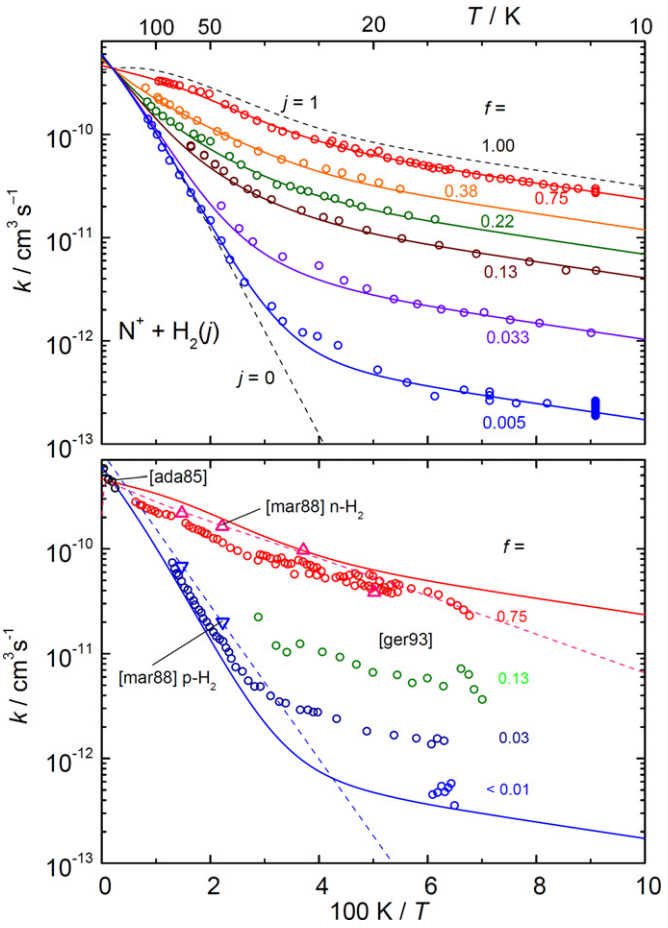

Figure 4. Arrhenius plot of experimental rate coefficients k for reaction (1), measured at different ortho-fractions f (upper panel). The data can be reproduced quite well with a thermally weighted superposition of state specific rate coefficients. The used function is given in Equation (3), the parameters in Table 1. The thin dashed lines are the analytical results for $f = 0$ (pure p-H_2) and $f = 1$ (pure o-H_2). In the lower panel, our data are compared to previous results. The triangles are CRESU results (Marquette et al. 1988), while the dots are ion trap results reported in (Gerlich 1993). The data at room temperature and above have been measured with an SIFDT instrument (Adams & Smith 1985). The dashed lines which go through the triangles indicate the functions used recently by Dislaire et al. (2012).

(A color version of this figure is available in the online journal.)

Table 1
State Specific Rate Coefficients for the Title Reaction, $k_{j,ja}$ (units 10^{-10} cm^3 s^{-1} and K), Derived from the $k(T)$

j, j_a	k_A	T_A
$k_{0,0}$	12	230
$k_{1,0}$	1.9	18
$k_{0,1}$	14	230
$k_{1,1}$	12	40

Notes. Results measured for various ortho fractions f (see Figures 4–6) and using Equation (2). $k_{0,2}$ and $k_{1,2}$ are set to zero (adiabatic approximation) and it is assumed that the ions are thermalized. For more information see the text.

quite well. The parameters obtained are presented in Table 1. More aspects of this analysis will be discussed below.

In the lower part of Figure 4, our data are compared to a variety of previously published measurements. For clarity and orientation, only our new analytical fits for $f = 0.75$ and 0.05 are included as solid lines. In addition, Table 2 presents numerical

Table 2
Previous Measured and Calculated Rate Coefficients for the Title Reaction (units 10^{-10} cm^3 s^{-1} and K)

k_A	T_A	n	Remarks	Reference
8.35	168.5	0	p-H_2	Marquette et al. (1988)
4.16	41.9	0	n-H_2	
15.3	177.5	0	p-H_2	Gerlich (1989)
4.06	42.5	0	n-H_2 (27–45 K)	
14.0	230	0	p-H_2	Gerlich (1993)
1.1	26	0	n-H_2 (10–40 K)	
4.2	44.5	−0.17	o-H_2	Dislaire et al. (2012)
9.0	220	0	p-H2	This work
1.5	180	−2.1	o-H2	
1.75	15	0		

Note. For comparison, the results from this work (last three lines) have also been parameterized using Equations (2) and (5).

values from other experiments and from a statistical theory. It can be seen that the previous ion trap results (Gerlich 1993) are slightly lower for n-H_2 ($f = 0.75$); however, they overlap within the combined uncertainties of absolute rate coefficients (typically 20%). The agreement of the steep decay of k between 100 K and 40 K for almost pure p-H_2, following the dotted line for $j = 0$ in the upper panel is gratifying. At temperatures below 25 K, the plots for the various mixtures run more or less parallel, indicating that k is mainly determined by the first half of Equation (3), i.e., the contributions from hydrogen in $j = 1$.

As explained in the context of Figure 2, the f values have been set absolutely by mixing n-H_2 and p-H_2. This method leads to very reliable values for $f > 0.2$. An analysis of possible errors indicates, that mixtures with less o-H_2 ($f < 0.2$) have an relative uncertainty of up to 10%. The ortho fractions given for "pure p-H_2" ($f < 0.01$) have been determined by fitting the experimental data using f as a free parameter. Note, however, that it is not yet clear whether the loss of N^+ in the low-temperature region is really just due to the reaction with the small o-H_2 admixtures or whether other processes, e.g., tunneling through a barrier, gas impurities such as HD or RF heating, are the reason for this.

In addition to the systematic variation of the temperature, the f dependence of the rate coefficients has also been recorded by increasing the ortho fraction in small steps from near zero to 0.75. The results, obtained at five different temperatures, are plotted in Figure 5. Comparison with the dashed lines reveals that all data follow a linear increase in good approximation. This is in accordance with Equation (3) predicting such an f dependence; however, it is only valid within the simple model used. Possible deviations could be expected due to more complex kinetics occurring in the trap, especially due to differences in FS relaxation for collisions of N^+ with $H_2(j = 0)$ or $H_2(j = 1)$. In this context, it is an interesting question whether the exothermic transfer of rotational energy into FS energy,

$$N^+\left(^3P_{ja}\right) + H_2(j = 1) \rightarrow N^+(^3P_{ja+1}) + H_2(j = 0), \qquad (4)$$

can affect the FS population at very low temperatures. Most probably, this process is forbidden by nuclear spin restriction, i.e., the required ortho–para conversion is very unlikely.

4. DISCUSSIONS

As long as there are no directly measured state specific cross sections, assumptions have to be made about the role of the different energy forms in driving the reaction. In the evaluation above, the reactivity of ions in the highest excited FS state has been set to zero, based on the adiabatic model, leading to very good fits of the data. This agreement, however, cannot be taken as a proof of the validity of this model, since other analytical functions, also used in the analysis of chemical systems, are of fitting capable them.

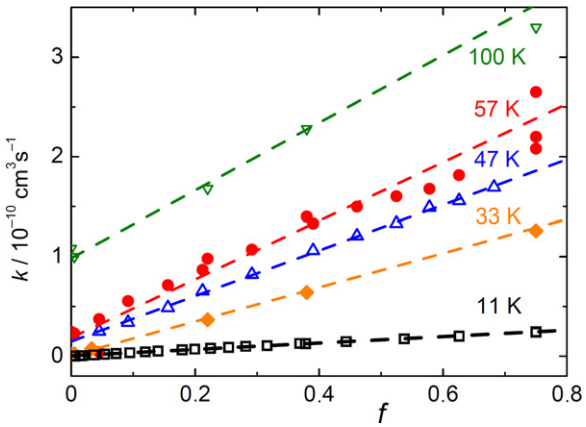

Figure 5. Rate coefficients for reaction (1) measured as a function of the ortho fraction for the indicated temperatures. As predicted from Equation (3) the data show a linear increase with increasing f. Nonetheless systematic deviations cannot be ruled out, especially at very low temperatures. It should be mentioned that the 11 K results extend over two orders of magnitude.

(A color version of this figure is available in the online journal.)

Deviations from the simple Arrhenius form (Equation (3)) are well known. They can be traced back to deviations of the threshold onset of an endothermic cross section from the functional form $\sim(E_t - E_o)^{1/2}/E_o$ (E_t is the translational energy; E_o is the threshold energy). In astrochemical data systems (see, for example, Equation (1) in Wakelam et al. 2012) it is common to account for this using a pre-exponential temperature-dependent factor with a free parameter n,

$$k = k_A(T/300\,\mathrm{K})^n \exp(-T_A/T). \qquad (5)$$

This function, which is called the Arrhenius–Kooij formula, has been used recently by Dislaire et al. (2012) for reevaluating the $N^+ + H_2$ data of Marquette et al. (1988). Ignoring the role of FS energy, they obtained a new set of parameters for o-H_2 (see Table 2, Figures 4 and 6). For p-H_2 they used the unaltered results reported by Marquette et al. (1988).

In Figure 6, the results of two different fitting procedures can be compared with each other. In the upper part, the $f = 0.75$ results from Figure 4 are reproduced together with the fit based on Equation (3). The four thin lines show the individual contributions $k_{j,ja}$ weighted with the thermal population of the FS states (ξ_{ja}) and the ortho fraction f. Inspection of these contributions reveals that in this model the curvature of the measured data is mainly caused by the change of the thermal population of the FS states. Between 50 K and 100 K the state specific rate coefficient $k_{1,1}$, i.e., reaction of $N^+(^3P_1)$ with $H_2(j = 1)$, prevails while the contribution from FS ground-state ions dominates at low temperatures. It is obvious that the results obtained for $f = 0.75$ are not very sensitive to $k_{0,0}$ and $k_{0,1}$. For these state specific rate coefficients more information has been derived from measurements with p-H_2 as can be seen in Figure 4. In the lower panel, the three indicated functions (thin lines, based on Equations (2) and (5)) have been used. With the parameters given in the lower part of Table 2, very good agreement

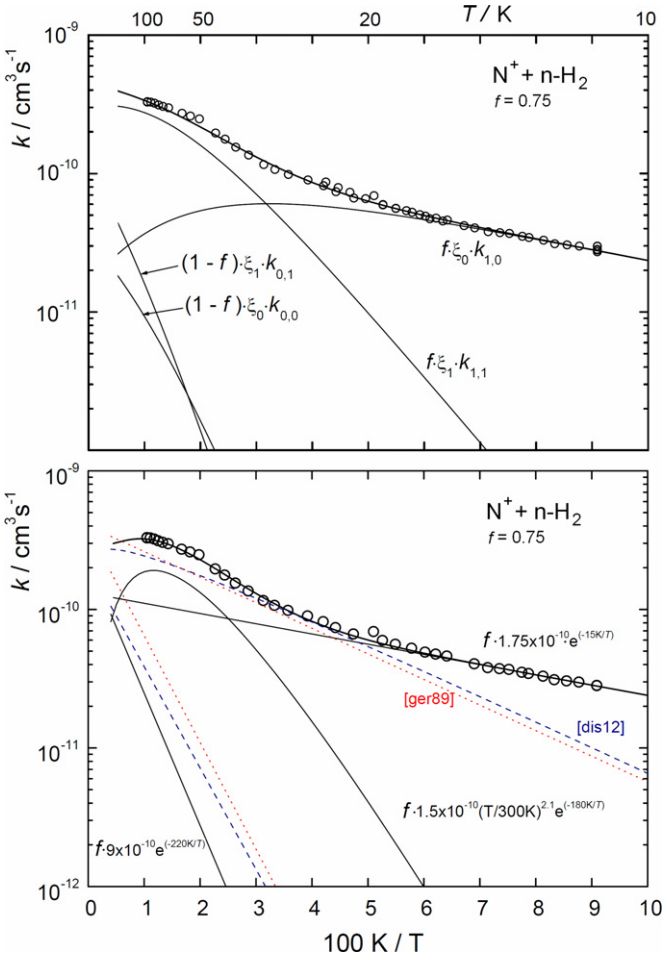

Figure 6. Two different fits of $k(T)$ measured with n-H_2. In the upper panel Equation (3) is used with the parameters given in Table 1. The four thin lines show the individual contributions $k_{j,ja}$, weighted with the thermal population of the FS states (ξ_{ja}) and the ortho fraction f. In the lower panel, the functions given in Equations (2) and (5) have been used directly. Three functions had to be used to get also a good fit. They are plotted as three thin lines together with the parameters used. In addition, this plot also shows the results from phase-space theory (short dashed line (Gerlich 1989) and the function used by Dislaire et al. (2012).

(A color version of this figure is available in the online journal.)

with the data points has also been reached. In this case, the curvature of the data is reproduced by the pre-exponential term. With the exception of the activation temperatures T_A, a scientific interpretation of these results is not obvious. Perhaps this can be taken as a hint that the $^3P_1$ state really plays a significant role at temperatures above 40 K.

The two examples shown in Figure 6 and discussed above illustrate that the analysis of the manifold of measured data is somehow arbitrary and that more experimental information is needed. Another problem, already mentioned in Section 1, is that our evaluation of the data is internally inconsistent since the $^3P_2$ state is excluded postulating adiabatic behavior on one side but it assumes efficient FS relaxation on the other side. In order to shed some more light on this conflict, additional experimental information is used, namely, the temporal changes of the ion composition in the trap as illustrated and discussed in Figure 3 and shown in Figure 7.

Since, due to the ionization process, the initially injected primary N^+ ions are in the $^3P_2$ state with a probability of 5/9 (3/9 in $^3P_1$, 1/9 in $^3P_0$) thermalization of the trapped ion ensemble and hydrogen abstraction reactions occur in competition with each other. In order to model the kinetics, one needs the relevant rate coefficients. A first attempt, based on state specific reaction rate coefficients calculated with phase-space theory (Gerlich 1989) and assuming relaxation rate coefficients $kr_{ja\to ja-1} = 10^{-n}$ cm^3 s^{-1} with $n = 11$, 10, and also 9, was reported in Tosi et al. (1994). While all measured decay curves were mono-exponential (after thermalizing the kinetic energy; see also Figure 4 of Gerlich 1993) the simulation always predicted an initial fast decay of primary ions followed by a slower one (see Figure 4 of Tosi et al. 1994). This curved behavior is obviously due to the high reactivity of the excited N^+ ions as predicted by the phase-space theory. In Tosi et al. (1994), a trivial solution has been proposed: fine structure energy is just not available, i.e., all ions react with the same rate coefficient. Looking at the potential energy surface and Figure 1, there is no obvious reason for such an extreme behavior.

Table 3
Experimental Parameters Used in the Measurements Shown in Figure 7

	a	*b*	*c*	*d*
T (K)	110	98	11	11
[H_2] (cm^{-3})	1.8E12	2.6E11	2.0E12	2.8E13
f	0.75	0.0055	0.75	0.0093
[He] (cm^{-3})	2.4E12	2.3E12	1.2E12	2.4E12
$\langle k \rangle$	3.20E−10	1.00E−10	2.20E−11	2.20E−13

For testing various assumptions, additional measurements have been performed under different experimental conditions. The number density of H_2 has been varied over more than two orders of magnitude. In addition, He buffer gas has been added with a number density of some 10^{12} cm^{-3} so far without any significant changes. A selection of new results is plotted in Figure 7. The upper part shows the decay of the relative number of N^+ ions at about 100 K, the lower part of figure shows decay at 11 K. In the measurements on the left, n-H_2 was been used; on the right p-H_2 was used. All relevant experimental parameters are collected in Table 3. As can be seen from the thin lines, all four data sets can be fitted almost perfectly with a simple exponential decay function,

$$N_{N^+}(t) = N_0\, e^{-t/\tau}. \quad (6)$$

From the measured decay times τ and the hydrogen number densities [H_2], mean rate coefficients have been calculated

$$\langle k \rangle = (\tau\, [H_2])^{-1}. \quad (7)$$

The resulting parameters $\langle k \rangle$, which are an average over the time dependent FS population, are included in Table 3. In order to understand these observations in more detail, several additional facts need to be mentioned. (1) The decay rate of all N^+ ions is at all times the same. The slight deviations during the thermalization of the translational energy after ion injection can be ignored at the timescales used in Figure 7. (2) The monotonous decay can be followed until storage times where only 10^{-4} of the injected ions are left over. (3) Simulations with rate coefficients from phase-space theory always lead to a faster decay at the beginning (concave curvature). (4) Setting the rate coefficient for the $^3P_2$ state to zero (strict adiabatic model) but allowing for relaxation always leads to a convex curvature.

Guided by these facts we have developed a kinetic model that includes reaction of all three states of N^+ and also FS-changing

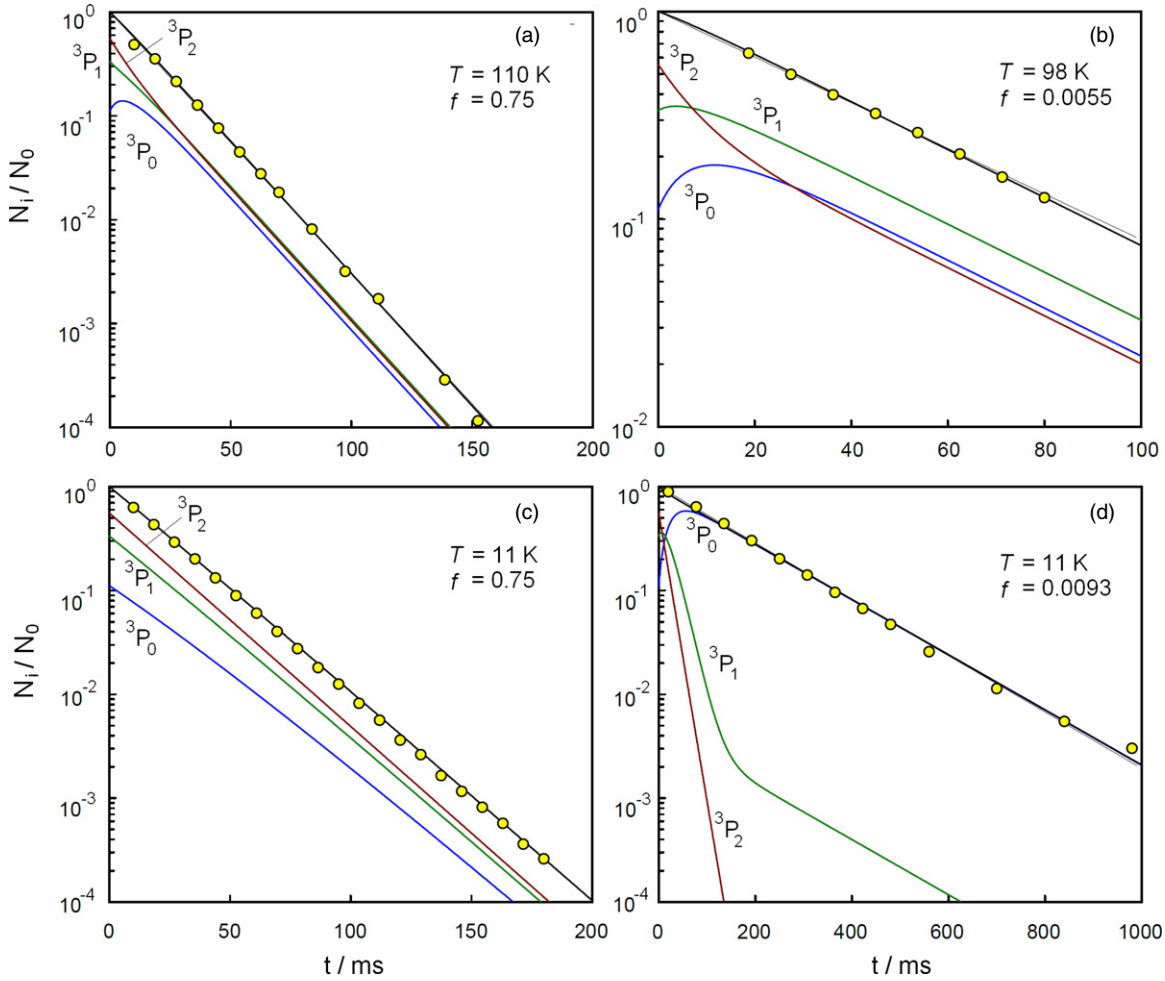

Figure 7. Decay of N^+ ions measured at the indicated temperatures and for n-H_2 (left, $f = 0.75$) and for p-H_2 with minor o-H_2 impurities (right, $f < 0.01$). Note the different scales. All relevant experimental parameters are collected in Table 3. The experimental data (circles) can be fitted well with a first-order exponential decay resulting in the mean rate coefficients $\langle k \rangle$ (also given in Table 3). In reality, the kinetics are more complicated due to the competition of FS-changing collisions and reactions with H_2. The three thin lines, marked with $^3P_{ja}$ ($j_a = 0, 1, 2$) show a special solution of the changes of the relative number of N^+ ions in specific FS states. In all cases, the high-temperature ratio 5:3:1 has been assumed for the initial population. The state specific rate coefficients for reaction and relaxation are given in Tables 1 and 4. Note that this result is not unique.

(A color version of this figure is available in the online journal.)

collisions. In order to restrict the number of free parameters of the simulation, we started with the state specific rate coefficients derived form our experiment, i.e., with the values given in Table 1. Then the rate coefficients $k_{0,2}$ and $k_{1,2}$, which have been set to zero in the adiabatic model, have been increased slowly. Motivated by the interaction shown schematically in Figure 1 only FS transitions from 2 to 1 and 1 to 0 have been accounted for with the relaxation rate coefficients $kr_{2\to1}$ and $kr_{1\to0}$. The reverse rate coefficients, $kr_{1\to2}$ and $kr_{0\to1}$, have been included in the calculation, making use of micro-reversibility. Direct transitions between 2 and 0 are assumed to be inefficient.

It has been rather easy to find parameters describing each individual data set. It also became evident that there are many specific solutions although there is a strong correlation between the competing processes imposed by the mono-exponential decay of the experimental data. The relaxation and reaction rate coefficients strongly depend on each other. To our surprise we finally found a very simple solution, taking the four unchanged rate coefficients given in Table 1 and also using simple Arrhenius-type rate coefficients for the highest FS state and for relaxation.

The resulting parameters fitting all our data sets are given in Table 4. The solutions for the temporal changes of the number of N^+ ions in specific $^3P_{ja}$ states and their sum are plotted in Figure 7. In all cases, the sum (solid line) follows nicely the mono-exponential decay of the measured data. A detailed inspection of (a) and (b) reveals that FS thermalization is achieved only after 30 ms since the relaxation rate coefficient is rather slow (4×10^{-11} cm^3 s^{-1}). In order to get the mono-exponential decay during this time the concave function describing the decay of ions in the $^3P_2$ state is compensated by the two convex functions. At 11 K relaxation is even slower

Table 4
State Specific Rate Coefficients for Reaction, $k_{j,ja}$, and Relaxation, $kr_{ja\to ja'}$, Derived from the Fits Shown in Figure 7 (units 10^{-10} cm^3 s^{-1} and K)

	k_A	T_A
$k_{0,2}$	0.51	53.4
$k_{1,2}$	1.44	18.4
$kr_{2\to1}$ $kr_{1\to0}$	0.58	37.0

Note. Rate coefficients needed in addition to those in Table 1 for fitting the exponential decay shown in Figures 7(a)–(d).

(2×10^{-12} cm^3 s^{-1}) and with n-H_2 (panel (c)) reaction is faster than relaxation. In order to get the mono-exponential time dependence, the three rate coefficients are similar. Impressive is the result (d), where the N^+ can only react with the traces of H_2 ($j = 1$). Since in this case the H_2 number density is more than 10 times higher than in (c), thermalization of the FS population is achieved in 200 ms. For further conclusions, more measurements and a detailed mathematical analysis of the coupled differential equations are needed.

In summary, the results of our model allow several conclusions. (1) FS-changing collisions are rather slow, especially at low temperatures indicating nearly adiabatic behavior. (2) In contradiction to the strict adiabatic model, the highest FS state contributes to the formation of NH^+ products, but much slower than predicted from statistical calculations. (3) Our experimental observations are qualitatively in accordance with the nonadiabatic couplings indicated in the oversimplified Figure 1. For a more quantitative understanding, one needs a detailed adiabatic or nonadiabatic formulation of the multi-surface problem. The first approach may be similar to the N^+–He system (Soldan & Hutson 2002); however, in addition to the spin–orbit coupling, one must include the correct long-range attraction (charge-induced dipole and charge–quadrupole) and the couplings induced by the anisotropy, and one has to account for the effects caused by the rotation of H_2. At very low energies hyperfine-interaction may also finally play a role. All this leads to a complex switch yard of crossings and needs help from theory to be sorted out!

5. CONCLUSIONS AND OUTLOOK

Based on an extensive set of new experimental rate coefficients $k(T; f)$ as well as on a careful analysis of the decay curves of trapped N^+ ions, for the first time state specific rate coefficients for the interaction of $N^+(^3P_{ja})$ with $H_2(j)$ have been extracted. There are still uncertainties concerning the role of the FS energy. Nonetheless it is rather clear that excitation of N^+ to the $^3P_2$ state reduces its reactivity, but not completely to zero as predicted from strict adiabatic assumptions (Wilhelmsson & Nyman 1992; Russell & Manolopoulos 1999).

As long as astrochemical models ignore the FS states of the N^+ ions, it is recommended that the rate coefficients for $j = 0$ and 1, presented in the lower part of Figure 6 and in Table 2, be used. However, it must be noted that the two N^+ lines ($^3P_2 \rightarrow {}^3P_1$) at 121.9 μm and ($^3P_1 \rightarrow {}^3P_0$) at 205.2 μm play an important role in certain astrophysical environments, e.g., in photo-dissociation regions, where matter is heated via penetrating far-ultraviolet photons and cooled via forbidden atomic fine-structure transitions. A detailed discussion of such cooling lines observed in the Orion Bar can be found in a recent publication by Bernard-Salas et al. (2012). It is obvious that one needs detailed rate coefficients for inelastic and reactive collisions with electrons, atoms, and molecules in order to model such observations.

The presented experimental results give some first information on the state specific rate coefficients $k_{j,ja}(T)$ for all combinations of $j_a = 0$–2 and $j = 0$–1. In order to check the results presented additional experiments must be performed. For example, using He number densities of several 10^{15} cm^{-3} and relaxation times of seconds or longer before hydrogen is leaked into the trap may finally lead to relaxation of the FS population prior to the reaction. An ultimate experiment would be the in situ state selected ionization of N-atoms via autoionizing resonances. Another striking idea is to maintain a stationary FS population of the trapped N^+ ions using an intense microwave wave field at the wavelengths mentioned above.

As established in Gerlich et al. (2011) the apparatus used in this work can also be operated with a neutral target beam. To fully understand the NH_2^+ collision system we plan to study the reverse reaction

$$NH^+ + H \rightarrow N^+ + H_2 \quad (8)$$

as a function of the temperature of the ion and the atomic beam source, similar to $CH^+ + H$ (Plasil et al. 2011). This beam-trap arrangement can also be used with a high-temperature accommodator for producing rotationally and vibrationally excited H_2. Finally, it must be mentioned that the various deuterated variants of reactions (1) and (8) including the endothermic D–H exchange in $ND^+ + H$ will provide deep insight into the role of zeropoint energies, barriers, and tunneling at low energies.

Since 2010, the AB 22PT instrument has been operated at the Faculty of Mathematics and Physics of Charles University in Prague. We thank the Technical University of Chemnitz and the DFG for lending us this instrument. This work is a part of research grant OC10046 financed by the Ministry of Education of the Czech Republic and was partly supported by GACR (P209/12/0233, 205/09/1183), by GAUK 388811, GAUK 406011, and by COST Action CM0805 (The Chemical Cosmos).

REFERENCES

Adams, N. G., & Smith, D. 1985, CPL, 117, 67
Amero, J. M., & Vazquez, G. J. 2005, IJQC, 101, 396
Barlow, S. E., Luine, J. A., & Dunn, G. H. 1986, IJMSI, 74, 97
Bernard-Salas, J., Habart, E., Arab, H., et al. 2012, A&A, 538, A37
Dislaire, V., Hily-Blant, P., Faure, A., et al. 2012, A&A, 537, A20
Gerlich, D. 1989, JChPh, 90, 3574
Gerlich, D. 1992, AdChP, 82, 1
Gerlich, D. 1993, J. Chem. Soc. Faraday Trans., 89, 2199
Gerlich, D. 1995, PhyS, T59, 256
Gerlich, D. 2008a, in Low Temperatures and Cold Molecules, ed. I. W. M. Smith (Singapore: Imperial College Press), 121
Gerlich, D. 2008b, in Low Temperatures and Cold Molecules, ed. I. W. M. Smith (Singapore: Imperial College Press), 295
Gerlich, D., Borodi, G., Luca, A., Mogo, C., & Smith, M. 2011, ZPC, 252, 475
Gerlich, D., Jusko, P., Roučka, Š., et al. 2012, ApJ, 749, 22
González, M., Aguilar, A., & Fernández, Y. 1986, CP, 104, 57
Jursic, B.S. 1998, AcTC, 99, 171
Le Bourlot, J. 1991, A&A, 242, 235
Mahan, B. H., & Ruska, W. E. W. 1976, JChPh, 65, 5044
Marquette, J. B., Rebrion, C., & Rowe, B. R. 1988, JChPh, 89, 2041
Nyman, G., & Wilhelmsson, U. 1992, JChPh, 96, 5198
Plasil, R., Mehner, T., Dohnal, P., et al. 2011, ApJ, 737, 60
Russell, C. L., & Manolopoulos, D. E. 1999, JChPh, 110, 177
Soldan, P., & Hutson, J. M. 2002, JChPh, 117, 3109
Sunderlin, L. S., & Armentrout, P. B. 1994, JChPh, 100, 5639
Tarroni, R., Palmieri, P., Mitrushenkov, A., Tosi, P., & Bassi, D. 1997, JChPh, 106, 10265
Tosi, P., Dmitriev, O., Bassi, D., Wick, O., & Gerlich, D. 1994, JChPh, 100, 4300
Wakelam, V., Herbst, E., Loison, J.-C., et al. 2012, ApJS, 199, 21
Wilhelmsson, U., & Nyman, G. 1992, JChPh, 96, 1886
Wilhelmsson, U., Siegbahn, P. E. M., & Schinke, R. 1992, JChPh, 96, 8202
Willitsch, S., Merkt, F., Kállay, M., & Gauss, J. 2006, MolPh, 104, 1457

III. State Specific Stabilization of $H^+ + H_2(J)$ Collision Complexes

Gerlich D., Plašil R., Zymak I., Hejduk M., Jusko P., Mulin D., and Glosík J. (2013)

The Journal of Physical Chemistry A, **117**(**39**), 10068.

THE JOURNAL OF PHYSICAL CHEMISTRY A

Article

pubs.acs.org/JPCA

State Specific Stabilization of $H^+ + H_2(j)$ Collision Complexes

D. Gerlich,*[,†,‡] R. Plašil,[†] I. Zymak,[†] M. Hejduk,[†] P. Jusko,[†] D. Mulin,[†] and J. Glosík[†]

[†]Faculty of Mathematics and Physics, Charles University, 121 16 Prague, Czech Republic

[‡]Department of Physics, University of Technology, 09107 Chemnitz, Germany

ABSTRACT: Stabilization of H_3^+ collision complexes has been studied at nominal temperatures between 11 and 33 K using a 22-pole radio frequency (rf) ion trap. Apparent binary rate coefficients, $k^* = k_r + k_3[H_2]$, have been measured for para- and normal-hydrogen at number densities between some 10^{11} and 10^{14} cm^{-3}. The state specific rate coefficients extracted for radiative stabilization, $k_r(T;j)$, are all below 2×10^{-16} cm^3 s^{-1}. There is a slight tendency to decrease with increasing temperature. In contrast to simple expectations, $k_r(11\ K;j)$ is for $j = 0$ a factor of 2 smaller than for $j = 1$. The ternary rate coefficients for p-H_2 show a rather steep T-dependence; however, they are increasing with temperature. The state specific ternary rate coefficients, $k_3(T;j)$, measured for $j = 0$ and derived for $j = 1$ from measurements with n-H_2, differ by an order of magnitude. Most of these surprising observations are in disagreement with predictions from standard association models, which are based on statistical assumptions and the separation of complex formation and competition between stabilization and decay. Most probably, the unexpected collision dynamics are due to the fact that, at the low translational energies of the present experiment, only a small number of partial waves participate. This should make exact quantum mechanical calculations of k_r feasible. More complex is three-body stabilization, because it occurs on the H_5^+ potential energy surface.

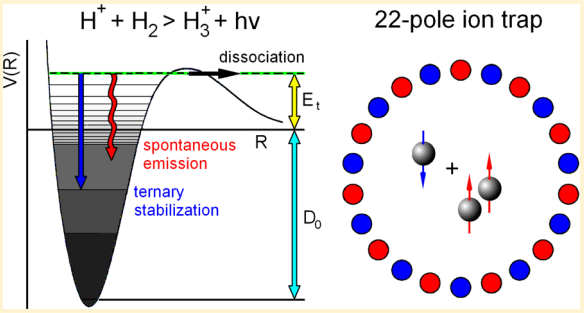

INTRODUCTION

In understanding the electronic structure of atoms and the formation of molecules, the hydrogen atom, the diatomic molecules H_2^+ and H_2, as well as the simplest polyatomic molecule H_3^+ play a fundamental role. Like H_2, the triatomic ion has only two electrons. But instead of one internuclear coordinate, already three are needed to describe the location or the motion of the three protons. Due to the importance of this special ion in fundamental science and in all kinds of hydrogen plasmas, including astrophysics, the last decades have seen many experimental and theoretical activities dealing with both bound and scattering states. In other word, H_3^+ is a benchmark system not only for understanding molecular structure but also for scattering dynamics.

Recently, Oka[1] has passed in review his personal engagement and involvement in searching for the IR spectrum of H_3^+ in the laboratory and in detecting this ion in space, finally in more and more astrophysical objects. It is a successful story, emphasizing the close interrelation between spectroscopy and astronomy. For identifying a molecule in space one must know its rotational−vibrational levels and the frequencies of photons that can be emitted or absorbed. Meanwhile, after more than 30 years, many transitions of H_3^+ and deuterated analogues have been measured and there is still space for filling more tables.[2,3] Present activities investigate the energy range where the three protons can leave their triangular structure and start to explore the configuration space toward linearity.[4] All these precisely measured lines are a challenge for rigorously testing ab initio theories. To determine the eigenstates and to predict transitions with spectroscopic accuracy, the quality of the ground state potential energy surface has been improved in many iterations. The most recent reports and references to previous publications can be found in refs 5 and 6. Despite all this, H_3^+ is far from being fully accessed experimentally or rigorously described by theory, especially if the total energy reaches the vicinity of the $H^+ + H_2$ continuum.

In the above-mentioned retrospective, Oka[1] also stated that the chemistry of H_3^+ is "extremely simple and allows one to interpret the observed abundances". Unfortunately, this is not true if one looks into the details of hydrogen chemistry leading to the formation or destruction of this central ion. Also inelastic collisions, just changing the vibrational−rotational state or inducing an ortho−para transition, are an unsolved experimental challenge, especially at low temperatures. Because H_3^+ is the most abundant polyatomic ion in the universe, it must be involved in many reactions with other atoms, molecules, anions, or electrons. Therefore, it certainly is a powerful sensor for probing specific astrophysical environments; however, more details on its role in chemistry are needed. One example is the still ongoing discussion on its recombination with electrons. The status of the $H_3^+ + e^-$ research was recently summarized

Special Issue: Oka Festschrift: Celebrating 45 Years of Astrochemistry

Received: January 27, 2013
Revised: March 14, 2013
Published: March 15, 2013

with the statement "But this was not the end of the story, not even the beginning of the end; it marked only the end of the beginning."[7] Another basic but not yet solved question is the ortho−para conversion of H_3^+ in low temperature collisions with H_2.[8]

In this contribution, we concentrate on the $H^+ + H_2$ collision system, i.e., at H_3^+ ions having a total energy above the dissociation limit. To be of importance for dense interstellar clouds, the energy is restricted to a few millielectronvolts, relative to the asymptote. At higher collision energies, proton scrambling plays an important role in converting translational energy into internal excitation of the molecule followed by conversion into radiation. Most probably this energy transfer is more efficient in cooling primordial gas than the H_3^+ molecule with its infrared active modes.[9] Another important aspect of this rather simple collision system is the conversion of ortho-H_2 into para-H_2 or vice versa, catalyzed by the proton. Only recently has this process, which has been described in detail with statistical theories,[10,11] been treated with an exact quantum mechanical method.[12,13] The obtained thermal state-to-state rate coefficients (see erratum[14]) are smaller than the statistical predictions and, surprisingly, they fall with falling temperature. Is this an indication that statistical models are not any more applicable in the 10 K range? Also, other recent theoretical studies (see ref 15 and references therein) provide evidence that theoreticians are close to describing, with exact quantum mechanical methods, the interaction of a proton or deuteron with H_2 and D_2 at translational energies of a few millielectronvolts. It is obvious that, in this energy range, a very good potential energy surface with the correct long-range behavior is required. For this purpose, it seems to be still the best to include analytical approximations of the long-range electrostatic interaction into the ab initio potential.[16] It is an open question whether the improved potentials[5,6] and the methods to describe the vibrational−rotational motion of H_3^+ with spectroscopic accuracy are finally also suited to find the resonances determining the cross section for converting hydrogen in $j = 1$ into $j = 0$ in a low energy collision with protons, or to predict the probability to stabilize such a collision complex via emission of a photon.

Radiative stabilization of collision complexes is an important process in the growth of molecules in low-density interstellar clouds. From a fundamental point of view, formation of H_3^+ via radiative association,

$$H^+ + H_2 \xrightarrow{k_r} H_3^+ + h\nu \quad (1)$$

is a so-called "half-collision", an important subfield of collision dynamics. Most related experiments start with a stable molecule (e.g., photoinduced dissociation or detachment of an electron); here a molecule in a more or less long-lived scattering state is stabilized by losing the energy $h\nu$. Because these states are embedded in the energy continuum, one needs a barrier (for example caused by a rotational angular momentum, Feshbach-type resonances) to keep them bound for some time or other dynamical restrictions. It also should be mentioned that the total number of states in the energy interval of interest is an important criterion.

For long time, information on association of reactants has been extracted from experiments operating at rather high pressures. Under such conditions, H_3^+ is formed with the help of a third body, i.e., via

$$H^+ + 2H_2 \xrightarrow{k_3} H_3^+ + H_2 \quad (2)$$

Using a drift-tube mass spectrometer apparatus and operating at number densities close to 10^{16} cm^{-3}, Graham et al.[17] determined a ternary rate coefficient k_3 of 3×10^{-29} cm^6 s^{-1} at 300 K. Johnson et al.[18] extended the temperatures range from room temperature down to 135 K and observed a slight increase of k_3. The mentioned results are included in Table 1.

Table 1. Rate Coefficients for Radiative and Ternary Association of Protons with Hydrogen Molecules[a]

T	k_r	Δk_r	k_3	Δk_3	remarks	ref
300			0.30	0.15	drift tube	17
300			0.30	0.03	drift tube	18
135			0.43	0.04		
230	1.0	0.2	0.74	0.2	first TV rf trap	21
80	1.3	0.2	0.54	0.2	80 K RET	22
11	1.6	0.3	0.27	0.08	n-H_2 (Figure 5)	24
22	0.5	0.2	0.25	0.08		
11	0.9	0.2	0.88	0.04	p-$H_2/j = 0$ (Figure 2)	this work
22	0.4	0.2	1.31	0.01		
33	0.4	0.7	1.75	0.04		
11	1.8	0.4	0.06	0.09	$j = 1$	

[a]Units: T in K, k_r in 10^{-16} cm^3 s^{-1}, and k_3 in 10^{-28} cm^6 s^{-1}. In the upper part, values from the literature are collected, all measured with n-H_2. The lower part presents state specific results from this work. The errors Δk_r and Δk_3 include only the statistical uncertainties.

In such studies the ternary association rate coefficient is derived from the measured apparent binary rate coefficient, k^*, by dividing it through the number density $[H_2]$, $k_3 = k^*/[H_2]$. This is suitable for high pressure environments, in fact, k^* has two contributions,

$$k^* = k_r + k_3[H_2] \quad (3)$$

Inspection of this equation reveals that, to get a similar number of products from the first and second term, one has to operate at number densities in the range of $[H_2] = k_r/k_3$. In the present case it means below 10^{13} cm^{-3}. It also must be noted that at the densities in the range of 10^{16} cm^{-3}, higher order collisions and saturation effects may play a role.[19]

The eighties have seen the development of innovative trapping techniques extending gas phase chemistry toward both lower densities and temperatures. First results for radiative association, measured in a liquid helium cooled Penning ion trap, were published by the group of Dunn.[20] First results for reactions 1 and 2, determined with an early version of an rf ring electrode trap operating between 300 and 230 K, have been reported in a conference contribution.[21] A similar trap, directly cooled with liquid nitrogen, provided results at 80 K.[22] All mentioned ternary and radiative rate coefficients are collected in Table 1 and discussed in more detail in an early review on radiative association.[19]

Although rf ion traps have been further improved,[23] they never have been used to extend the mentioned early experiments toward lower temperatures. However, due to continuous improvements of computers and methods, the $H^+ + H_2$ collision system is now within the reach of exact quantum mechanical calculations (see refs 13 and 15 and references therein). Therefore, it is timely to get more experimental information, especially state specific rate coefficients at very low temperatures.

dx.doi.org/10.1021/jp400917v | J. Phys. Chem. A 2013, 117, 10068−10075

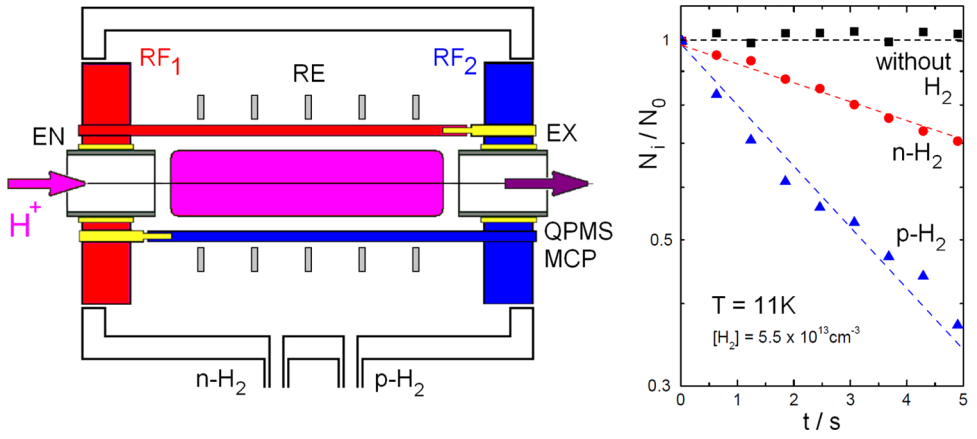

Figure 1. Left: 22-pole ion trap, the central part of the AB-22PT instrument.[36] Utilizing a cold head, wall temperatures down to T_{22PT} = 11 K can be reached. Mass selected H^+ ions are injected via the electrostatic entrance electrode (EN). For analyzing the ion cloud after various storage times *t*, the exit (EX) is opened using a suitable voltage. The ions pass a quadrupole mass spectrometer and are detected with a microchannel plate. The axial trapping potential, created by the rf field, can be corrected locally using five ring electrodes (RE). Right: normalized number of protons as a function of storage time. Without target gas, there is no change. Adding hydrogen (number density is in both cases 5.5 × 10^{13} cm^{-3}) leads to a decay of the number of protons due to formation of H_3^+. It is obvious that p-H_2 is more reactive than n-H_2.

In the following we give a short description of the instrument. New results for p-H_2 are presented and compared to results recently published for n-H_2.[24] Using well-prepared ortho−para mixtures allows us to extract state specific rate coefficients for radiative and ternary stabilization of $H^+ + H_2(j)$ collision complexes, $k_r(T;j)$ and $k_3(T;j)$. The discussion section emphasizes that the established models for explaining association processes are not able to provide sufficient explanations for the surprising result that k_r and k_3 show different temperature dependencies and that radiative association of protons with rotating H_2 is significantly faster than with ground state hydrogen.

EXPERIMENTAL SECTION

The measurements have been performed in the AB-22PT instrument the central part of which is the 22-pole rf ion trap, shown in Figure 1 on the left. It is surrounded by a copper box that is connected to the cold head of a closed-cycle helium refrigerator (Leybold RGD 210, lowest temperature 11 K). Because the principle of ion trapping[25] and the details of the 22-pole trap (first mentioned in ref 19) have been described often, only a few special hints are given below. Selected aspects of low temperature trapping have been discussed recently.[26,27]

Using magnetically suspended turbomolecular pumps, the vacuum chamber surrounding the trap is evacuated to a pressure below 10^{-7} Pa. Ultrahigh purity hydrogen gas has been used. In addition, traces of impurities are frozen out at low temperatures, with the exception of HD and D_2. As indicated in Figure 1, two separate gas inlets were installed, one for normal hydrogen (25% p-H_2, i.e., *j* = even and 75% o-H_2, i.e., *j* = odd) and one for para hydrogen. The purity of para hydrogen has been determined in situ using the reaction of N^+ with H_2.[28] Mixtures with a specific fraction of o-H_2, *f*, are set by adjusting the two separate leak valves. The gas density inside the trap is determined using an ionization gauge on the main chamber. This gauge is calibrated on a regular basis using a spinning rotor gauge that is connected to the interior of the 22-pole box.

For determining rate coefficients, the ion trap is periodically filled via the entrance electrode with a certain number of mass selected primary ions, in the present study typically a few hundred. The repetition period has been set to 10 s. Protons are created in a storage ion source via electron bombardment of hydrogen. After various storage times, *t*, the exit electrode is opened and the ions pass a quadrupole mass spectrometer and are detected with a microchannel plate. A typical set of raw data is shown in the right part of Figure 1. Without reactant gas, the number of stored ions (here normalized) is independent of the storage time. Adding n-H_2 through the left gas inlet or p-H_2 through the right one leads to a decrease of the number of protons. Because in both cases the same number density has been used (5.5 × 10^{13} cm^{-3}), it is immediately obvious that p-H_2 is more reactive than n-H_2.

A special difficulty in the present experiment is caused by the fact that the mass of the ion is only 1 *u* and, in addition, lower than the mass of the target gas, 2 u. Therefore, some remarks concerning the energy distributions of ions in rf traps must be made. In those applications where heavy ions are stored in H_2 or He, the influence of the rf field is very weak and can be neglected in most situations. One reason is that only small portions of energy are exchanged if the heavy ion hits the light buffer gas but cooling is finally very efficient. A second reason is that the translational temperature (i.e., the center of mass temperature) is determined by the mass weighted ratio of the cold gas temperature and the ion temperature (see eq 113 in ref 25). A simulation of the motion of protons stored in a ring electrode trap filled with H_2 indicate that, under similar conditions like here, 75% of the ions can be described with the nominal temperature, whereas 25% of them are at a 2.5 times higher temperature (see upper panel Figure 23 in ref 25). Unfortunately, real energy distributions of stored ions are usually less favorable due to potential distortions or parasitic time dependent fields which cause additional heating.

In the present experiment, the actual trapping conditions have been tested in situ via formation of He_2^+ dimers in He^+ + 2 He collisions, as discussed in detail by Plasil et al.[24] The results indicate *low* temperatures; however, deviations on the order of up to 10 K cannot be excluded. In addition, the ion to neutral mass ratio is 4:4 in this case and the trapping conditions have been superior because the test with He^+ has been performed with the same rf frequency (*f* = 19 MHz) used in the present work. Although the trap is still running in the safe operating mode (V_0 = 19 V, V^* = 34 meV, η = 0.15 at r_m/r_0 =

dx.doi.org/10.1021/jp400917v | J. Phys. Chem. A 2013, 117, 10068−10075

0.80 for m = 1 u, for details see ref 25), further experiments will be performed with higher frequencies. Moreover, additional work is going on for determining the actual velocity distribution of protons trapped in a 22PT with H_2 and D_2 gas. Due to all uncertainties that may add up to an estimated temperature increase of 30 K, the present results are just reported as a function of the nominal temperature.

RESULTS

From the decay rates of primary ions at various hydrogen number densities (right part of Figure 1), apparent second-order rate coefficients for the formation of H_3^+ from H^+ have been determined, predominantly for p-H_2 in the present work. Figure 2 shows a collection of such results as a function of the number density of p-H_2, determined at nominal temperatures of 11, 22, and 33 K. The data points are averages over several iterations of filling the trap and analyzing the content after different storage times. The measured rate coefficients, k^*, have been fitted using the density dependence predicted by eq 3. The fits are plotted as solid lines, the obtained fit parameters, k_3 and k_r, are included in Table 1. To emphasize the temperature dependent differences in ternary association, the data are plotted here in a lin−lin scale, certainly at the disadvantage of radiative association which is discussed below. Against standard expectations, which are based on an increase of the lifetime of the collision complex with decreasing temperature, the data show clearly that ternary association becomes less efficient at lower temperatures.

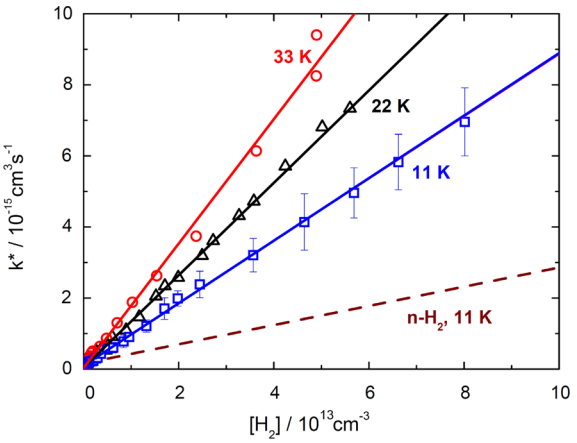

Figure 2. Apparent binary association rate coefficient k^* for T_{22PT} = 11, 22, and 33 K as a function of the p-H_2 number density. The data have been averaged over many iterations. For emphasizing the ternary rate coefficients, the results are plotted on a linear scale. The data are fitted with $k^* = k_r + k_3[H_2]$. The resulting parameters are in Table 1. The surprising result is that ternary association gets faster with increasing temperature. Concerning $k_r(T)$, see the text and Figure 3.

The obtained ternary and radiative rate coefficients are shown as a function of the nominal temperature in Figure 3 (rhomboids with crosses). To perform additional and faster measurements of the temperature dependence of k_r and k_3, it would be necessary to record H_3^+ formation at very low and very high number densities, respectively. In the present work, the apparent second-order rate coefficients k^* have been measured as a function of T_{22PT} between 11 and 45 K at the three different densities, given in Figure 3. The values for k_3 have been determined at 2.8 × 10^{13} cm^{-3} (squares, upper panel), by correcting k^* for the small contributions from

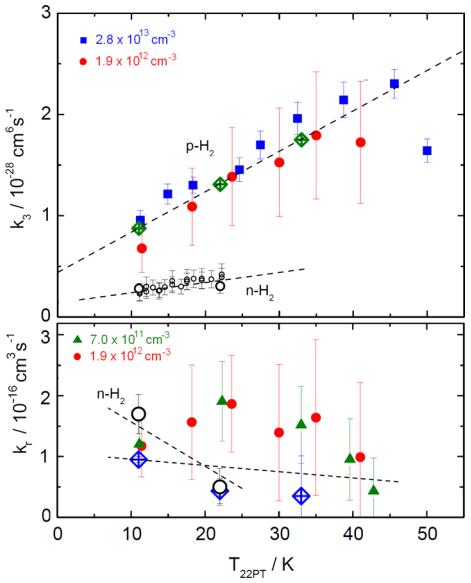

Figure 3. Temperature dependence of k_3 (upper panel) and k_r (lower panel). The large symbols (rhomboids with crosses inside) are results from fits to the density dependence of k^*. In addition, $k_3(T)$ has been determined at fixed p-H_2 densities (filled squares, 2.8 × 10^{13} cm^{-3}; filled circles, 1.9 × 10^{12} cm^{-3}) by correcting the measured k^* values individually for the small contribution from k_r. In analogy, $k_r(T)$ has been extracted from k^* measures at low densities (filled triangles, 7.0 × 10^{11} cm^{-3}; filled circles, 1.9 × 10^{12} cm^{-3}) and subtracting the contribution from ternary processes. For comparison, the previously published results[24] from experiments with n-H_2 are plotted as open circles. The trends (dashed lines) are discussed in the text.

radiative association. Correspondingly, the values for k_r have been obtained from k^* at 7.0 × 10^{11} cm^{-3} by subtracting the mean value of $k_3[H_2]$ (triangles, lower panel). The filled circles indicate that correction of k^* with nominal values of k_3 and k_r also works reasonably well at a density (1.9 × 10^{12} cm^{-3}) where the two contributions $k_3[H_2]$ and k_r are nearly equal. Also included in Figure 3 are dashed lines that indicate the temperature trend. The increase of k_3 for p-H_2, which follows the linear function

$$k_3(T;j{=}0) = (4.4 + 0.4 \times T/\mathrm{K}) \times 10^{-29}\ \mathrm{cm}^6\ \mathrm{s}^{-1} \quad (4)$$

is rather obvious but needs explanations (see below). For n-H_2 (data from Plasil et al.[24]), the trend is not so evident, partly due to the smaller temperature interval. The minor increase indicated by the dashed line,

$$k_3(T;\text{n-}H_2) = (1.4 + 0.1 \times T/\mathrm{K}) \times 10^{-29}\ \mathrm{cm}^6\ \mathrm{s}^{-1} \quad (5)$$

can be fully explained with the contribution of the 25% of $H_2(j{=}0)$ in n-H_2. This leads to the conclusion that $k_3(T;j{=}1)$ does not change with temperature. The results for radiative association (lower panel) are rather uncertain due to the large errors of the individual points. Therefore, the two functions

$$k_r(T;j{=}0) = (1 - 0.01 \times T/\mathrm{K}) \times 10^{-16}\ \mathrm{cm}^3\ \mathrm{s}^{-1} \quad (6)$$

$$k_r(T;\text{n-}H_2) = (2.3 - 0.07 \times T/\mathrm{K}) \times 10^{-16}\ \mathrm{cm}^3\ \mathrm{s}^{-1} \quad (7)$$

should not be overinterpreted. However, it is rather certain that radiative association decreases with temperature; i.e., it does not follow the temperature trend of ternary association.

Important for deriving state specific rate coefficients for j = 1 are the differences between p-H_2 and n-H_2. In Figure 4, the

dx.doi.org/10.1021/jp400917v | J. Phys. Chem. A 2013, 117, 10068−10075

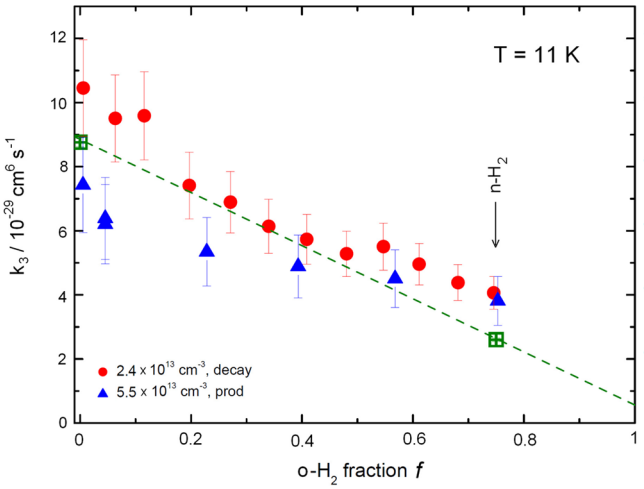

Figure 4. Ternary rate coefficients k_3 measured at T_{22PT} = 11 K as a function of the ortho fraction f (f = 0, p-H_2; f = 0.75, n-H_2). The squares with crosses inside have been determined from fits to the density dependence of k^*, and the other points have been measured at the indicated fixed densities and corrected for minor contributions from k_r. The filled circles have been derived from the decay of primary protons, and the triangles show rate coefficients determined from the products H_3^+. The slight systematic difference is discussed in the text. The dotted line indicates that the f dependence can be approximated with a linear function resulting in state specific rate coefficients for H_2 in j = 0 and j = 1 (see the text and Table 1).

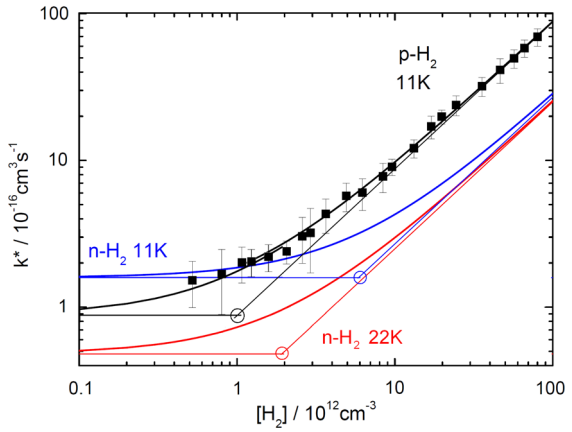

Figure 5. Apparent binary association rate coefficients k^*. For better comprehensibility only the T_{22PT} = 11 K data are shown for p-H_2. As in Figure 2, they are fitted with eq 3. Due to the log−log plot, the contributions from radiative association become apparent by the curvature of the fit. These results can be compared with the fitting curves, determined for n-H_2 at 11 and 22 K.[24] The circles mark the locations, where ternary and radiative association are equally efficient. It is obvious that ternary association with p-H_2 is significantly faster than with n-H_2 whereas the differences for radiative association are rather small and not so obvious because of the errors. For more detail, see the text and Table 1.

mean ternary rate coefficient is plotted as a function of the ortho fraction f. The two large symbols (squares with crosses inside) are the above presented results determined from the density dependence of k^* whereas the other points have been measured directly at the indicated f values. As discussed above, the contributions from k_r, which have been subtracted from k^*, are rather small at the indicated hydrogen densities. The rate coefficients plotted as filled circles have been derived from the decay of the protons, as most of the results presented in this work. The triangles show rate coefficients where the formation of H_3^+ products has been evaluated. Inspection reveals that they are smaller, which may be due to minor differences in the detection or trapping efficiency of H^+ and H_3^+. Remarkable is a systematic increase of the deviations toward pure p-H_2. This may be due to additional loss of H_3^+ because it is faster converted into H_5^+ ions. It is known from ion trap experiments[29] that, in pure p-H_2, H_5^+ clusters grow 4 times faster than in n-H_2. The overall dependence on f can be reasonably well described with a linear function (dashed line)

$$k_3(f) = (1 - f)k_3(j{=}0) + f\ k_3(j{=}1) \quad (8)$$

although one also could expect deviations from linearity because hydrogen plays a triple role: (i) thermalization of the ions, (ii) formation of the complexes, and (iii) stabilization of them. The fit with eq 8 results in the two state specific rate coefficients $k_3(11\ \mathrm{K}; j{=}0) = 8.8 \times 10^{-29}$ cm^6 s^{-1} and $k_3(11\ \mathrm{K}; j{=}1) = 0.6 \times 10^{-29}$ cm^6 s^{-1}. It is an open question whether this huge difference is due to complex formation or complex stabilization or due to both processes. Also the protons may be on average faster if more hydrogen molecules are rotationally excited (ortho−para transitions).

To illustrate the limitations in extracting radiative rate coefficients, Figure 5 compares selected results in a log−log presentation. As in Figure 2, the data (11 K, p-H_2) are fitted with the function given in eq 3. The results for n-H_2 at 11 and 22 K, reported by Plasil et al.,[24] are represented here only via their fit function for clarity. The thin straight lines mark the separate contributions from radiative (horizontal) and ternary (increasing) association. The circles indicate the locations, where they are equally efficient. Because all rate coefficients for radiative association are below 2×10^{-16} cm^3 s^{-1} and have rather large errors (see also Figure 3), future experiments should be extended to lower number densities. Note, however, that this requires very long storage times and no perturbations.

DISCUSSION

Collisions with hydrogen molecules are by far the most abundant processes in the universe, and therefore, it is of central importance to determine the ortho−para ratio in the various astrophysical environments and to understand how the 14.4 meV energy, provided by hydrogen in j = 1, and the total nuclear spin 1 affect physical and chemical processes. This is especially important at low temperatures. The result from the present work that ternary association is significantly more efficient with nonrotating hydrogen, is in accordance with previous ion trap studies performed with C^+, CH_3^+, and $C_2H_2^+$ ions, showing that both radiative and ternary association is several times faster with p-H_2 than with n-H_2.[30] Surprising on the new results is the temperature dependence of k_3 and the fact that radiative association is always very slow.

Previous measurements of ternary and radiative association rate coefficients have been evaluated using rather simple statistical models that have been reviewed by Gerlich and Horning.[19] The basic assumption is that the overall process can be described by the formation of a long-lived complex followed by (i) dissociation, (ii) ternary stabilization, or (iii) emission of a photon. The outcome of such calculations is that k^*, as defined in eq 3, can be approximated by the equation

$$k^* = k_c(1/\tau_{H_2} + 1/\tau_r)/(1/\tau_{diss} + 1/\tau_{H_2} + 1/\tau_r) \quad (9)$$

dx.doi.org/10.1021/jp400917v | J. Phys. Chem. A 2013, 117, 10068−10075

Here k_c is the rate coefficient for forming the collision complex and the time constants τ_{diss}, τ_{H_2}, and τ_r describe its dissociation, its stabilization via the second H_2, and its radiative stabilization, respectively. It is also common to describe ternary stabilization by the product of a collision rate coefficient k_{H_2} and a stabilization factor f_s. Under such assumptions complex and radiative lifetimes can be inferred from the experimental data. Results for several systems are collected in the above-mentioned review[19] where one also finds for H^+ + n-H_2 at 80 K $\tau_{diss} = 5.5 \times 10^{-11}$ s and $\tau_r = 1.1$ ms. Using classical trajectory calculations,[31] the complex lifetime has been estimated to be $\tau_{diss} \sim 10^{-11}$ s at 0.1 eV and to change proportional to $T^{-1.9}$. This steep increase with falling temperature is in obvious contrast to our very small values of k_r. The question is whether this is due to k_c, τ_{diss}, or τ_r, the only parameters relevant at low densities. Concerning the radiative lifetime of highly excited H_3^+, an independent trapping experiment has provided additional information. It is based on CO_2 laser photofragmentation after different storage times; for details, see refs 10 and 19. The resulting lifetime, $\tau_r = 0.37$ ms, is in accordance with the expectation that IR emissions are in the millisecond range. The conclusion is that something must be wrong with the simple statistical concept of complex formation and decay.

For systems with many active internal degrees of freedom, statistical approaches are certainly useful; however, $H^+ + H_2$ collisions at translational energies of a few millielectronvolts populate only a rather small number of resonances. These scattering states may have quite different lifetimes and emission probabilities (dipole moments). Unfortunately, H_3^+ in the vicinity of the dissociation limit is still an unsolved problem, although there have been many theoretical activities, stimulated by the predissociation spectra reported by Carrington and co-workers.[32] For more than 25 years they have been unassigned! Can one expect under such conditions that modern theories are capable of predicting radiative association in $H^+ + H_2$ collisions?

To answer this question, it first should be emphasized that the Carrington states[32] are very specific ones, preselected by the experimental conditions. They have microsecond lifetimes and also excitation energies up to 3000 cm^{-1} above the dissociation limit. Because the ions are produced in reactive collisions of H_2^+ with H_2, angular momenta of 25 $\hbar$ or higher must be expected. In the present ion trap experiment, the energy interval of interest is 100 times smaller and the total orbital angular momenta J are restricted to a few $\hbar$. Based on the simple Langevin criterion and using just the polarization interaction, the maximum orbital angular momentum is $l_m = 6\ \hbar$ at 1 meV translational energy. All this leads to a rather low total number of H_3^+ continuum states populated in the collision complex. These quasibound states have been calculated rather often;[33] however, one of the problems is to get an accurate potential energy surface, describing also correctly the long-range part. Note that, in linear approach, the H^+-H_2 interaction has a 3.2 meV barrier at 11 a_0 and that, for C_{2v} geometry, it is still −1 meV attractive at 22 a_0.[16] A systematic investigation of the ground state potential energy surface of H_3^+ together with all bound vibrational states, including resonances above the dissociation limit has been reported recently by Jaquet and Khoma,[6] so far only for the total angular momentum $J = 0$. As already mentioned in the Introduction, first quantum mechanical scattering calculation have been reported for the $H^+ + H_2$ system and isotopic variants by Honvault et al.[14,15] For ortho−para transitions, the cross sections calculated at millielectronvolt translational energies, show a pronounced resonance structure (see Figure 1 in ref 12). It seems to be rather certain that such long-lived resonances are responsible for radiative association. Therefore, one can hope that theoreticians may find sooner or later explanations for the results from this work and especially for the fact that the largest value so far measured ($k_r = 1.8 \times 10^{-16}$ $cm^3\ s^{-1}$) is for the collision of a proton with the hydrogen molecule in the first rotational state!

Significantly more difficult than radiative association is to understand the measured ternary association rate coefficients and their temperature dependencies. In this case it is evident that the simple model mentioned above is not valid. Statistical theories always have predicted that the lifetime of a complex increases with decreasing temperature. In most model calculations, the proportionality $\sim T^{-s}$ is taken, where s is the so-called number of active degrees of freedom. At the moment we can only speculate that, from the few resonances populated under the conditions of our experiment, only selected ones can contribute to ternary association and that the number of such active resonances becomes bigger when the nominal temperature increases from 11 to 33 K. A second, even bigger uncertainty in ternary association is the stabilization of the intermediate complex by the collision with a second hydrogen molecule. This interaction takes place on the rather well-characterized potential energy surface of H_5^+.[34] One of the remarkable characteristics is that the proton can easily be exchanged between the two hydrogen molecules.[35] As a consequence of this "shared proton structure", one may suppose that the H_2 approaching the H_3^+ complex pulls out the proton in many cases instead of stabilizing the collision complex. Such specific processes certainly may have quite different temperature dependences. An interesting related information mentioned by Gerlich and Horning,[19] is that helium as stabilizer is more than four times more efficient than hydrogen.

CONCLUSIONS

With para- and normal-hydrogen new measurements have been performed at low temperatures for obtaining state specific rate coefficients for forming H_3^+ via radiative and ternary association. The extracted results, $k_r(T;j)$ and $k_3(T;j)$, show surprising temperature dependences that cannot be explained with simple statistical models. Due to the very unfavorable ion:neutral mass ratio, the actual velocity distribution deviates probably from the thermal one, and one needs at least two temperatures for describing it. Nonetheless, the interesting observations are unchanged, and it can be expected that the temperature dependences become even more pronounced. A significant improvement of the results can be achieved if the target gas is leaked in using a cold effusive or supersonic beam of hydrogen molecules. This is possible with the present instrument.[36]

It has been mentioned several times that more support from theory is needed for understanding the role of the $(H-H_2)^+$ scattering states populated at translational energies of a few millielectronvolts. Sufficiently accurate potential energy surfaces and the tools to solve the collision dynamics seem to be available today. Not mentioned so far but also of central importance are certainly the restrictions imposed by the nuclear spin of the three or five protons. For describing radiative

association, a suitable dipole moment surface is needed for predicting the emission of photons. An experimental challenge is finally the laser induced association of the collision complex, allowing one to perform spectroscopy on it. All this finally may help also to understand the Carrington lines.[32]

A completely different theoretical approach for exploring H_3^+ close to the dissociation limit has been reported recently by Kylänpää and Rantala.[37] In this work, a quantum statistical method has been used to explore the structure and energetics of H_3^+ as a function of temperature up to the thermal dissociation limit which has been found to be around 4000 K. Corresponding trapping experiments are possible and are in preparation.

AUTHOR INFORMATION

Corresponding Author

*E-mail: gerlich@physik.tu-chemnitz.de.

Notes

The authors declare no competing financial interest.

ACKNOWLEDGMENTS

We thank the DFG and the TU Chemnitz for making these studies possible by lending the Charles University in Prague the AB-22PT instrument. This work was partly supported by GACR (P209/12/0233, 205/09/1183), GAUK 388811, GAUK 406011, and GAUK 659112.

REFERENCES

(1) Oka, T. H_3^+ from the Laboratory to the Galactic Center. *Faraday Discuss.* **2011**, *150*, 9−22.

(2) Morong, C. P.; Gottfried, J. L.; Oka, T. H_3^+ as the Benchmark for Rigorous ab initio Theory. *J. Mol. Spectrom.* **2009**, *255*, 13−23.

(3) Pavanello, M.; Adamowicz, L.; Alijah, A.; Zobov, N. F.; Mizus, I. I.; Polyansky, O. L.; Tennyson, J.; Szidarovszky, T.; Császár, A. G. Calibration-Quality Adiabatic Potential Energy Surfaces for H_3^+ and its Isotopologues. *J. Chem. Phys.* **2012**, *136*, 184303-1−184303-14.

(4) Polansky, O. L.; Alijah, A.; Zobov, N. F.; Mizus, I. I.; Ovsyannikov, R. I.; Tennyson, J.; Lodi, L.; Szidarovsky, T.; Császár, A. G. Spectroscopy of H_3^+ Based on a New High-accuracy Global Potential Energy Surface. *Philos. Trans. R. Soc. A* **2012**, *370*, 5014−5027.

(5) Pavanello, M.; Adamowicz, L.; Alijah, A.; Zobov, N. F.; Mizus, I. I.; Polyansky, O. L.; Tennyson, J.; Szidarovszky, T.; Császár, A. G; Berg, M.; et al. Precision Measurements and Computations of Transition Energies in Rotationally Cold Triatomic Hydrogen Ions up to the Midvisible Spectral Range. *Phys. Rev. Lett.* **2012**, *108*, 023002−023007.

(6) Jaquet, R.; Khoma, M. V. A Systematic Investigation of the Ground State Potential Energy Surface of H_3. *J. Chem. Phys.* **2012**, *136*, 154307-1−154307-11.

(7) Larsson, M. Dissociative Recombination of H_3^+: 10 Years in Retrospect. *Philos. Trans. R. Soc. A* **2012**, *370*, 5118−5129.

(8) Crabtree, K.; McCall, B. The Ortho:Para Ratio of H_3^+ in Laboratory and Astrophysical Plasmas. *Philos. Trans. R. Soc. A* **2012**, *370*, 5055−5056.

(9) Glover, S.; Savin, D. W. H_3^+ Cooling in Primordial Gas. *Philos. Trans. R. Soc. London, Ser. A* **2006**, *364*, 3107−3112.

(10) Gerlich, D. Ortho - Para Transitions in Slow $H^+ + H_2$ Collsions. *J. Chem. Phys.* **1990**, *92*, 2377−2388.

(11) Grozdanov, T. P.; McCarroll, R. Low-Energy $H^+ + H_2$ Reactive Collisions: Mean-Potential Statistical Model and Role of Permutation Symmetry. *J. Phys. Chem. A* **2012**, *116*, 4569−4577.

(12) Honvault, P.; Jorfi, M.; Gonzalez-Lezana, T.; Faure, A.; Pagani, L. Ortho-Para H_2 Conversion by Proton Exchange at Low Temperature: An Accurate Quantum Mechanical Study. *Phys. Rev. Lett.* **2011**, *107*, 023201-1−023201-4.

(13) Honvault, P.; Jorfi, M.; Gonzalez-Lezana, T.; Faure, A.; Pagani, L. Quantum Mechanical Study of the Proton Exchange in the Ortho−Para H_2 Conversion Reaction at low Temperature. *Phys. Chem. Chem. Phys.* **2011**, *13*, 19089−19100.

(14) Honvault, P.; Jorfi, M.; Gonzalez-Lezana, T.; Faure, A.; Pagani, L. Erratum: Otho-Para H_2 Conversion by Proton Exchange at Low Temperature: An Accurate Quantum Mechanical Study. *Phys. Rev. Lett.* **2012**, *108*, 109903-1.

(15) Jambrina, P. G.; Alvarino, J. M.; Gerlich, D.; Hankel, M.; Herrero, V. J.; Saez- Rabanos, V.; Aoiz, F. J. Dynamics of the $D^+ + H_2$ and $H^+ + D_2$ Reactions: A Detailed Comparison Between Theory and Experiment. *Phys. Chem. Chem. Phys.* **2012**, *14*, 3346−3359.

(16) Velilla, L.; Lepetit, B.; Aguado, A.; Beswick, J. A.; Paniagua, M. The H_3^+ Rovibrational Spectrum Revisited with a Global Electronic Potential Energy Surface. *J. Chem. Phys.* **2008**, *129*, 084307−1−084307−11.

(17) Graham, E.; James, D. R.; Keever, W. C.; Gatland, I. R.; Albritton, D. L.; McDaniel, E. W. Measurement of the Rate Coefficient of the Reactions $H^+ + 2H_2 \rightarrow H_3^+ + H_2$ and $D^+ + 2D_2 \rightarrow D_3^+ + D_2$ in a Drift Tube Mass Spectrometer. *J. Chem. Phys.* **1973**, *59*, 4648−4651.

(18) Johnson, R.; Huang, C.-M.; Biondi, M. A. Three-Body Association Reactions of H^+ and H_3^+ Ions in Hydrogen from 135 to 300 K. *J. Chem. Phys.* **1976**, *65*, 1539−1541.

(19) Gerlich, D.; Horning, S. Experimental Investigations of Radiative Association Processes as Related to Interstellar Chemistry. *Chem. Rev.* **1992**, *92*, 1509−1539.

(20) Barlow, S. E.; Luine, J. A.; Dunn, G. H. Measurement of Ion/Molecule Reactions Between 10 and 20 K. *Int. J. Mass. Spectrom. Ion Phys.* **1986**, *74*, 97−128.

(21) Gerlich, D.; Kaefer, G. Measurements of Extremely Small Rate Coefficients in an RF Trap: The Association Reaction of C^+ and H^+ with H_2 at 230 and 320 K. *Proceedings of the 5th International Swarm Seminar*; Adams, N. G., Smith, D., Eds.; Birmingham University: Birmingham, U.K., 1987; pp 133−137.

(22) Gerlich, D.; Kaefer, G.; Paul, W. Ion Trap Studies of Ternary and Radiative Association Processes. In *7th Symposium on Atomic and Suface Physics*; Märk, T. D. , Howorka, F., Eds.; University of Innsbruck: Innsbruck, 1990; pp 332−337; http://repository.uibk.ac.at/alo?objid=1026217.

(23) Gerlich, D. Ion-Neutral Collisions in a 22-Pole Trap at Very Low Energies. *Phys. Scr.* **1995**, *T59*, 256−263.

(24) Plašil, R.; Zymak, I.; Jusko, P.; Mulin, D.; Gerlich, D.; Glosík, J. Stabilization of H^+ - H_2 Collision Complexes Between 11 and 28 K. *Philos. Trans. R. Soc. A* **2012**, *370*, 5066−5073.

(25) Gerlich, D. Inhomogeneous Electrical Radio Frequency Fields: A Versatile Tool for the Study of Processes with Slow Ions. *Adv. Chem. Phys.* **1992**, *LXXXII*, 1−176.

(26) Gerlich, D. The Study of Cold Collisions Using Ion Guides and Traps. In *Low temperatures and cold molecules*; Smith, I. W. M., Ed.; World Scientific Publishing Co. Pte. Ltd.: Singapore, 2008; pp 121−174.

(27) Gerlich, D. The Production and Study of Ultra-Cold Molecular Ions. In *Low temperatures and cold molecules*; Smith, I. W. M., Eds.; World Scientific Publishing Co. Pte. Ltd.: Singapore, 2008; pp 295−343.

(28) Zymak, I.; Hejduk, M.; Mulin, D.; Plašil, R.; Glosík, J.; Gerlich, D. Low Temperature Ion Trap Studies of $N^+(^3P_{ja}) + H_2(j) \rightarrow NH^+ + H$. *Astrophys. J.* **2013**, in press.

(29) Paul, W.; Lücke, B.; Schlemmer, S.; Gerlich, D. On the Dynamics of the Reaction of Positive Hydrogen Cluster Ions (H_5^+ to H_{23}^+) with Para and Normal Hydrogen at 10 K. *Int. J. Mass. Spectrom. Ion Phys.* **1995**, *150*, 373−387.

(30) Gerlich, D. Recent Progress in Experimental Studies of Ion−Molecule Reactions Relevant to Interstellar Chemistry. In *Molecules and Grains in Space*; Nenner, I., Ed.; AIP Press: New York, 1994; pp 489−500.

(31) Schlier, Ch.; Vix, U. Lifetimes of Triatomic Collision Complexes. *Chem. Phys.* **1985**, *95*, 401−409.

(32) Carrington, A.; McNab, I. R.; West, Y. D. Infrared Predissociation Spectrum of the H_3^+ Ion. II. *J. Chem. Phys.* **1993**, *98*, 1073−1092.
(33) Tennyson, J.; Barletta, P.; Munro, J. J.; Silva, B. C. The Role of Asymptotic Vibrational States in H_3. *Philos. Trans. R. Soc. London, Ser. A* **2006**, *364*, 2903−2916.
(34) Aguado, A.; Barragán, P.; Prosmiti, R.; Delgado-Barrio, G.; Villarreal, P.; Roncero, O. A New Accurate and Full Dimensional Potential Energy Surface of H_5^+ Based on a Triatomics-in-Molecules Analytic Functional Form. *J. Chem. Phys.* **2010**, *133*, 024306-1−024306-15.
(35) de Tudela, R. P.; Barragán, P.; Prosmiti, R.; Villarreal, P.; Delgado-Barrio, G. Internal Proton Transfer and H_2 Rotations in the H_5^+ Cluster: A Marked Influence on its Thermal Equilibrium State. *J. Phys. Chem. A* **2011**, *115*, 2483−2488.
(36) Gerlich, D.; Borodi, G.; Luca, A.; Mogo, C.; Smith, M. Reactions Between Cold CH_n^+ with H and H_2. *Z. Phys. Chem.* **2011**, *252*, 475−492.
(37) Kylänpää, I.; Rantala, T. T. Finite Temperature Quantum Statistics of H_3^+ Molecular Ion. *J. Chem. Phys.* **2010**, *133*, 044312-1−044312-5.

IV. Stabilization of H^+-H_2 Collision Complexes between 11 and 28 K

Plašil R., Zymak I., Jusko P., Mulin D., Gerlich D., Glosík J. (2012)

Philosophical Transactions of the Royal Society A, **370**, 5066.

PHILOSOPHICAL TRANSACTIONS OF THE ROYAL SOCIETY A

CrossMark click for updates

Phil. Trans. R. Soc. A (2012) **370**, 5066–5073
doi:10.1098/rsta.2012.0098

Stabilization of H^+–H_2 collision complexes between 11 and 28 K

By Radek Plašil*, Illia Zymak, Pavol Jusko, Dmytro Mulin, Dieter Gerlich and Juraj Glosík

Faculty of Mathematics and Physics, Charles University, Prague, Czech Republic

Formation of H_3^+ via association of H^+ with H_2 has been studied at low temperatures using a 22-pole radiofrequency trap. Operating at hydrogen number densities from 10^{11} to $10^{14}\,cm^{-3}$, the contributions of radiative, k_r, and ternary, k_3, association have been extracted from the measured apparent binary rate coefficients, $k^* = k_r + k_3[H_2]$. Surprisingly, k_3 is constant between 11 and 22 K, $(2.6 \pm 0.8) \times 10^{-29}\,cm^6\,s^{-1}$, while radiative association decreases from $k_r(11\,K) = (1.6 \pm 0.3) \times 10^{-16}\,cm^3\,s^{-1}$ to $k_r(28\,K) = (5 \pm 2) \times 10^{-17}\,cm^3\,s^{-1}$. These results are in conflict with simple association models in which formation and stabilization of the complex are treated separately. Tentative explanations are based on the fact that, at low temperatures, only few partial waves contribute to the formation of the collision complex and that ternary association with H_2 may be quite inefficient because of the 'shared proton' structure of H_5^+.

Keywords: interstellar chemistry; H^+; H_3^+; association; ion traps

1. Introduction

As Oka summarized in his introductory remarks of the 2006 meeting, H_3^+ plays an important role in many fields ranging from astrochemistry via applications in hydrogen plasmas to fundamental aspects [1]. The combination of three protons (or deuterons) and two electrons represents a benchmark system for both understanding molecular structure and scattering dynamics. Accurate ground-state potential energy surfaces today allows us to predict low-lying rotation–vibrational states and infrared and sub-millimetre transitions with spectroscopic accuracy [2,3]. With increasing total energy, more states become accessible. The present spectroscopic activities work in an energy range where the atoms start to explore not only the triangular, but also the linear, configuration space. Here, H_3^+ becomes floppy and, owing to nonlinear couplings, the classical motion can become chaotic. All this and strong Coriolis coupling between rotation–vibrational states make precise *ab initio* calculations a challenge.

Even more complications arise if the total energy of the H_3^+ system reaches the dissociation limit. In this regime, specific bound or quasibound states exist, which are responsible for the pre-dissociation spectra reported by Carrington *et al.* [4,5].

*Author for correspondence (radek.plasil@mff.cuni.cz).

One contribution of 21 to a Theo Murphy Meeting Issue 'Chemistry, astronomy and physics of H_3^+'.

So far, there is no clear assignment of the observed transitions; however, there are interesting explanations [6,7]. Similar scattering states are populated in low-energy $H^+ + H_2$ collisions, leading to energy exchange, ortho–para transitions, chemical reactions (scrambling) or, the subject of this paper, to association, i.e. to continuum-bound transitions. The theoretical treatment of H_3^+ in the vicinity of the dissociation limit requires a potential with the correct long-range behaviour and sophisticated methods for describing the dynamics.

Addition of molecules via association is an important process for forming complex structures in many plasma environments. Radiative association plays an important role in the formation of interstellar molecules. Although under most conditions, H_3^+ is formed via H-atom abstraction in $H_2^+ + H_2$ collisions, association of H^+ with H_2 also plays a role under specific conditions [8]. In any case, it is of fundamental interest as the inverse process to photofragmentation. In the following, we report results for radiative association, i.e. stabilization via emission of a photon,

$$H^+ + H_2 \xrightarrow{k_r} H_3^+ + h\nu, \tag{1.1}$$

and ternary association,

$$H^+ + 2H_2 \xrightarrow{k_3} H_3^+ + H_2, \tag{1.2}$$

where the formed complex is stabilized via collision with a third body. At the number densities $[H_2]$ we use in the present study, the radiative association rate coefficient k_r and the ternary association rate coefficient k_3 contribute both significantly to the apparent binary rate coefficient,

$$k^* = k_r + k_3[H_2]. \tag{1.3}$$

For many decades, the determination of association rate coefficients has been the domain of swarm techniques operating at rather high pressures. With number densities above $10^{16}\,\mathrm{cm}^{-3}$ and rate coefficients of $10^{-29}\,\mathrm{cm}^6\,\mathrm{s}^{-1}$, reaction time constants were shorter than millieseconds and, therefore, became measurable. For reaction (1.2), Graham *et al.* determined a ternary rate coefficient at 300 K [9], using a drift-tube mass spectrometer apparatus. Johnsen *et al.* extended the temperature range from room temperature down to 135 K [10] and reported rate coefficients increasing from 3.0×10^{-29} to $4.3 \times 10^{-29}\,\mathrm{cm}^6\,\mathrm{s}^{-1}$. Swarm techniques could not provide direct results for radiative association because the high densities lead to $k_3[H_2] \gg k_r$. This situation has changed by the development of ion-trapping techniques in the 1980s. First results for reactions (1.1) and (1.2) at 230 K have been reported in Gerlich & Kaefer [11]. An early summary can be found in Gerlich & Horning [12]. Because of the high sensitivity of ion traps, one can operate at such low number densities that ternary association becomes even slower than radiative association.

In the last few years, new interest in the $H^+ + H_2$ collision system has grown, mainly owing to the fact that this fundamental three-proton two-electron system got within the reach of 'exact' quantum mechanical calculations (see [13,14] and references therein). Therefore, we have started a research programme to measure low-temperature rate coefficients for collisions between hydrogen ions and hydrogen atoms or molecules, including also anions. First results determined

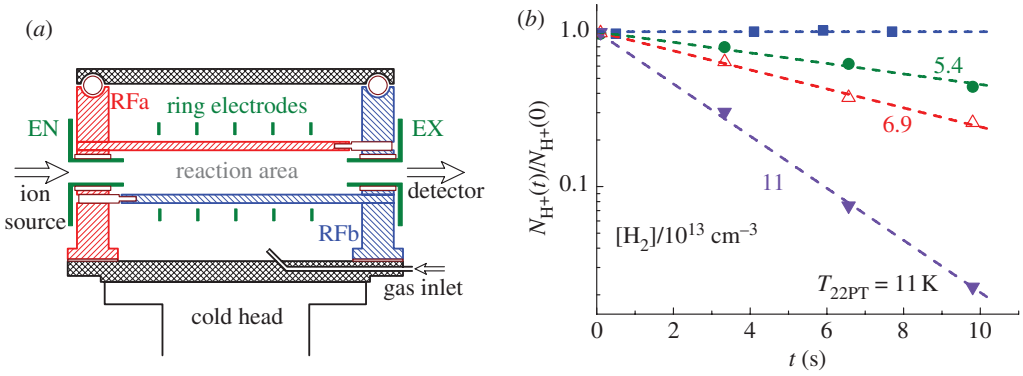

Figure 1. (*a*) The 22-pole ion trap scheme. In the radial direction, ions are confined by the radiofrequency field, created by two sets of 11 poles (RFa and RFb) precisely mounted on opposite sides ($f = 18$ MHz, $V_0 = 19$ V for H^+, $V_0 = 26$ V for He^+). The entrance and exit electrodes (EN and EX) are used to open and close the trap with electrostatic barriers of some tens of meV. (*b*) Typical decrease of the relative number of trapped H^+ ions due to reactions with H_2. The number density of H_2 has been varied from 10^{12} to 10^{14} cm^{-3}, leading to decay time constants between many minutes and 2.5 s. (Online version in colour.)

at 11 K for ternary association, were reported recently in a conference contribution [15]. The new results cover the temperature range from 11 to 28 K and include radiative association.

2. Experiments

To study reactions (1.1) and (1.2) and to determine separately their rate coefficients, the AB-22PT instrument has been used. The principle of ion trapping and the experimental details have been described elsewhere [16]. The central part of the instrument, the 22-pole ion trap, is shown schematically in figure 1*a*. In the present study, normal hydrogen (one-quarter para-H_2 and three-quarters ortho-H_2) was introduced into the trap volume. A few collisions with the walls are sufficient to get the neutral gas into thermal equilibrium with the box, with the exception of the ortho–para ratio. The background pressure of the main chamber is lower than 10^{-7} Pa. The level of reactive impurities in a gas leaked into the reaction volume has to be below 0.1 ppm. Impurities with the exception of HD and D_2 are mostly frozen out at 11 K.

The measuring procedure is based on iterative filling of the trap with a well-defined number of primary ions and analysis of the content after different times using a quadrupole mass spectrometer and micro-channel plate detector. In the present experiment, the storage times have been extended up to 30 s.

In order to test the actual conditions of the instrument, formation of He_2^+ dimers via the $He^+ + 2$ He reaction has been used. Although the new data shown in figure 2 are somewhat larger than the previous ion-trapping results [12], there is a good overall agreement with them and also with the analytical function extrapolating the data from Böhringer *et al.* [18].

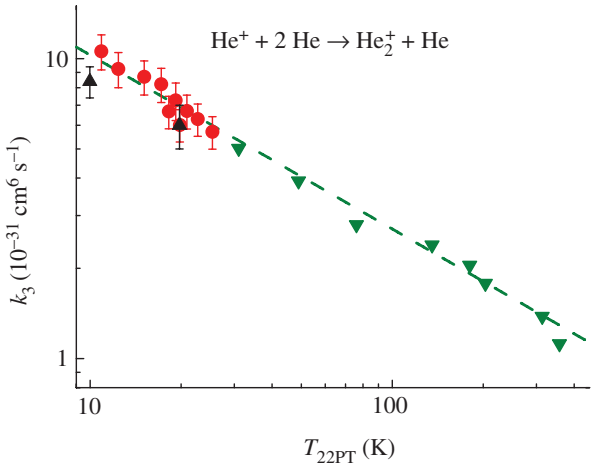

Figure 2. Formation of He_2^+ dimers via the $He^+ + 2\,He$ reaction. Filled circles show the measured temperature dependence of $k_3(T)$ used as a thermometer in the trap, as proposed in Gerlich [17]. The inverted triangles indicate previous results obtained using a selected ion drift tube by Böhringer *et al.* [18] and triangles show a ring electrode trap by Gerlich, at low temperatures [12]. The dashed line extrapolates Böhringer's fit. (Online version in colour.)

3. Results

A typical set of raw data, recorded at a 22-pole temperature of 11 K, is shown in figure 1*b*. In order to increase the sensitivity, a repetition period of 10 s has been chosen. About 100 H^+ ions have been injected each time. For better comparison of the results, the number of remaining primary ions is normalized to the initially injected ones. The number of ions in the trap has been counted at four different storage times. As can be seen from the dashed lines, N_{H^+} decreases exponentially with a characteristic decay time $\tau = (k^*[H_2])^{-1}$. The number density of H_2 has been varied over more than two orders of magnitude, leading to a variation of τ from 2.5 s to conditions where statistical errors limit the measurement. The rate coefficients can also be determined from the number of produced H_3^+ ions; however, this requires the determination of the detection efficiencies of the two different ions.

From such data, the apparent binary rate coefficient k^* is determined. Figure 3 shows averages over a large set of such measurements, performed at 11 and 22 K and at H_2 densities as low as $4 \times 10^{11}\,cm^{-3}$. The errors are smaller than the dot size, with the exception of the results at low densities where the bars indicate the uncertainties. For separating bi- and termolecular contributions, the data have been fitted with equation (1.3), resulting in the solid lines. Comparison of the dashed and dotted lines with the experimental results reveals that at densities below $10^{12}\,cm^{-3}$, most products are $H_3^+ + h\nu$, while above $10^{13}\,cm^{-3}$, stabilization of the H^+–H_2 collision complex with H_2 prevails and k^* rises proportional to $[H_2]$. In accordance with expectations, the results show $k_r(11\,K) > k_r(22\,K)$, while, to our surprise, the ternary rate coefficients are the same at the two temperatures.

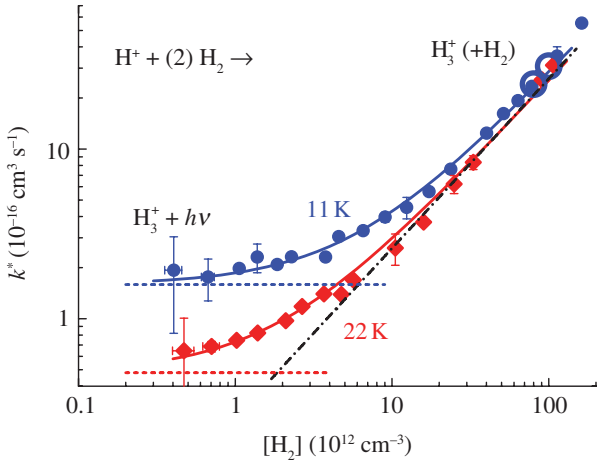

Figure 3. Apparent binary association rate coefficient k^* for $T_{22PT} = 11$ K, circles, and 22 K, squares (averaged over many measurements). In order to extract information on radiative and ternary association, the density has been varied over a wide range. The data have been fitted with $k^* = k_r + k_3[H_2]$. The dashed and the dashed-dotted lines show the individual contributions. The surprising observation that the ternary association rate coefficient is the same for both temperatures while radiative association becomes faster with decreasing temperature is discussed in the text. (Online version in colour.)

The results from the fits of figure 3 are plotted in figure 4 as solid circle points. In order to obtain more information on the temperature dependence of H_3^+ formation, the density has been kept constant at three different values, and the temperature has been varied between 11 and 28 K. At the low density (9×10^{11} cm^{-3}), the values for k_r have been determined by subtracting from the measured rate coefficients k^* the contribution from ternary association. Values for k_3 have been determined by measuring k^* at two higher densities (8×10^{12} cm^{-3}, 1.6×10^{13} cm^{-3}) and by subtracting the contributions from radiative association.

4. Discussion and conclusion

The basics of an empirical description of association reactions have been summarized in Gerlich & Horning [12]. It is based on the assumption that one can separate two independent sequential steps, first the formation of a long-lived complex followed by its stabilization. The collision complex is formed with a bimolecular rate coefficient k_c. Assuming that there are no other product channels, this complex decays back to the reactants with a time constant τ_{diss}. Usually, a small fraction may be stabilized via emission of a photon (time constant τ_r) or stabilized via collision with a third body. In the present study, we use only H_2 (time constant τ_{H_2}). With these elementary processes, the overall formation of stable products can be described by the apparent second-order rate coefficient

$$k^* = k_c \frac{1/\tau_{H_2} + 1/\tau_r}{1/\tau_{diss} + 1/\tau_{H_2} + 1/\tau_r}. \tag{4.1}$$

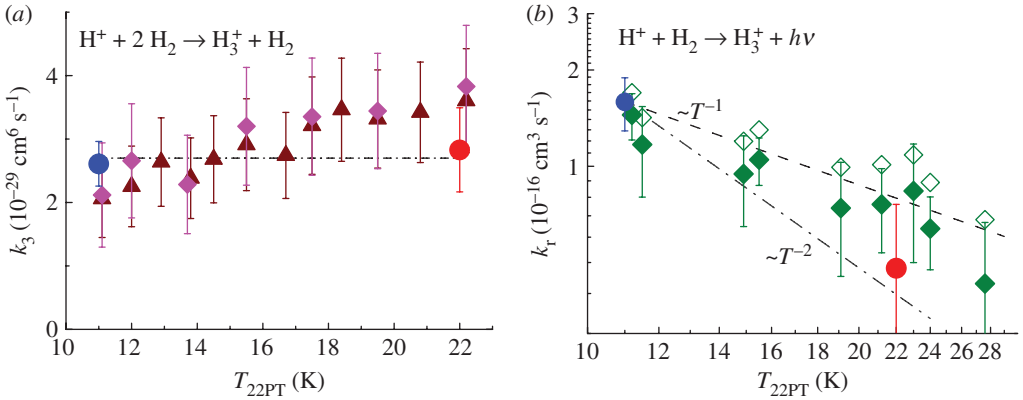

Figure 4. Temperature dependences of k_r and k_3. The solid circles are the results from the fits shown in figure 3. (*a*) $k_3(T)$ was measured at two densities (squares, $8 \times 10^{12}\,cm^{-3}$; triangles, $1.6 \times 10^{13}\,cm^{-3}$). The results have been corrected individually for contribution from radiative association. The apparent increase of k_3 with T is within the overall uncertainty of the data. (*b*) $k_r(T)$ was measured at a density of $9 \times 10^{11}\,cm^{-3}$. The results have been corrected individually for contributions from ternary association. The uncorrected values are plotted as open symbols. The dashed line indicates a T^{-1} law, the dashed-dotted a T^{-2} law. (Online version in colour.)

A rigorous calculation of this requires, in general, a master equation approach accounting for the elementary steps that either contribute to stabilization or compete against it.

In such a model, the temperature dependence of the overall process is mainly determined by τ_{diss}, while one assumes that τ_r and τ_{H_2} do not change much with temperature. Under such conditions, one gets the same T dependence for k_3 and k_r, in contrast to our experimental observation. Here, we can give only some first hints to possible reasons. One is based on the special shape of the H_5^+ potential energy surface, the so-called shared proton structure [19]. Owing to this interaction, a H_2 approaching the H_3^+ collision complex slowly may pull out the proton from the collision complex instead of stabilizing it. Other explanations may be based on the fact that statistical arguments do not hold anymore at the low temperatures of our experiment. On the basis of the simple Langevin criterion using only the polarization interaction, one obtains for the total orbital angular momentum $l_m < 6$ at 10 K and $l_m < 8$ at 20 K. This leads to a rather low number of states accessible to the H_3^+ complex [6].

More theoretical and experimental work is needed to understand these scattering states of H_3^+. One of our aims is to go to higher temperatures for comparing our results with previous measurements. It is very important to use para-H_2 and to study the influence of the various nuclear spin configurations.

Finally, there are various interesting aspects of the astrophysical relevance of $H^+ + H_2$ collisions. Its role in ortho–para conversion has been reevaluated recently ([13], see also the erratum). It is an open question as to whether scattering of H^+ on H_2 is more efficient in cooling primordial gas than the H_3^+ molecule with its infrared active modes [20]. Another important subject is the chemical lifetime of protons in various environments. Electron transfer from atoms

(e.g. O, P, S [21,22]) competes with radiative recombination with free electrons and with neutralization in collisions with negatively charged molecules or small dust particles. Depending on the conditions and fractional abundances of the relevant targets, detailed models will predict regions where radiative association with H_2 is an important sink for protons and a source for excited H_3^+ ions.

This work is a part of the research grant OC10046 financed by the Ministry of Education of the Czech Republic and was partly supported by GACR (P209/12/0233, 205/09/1183), by GAUK 388811, GAUK 406011 and by COST Action CM0805 (The Chemical Cosmos). Since 2010, the instrument has been operated at the Faculty of Mathematics and Physics of Charles University in Prague. We thank the Technical University of Chemnitz and the DFG for lending us this instrument.

References

1 Oka, T. 2006 Introductory remarks. *Phil. Trans. R. Soc. A* **364**, 2847–2853. (doi:10.1098/rsta.2006.1870)
2 Pavanello, M., Tung, W.-C., Leonarski, F. & Adamowicz, L. 2009 New more accurate calculations of the ground state potential energy surface of H_3^+. *J. Chem. Phys.* **130**, 074105. (doi:10.1063/1.3077193)
3 Morong, C. P., Gottfried, J. L. & Oka, T. 2009 H_3^+ as the benchmark for rigorous *ab initio* theory. *J. Mol. Spectrosc.* **255**, 13–23. (doi:10.1016/j.jms.2009.02.010)
4 Carrington, A. & Kennedy, R. A. 1984 Infrared predissociation spectrum of the H_3^+ ion. *J. Chem. Phys.* **81**, 91–112. (doi:10.1063/1.447357)
5 Carrington, A., McNab, I. R. & West, Y. D. 1993 Infrared predissociation spectrum of the H_3^+ ion. II. *J. Chem. Phys.* **98**, 1073–1092. (doi:10.1063/1.464331)
6 Berblinger, M. & Schlier, Ch. 1988 Classical radiation spectra of long-lived H_3^+ complexes. *Mol. Phys.* **63**, 779–790. (doi:10.1080/00268978800100561)
7 Tennyson, J., Barletta, P., Munro, J. J. & Silva, B. C. 2006 The role of asymptotic vibrational states in H_3^+. *Phil. Trans. R. Soc. A* **364**, 2903–2916. (doi:10.1098/rsta.2006.1890)
8 Bayet, E., Williams, D. A., Hartquist, T. W. & Viti, S. 2011 Chemistry in cosmic ray dominated regions. *Mon. Not. R. Astron. Soc.* **414**, 1583–1591. (doi:10.1111/j.1365-2966.2011.18500.x)
9 Graham, E., James, D. R., Keever, W. C., Gatland, I. R., Albritton, D. L. & McDaniel, E. W. 1973 Measurement of the rate coefficient of the reactions $H^+ + 2H_2 \rightarrow H_3^+ + H_2$ and $D^+ + 2D_2 \rightarrow D_3^+ + D_2$ in a drift tube mass spectrometer. *J. Chem. Phys.* **59**, 4648–4651. (doi:10.1063/1.1680676)
10 Johnsen, R., Huang, C.-M. & Biondi, M. A. 1976 Three-body association reactions of H^+ and H_3^+ ions in hydrogen from 135 to 300 K. *J. Chem. Phys.* **65**, 1539–1541. (doi:10.1063/1.433209)
11 Gerlich, D. & Kaefer, G. 1987 Measurements of extremely small rate coefficients in an RF trap: the association reaction of C^+ and H^+ with H_2 at 230 and 320 K. In *Proc. 5th Int. Swarm Seminar* (eds N. G. Adams & D. Smith), p. 133. Birmingham, UK: University of Birmingham.
12 Gerlich, D. & Horning, S. 1992 Experimental investigations of radiative association processes as related to interstellar chemistry. *Chem. Rev.* **92**, 1509–1539. (doi:10.1021/cr00015a003)
13 Honvault, P., Jorfi, M., Gonzalez-Lezana, T., Faure, A. & Pagani, L. 2011 Quantum mechanical study of the proton exchange in the ortho–para H_2 conversion reaction at low temperature. *Phys. Chem. Chem. Phys.* **13**, 19 089–19 100. (doi:10.1039/C1CP21232J) [Erratum in *Phys. Rev. Lett.* 2012 **108**, 109903.]
14 Jambrina, P. G., Alvarino, J. M., Gerlich, D., Hankel, M., Herrero, V. J., Saez-Rabanos, V. & Aoiz, F. J. 2012 Dynamics of the $D^+ + H_2$ and $H^+ + D_2$ reactions: a detailed comparison between theory and experiment. *Phys. Chem. Chem. Phys.* **14**, 3346–3359. (doi:10.1039/C2CP23479C)
15 Zymak, I., Jusko, P., Roucka, S., Plasil, R., Rubovic, P., Gerlich, D. & Glosik, J. 2011 Ternary association of H^+ ion with H_2 at 11 K. *Eur. Phys. J. Appl. Phys.* **56**, 24010. (doi:10.1051/epjap/2011110172)

16 Gerlich, D. 1992 Inhomogeneous rf fields: a versatile tool for the study of processes with slow ions. In *Advances in chemical physics: state-selected and state-to-state ion-molecule reaction dynamics, part 1. Experiment*, vol. 82 (eds C.-Y. Ng, M. Baer, I. Prigogine & S. A. Rice). Hoboken, NJ: Wiley & Sons, Inc. (doi:10.1002/9780470141397.ch1)
17 Gerlich, D. 2008 The study of cold collisions using ion guides and traps. In *Low temperatures and cold molecules* (ed. I. W. M. Smith), pp. 121–174. Singapore: Imperial College Press.
18 Böhringer, H., Glebe, W. & Arnold, F. 1983 Temperature-dependence of the mobility and association rate coefficient of He^+ ions in He from 30–350 K. *J. Phys. B* **16**, 2619–2626. (doi:10.1088/0022-3700/16/14/022)
19 Sanz-Sanz, C., Roncero, O., Valdés, A., Prosmiti, R., Delgado-Barrio, G., Villarreal, P., Barragán, P. & Aguado, A. 2011 Infrared spectrum of H_5^+ and D_3^+. *Phys. Rev. A* **84**, 060502. (doi:10.1103/PhysRevA.84.060502)
20 Glover, S. & Savin, D. W. 2006 H_3^+ cooling in primordial gas. *Phil. Trans. R. Soc. A* **364**, 3107–3112. (doi:10.1098/rsta.2006.1867)
21 Crabtree, K. N., Indriolo, N., Kreckel, H., Tom, B. A. & McCall, B. J. 2011 On the ortho:para ratio of H_3^+ in diffuse molecular clouds. *Astrophys. J.* **729**, 15. (doi:10.1088/0004-637X/729/1/15)
22 Woodall, J., Agúndez, M., Markwick-Kemper, A. J. & Millar, T. J. 2007 The UMIST database for astrochemistry 2006. *Astron. Astrophys.* **466**, 1197–1204. (doi:10.1051/0004-6361:20064981)

V. Interaction of O^- and H_2 at Low Temperatures

Jusko P., Roučka Š., Mulin D., Zymak I., Plašil R., Gerlich D.,
Čížek M., Houfek K., Glosík J. (2015)
The Journal of Chemical Physics, **142**(**1**), 014304.

Interaction of O^- and H_2 at low temperatures

P. Jusko,[1] Š. Roučka,[1,a)] D. Mulin,[1] I. Zymak,[1] R. Plašil,[1] D. Gerlich,[1] M. Čížek,[2] K. Houfek,[2] and J. Glosík[1]

[1]*Department of Surface and Plasma Science, Faculty of Mathematics and Physics, Charles University in Prague, Prague 180 00, Czech Republic*

[2]*Institute of Theoretical Physics, Faculty of Mathematics and Physics, Charles University in Prague, Prague 180 00, Czech Republic*

(Received 10 September 2014; accepted 15 December 2014; published online 6 January 2015)

Reactive collisions between O^- and H_2 have been studied experimentally at temperatures ranging from 10 K to 300 K using a cryogenic radiofrequency 22-pole ion trap. The rate coefficients for associative detachment, leading to $H_2O + e^-$, increase with decreasing temperature and reach a flat maximum of 1.8×10^{-9} cm^3 s^{-1} at temperatures between 20 K and 80 K. There, the overall reaction probability is in good agreement with a capture model indicating efficient non-adiabatic couplings between the entrance potential energy surfaces. Classical trajectory calculations on newly calculated potential energy surfaces as well as the topology of the conical intersection seam leading to the neutral surface corroborate this. The formation of $OH^- + H$ via hydrogen transfer, although occurring with a probability of a few percent only (about 5×10^{-11} cm^3 s^{-1} at temperatures 10–300 K), indicates that there are reaction paths, where electron detachment is avoided. © *2015 AIP Publishing LLC.* [http://dx.doi.org/10.1063/1.4905078]

I. INTRODUCTION

The reaction of O^- with H_2 is one of the simplest anion-neutral systems and as such it has been studied many times theoretically and experimentally. To our knowledge, there are no measured reaction rate coefficients for temperatures below 170 K. At low temperatures, two exothermic reaction channels are open. These are associative detachment (AD),

$$O^- + H_2 \xrightarrow{k_1} H_2O + e^-, \qquad \Delta H = -3.58 \text{ eV} \tag{1}$$

and hydrogen atom transfer

$$O^- + H_2 \xrightarrow{k_2} OH^- + H, \qquad \Delta H = -0.28 \text{ eV}, \tag{2}$$

with reaction rate coefficients k_1 and k_2, respectively. The given reaction enthalpies were calculated from the enthalpies of formation of neutrals[1] and electron affinities.[2,3] The formation of metastable H_2O^- via radiative association is also energetically allowed,[4] but this process has not yet been confirmed experimentally. Studying the temperature dependence of the two reactions provides a probe for investigating the structure and reactivity of the fundamental H_2O^- system at low energies. At higher energies, this system has recently been studied theoretically[5] and experimentally[6–8] by means of dissociative electron attachment to the neutral water molecule. Other studies include the work of Claydon *et al.*[9] and the detailed potential energy surface calculations of Werner *et al.*[4]

Experimental studies of the rate coefficients of reactions (1) and (2) and their temperature dependencies have been carried out before at room temperature and above using drift tubes, flowing afterglow, tandem mass spectrometry, and an octopole ion trap instrument.[10,11] A study at mean collision energies down to 0.02 eV was carried out using a temperature variable flow/drift tube.[12] Furthermore, the kinetic energy distribution of the electrons produced in associative detachment has been studied by Mauer and Schulz,[13] Esaulov *et al.*,[14] and Jusko *et al.*[11] Using crossed beams, energy partitioning in the $O^- + D_2 \rightarrow OD^- + D$ reaction has been reported recently by Lee and Farrar.[15] The results of all these studies indicate high internal excitation of the produced H_2O neutrals and slow electrons. For further details and references see Ref. 11.

When $O^-(^2P)$ approaches $H_2(X^1\Sigma_g^+)$, the collision system can follow three electronic surfaces which can be marked according to their corresponding irreducible representations as $1^2A'$, $1^2A''$, and $2^2A'$. Furthermore, the O^- ion can be present in two fine structure states, $O^-(^2P_{3/2})$ and $O^-(^2P_{1/2})$, which is 22 meV higher.[16] Molecular hydrogen is present in two nuclear spin configurations: *ortho*- and *para*-H_2. The lowest rotational states of *ortho*- and *para*-H_2 are separated by ≈15 meV. In the present experiments, we are using normal hydrogen; hence, the ratio of *ortho*-/*para*-H_2 concentrations is fixed at the statistical value, 3:1 (see discussion in Ref. 17). Concerning the population of the two O^- fine structure states, reached in the trap via collisions with He and H_2, we can only speculate. Analysis of drift tube experiments by Viehland *et al.*[18] suggests that the relaxation of fine structure states of O^- by collisions with helium is slow and the ratio of $O^-(^2P_{1/2})$ to $O^-(^2P_{3/2})$ concentration is 1:2 according to the statistical probability of production in the ion source. Collisions with H_2 are not expected to contribute to relaxation, because at low temperatures almost every collision of O^- with H_2 is reactive.

This work presents an experimental and theoretical study of collisions of O^- with H_2 at low temperatures. In the following, we will first describe the experiment and the measured temperature dependencies of rate coefficients for AD and hydrogen atom transfer. In the section Calculations and

a)Author to whom correspondence should be addressed. Electronic mail: Stepan.Roucka@mff.cuni.cz

theory, we introduce briefly into the calculation of the H_2O^- potential energy surfaces and provide a detailed basis for explaining the measured results. In Conclusions, we summarize the results and provide some information on planned work.

II. EXPERIMENT

To study reactive collisions of O^- ions with H_2, we used the cryogenic 22-pole radiofrequency ion trap. Because a thorough description of the instrument can be found elsewhere,[19–21] only a few hints are given here. Primary O^- ions are produced by electron bombardment of N_2O precursor gas in a storage ion source.[22] The ions are extracted from the ion source, mass selected, and injected into the linear 22-pole radiofrequency ion trap.[22,23] The trap is cooled by a cryocooler reaching temperatures down to 10 K. The injected ions are thermalized to the trap temperature by collisions with helium buffer gas. The number density of helium is typically 100 times higher than the number density of the H_2 reactant gas, which is also leaked into the trap. The absolute number density of the reactant, which is required for determination of absolute rate coefficients, is determined using a Bayard-Alpert ionization gauge. A standard procedure for calibrating the ionization gauge using a spinning rotor gauge is used. We estimate that the total systematic error of the number density is below 20%. After a certain trapping/reaction time, the ions are extracted from the trap, mass selected, and counted using a microchannel plate detector. By repeating this procedure for different selected masses, trapping times, and H_2 densities, one can obtain the time evolution of relative numbers of ions in the trap. In particular, the relative numbers of O^- and OH^- ions, denoted by N_O and N_{OH}, respectively, were measured for several H_2 densities as a function of time after injection of O^- ions to the trap.

III. EXPERIMENTAL RESULTS

A typical measured time evolution of the numbers of trapped primary O^- and product OH^- ions, N_O and N_{OH}, is shown in Fig. 1, at various trap temperatures. The measurements were performed at constant H_2 flux resulting in different hydrogen densities at different temperatures. In order to make the results comparable, we show how the data would appear if the $[H_2]$ were equal 10^{10} cm^{-3} in each measurement. This is achieved by using a reduced trapping time $t^{\#} = t \times [H_2]/(10^{10}\ \text{cm}^{-3})$. In this way, the slopes of the O^- number decays are proportional to the reaction rate coefficients at the respective temperatures. Since the H_2 flux was not adjusted between the presented measurements, the relative values are not affected by the systematic uncertainty of $[H_2]$.

The data were analyzed by least-squares fitting the measured numbers of ions with the analytic solutions of the corresponding kinetic equations. The good agreement of the fit with the measured data is illustrated in Fig. 1. At temperatures above 200 K, we observed a loss of O^- ions even without adding H_2. One of the reasons is the N_2O gas from the ion source, which is efficiently cryopumped at lower temperatures. In such cases, the loss rate is measured separately for the given temperature and it is included in our analysis. Also for OH^- ions, an additional loss was observed at temperatures above 200 K and included in the kinetic equations as an additional term. This increased the uncertainty of the fitted values of k_2; hence, more datasets had to be averaged in order to reach the desired accuracy at 300 K. At temperatures below 200 K, the OH^- loss is negligible as verified by repeating the analysis with the OH^- loss process included.

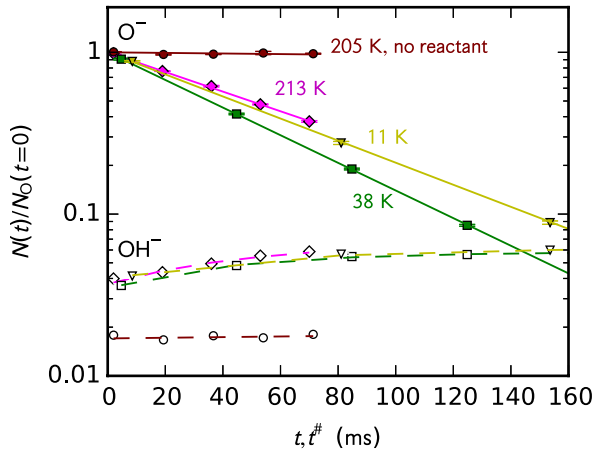

FIG. 1. Decay of the number of primary O^- ions and increase of the number of OH^- product ions due to interaction of O^- ions with H_2. The data were measured at several trap temperatures (indicated in the graph). The numbers of O^- and OH^- ions relative to the initial number of O^- ions are indicated by full and empty symbols, respectively. The number density of H_2 at 213 K was 1.0×10^{10} cm^{-3}. The data at 11 K and 38 K are plotted as a function of reduced trapping time $t^{\#}$, accounting for the change of density with temperature at constant gas flux (see text). The fitted curves are indicated by lines. The data measured at 205 K without H_2 reactant present are shown for comparison.

From the evaluated time dependencies and the known number densities of H_2, the reaction rate coefficients for both reaction channels were calculated. Measured linear dependencies of the loss rate on $[H_2]$ confirmed that the evaluated rate coefficients correspond to a binary reaction with H_2. By varying the trap temperature, the rate coefficients of both reactions were measured in the temperature range of 10–300 K. For reaction (2), the accuracy of measurements at temperatures above 200 K is limited due to parasitic reactions. In order to test the influence of desorbing impurities, measurements were performed during the cooling down phase as well as the warming up phase (cold head switched off). As can be seen from Fig. 2, there are no significant differences in the results. The rate coefficient of reaction (1) has a flat maximum of about 1.8×10^{-9} cm^{3}s^{-1} in the temperature range of 20–80 K, which exceeds the Langevin rate coefficient $k_{\text{Lang}} = 1.56 \times 10^{-9}$ cm^3 s^{-1} (the polarizability of normal-H_2 at 77 K was used to calculate k_{Lang},[24] neglecting the small temperature dependence). Similar temperature dependence was recently observed for reaction of NH_2^- with H_2.[25] Reaction (2) proceeds with a nearly constant rate coefficient of 5×10^{-11} cm^3 s^{-1} corresponding to a reaction probability of approximately $k_2/k_{\text{Lang}} \approx 0.03$. The slight decrease down to 10 K may indicate an increase of adiabatic behavior at these low velocities.

For comparison, Fig. 2 also shows a collection of results obtained in previous studies (see figure caption). The value

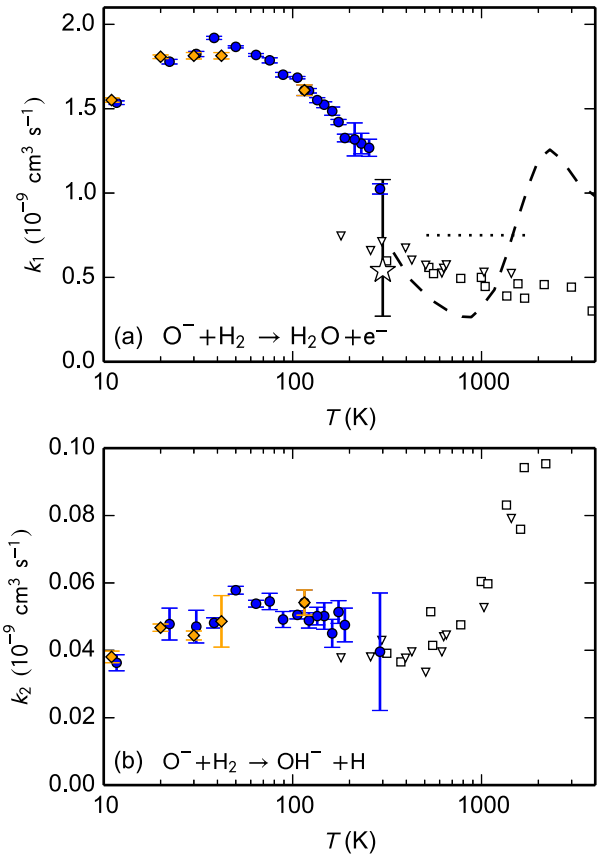

FIG. 2. Temperature dependence of the rate coefficients for associative detachment (panel (a)) and H atom transfer reactions (panel (b)). The data measured in the present experiments are indicated by the filled symbols (diamonds: warming up phase and circles: cooling down phase). The error bars indicate only the statistical errors of the fits. The overall uncertainty of the absolute values is ±20%. The hollow star indicates data measured recently using an octopole ion trap at 300 K in our laboratory.[11] The figures also show various results measured with drift tubes: hollow squares: McFarland *et al.*,[10] triangles: Viggiano *et al.*,[12] and dotted lines: Moruzzi *et al.*[26] The dashed line shows ion beam data[13] reported by McFarland *et al.*[10]

marked by a hollow star in panel (a) of Fig. 2 was measured in an octopole radiofrequency ion trap at 300 K by detecting the electrons produced in AD (reaction (1)).[11] This result is accurate within a factor of 2 due to systematic errors. Note that the primary goal of those studies was to record the energy distribution of electrons produced in AD.

Inspection of the overall temperature dependence of the rate coefficients indicates interesting trends. Note, however, that our results are thermal rate coefficients at temperatures ≤300 K while drift tube data were obtained at mean collision energies KE_{CM}. They are plotted at corresponding temperatures above 300 K (with exception of one value at 176 K[12]). The rate coefficient of reaction (2) is certainly a continuous extension of the data by McFarland *et al.*[10] and Viggiano *et al.*[12] while the rate coefficients of reaction (1) show a step at 300 K. However, considering that the overall uncertainty of our data is 20%, and the systematic and statistical errors of Viggiano *et al.*[12] are 25% and 15%, respectively, this step is nearly insignificant. It may be caused partly due to parasitic reactions in the trap at temperatures above 200 K but also due to errors in the older experiments. Nonetheless, there is no doubt that the overall reactivity of O^- and H_2 increases steeply with temperature decreasing below 300 K. In the following, we provide a tentative explanation based on nonadiabatic coupling of the repulsive potential energy surfaces to the reactive one.

IV. CALCULATIONS AND THEORY

The complete theoretical description of the reactive $O^- + H_2$ scattering is beyond the scope of this article and it will be subject of a subsequent paper. Here, we present some preliminary calculations and qualitative reasoning giving some insight into the dynamics of the processes of the interest. This section is organized as follows. We present the details of the *ab initio* calculation in Subsection IV A. The cuts of the lowest three potential energy surfaces (PES) along the reactive coordinate are also discussed there. These cuts indicate that only one of the three PES contributes to AD reaction. Finally, we discuss briefly the global topology of these surfaces including the information about the conical intersection structure. In Subsection IV B, we argue that the conical intersection is responsible for the fact that all three surfaces finally contribute to the process (as suggested by the size of the measured rate exceeding the Langevin rate). This argument is supported by classical trajectory calculations that are limited to individual uncoupled surfaces (calculation of the nonadiabatic coupling of the surfaces is left for the subsequent work). No quantitative information on reaction cross sections and branching ratios can be given as long as we neglect the nonadiabatic coupling. We thus remain on the qualitative level of discussion there. In Subsection IV C, a simplified quantitative model is, nevertheless, developed for the capture cross section. We believe that this model is relevant for explaining the shallow maximum in measured rates near 40 K.

A. *Ab initio* potential energy surfaces

First, we have calculated the potential energy surfaces for the three lowest electronic states leading to the $O^-(^2P) + H_2(X^1\Sigma_g^+)$ asymptote ($1^2A'$, $1^2A''$, and $2^2A'$). The positions of the nuclei were parameterized with Jacobi coordinates R (distance between nucleus of O and the center of mass of H_2), r (mutual distance of the two H atoms), and θ (angle between R and r vectors). Calculations have been done with the MOLPRO package[27,28] using the internally contracted multireference configuration interaction (MRCI) method[29] starting from MCSCF[30,31] with 1 closed orbital and 9 electrons in 10 active orbitals. In order to obtain the best results possible today, we did all calculations with aug-cc-pVTZ.[32] To localize the two-dimensional surface, where the anion states are embedded in the electron continuum, also the lowest state of the neutral H_2O molecule has been determined on the same level of theory. The potential energy surfaces were obtained on a fine grid with $\theta \in \langle 0°, 90° \rangle$ with step 10°, $R \in \langle 2a_0, 10a_0 \rangle$ and $\langle 10a_0, 20a_0 \rangle$ with steps $0.2a_0$ and $0.5a_0$, respectively, and $r \in \langle 1.0a_0, 2.0a_0 \rangle$ and $\langle 2.0a_0, 2.9a_0 \rangle$ with steps $0.05a_0$ and $0.1a_0$, respectively. All distances here and in the rest of the

paper are given in atomic units (Bohr radius a_0). As compared to previous calculation of Werner *et al.*,[4] our active space is bigger and we used all configurations from the active space as reference wave functions in MRCI calculations. Although our MRCI results include more electron correlation than those of Werner *et al.*,[4] the asymptotic energy difference between $O^- + H_2$ and $OH^- + H$ channels by 0.1 eV is too small as compared to the experimental value of 0.28 eV. To improve the asymptotic behavior of the PES, we used the Davidson correction as implemented in MOLPRO[33] for which the energy difference is 0.23 eV.

To visualize the PES relevant for the understanding reactions (1) and (2), Fig. 3 shows one-dimensional cuts of PES along two paths connecting $O^- + H_2$ and $OH^- + H$ asymptotic regions. In panel (a), the adiabatic potential energy for all three ($1^2A'$, $1^2A''$, and $2^2A'$) states is plotted along the reaction coordinate (minimum energy path), together with the potential energy of the neutral molecule H_2O. The autodetachment can occur in the region where the anionic curve is above the neutral (this region is responsible for $e^- + H_2O$ product channel). Strictly speaking, the electron-molecule scattering

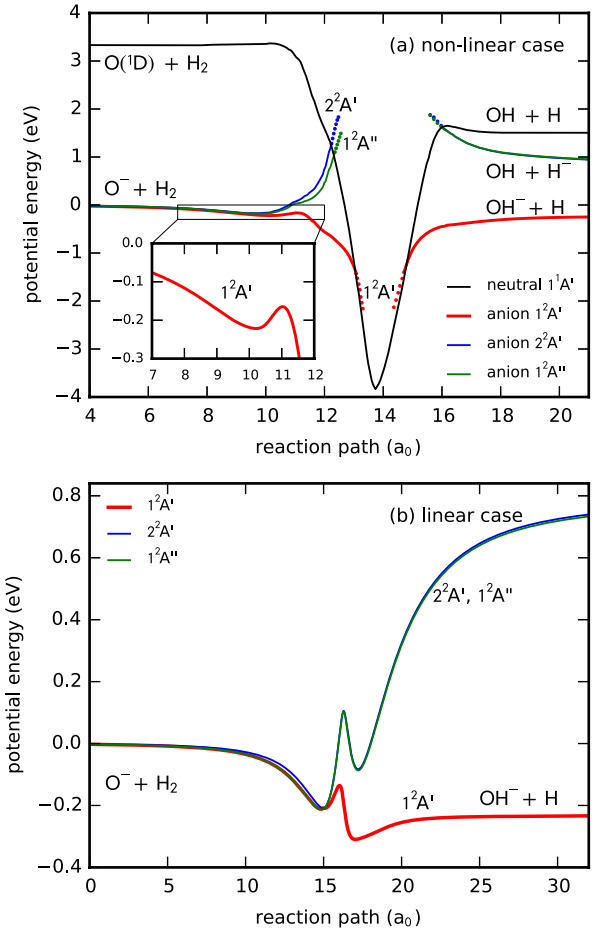

FIG. 3. Panel (a)—PES of H_2O^- and H_2O along the minimum energy path going from $O^- + H_2$ to $OH^- + H$ on the $1^2A'$ PES. The anionic curves in the autodetachment region, where they are above the neutral PES, are indicated by points. The local minimum of the $1^2A'$ PES, where some metastable H_2O^- states may exist, is magnified in the inset. In Panel (b), the path is constrained to the linear geometry, $\theta = 0°$. In this case, the potential energy of the neutral H_2O is too high—outside of the graph.

calculation must be used to continue the curves deep into this region. We thus show only short portion of the PES calculated from quantum chemistry with the dashed lines. In panel (b), the minimum energy path is restricted to a linear molecular geometry (similar potential curve was shown for older calculation by Werner *et al.*[4]). Here, the neutral H_2O PES cannot be shown because it is far up, out of the energy scale of the graph. Inspection of the upper panel reveals that the system following the minimum energy path on the ground $1^2A'$ PES passes through the autodetachment region, while the PES of the other two states are repulsive and do not allow to reach this region in low-energy collisions directly. There are also trajectories possible (e.g., along the linear PES shown in (b)) where the autodetachment region is avoided and one may reach the $OH^- + H$ product channel without electron detachment. However, it is energetically preferable to bend the molecule and to follow the path shown in Fig. 3(a). This, together with a high probability of autodetachment, provides a first qualitative explanation for the small k_2 observed in the experiment.

More qualitative insight into the collision dynamics can be gained by inspecting the three surfaces that the $O^- + H_2$ system has to follow during the first approach. In statistical theories, it is common to account for repulsive surfaces with a weighting factor which would be here 1/3 if the surfaces are not coupled at all. However, this does not apply to the present anionic system, because all three PES are first attractive before they split. This situation is shown in more detail in Fig. 4(a). The data in this figure are calculated in linear geometry (with $\theta = 0°$, $r = 1.4a_0$) since the minimum energy path follows this line down to an $O^- - H_2$ distance of $4.5a_0$. Note that two of the three states are degenerate, forming a $^2\Pi$ state due to the additional symmetry in linear geometry. All three PES follow the asymptotic behavior within ~10 meV. We can therefore expect that first capture at low collision energies can be rather well understood from the motion in a potential that is close to the average of the three PES. Another important feature seen in Fig. 4(a) (see also the inset) is the conical intersection near $R = 4.6a_0$, which couples all three states in the vicinity of the local potential minimum. To understand the global geometry of the conical intersection, we have to keep in mind that two of the PES are degenerate at linear geometry (it is $1^2A'$ and $1^2A''$ for R larger than the intersection point and $2^2A'$ and $1^2A''$ for small R). The three PES are thus just the three branches of one 3-dimensional self-intersecting surface, which intersects itself at linear geometry (2-dimensional intersection) and at a 1-dimensional curve ($R = 4.6a_0$, $\theta = 0°$, $r = 1.4a_0$ is one representative point of this triple intersection). It is beyond the scope of the present paper to describe the nonadiabatic dynamics on this PES manifold and how and where the electron is ejected. Autoionization widths and the coefficients for nonadiabatic and spin-orbit coupling have to be found first. However, we will try to learn from the classical trajectory calculations on the three PES, disregarding any coupling.

B. Classical trajectories on uncoupled PES

First, we followed a set of trajectories on the lowest PES. All trajectories start in the asymptotic region $R \to \infty$ with the hydrogen molecule close to its equilibrium geometry $r = 1.4a_0$

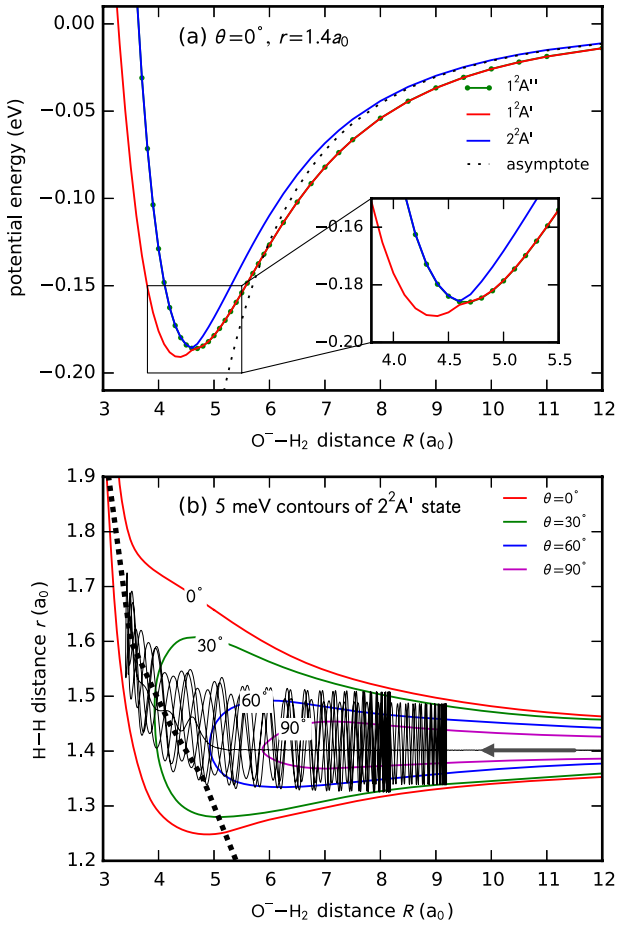

FIG. 4. Panel (a)—Section of the three potential energy surfaces for $\theta = 0°$, $r = 1.4014a_0$, showing the attraction of O^- and H_2 and the conical intersection at $4.6a_0$, coupling them. The sum of quadrupole and polarization potential is marked with a dotted line. Panel (b)—Typical classical trajectory on the $2^2A'$ PES for a collision energy of 5 meV projected on the $\theta = 0°$ plane. The conical intersection at $\theta = 0°$ is marked by the dashed line. The equipotential lines for $V = 5$ meV are also shown for the indicated values of θ. This picture shows a section of a trajectory with a duration of 700 vibrational periods of H_2. Most trajectories remain trapped for typically 10^4–10^5 vibrational periods, passing beyond the conical intersection several hundred times.

and with arbitrary initial orientation θ. The behavior of typical trajectories is as follows. As the colliding particles approach each other, the molecule has a tendency to align ($\theta \to 0°$) due to the long range quadrupole potential, staying close to reaction path (Fig. 3(a)). When reaching the interaction region $R \approx 3a_0$ on the PES of the ground state $1^2A'$, the trajectory is deflected towards the $OH^- + H$ asymptote by stretching r. The angle θ increases at the same time. When moving on the $1^2A'$ ground electronic PES the trajectory can continue to the autodetachment region at $r \approx 2.2a_0$ and $\theta \approx 60°$. For treating electron detachment, the autodetachment mechanism must be quantified (autodetachment width). The measured energy distribution of electrons[11] suggests that the detachment is efficient, as it occurs soon after crossing the PES of the neutral. Also the measured rate coefficient of associative detachment between OH^- and H shows that nearly every collision leads to detachment.[34] We also expect, in accordance with Fig. 3(b) that some trajectories can reach the $OH^- + H$ exit channel, avoiding the detachment region. According to the experimental results, this process occurs with small probability.

As shown already in Fig. 3(a), trajectories on the upper two electronic states cannot lead directly to autodetachment or rearrangement at low collision energies. A typical trajectory for the $2^2A'$ PES and the position of the conical intersection among the three electronic states at $\theta = 0°$ (black dashed line) are shown in Fig. 4(b). The starting point of the trajectory is at the right ($R = 12a_0$ and $r = 1.4a_0$) and the particles are approaching each other on a straight line. During the reflection at short distances, vibration along the coordinate r is excited. The conversion of translational energy into vibration of H_2 hinders or forbids dissociation back to the initial channel. The trajectory thus becomes trapped in a long lived collision complex. It is easy to see that it passes beyond the conical intersection many times. Strictly speaking, the trajectory on single PES does not make sense beyond the conical intersection point since the $2^2A'$ becomes degenerate with $1^2A''$ each time the system passes through the linear geometry enhancing the nonadiabatic coupling among PES. This corroborates our speculation from above: the many attempts accumulate to a large probability to jump to the lowest $1^2A'$ state from where it does not come back because it can continue its way towards the autodetachment region or to the H atom transfer channel. It is thus plausible to assume that all three PES contribute to the detachment cross section (the lowest one directly and upper two through the conical intersection). We have already stressed that we cannot give more quantitative statement about the branching into individual product channels without accounting for nonadiabatic coupling, but in Subsection IV C we try to quantify the capture cross section for the formation of just described long lived collision complex.

C. Model for low-energy capture rate

Qualitative discussion in Subsections IV A and IV B suggests, that at low enough energies, the sum of the AD (the dominant channel) and the H atom transfer rate coefficients will become close to the total capture rate coefficient. To explain qualitatively the behavior of the rate coefficient at very low energies (where experiment shows deviations from the Langevin rate), we performed calculation of the cross section of capture within a simple 1D model with the following effective 1D potential model (in hartrees):

$$\frac{V(R/a_0)}{\text{Ha}} = -\frac{2.74}{R^4} + 0.001\,5(e^{-1.4(R-5.5)} - 2e^{-0.7(R-5.5)}). \tag{3}$$

This function is obtained from *ab initio* data for $R > 3a_0$. To take into account possibility of reorientation and stretching of the molecule, we take the *ab initio* data at fixed-R and diagonalize the Hamiltonian in r, θ space. The R-dependence of the lowest eigenvalue then produces the one dimensional potential energy curve for each of the three PES. Finally, the function $V(R)$ above is the least squares fit to the average of the three thus obtained curves. $V(R)$ is replaced by a constant for $R < 3a_0$, since this region is not important for capture at low energies. Furthermore, at small R, we include the complex

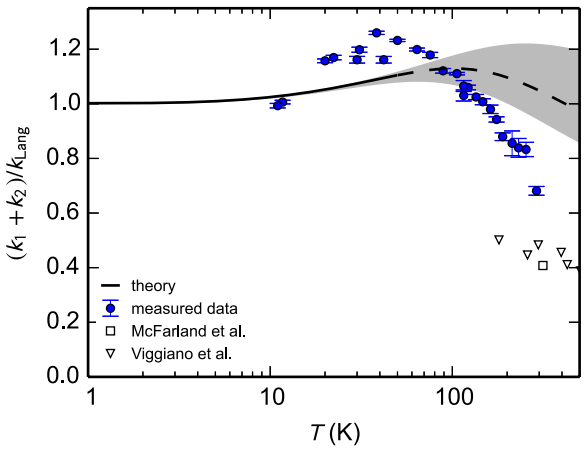

FIG. 5. Comparison of the measured total reaction rate coefficients $k_1 + k_2$ with the values calculated with the 1D capture model described in the text. The data are normalized with the Langevin capture rate coefficient. Sensitivity test of the model is indicated with the gray area. The part of the theoretical curve which is significantly sensitive to the parameters of the absorption potential, is shown as a dashed line. Experimental results of McFarland *et al.*[10] and Viggiano *et al.*[12] are shown for comparison.

absorbing potential equal to $-i/2\times\Gamma(R)$, with

$$\frac{\Gamma(R/a_0)}{\text{Ha}} = A[1+e^{5(R-R_c)}]-1. \quad (4)$$

The total absorption cross section for this potential is calculated solving the radial Schrödinger equation for sufficient number of partial waves. The cross section is integrated over Maxwell-Boltzmann collision energy distribution. The resulting capture rate coefficient is shown in Fig. 5, together with our experimental data for AD. We also show the uncertainty of the capture model due to the absorbing function $\Gamma(R)$ by varying the strength A between 0.2 and 1.0 and the position R_c between $2.5a_0$ and $3.5a_0$. To emphasize the small deviations from the simple Langevin model, we show in Fig. 5 the rate coefficient of reaction (1) normalized to the Langevin capture rate coefficient.

The calculated rate coefficient qualitatively agrees with the measured curve. Its size even slightly exceeds the Langevin value due to additional short range attractive term somewhat strengthening the polarization potential. The presence of the maximum (and the associated drop in rate towards the lowest temperatures) can thus be directly related to the shape of the potential. The exact position of the maximum does not match the observed data. We attribute this mismatch to the averaging procedure used to produce the capture model. For more precise capture coefficient, we need to take into account the nonadiabatic coupling and not just the average, since two of the three PES are degenerate in linear geometry for each value of R. The calculated data also show the decrease of the rate at higher temperature but we expect that the simple capture model is not correct at higher end of temperature axis in Fig. 5.

V. CONCLUSIONS AND OUTLOOK

The rate coefficients of associative detachment and hydrogen atom transfer between O^- and H_2 have been measured at temperatures between 10 K and 300 K. This work thus provides data at so far unexplored temperatures below 176 K. The rate coefficient of associative detachment increases with decreasing temperature between 300 K and 80 K, then levels off at 1.8×10^{-9} cm^3 s^{-1} between 80 K and 20 K, and finally decreases again to the value of 1.5×10^{-9} cm^3 s^{-1} at 10 K. The rate coefficient of hydrogen atom transfer has a nearly constant value of 5×10^{-11} cm^3 s^{-1} with a slight decrease at 10 K. The unexpectedly high value of the associative detachment rate coefficient is explained with the aid of calculated PES of H_2O^-. The classical trajectory simulations suggest that a long-lived complex is formed in collisions on the attractive PES at low collision energies and that there is a high probability of transition to the reactive PES due to the conical intersection, which means that the reaction rate coefficient will be close to the capture rate coefficient. Since all three potentials are following closely the quadrupole + polarization behavior at large $O^- + H_2$ separation, this capture rate is close to Langevin rate at low temperature. The Langevin value is even little bit exceeded (in accordance with measured data) since the PES are even slightly more attractive than the quadrupole + polarization. With increasing collision energy, the lifetime of the collision complex decreases due to easier possibility to escape back through attractive potential energy well and the rate coefficient approaches the fraction of Langevin rate. Furthermore, the presence of long-lived H_2O^- complexes points to the possibility of ternary association, i.e., stabilization by collision with third particle and consequent formation of metastable H_2O^-. Experimentally determined branching ratios show that hydrogen atom transfer occurs in less than 5% of reactive collisions. This observation can be explained by noticing that the reaction path of hydrogen atom transfer passes through autodetachment region. The paths that avoid autodetachment have to balance on the higher potential energy shelf, which is less probable.

The observed data are thus in good agreement with the theoretical arguments that follow from the calculated PES. However, to get a deeper understanding, further experimental and theoretical studies are needed. Experimental study of the isotopic effect of exchanging H_2 for D_2 is in preparation and we are planning to study the differences in reactivity between *ortho* and *para* nuclear spin configurations of H_2 by means of the 22-pole trap combined with a para-hydrogen generator.

We also plan to deepen our theoretical understanding of the dynamics in several respects. First, we will determine the autodetachment widths by running the R-matrix calculation[35,36] of electron scattering on water molecule with relevant geometries. From this calculation, we plan to construct the nonlocal resonance model for the associative detachment, as we did previously for several diatomic systems.[37–39] Finally, we will also calculate the nonadiabatic and spin-orbit coupling among the three anionic states and run the scattering calculation of the nuclear dynamics to get state to state cross sections for both reactions (1) and (2).

ACKNOWLEDGMENTS

We thank the Technische Universität Chemnitz and the Deutsche Forschungsgemeinschaft for lending the 22-pole trap

instrument to the Charles University. This work was partly supported by the Czech Grant Agency (GACR P209/12/0233, GACR 14-14715P, GACR 208/10/1281) and by the Charles University (UNCE 204020/2012, GAUK 659112).

[1]M. W. Chase and National Institute of Standards and Technology (U.S.), *NIST-JANAF Thermochemical Tables* (American Chemical Society, Woodbury, NY; American Institute of Physics for the National Institute of Standards and Technology, Washington, DC, 1998).
[2]J. R. Smith, J. B. Kim, and W. C. Lineberger, Phys. Rev. A **55**, 2036 (1997).
[3]C. Blondel, W. Chaibi, C. Delsart, C. Drag, F. Goldfarb, and S. Kröger, Eur. Phys. J. D **33**, 335 (2005).
[4]H. J. Werner, U. Manz, and P. Rosmus, J. Chem. Phys. **87**, 2913 (1987).
[5]D. J. Haxton, C. W. McCurdy, and T. N. Rescigno, Phys. Rev. A **75**, 012710 (2007).
[6]H. Adaniya, B. Rudek, T. Osipov, D. J. Haxton, T. Weber, T. N. Rescigno, C. W. McCurdy, and A. Belkacem, Phys. Rev. Lett. **103**, 233201 (2009).
[7]D. J. Haxton, H. Adaniya, D. S. Slaughter, B. Rudek, T. Osipov, T. Weber, T. N. Rescigno, C. W. McCurdy, and A. Belkacem, Phys. Rev. A **84**, 030701(R) (2011).
[8]N. B. Ram, V. S. Prabhudesai, and E. Krishnakumar, J. Phys. B: At. Mol. Opt. Phys. **42**, 225203 (2009).
[9]C. R. Claydon, G. A. Segal, and H. S. Taylor, J. Chem. Phys. **54**, 3799 (1971).
[10]M. McFarland, D. L. Albritton, F. C. Fehsenfeld, E. E. Ferguson, and A. L. Schmeltekopf, J. Chem. Phys. **59**, 6629 (1973).
[11]P. Jusko, Š. Roučka, R. Plašil, and J. Glosík, Int. J. Mass Spectrom. **352**, 19 (2013).
[12]A. A. Viggiano, R. A. Morris, C. A. Deakyne, F. Dale, and J. F. Paulson, J. Phys. Chem. **95**, 3644 (1991).
[13]J. L. Mauer and G. J. Schulz, Phys. Rev. A **7**, 593 (1973).
[14]V. A. Esaulov, R. L. Champion, J. P. Grouard, R. I. Hall, J. L. Montmagnon, and F. Penent, J. Chem. Phys. **92**, 2305 (1990).
[15]S. T. Lee and J. M. Farrar, J. Chem. Phys. **111**, 7348 (1999).
[16]C. Blondel, C. Delsart, C. Valli, S. Yiou, M. R. Godefroid, and S. Van Eck, Phys. Rev. A **64**, 052504 (2001).
[17]I. Zymak, M. Hejduk, D. Mulin, R. Plašil, J. Glosík, and D. Gerlich, Astrophys. J. **768**, 86 (2013).
[18]L. A. Viehland, R. Webb, E. P. Lee, and T. G. Wright, J. Chem. Phys. **122** (2005).
[19]D. Gerlich, G. Borodi, A. Luca, C. Mogo, and M. A. Smith, Z. Phys. Chem. **225**, 475 (2011).
[20]I. Zymak, P. Jusko, Š. Roučka, R. Plašil, P. Rubovič, D. Gerlich, and J. Glosík, Eur. Phys. J. Appl. Phys. **56**, 24010 (2011).
[21]D. Gerlich, P. Jusko, Š. Roučka, I. Zymak, R. Plašil, and J. Glosík, Astrophys. J. **749**, 22 (2012).
[22]D. Gerlich, Adv. Chem. Phys. **82** (1992).
[23]D. Gerlich, Phys. Scr. **1995**, 256.
[24]Y. Y. Milenko, L. V. Karnatsevich, and V. S. Kogan, Physica **60**, 90 (1972).
[25]R. Otto, J. Mikosch, S. Trippel, M. Weidemüller, and R. Wester, Phys. Rev. Lett. **101**, 063201 (2008).
[26]J. L. Moruzzi, J. J. W. Ekin, and A. V. Phelps, J. Chem. Phys. **48**, 3070 (1968).
[27]H.-J. Werner, P. J. Knowles, G. Knizia, F. R. Manby, and M. Schütz, Wiley Interdiscip. Rev.: Comput. Mol. Sci. **2**, 242 (2012).
[28]H.-J. Werner, P. J. Knowles, G. Knizia, F. R. Manby, M. Schütz, P. Celani, T. Korona, R. Lindh, A. Mitrushenkov, G. Rauhut, K. R. Shamasundar, T. B. Adler, R. D. Amos, A. Bernhardsson, A. Berning, D. L. Cooper, M. J. O. Deegan, A. J. Dobbyn, F. Eckert, E. Goll, C. Hampel, A. Hesselmann, G. Hetzer, T. Hrenar, G. Jansen, C. Köppl, Y. Liu, A. W. Lloyd, R. A. Mata, A. J. May, S. J. McNicholas, W. Meyer, M. E. Mura, A. Nicklass, D. P. O'Neill, P. Palmieri, D. Peng, K. Pflüger, R. Pitzer, M. Reiher, T. Shiozaki, H. Stoll, A. J. Stone, R. Tarroni, T. Thorsteinsson, and M. Wang, MOLPRO, *Version 2012.1, A Package of Ab Initio Programs* (University College Cardiff Consultants Limited, Cardiff, UK, 2012).
[29]P. Knowles and H.-J. Werner, Theor. Chim. Acta **84**, 95 (1992).
[30]H.-J. Werner and P. J. Knowles, J. Chem. Phys. **82**, 5053 (1985).
[31]P. J. Knowles and H.-J. Werner, Chem. Phys. Lett. **115**, 259 (1985).
[32]T. H. Dunning, J. Chem. Phys. **90**, 1007 (1989).
[33]H.-J. Werner, M. Kállay, and J. Gauss, J. Chem. Phys. **128**, 034305 (2008).
[34]C. J. Howard, F. C. Fehsenfeld, and M. McFarland, J. Chem. Phys. **60**, 5086 (1974).
[35]J. Tennyson, Phys. Rep. **491**, 29 (2010).
[36]J. M. Carr, P. G. Galiatsatos, J. D. Gorfinkiel, A. G. Harvey, M. A. Lysaght, D. Madden, Z. Mašín, M. Plummer, J. Tennyson, and H. N. Varambhia, Eur. Phys. J. D **66**, 58 (2012).
[37]M. Čížek, J. Horáček, and W. Domcke, J. Phys. B: At. Mol. Opt. Phys. **31**, 2571 (1998).
[38]K. Houfek, M. Čížek, and J. Horáček, Phys. Rev. A **66**, 062702 (2002).
[39]S. Živanov, M. Allan, M. Čížek, J. Horáček, F. A. U. Thiel, and H. Hotop, Phys. Rev. Lett. **89**, 073201 (2002).